Titre: Title:	Réactions homogènes en phase gazeuse dans les lits fluidisés
Auteur: Author:	Jean-Philippe Laviolette
Date:	2010
Type:	Mémoire ou thèse / Dissertation or Thesis
Référence: Citation:	Laviolette, J.-P. (2010). Réactions homogènes en phase gazeuse dans les lits fluidisés [Thèse de doctorat, École Polytechnique de Montréal]. PolyPublie. https://publications.polymtl.ca/340/

UNIVERSITÉ DE MONTRÉAL

RÉACTIONS HOMOGÈNES EN PHASE GAZEUSE DANS LES LITS FLUIDISÉS

JEAN-PHILIPPE LAVIOLETTE

DÉPARTEMENT DE GÉNIE CHIMIQUE

ÉCOLE POLYTECHNIQUE DE MONTRÉAL

THÈSE PRÉSENTÉ EN VUE DE L'OBTENTION

DU DIPLÔME DE PHILOSOPHIAE DOCTOR (Ph.D.)

(GÉNIE CHIMIQUE)

JUIN 2010

UNIVERSITÉ DE MONTRÉAL

ÉCOLE POLYTECHNIQUE DE MONTRÉAL

Cette thèse intitulée:

RÉACTIONS HOMOGÈNES EN PHASE GAZEUSE DANS LES LITS FLUIDISÉS

présentée par : LAVIOLETTE, Jean-Philippe

en vue de l'obtention du diplôme de : Philosophiae Doctor

a été dûment acceptée par le jury d'examen constitué de :

M. LEGROS Robert, Ph.D., président

M. PATIENCE Gregory S, Ph.D., membre et directeur de recherche

M. CHAOUKI Jamal, Ph.D., membre et codirecteur de recherche

Mme LA MARCA Concetta, Ph.D., membre et codirecteur de recherche

M. FRADETTE Louis, Ph.D., membre

M. HEMATI Mehrdji, Doct.Ing., membre

REMERCIEMENTS

Je remercie mes directeurs de thèse, Jamal Chaouki et Gregory Patience, pour m'avoir accueilli dans leur équipe de recherche, pour l'aide qu'ils m'ont apportée, pour leur patience et pour leur encouragement. Leurs nombreuses critiques m'ont été très précieuses dans mes travaux.

Je remercie également ma co-directrice de thèse, Concetta La Marca, qui m'a accueilli chez E.I. du Pont de Nemours afin que je puisse mettre en pratique mes connaissances dans un contexte industriel. Nos discussions sur la modélisation des réactions m'ont été très utiles.

Je tiens à remercier Jean Huard, Daniel Dumas, Carol Painchaud, Robert Delisle, Gino Robin et Martine Lamarche sans qui, je n'aurais pas pu réaliser ce travail.

Le déroulement de mon doctoratn'aurait pas été aussi agréable sans avoir rencontré Farhad Azar, Ali Shekari, Babak Esmaeili, Rouzbeh Jafari, Mania, Jocelyn Doucet, Jonathan Bouffard et Olivier Dubé.

Je remercie ma famille qui m'a soutenu pendant ce travail et plus spécifiquement mes parents qui ont toujours eu mon bien-être à cœur. C'est en grande partie grâce à eux si je me trouve là où je suis présentement.

Finalement, je remercie ma conjointe, Florence, qui a quitté Marseille pour m'accompagner dans cette aventure qui devait à l'origine durer… 3 ans.

RÉSUMÉ

Cette thèse présente une étude sur les réactions homogènes en phase gazeuse dans les lits fluidisés. L'objectif principal est de développer des outils de modélisation et de caractérisation des réactions homogènes en phases gazeuses dans les réacteurs à lit fluidisé.

Minimiser l'occurrence de réactions homogènes dans les lits fluidisés est un enjeu majeur puisqu'elles peuvent causer une baisse de production suite à la dégradation des réactifs et des produits désirés. Par ailleurs, ces réactions peuvent représenter un risque pour la sécurité lorsqu'elles sont rapides et exothermiques comme c'est le cas pour les réactions d'oxydations. Dans la région du lit fluidisé, la fraction de solides augmente le taux de recombinaison des radicaux libre et évite l'initiation de réactions homogènes ou réduit leur vitesse de réaction. Il existe toutefois des régions de haute porosité où des réactions homogènes peuvent être produites par de fortes concentrations de réactifs combinés à des températures et pressions élevées (caractéristiques de nombreux procédés incluant les procédés d'oxydation). Dans ces régions, le taux de recombinaison des radicaux libres peut être insuffisant pour empêcher l'initiation de réactions en phases gazeuses. Dans un réacteur à lit fluidisé, les régions de faible fraction de solides incluent principalement:

- La zone du distributeur et des injecteurs dans le lit fluidisé
- La phase bulle dans le lit fluidisé
- Les régions en aval du lit fluidisé (zone de désengagement, cyclone, etc.)

Dans la première partie de ce travail, la combustion en lit fluidisé du méthane, éthane, propane et n-butane avec de l'air a été étudiée en mode d'injection séparée. Un lit fluidisé de particules inertes de sables a été opéré dans le régime à bulle et à des températures intermédiaires : $923\ K \leq T_B \leq 1123\ K$. Pour l'éthane, le propane et le n-butane, la combustion avait lieu principalement dans la région de désengagement lorsque la température du lit fluidisé était inférieure à $T_1 = 923\ K$. D'un autre côté, la combustion se produisant entièrement dans une distance de 0.2 m de l'injecteur lorsque la température du lit était supérieure à $T_2 = 1073\ K$. Pour

le méthane, les valeurs de T_1 et T_2 étaient significativement plus élevées avec des mesures respectives de 1023 K et 1123 K. La combustion dans le lit fluidisé a été modélisée avec précision à l'aide d'une cinétique globale de première ordre et une modèle hydrodynamique composé de deux réacteurs pistons en séries : un qui caractérisait la région près de l'injecteur et un autre pour la région de lit fluidisé en aval. La cinétique globale de réaction a été mesurée pour chacun des hydrocarbures. Pour les n-alcanes C_2 à C_4, la cinétique globale était caractérisé par une seule expression de type Arrhenius, alors que la cinétique du méthane était significativement plus lente. Les propriétés de la région de l'injecteur causaient soit une conversion importante dans cette région, soit un délai d'auto-allumage dans le lit fluidisé. La conversion des réactifs près de l'injecteur augmentait avec une hausse de la température du lit fluidisé et diminuait avec une hausse de la vitesse d'injection du gaz à l'extrémité de l'injecteur. Afin de prendre ce phénomène en compte dans le modèle de réaction, une analogie a été effectuée avec le concept de temps d'induction. Ainsi, la longueur du réacteur piston caractérisant la région de l'injection a été corrélée à la température du lit fluidisé et la vitesse d'injection avec une expression de type Arrhenius.

Dans la seconde partie de cette thèse, la combustion du propane dans la zone de désengagement d'un lit fluidisé de sable a été étudiée. La température du lit fluidisé a été maintenue faible entre 818 K et 923 K afin que la combustion se produise essentiellement en aval du lit fluidisé. De plus, une vitesse superficielle de gaz deux fois supérieure à la vitesse minimale de fluidisation a été utilisée pour minimiser l'emportement de solides. Durant les expériences, la zone de désengagement a été caractérisée par des mesures simultanées de flux de solides, de composition chimique de la phase gazeuse, de température et de pression. L'auto-allumage de la mixture propane/air a été observé à seulement 0.06 m de la surface du lit pour des températures de lit fluidisé supérieures à 833 K. Six mécanismes de microcinétique ont été utilisés afin de reproduire le profil axial de conversion du propane: tous les modèles ont sous-estimé le taux de réaction dans la zone de désengagement. Or, lorsque le modèle considérait le H_2O_2 produit lors de la combustion dans le lit fluidisé, la vitesse de réaction calculée dans la zone de désengagement étaient significativement plus élevée et causait une meilleure concordance entre le modèle et les résultats expérimentaux.

La troisième partie de ce travail relate le développement d'une nouvelle méthode spectroscopique pour la mesure quantitative et simultané de la fraction de solides (1-ε) et de la composition chimique dans la phase gazeuse (Y_i) dans un système gaz/solide. La méthode a été utilisée avec une FT-IR connecté à une sonde à fibres-optiques à laquelle des mesures en temps réel et in situ pouvaient être effectuées. L'effet de (1-ε) et Y_i sur le spectre d'absorbance mesuré étaient additifs et pouvaient être calibrés de manière indépendante. Des mesures ont été effectuées avec des mixtures alkane/azote et deux types de particules: du sable et du catalyseur FCC. La fraction volumétrique de l'hydrocarbure et (1-ε) ont été variées entre des valeurs respectives de 1.8 - 10.1 mol% et 0 - 0.45. Les erreurs relatives sur la mesure de Y_i étaient toujours inférieures à 6% and l'erreur augmentait avec une baisse de l'intensité du rayon infrarouge. Une preuve de concept a été effectuée dans un lit fluidisé: la sonde à fibres-optiques a été utilisée pour mesurer la fraction volumétrique d'un traceur gazeux dans la phase bulle et émulsion.

Les résultats ont également démontré que la méthode est limitée par deux paramètres:

- L'intensité du rayon infrarouge transmis dans l'échantillon et récolté par le détecteur du spectromètre.
- La vitesse de mouvement des solides et la fréquence de modulation du spectromètre.

Un signal infrarouge faible augmente l'erreur sur les mesures instantanées. L'erreur relative sur la mesure peut toutefois être significativement diminuée en-dessous de 5% si une moyenne temporelle est effectuée. L'intensité du rayon infrarouge pourrait être accrue en:

- Augmentant l'intensité de la source IR
- Optimisant le transfert du rayon IR à l'interface spectromètre/sonde à fibres-optiques
- Optimisant le transfert du rayon IR l'extrémité de la sonde
- Augmentant la sensibilité du détecteur

Le mouvement des particules solides produit du bruit dans le spectre d'absorbance mesuré de sorte que la fréquence de modulation doit être suffisamment élevée afin de déplacer le bruit vers les basses fréquences à l'extérieur des longueurs d'ondes d'intérêts.

ABSTRACT

This thesis presents a study on homogeneous gas-phase reactions in fluidized beds. The main objective is to develop new tools to model and characterize homogeneous gas-phase reactions in this type of reactor.

Minimizing the risk of gas-phase reactions in fluidized beds is critical since they may cause a decrease in production by degrading reactants and desired products. Furthermore, they may constitute a safety concern in the case of fast and exothermic reactions such as oxidation reactions. In the fluidized bed region, the high solids volume fraction quenches free radicals, which minimizes gas-phase reactions. However, fluidized bed reactors are characterized by several regions of low solids volume fractions where gas-phase reactions may occur due to high temperatures, pressures and reactants concentrations. In these regions, the rate at which free radicals are quenched may be insufficient. In a fluidized bed reactor, the regions of low solids volume fraction mainly include:

- The regions close to the distributor and the injectors
- The bubble phase
- The regions downstream of the fluidized bed surface (freeboard, cyclones, etc.)

Chemical processes in fluidized beds should be designed in order to prevent the initiation of homogeneous gas-phase reactions in these regions.

In the first part of this work, the non-premixed combustion of C_1 to C_4 n-alkanes with air was investigated inside a bubbling fluidized bed of inert sand particles at intermediate temperatures: $923\ K \leq T_B \leq 1123\ K$. For ethane, propane and n-butane, combustion occurred mainly in the freeboard region at bed temperatures below $T_1 = 923$ K. On the other hand, complete conversion occurred within 0.2 m of the injector at: $T_2 = 1073$ K. For methane, the measured values of T_1 and T_2 were significantly higher at 1023 K and above 1123 K, respectively. The fluidized bed combustion was accurately modeled with first-order global kinetics and two one-phase PFR

models in series: one PFR to model the region close to the injector and another to represent the main fluidized bed body. The measured global reaction rates for C_2 to C_4 n-alkanes were characterized by a uniform Arrhenius expression, while the global reaction rate for methane was significantly slower. Reactions in the injector region either led to significant conversion in that zone or an autoignition delay inside the main fluidized bed body. The conversion in the injector region increased with rising fluidized bed temperature and decreased with increasing jet velocity. To account for the promoting and inhibiting effects, an analogy was made with the concept of induction time: the PFR length (b_i) of the injector region was correlated to the fluidized bed temperature and jet velocity using an Arrhenius expression.

In the second part of this work, propane combustion experiments were conducted in the freeboard of a fluidized bed of sand particles at temperatures between 818 K and 923 K and at superficial gas velocity twice the minimum fluidization velocity. The freeboard region was characterized by simultaneous measurements of solids flux, chemical composition, temperature and pressure. Autoignition was only recorded within 0.06 m of the bed surface at temperatures greater than 833 K. Propane conversion predicted by six different microkinetic mechanistic models were compared to the experimental measurements: all six models underestimated the reaction rate above the bed surface. However, accounting for the production of H_2O_2 during in-bed combustion significantly increased the calculated reaction rates and resulted in a better agreement between predicted and measured propane conversion.

In the third part of this work, a novel spectroscopic method was developed to measure quantitatively and simultaneously solids volume fraction ($1-\varepsilon$) and gaseous species composition (Y_i) in a gas/solid system. The method was comprised of an FT-IR coupled to a fibre-optic probe that could perform real-time and in-situ measurements of absorbance. The effect of ($1-\varepsilon$) and Y_i on the absorbance spectra were additive and could be independently calibrated. Experiments were conducted with alkane/nitrogen mixtures and two types of particles: sand and FCC. Fuel mole fractions and ($1-\varepsilon$) were varied between 1.8 - 10.1 mol% and 0 - 0.45, respectively. The relative errors for Y_i time-averaged measurements were below 6% and the error increased significantly with decreasing beam intensity. A proof of concept for a novel application in fluidized beds was

also completed: the fibre-optic probe was used to measure the molar fraction of a tracer gas inside the emulsion and bubble phases during gas tracer experiments.

TABLE DES MATIÈRES

LISTE DES TABLEAUX

LISTE DES ANNEXES

LISTE DES FIGURES

LISTE DES SIGLES ET ABRÉVIATIONS

CHAPITRE IV

A Cross-sectional area (m^2)

b_i Parameter in equation (7) for i^{th} species (m)

D_j Injector nozzle diameter (m)

E_A Activation energy (J)

g Gravitational constant (9.81 m/s^2)

H_B Fluidized bed height (m)

k_0 First-order reaction rate constant (m^{-1})

L_j Jet penetration length (m)

Q_n Jet volumetric flow rate at 0^oC & 101.3 kPa (litres)

R Universal gas contant (8.314 J/Kmol)

r Radial position (m)

t_j Average gas residence time in injector region (s)

T Temperature (K)

T_B Fluidized bed temperature (K)

T_1 Lower critical temperature (K)

T_2 Upper critical temperature (K)

U_j Gas injection velocity at the sparger tip (m/s)

U_{mf} Minimum fluidization velocity (m/s)

U_g Superficial gas velocity (m/s)

v Volumetric flow rate (m^3/s)

w Nozzle thickness (cm)

X_i Conversion of i^{th} species (%)

Y_i Volume fraction of i_{th} species (vol%)

Z Axial position above the distributor (m)

Z_j Axial position above the injector tip (m)

Greek letters

ε Average void fraction in fluidized bed

ρ_b Fluidized bed density (kg/m^3)

ρ_g Fluidizing gas density (kg/m^3)

ρ_j Gas density at injector nozzle (kg/m^3)

ρ_p Particle density (kg/m^3)

τ Induction time (s)

CHAPITRE V

d_P average particle size (μm)

G_{SU} solids upward flux or entrainment flux (kg/m^2s)

r radial position (m)

R reaction radius (0.2 m)

τ_B average gas residence time in fluidized bed (s)

T temperature (K)

T_B fluidized bed temperature (K)

U_g superficial gas velocity (m/s)

U_{mf} minimum fluidization velocity (m/s)

Y_i volume fraction of species i (vol%)

Z axial position (m)

Z_F axial position in the freeboard (m)

CHAPITRE VI

A Absorbance

d_p Average particle size (μm)

f Modulation frequency (kHz)

t Distance between probe tip and mirror (mm)

Y_i Molar fraction of specie i (vol%)

Greek symbols

$(1-\varepsilon)$ Solids volume fraction

λ Wavelength (μm)

σ Variance

INTRODUCTION

Plusieurs procédés catalytiques industriels gaz sont caractérisés par une compétition entre des réactions homogènes en phase gazeuse et des réactions hétérogènes à la surface de particules solides. Les réactions homogènes peuvent mener à une baisse de production en causant la dégradation du catalyseur, des réactifs et des produits désirés. Par ailleurs, ces réactions peuvent représenter un risque pour la sécurité lorsqu'elles sont rapides et exothermiques comme c'est le cas pour les réactions d'oxydations. Tandis que les procédés catalytiques impliquant des réactions d'oxydation sélectives d'hydrocarbures sont de plus en plus répandus dans l'industrie, de nouveaux procédés sont présentement en développement. Par exemple, des recherches sur les procédés d'oxydation d'alcanes produisant différents produits chimiques de valeur visent à réduire l'utilisation d'alcènes, dans ces procédés, afin de diminuer les coûts. Par ailleurs, il existe plusieurs autres types de procédés gaz/solides impliquant des réactions d'oxydation où les réactions homogènes peuvent avoir des effets néfastes: regénération de catalyseur, gazéification, calcination, combustion, etc. Or, les réacteurs à lit fluidisé sont utilisés ou considérés pour plusieurs de ces procédés en raison de leur capacité à dissiper la chaleur produite localement. En effet, le mouvement des solides minimise la création de zones locales chaudes (« hot spots ») étant donné que la capacité thermique des solides est significativement plus élevée que celle du gaz.

Afin de maximiser le rendement d'un procédé, les réacteurs à lit fluidisé peuvent opérer à l'intérieur des limites d'inflammabilité en injectant l'oxydant et les hydrocarbures séparément dans le lit fluidisé de solides. La fraction de solides élevée dans le lit, augmentant le taux de recombinaison des radicaux libres, évite l'initiation de réactions homogènes ou réduit leur vitesse de réaction. Toutefois, il demeure des régions où la fraction de solides est significativement plus faible. Dans ces régions de faible fraction de solides, des réactions homogènes peuvent être produites par de fortes concentrations de réactifs combinés à des températures et pressions élevées (caractéristiques de nombreux procédés incluant les procédés d'oxydation). Aussi, le taux de recombinaison des radicaux libres peut être insuffisant et ainsi empêcher l'initiation de réactions en phases gazeuses. Dans un réacteur à lit fluidisé, les régions de faible fraction de solides incluent principalement:

- La zone du distributeur et des injecteurs dans le lit fluidisé
- La phase bulle dans le lit fluidisé
- Les régions en aval du lit fluidisé (zone de désengagement, cyclone, etc.)

À proximité du distributeur et des injecteurs, l'injection de gaz produit des zones de forte porosité. Or, lorsque les réactions homogènes en phase gazeuse sont rapides, la conversion de réactifs dans ces régions peut être élevée. Près des injecteurs, des réactions en phases gazeuse peuvent dégrader les réactifs, les produits désirés et produire une zone de haute température qui désactive le catalyseur. La phase bulle est une autre région propice aux réactions homogènes, mais elle peut également causer un court-circuit de réactifs qui sont entraînés dans la zone de désengagement.

Des réactifs peuvent également être entraînés dans la zone de désengagement en raison de contraintes opératoires qui limitent la conversion dans la région du lit fluidisé. Par exemple, la sélectivité des procédés d'oxydation partielle décroît généralement avec une augmentation de la conversion en raison de réactions secondaires qui dégradent le(s) produit(s) désiré(s). Les réactifs restant sont emportés dans la zone de désengagement propice à l'initiation de réactions homogènes: porosité, température et pression élevées. Dans cette région, des réactions homogènes rapides et exothermiques peuvent mener à une explosion. La combustion dans la zone de désengagement représente un danger pour tous les procédés gaz/solides impliquant des réactions d'oxydation.

Il est donc primordial de minimiser l'occurrence de réactions homogènes dans les régions de faibles fractions de solides. Toutefois, la caractérisation de ces régions et des réactions qui s'y produisent est une tâche ardue en raison du couplage entre la fraction de solides et la composition chimique de la phase gazeuse. Or, les méthodes de mesures actuelles évaluent ces deux paramètres de manière indépendante et non simultanée.

Une technique de mesure permettant la mesure simultanée et in situ de la composition chimique et la fraction de solides présenterait plusieurs avantages pour la conception, la caractérisation et le dépannage de procédés. Principalement, elle permettrait de déterminer la composition dans la phase bulle et émulsion. À proximité du distributeur et des injecteurs, les zones de faibles fractions de solides pourrait être cartographiées et l'effet sur les réactions homogènes/hétérogènes mesuré. La caractérisation de la zone de désengagement serait simplifiée puisque la relation entre la porosité et la composition chimique serait saisie. Ce type de mesures ne peut être effectué que difficilement à l'aide des techniques existantes.

L'objectif principal de cette thèse est de développer des outils de modélisation et de caractérisation des phénomènes de réactions homogènes en phases gazeuses dans les réacteurs à lit fluidisé.

CHAPITRE 1 REVUE DE LITTÉRATURE

Ce chapitre présente une revue de la littérature scientifique sur la combustion en lit fluidisé, la combustion dans la zone de désengagement et la caractérisation des systèmes multiphasiques.

1.1 COMBUSTION EN LIT FLUIDISÉ

La combustion du méthane et du propane dans un lit fluidisé de solides inertes a fait l'objet de plusieurs études en mode d'injection séparée (Hesketh et Davidson 1991, Van der Vaart 1988, Van der Vaart 1988a, Friedman et Li 2005, Dounit et al. 2008, Pre et al. 1998, Zukowski 2003, Baron et al. 2002, Dennis et al. 1982, Srinivasan et al. 1998) et en mode pré-mélangé (Mabrouk et al. 2008, Ross et al. 2001, Sotudeh-Gharebaagh 1998, Singh et al. 1975, Stubington et Davidson 1981, Sotudeh-Gharebaagh et Chaouki 2007). La température du lit fluidisé a été décrite comme un paramètre important qui détermine le taux de conversion dans la région du lit. Accroître la température entraîne un autoallumage plus rapide dans le lit fluidisé de solides. En mode d'injection pré-mélangé, une augmentation de la température du lit fluidisé cause le déplacement du front de combustion vers le distributeur: le front de combustion se déplace initialement de la zone de désengagement vers les bulles qui éclatent à la surface du lit, ensuite dans les bulles à l'intérieur du lit et finalement dans de petites bulles au niveau du distributeur (Zukowski 2003, Dennis et al. 1982). Alors que certaines études affirment que la combustion se produit essentiellement dans la phase émulsion (Dennis et al. 1982), la combustion du méthane et du propane a été observée dans des lits fixes de sables à des températures supérieures à 1023 K et 973 K, respectivement (Hesketh et Davidson 1991, Sotudeh-Gharebagh et Chaouki 2003).

Deux températures critiques ont été définies pour la combustion dans un lit fluidisé de particules inertes. En-dessous de la température critique inférieure (T_1), la combustion se produit en aval de la surface du lit fluidisé (dans la région de désengagement). Lorsque la température du lit se trouve entre T_1 et la température critique supérieure (T_2), le front de combustion se déplace dans la phase bulle à l'intérieur du lit. Finalement, lorsque la température du lit est supérieure à T_2, la combustion se produit entièrement dans le lit fluidisé de solides et à proximité du distributeur. Pour la combustion du méthane dans un lit fluidisé de sable, les valeurs de T_1 et T_2 mesurées oscillent entre 823-1018 K et 1133-1250 K, respectivement (Laviolette et al. 2010). Pour la

combustion du propane, T_2 a été mesuré dans un lit fluidisé de sable peu profond ($H_B \approx 0.1$ m) en tant que 1123 K (Van der Vaart 1988, Dennis et al. 1982). Toutefois, peu d'études se sont attardées à la combustion d'autres alcanes en lit fluidisé de particules inertes.

Le taux de conversion lors de la combustion en lit fluidisé peut également être estimé à l'aide d'un modèle qui combine l'hydrodynamique gaz/solide et la cinétique de réaction. Plusieurs modèles d'hydrodynamique de la phase gazeuse ont été proposés dans la littérature et ses modèles varient en complexité (Laviolette et al. 2010). L'hydrodynamique de la phase gazeuse varie entre le réacteur piston et un réacteur parfaitement mélangé selon les conditions d'opération et la nature de la réaction. Une étude récente de traceur gazeux par Lorences et al. (2006) a démontré que l'hydrodynamique de la phase gazeuse est comparable à celle d'un réacteur piston lorsque $U_g \leq 6\ U_{mf}$.

La région à proximité du distributeur et des injecteurs est caractérisée par un transfert de masse plus intense comparativement au lit fluidisé (Laviolette et al. 2010). Lorsque les réactions sont rapides, comme la combustion, une conversion importante peut survenir à l'extrémité des injecteurs. En conséquence, la modélisation de la réaction près des injecteurs et dans le lit fluidisé nécessite deux modèles hydrodynamiques distincts. Pour un injecteur orienté vers le bas, les études portant sur l'auto-allumage d'hydrocarbures dans des écoulements à contre-courant mènent à une meilleure compréhension des paramètres pouvant influencer la conversion à l'extrémité de l'injecteur (Humer et al. 2002, Fotache et al. 1999, Jomaas et al. 2005). Ces études démontrent que l'inflammabilité et la conversion décroissent avec la diminution de la température et l'augmentation de la vitesse des gaz à contre-courant. En effet, les réactions menant à l'auto-allumage des hydrocarbures impliquent des espèces chimiques intermédiaires très réactives. Or, leur durée de vie peut être du même ordre que l'échelle de temps caractéristique du transfert de masse et d'énergie. Afin de modéliser la région de l'injecteur, des modèles à une et deux phases ont été proposés dans la littérature (Laviolette et al. 2010).

Plusieurs types de modèles de cinétique de réaction sont disponibles dans la littérature pour les systèmes homogènes en phase gazeuse: modèles de microcinétique et modèles globaux

(Dounit et al. 2008, Pre et al. 1998, Ross et al. 2005). Certains mécanismes de microcinétique ont été modifiés afin d'inclure les réactions de recombinaison des radicaux libres à la surface des particules solides (Sotudeh-Gharebagh et Chaouki 2003, Jeng et al. 2001). Les modèle de microcinétique sont complexes, mais essentiel afin de prédire la production et la consommation d'espèces chimiques intermédiaires. Toutefois, dans des conditions de combustion pauvre, la conversion de l'hydrocarbure dans un lit fluidisé est bien représentée par une cinétique globale de premier ordre (Sotudeh-Gharebagh et Chaouki 2003, Foka et al. 1994, Chaouki et al. 1999). Des expressions de cinétiques globales pour une combustion homogènes en phase gazeuse ont été proposées pour le méthane, mais demeurent rares pour l'éthane et les alcanes plus complexes (C_{2+}) (Ross et al. 2004).

Il peut être possible d'exprimer la cinétique globale de premier ordre ou la conversion pour les alcanes C_{2+} à l'aide d'une seule expression ou corrélation. Plusieurs études ont fait état de similitudes entre la chimie de combustion des alcanes : le taux de combustion est contrôlé par les mêmes réactions radicalaires. Ces réactions peuvent être résumées par les réactions élémentaires suivantes à températures intermédiaires (~ 850 K à 1200 K) (Horning et al. 2002, Burcat et al. 1971, Westbrook 2000):

$$H + O_2 + M \rightarrow HO_2 + M \tag{1.1}$$

$$RH + HO_2 \rightarrow R + H_2O_2 \tag{1.2}$$

$$H_2O_2 + M \rightarrow OH + OH + M \tag{1.3}$$

Dans les réactions ci-dessus, le symbole RH correspond à un alcane, R est un alkyle et M est partenaire de collision. Saxena et al. (2007) ont démontrés que le temps d'induction à haute température (> 1200 K) du propane et alcanes plus complexes peut être estimé de manière précise en employant les paramètres décrivant la vitesse des réactions (2) à (4):

$$HO_2 + HO_2 \rightarrow H_2O_2 + O_2 \tag{1.4}$$

Plusieurs études ont démontré que le temps d'induction des alcanes C_2-C_5 mesuré dans des tubes à chocs exhibe une dépendance similaire à la température, pression and composition chimique: une corrélation avec une énergie d'activation constante suffit (Horning et al. 2002, Burcat et al. 1971). Des études précédentes rapportent également qu'à une stoichiométrie température et pression similaire, le temps d'induction décroît telle que $C_2H_6 < n\text{-}C_4H_{10} < C_3H_8$ (Horning et al. 2002, Burcat et al. 1971, Lamoureux et al. 2002). D'un autre côté, le méthane est caractérisé par des temps d'induction significativement supérieurs résultant de la production d'un radical méthyle dans l'équation (1.2). Le radical méthyle se recombine pour former de l'éthane dans une réaction de terminaison. Si la chimie de combustion et d'autoallumage des alcanes C_{2+} démontre de telles similarités, un parallèle peut possiblement être fait entre leurs cinétiques de réaction respective.

1.2 COMBUSTION DANS LA ZONE DE DÉSENGAGEMENT

Les procédés en lit fluidisé sont souvent opérés à l'intérieur des limites d'inflammabilité afin d'augmenter le rendement. Dans ce cas, l'oxydant et l'hydrocarbure sont injectés séparément à l'intérieur du lit fluidisé de solides. La fraction de solides élevée à l'intérieur du lit inhibe les réactions homogènes en phase gazeuse (combustion) tout en promouvant les réactions sélectives en phase hétérogène. Toutefois, en raison de contraintes opératoires, les procédés peuvent être opérés avec une conversion partielle des réactifs à l'intérieur du lit de solides. Par exemple, les réactions d'oxydation sélective sont caractérisées par une sélectivité qui décroît en fonction de l'augmentation de la conversion (Botella et al. 2002, Lorences et al. 2006a, Malleswara Rao and Deo 2007, Hutchenson et al. 2009). Par conséquent, en aval du lit fluidisé – dans la zone de désengagement, les cyclones et les multiples conduites associées – la mixture gazeuse est potentiellement explosive puisque caractérisée par une concentration de réactifs (hydrocarbure et oxygène), une température, une pression et une porosité élevées (Van der Vaart 1988, Van der Vaart 1988a). Minimiser le risque de réactions homogènes dans ses régions constitue un enjeu important.

Plusieurs indices d'explosions sont disponibles dans la littérature pour des systèmes homogènes en phase gazeuse: limites d'inflammabilité, température d'auto-allumage et corrélations de temps d'induction (Brokaw et Jackson 1955, Chang et al. 1959, Burcat et Lifshitz 1971,

Burcat et al. 1971, Cathonnet et al. 1981, Kin et Soo Shin 2001, Penyazkov et al. 2005, Horning et al. 2002, Zhukov et al. 2005, Freeman et Lefebvre 1984, Cadman et al. 2000). Hesketh et al. (1991) ont démontré que les corrélations de temps d'induction peuvent prédire avec précision les délais d'auto-allumage au-dessus d'un lit fixe pour $T_B \leq 973$ K et lorsque la combustion dans le lit est négligeable. Toutefois, utiliser les résultats de ces corrélations afin de prédire le temps d'induction dans des réacteurs à lit fluidisé est incertain. En effet, les particules sont emportées en aval du lit fluidisé où elles inhibent les réactions homogènes en phase gazeuse. De plus, la distribution axiale et radiale des solides au-dessus du lit n'est pas uniforme: la quantité de solides emportés décroît exponentiellement à partir de la surface du lit fluidisé et atteint une valeur constante à une distance appelée « hauteur limite de désengagement des particules » (Wen et Chen 1982, Kunii et Levenspiel 1990). La zone de désengagement peut également être caractérisée par des gradients radiaux et axiaux de température et de concentrations d'espèces chimiques. Finalement, la conversion partielle des réactifs dans le lit fluidisé de solides produits des espèces chimiques intermédiaires et des radicaux libres qui peuvent participer aux réactions dans la zone de désengagement.

Afin de prédire le temps d'induction et la vitesse de combustion d'une mixture inflammable dans la zone de désengagement et ce pour différentes conditions opératoires, un modèle de combustion combinant l'hydrodynamique gaz/solide, la cinétique de réaction, le gradient de température et la condition limite adéquate doit être développé. Des modèles en régime permanent ont été proposés par De Lasa et al. (1979), Chen et al. (1982), Walsh et al. (1982), Sotudeh-Gharebagh et Mostoufi (2003), Dounit et al. (2008), and Hartman et al. (2010) pour représenter différentes réactions dans la zone de désengagement. Toutefois, ces modèles utilisent des cinétiques globales qui sont incapables de simuler la chimie radicalaire et le temps d'induction. Également, ces modèles utilisent des corrélations afin d'estimer la fraction de solides, ce qui risque d'introduire des erreurs significatives.

Un mécanisme de microcinétique est nécessaire afin de caractériser le temps d'induction et de considérer l'effet des espèces chimiques intermédiaires sur les réactions. Plusieurs modèles de microcinétique pour des systèmes homogènes en phase gazeuse sont disponibles dans la

littérature pour les régimes de basse température (T < 600 K) (Buda et al. 2006), de température intermédiaire (650-1000K) (Marinov et al. 1998, Dagaut et al. 1987) et de température élevée (T > 1000 K) (Qin et al. 2000, Sung et al. 1998, San Diego Mechanism, Smith et al. 2010). Ainsi, la cinétique de combustion du propane subit une transition d'un mécanisme à faible température (T < 600 K) à un mécanisme à température intermédiaire (T > 650 K). Ces deux régimes sont séparés par une région à coefficient de température négatif (600 – 650 K). La production de flammes froides a été observée à température faible et intermédiaire. La création de flammes froides est associée à un changement d'agent de réaction radicalaire en chaîne des hydroperoxydes au peroxyde d'hydrogène (Ranzi et al. 1994, Wilk et al. 1986). Certains mécanismes de microcinétique ont été modifiés afin d'inclure les réactions de recombinaison des radicaux libres (Jeng et al. 2001, Sotudeh-Gharebagh et Chaouki 2003).

Un modèle de microcinétique a été utilisé par Hutchenson et al. (2010) afin de prédire la conversion d'oxygène dans la zone de désengagement d'un réacteur à lit fluidisé pilote (0.128 m I.D.) contenant un catalyseur de pyrophosphate de vanadium (VPP) pendant l'oxydation sélective de n-butane. Les conversions calculées ont été comparées aux résultats expérimentaux: les prédictions étaient significativement plus faibles que les valeurs mesurées. Deux explications ont été avancées par les auteurs:

1. Des réactions importantes en phase homogène et hétérogènes étaient manquantes dans le modèle de microcinétique
2. La production de radicaux libres dans la région du lit fluidisé de solides n'était pas considérée dans le modèle.

Toutefois, cette étude était basée sur une caractérisation limitée de la zone de désengagement: la température et la composition chimique de la phase gazeuse étaient mesurées uniquement à une position de telle sorte que la zone de désengagement était considérée parfaitement mélangée.

Le modèle de réaction doit être validé à l'aide de données expérimentales où les paramètres influençant la combustion dans la zone de désengagement sont mesurés précisément:

composition chimique de la phase gazeuse, la fraction de solides et la température. De plus, puisque ces paramètres sont dépendants l'un de l'autre, ils doivent être mesurées simultanément, ce qui représente un défi important.

1.3 CARACTÉRISATION DES SYSTÈMES MULTIPHASIQUES

La mesure simultanée de la fraction de solides et de la composition chimique de la phase gazeuse est importante afin de caractériser les lits fluidisés gaz/solides. Or elle l'est également pour plusieurs autres types de systèmes. Les procédés multiphasiques sont répandus dans plusieurs industries: pétrochimique, chimique, pharmaceutique, alimentaire, pâte et papier, etc. Ils sont également présents dans l'ensemble de la chaîne de production: génération d'énergie (chambres à combustion), les procédés de transformation (gazéifieurs, réacteurs chimiques, mélangeurs et sécheurs), les procédés de purification/séparation (cyclones et précipitateurs), l'évacuation de déchets (cheminés), etc. La caractérisation des ces systèmes par la mesure de la composition chimique et la fraction de solides est critique à des fins de contrôle, d'optimisation et de dépannage dans les laboratoires et les industries. Ces mesures sont également essentielles pour le développement de modèles hydrodynamiques (gaz/solide/liquide) et de cinétique de réaction. Présentement, la composition et la fraction de solides sont mesurées par deux techniques distinctes.

Plusieurs techniques invasives et non-invasives de mesures ont été développées afin de mesurer la fraction de solides dans les systèmes di- et tri-phasiques. Les techniques invasives nécessitent l'introduction d'une sonde pour mesurer localement la capacité (Werther et Molerus 1972, Yates et Simons 1994, Hage et Werther 1997), la conductivité (Begovich et Watson 1978, Uribe-Salas et Gomez 1994, Liu et al. 2007), la fluorescence (Huizenga et al. 1998) ou la diffusion d'un rayon lumineux dans le milieu (Yates et Simons 1994, Cutolo et al. 1990, Ishida et Tanaka 1982, Hu et al. 1986, Esmaeili et al. 2008). La fraction de solides est dérivée de la mesure qui peut être effectuée in situ et en temps réel. Dans les systèmes liquide/solide ou gaz/liquide/solide, la phase coulis peut être également échantillonnée par l'entremise de sondes spéciales afin de mesurer la fraction volumique de liquide et solide (Huizenga et al. 1998, Gandhi et al. 1999). Les techniques non-invasives incluent la tomographie (Chaouki et al. 1997, Pugsley et al. 2003, Marashdeh et al. 2008, Razzak et al. 2009), la densitométrie (Esmaeili et al. 2008) et l'analyse de

la distorsion d'ondes ultrasoniques (Uchida et al. 1989). Ces techniques produisent des cartes de fraction de solides moyennées dans le temps ou l'espace avec une résolution variable.

La mesure de la composition chimique dans les phases gazeuse, liquide et solide peut être effectuée en continu ou de manière intermittente (Gandhi et al. 1999) à l'aide d'instruments analytiques (chromatographe, spectromètre, etc) et peut nécessiter l'arrêt du procédé (Luypaert et al. 2007, Swarbrick 2007). L'échantillonnage peut présenter plusieurs désavantages: perte de production suite à un arrêt, perturbation du système en raison de l'introduction de la sonde (l'erreur de mesure peut être de l'ordre de 5% à 100%), destruction de l'échantillon et perte du produit (Luypaert et al. 2007, Swarbrick 2007). Dans le contexte du « process analytical technology » (PAT) de la « U.S. Food and Drug Administration » (FDA), plusieurs publications présentent le développement d'application en spectroscopie infrarouge permettant la mesure de la composition chimique dans les systèmes multiphasiques (Armaroli et al. 2004, Kondo et al. 2007). Des techniques similaires ont également été mises au point afin de caractériser les réactions se produisant à la surface de catalyseurs solides (Corveleyn et al. 1997, Rantanen et al. 2000a). Ces applications fonctionnent en mode transmission ou réflexion diffuse (à la surface des solides) et peuvent mesurer la composition chimiques dans la phase dispersée (particules solides et gouttelettes liquides) et la phase continue (liquide ou gazeuse) (Rantanen et al. 2000, Cogdill et al. 2005, Triadaphillou et al. 2007, Andersson et al. 1999, Kirsch et Drennen 1995). La spectroscopie infrarouge présente l'avantage d'effectuer des mesures in situ et en temps réel par l'entremise d'une sonde à fibres optiques.

Une technique de mesure permettant la mesure simultanée de la composition chimique et la fraction de solides présenterait de nombreux avantages. Premièrement, la mesure de ces deux paramètres nécessiterait un seul instrument comparativement à deux, ce qui réduirait potentiellement la complexité de la mesure et le coût des équipements. Deuxièmement, une telle méthode offrirait beaucoup plus d'information sur le procédé puisque la fraction de solides et la composition chimique sont dépendantes. En effet, ceux deux paramètres sont liés par la cinétique de réaction et l'hydrodynamique. Les particules solides influencent les réactions au moyen d'effets inhibitifs et/ou catalytiques et également par le biais du bilan calorifique. De plus, au

niveau de l'hydrodynamique, les systèmes multiphasiques sont souvent composés de différentes régions caractérisées par une fraction de solides distinctes. La mesure de la composition chimique dans ses régions est fondamentale à la description d'un procédé. Par exemple, les lits fluidisés gaz/solide à bulles et turbulents possèdent une phase dense (émulsion) et une phase diluée (bulle). Les bulles causent un court-circuit des réactifs qui réduit le rendement d'un procédé. La mesure simultanée de la fraction de solide et la composition chimique dans la phase gazeuse permettraient de déterminer la composition dans la phase dense et diluée. Ce type de mesure peut difficilement être effectué à l'aide des techniques existantes.

La spectroscopie infrarouge présente un potentiel important pour la mesure simultanée de fraction de solides et de la composition chimique de la phase gazeuse. Les applications de spectroscopie infrarouge actuelles sont affectées par la phase solide. La fraction de solides et la taille des particules affectent l'interaction entre la lumière et le système en influençant sur la longueur du trajet d'absorption et la taille d'échantillon (Corveleyn et al. 1997, Cogdill et al. 2005). En effet, une augmentation de la taille des particules diminue l'intensité de lumière diffuse et accroît le trajet d'absorption du rayon lumineux produisant une augmentation de l'absorbance et un déplacement de la ligne de base en mode réflexion diffuse (Cogdill et al. 2005). Conséquemment, les techniques actuelles de spectroscopie infrarouge utilisées dans les systèmes multiphasiques nécessitent que l'échantillon soit uniforme dans le temps (d'une mesure à l'autre). Ceci est réalisé concrètement en effectuant des mesures dans des systèmes immobiles comme les comprimés pharmaceutiques (Andersson et al. 1999, Kirsch et Drennen 1996, Abrahamsson et al. 2005, Hailey et al. 1996, Sonja Sekulic et al. 1998). Pour les systèmes multiphasiques où la phase solide est en mouvement (lits fluidisés et mélangeurs, par exemple), les mesures nécessitent un arrêt du procédé (Sonja Sekulic et al. 1996, Frake et al. 1997), la synchronisation de l'acquisition du spectre avec une position spécifique de la cuve (Bellamy et al. 2008) ou la mesure dans les régions de faible porosité (Cui et al. 2001). Des mesures de porosité ont également été effectuées dans des mélangeurs symétriques afin d'assurer l'uniformité de la fraction de solides une fois le système parfaitement mélangé (De Paepe et al. 1997). Finalement, le traitement mathématique des spectres mesurés est souvent utilisé afin de minimiser les effets du déplacement de la ligne de base causé par le mouvement des solides (Cogdill et al. 2005). Toutefois, les systèmes multiphasiques sont généralement

caractérisés par des fractions de solides qui varient dans le temps et l'espace. Par conséquent, la mesure in situ et en temps réel de la composition chimique dans les différentes régions du système nécessite la détermination simultanée de la fraction de solides. Le taille d'échantillon peut être indépendant des propriétés des particules si les fibres optiques émettrices et réceptrices sont inclinées l'une vers l'autre (Berntsson et al. 2001). Ce principe peut être utilisé sur une fibre optique infrarouge pour mesurer la composition chimique.

Dans les systèmes multiphasiques, le mouvement des particules solides rend les mesures spectroscopiques et leurs interprétations plus complexes. La mesure d'absorbance est influencée par les variations de fractions de solides et la distance moyenne entre l'échantillon et la sonde. Lorsque les échantillons sont en mouvement, les régions du spectre peuvent être influencées différemment par les hétérogénéités locales. L'effet du mouvement de particules sur la spectroscopie par transformée de Fourier a été étudié par De Paepe et al. (1997), Berntsson et al. (2001) and Andersson et al. (2005). Il a été démontré que le mouvement des solides produit du bruit dans le spectre mesuré à certains nombres d'ondes qui dépendent de l'échelle de temps du balayage spectral comparativement à la vitesse des particules. Le nombre d'onde auquel le bruit apparaît augmente en fonction de l'accroissement de la fréquence de modulation. Ainsi, l'effet des solides peut être complètement éliminé aux nombres d'ondes d'intérêts si la fréquence de modulation est suffisamment élevée.

CHAPITRE 2 PRÉSENTATION DES ÉTAPES DE TRAVAIL

Minimiser l'occurrence de réactions homogènes dans les régions de faibles fractions de solides nécessite une bonne capacité de modélisation des réactions dans le lit fluidisé afin d'y obtenir une conversion élevée et empêcher la formation d'une mixture inflammable dans la zone de désengagement.

Si des contraintes opératoires limitent la conversion qui peut être obtenue dans la région du lit fluidisé, il est essentiel de caractériser le risque d'auto-allumage dans la zone de désengagement en fonction des conditions qui y règnent: composition chimique de la phase gazeuse, profils de fraction de solides, température et pression.

La fraction de solides et la composition chimique de la phase gazeuse sont deux paramètres dépendants qui doivent être mesurés simultanément. Une telle mesure est critique pour la caractérisation de la zone de désengagement et des régions de faibles fractions de solides dans le lit fluidisé: les régions à proximité des injecteurs et la phase bulle. Or, une telle mesure est difficile avec les techniques actuellement disponibles.

Les objectifs spécifiques de cette thèse sont:

1. Étudier expérimentalement la combustion d'hydrocarbures dans un lit fluidisé de solides inertes afin d'identifer les paramètres de fluidization menant à une conversion complète et d'améliorer les moyens disponibles pour y modéliser les réactions.
2. Étudier l'auto-allumage de mixtures hydrocarbure/air dans la zone de désengagement et tenter de modéliser les réactions avec une microcinétique afin de reproduire le temps d'induction et le taux de réaction.
3. Développer une nouvelle méthode pour mesurer simultanément la fraction de solides et la composition chimique de la phase gazeuse. Cette méthode devrait permettre d'effectuer des mesures en ligne et in situ dans des systèmes multiphasiques.

Afin de répondre à ces objectifs, le chapitre 4 décrit une étude expérimentale sur la combustion des alcanes C_1-C_4 dans un lit fluidisé de particules inertes. Les températures nécessaires à la conversion complète des alcanes C_1-C_4 dans la région du lit fluidisé (températures critiques de transition) sont mesurées. De plus, une cinétique de réaction globale et de premier ordre est mesurée pour chacun des alcanes. Finalement, un modèle pour prédire la conversion dans la région de l'injecteur et la région du lit fluidisé est proposé.

Le chapitre 5 présente une étude sur la combustion du propane dans la zone désengagement d'un lit fluidisé. Le temps d'induction et le taux de réaction du propane sont modélisés avec plusieurs modèles de microcinétique de combustion homogène en phase gazeuse.

Le chapitre 6 relate le développement d'une nouvelle méthode de spectroscopie infrarouge qui permet la mesure simultanée de la fraction de solides et de la composition chimique dans la phase gazeuse. La méthode est utilisée avec une sonde à fibres optiques infrarouges afin d'effectuer des mesures in situ et en ligne dans des systèmes gaz/solides. Des mesures sont effectuées dans un lit fluidisé afin de mesurer la fraction volumétrique d'un traceur gazeux dans la phase bulle et la phase émulsion.

Le chapitre 3 présente la méthodologie pour effectuer ces travaux.

CHAPITRE 3 MÉTHODOLOGIE

Ce chapitre présente la méthodologie suivie pour effectuer les expériences et la modélisation.

3.1 EXPÉRIENCES DE COMBUSTION EN LIT FLUIDISÉ

Les expériences sur la combustion en lit fluidisé des alcanes C_1-C_4 ont été effectuées sur le réacteur à lit fluidisé de la Figure 2-1. La région du lit fluidisé de solides avait un diamètre interne de 0.2 m et une hauteur d'environ 1.0 m. Des particules inertes de sables de silice (Geldart B, ρ_s = 2650 kg/m^3, d_p = 290 μm et U_{mf} = 0.08 m/s) ont été utilisées dans le lit. Le lit de particules était fluidisé avec de l'air injecté par le distributeur et l'hydrocarbure (méthane, éthane, propane ou n-butane) était acheminé séparément par un injecteur orienté vers le bas (4.1 mm D.I.). L'extrémité de cet injecteur se trouvait à une distance de 0.1 m au-dessus du distributeur. Avant chaque expérience, le réacteur à lit fluidisé était chauffé à la température désirée par l'entremise d'un brûleur de gaz naturel connecté à la boîte à vent. De l'huile lourde était également brûlée dans le lit afin d'accélérer le processus de chauffage. Une fois la température du lit atteinte, l'injection d'huile lourde et de gaz naturel était arrêtée et le lit fluidisé était chauffé avec du propane pendant au moins une heure afin de brûler tous les résidus d'huile lourde.

Les expériences ont été effectuées à une vitesse superficielle de gaz de 0.4 m/s et cinq températures de lit : 923 K, 973 K, 1023 K, 1073 K et 1123 K. La température à l'intérieur du réacteur était mesurée à neuf positions axiales différentes à l'aide de thermocouples. Le gaz était échantillonné à six positions axiales où une mesure était effectuée à cinq positions radiales. Le gaz échantillonné était ensuite analysé par un analyseur Ultramat™ de Siemens (CO/CO_2) et un micro-chromatographe en phase gazeuse CP-4900™ de Varian afin de mesurer la fraction volumétrique des espèces chimiques suivantes: H_2, CH_4, C_2H_4, C_2H_6, C_3H_8, n-C_4H_{10}, O_2, N_2, CO et CO_2. Pour chaque position axiale, une moyenne de la composition chimique était calculée sur la surface.

Du gaz était également échantillonné dans la section de désengagement afin de mesurer la fraction volumétrique d'oxygène à l'aide d'un Oxymat™ de Siemens. Lors des expériences, le débit de la mixture d'hydrocarbure était ajusté afin d'obtenir un débit calorifique constant de

3.8 kW (calculé à partir du pouvoir calorifique inférieur). Pour le méthane, l'éthane, le propane et le n-butane, les fractions volumétriques correspondantes à l'extrémité de l'injecteur étaient respectivement de 5.1%, 2.5%, 1.9% et 1.3%. Ceci correspondait à des vitesses d'injection de 52 m/s, 25 m/s, 18 m/s et 13 m/s pour le méthane, l'éthane, le propane et le n-butane, respectivement.

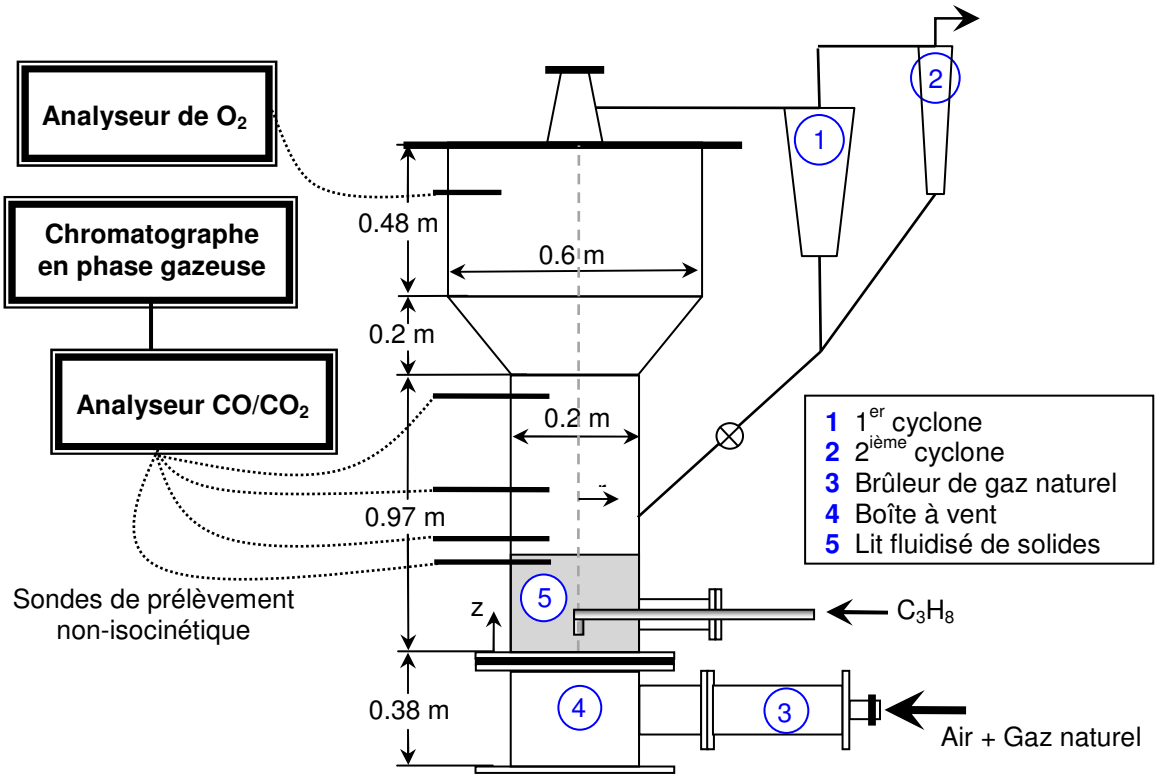

Figure 3-1: Réacteur à lit fluidisé

3.2 EXPÉRIENCES DE COMBUSTION DANS LA ZONE DE DÉSENGAGEMENT

Les expériences sur la combustion du propane dans la zone de désengagement ont été effectuées dans le même réacteur à lit fluidisé (figure 3-1) avec les mêmes particules inertes de sables de silice. La zone de désengagement était caractérisée par un diamètre interne de 0.2 m. Le propane était injecté séparément au moyen de l'injecteur orienté vers le bas. Pour toutes les expériences, une vitesse superficielle de 0.17 m/s ($U_g = 2.1\ U_{mf}$) et de faibles températures de lit

($818\ K \leq T_B \leq 923\ K$) ont été utilisées. La surface du lit fluidisé de solides et la zone de désengagement ont été caractérisées via la mesure simultanée du flux d'entraînement de particules, de la composition chimique de la phase gazeuse et de la température.

Les particules solides et le gaz étaient échantillonnés au moyen d'une sonde de prélèvement non-isocinétique similaire à celles décrites par Rhodes et Laussmann (1992), Reinhardt et al. (1999) et Van der Meer et al. (2000). Le flux de solides était déduit de la masse de solide récupérée:

$$G_{SU,D} = \frac{m_S}{A\ t}$$

De plus, la composition chimique du gaz était déterminée avec un chromatographe en phase gazeuse CP-4900™ de Varian et un Ultramat™ de Siemens. La figure 3-2 illustre le système d'échantillonnage. La température dans le réacteur était mesurée par 10 thermocouples positionnés sur la longueur du réacteur. Plus d'informations sur la sonde à prélèvement non-isocinétique et les techniques utilisées afin de mesurer simultanément le flux de solides, la composition chimique de la phase gazeuse et la température sont disponibles dans l'annexe 2.

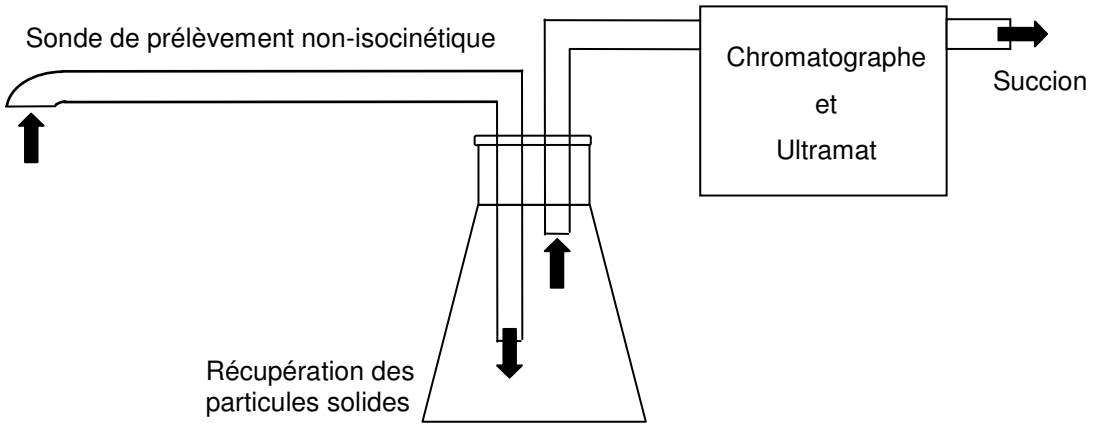

Figure 3-2: Mesure simultanée des particules et de la composition chimique du gaz

3.3 MODÉLISATION DE LA COMBUSTION EN LIT FLUIDISÉ

L'hydrodynamique de la phase gazeuse dans le lit fluidisé a été représentée à l'aide d'un modèle composé de deux réacteurs pistons en séries. De plus, une cinétique de réaction globale de premier ordre a été utilisée. Ces choix se justifient tel que mentionné dans la revue de littérature, car ils permettent de représenter de façon appropriée l'hydrodynamique de la phase gazeuse dans un lit fluidisé de faible vitesse superficielle et une combustion pauvre (Lorences et al. (2006), Laviolette et al. (2010)).

Le lit fluidisé a été séparé en deux zones distinctes:

1. La région de l'injecteur caractérisée par un taux de mélange gaz/gaz et gaz/solide élevé
2. Le lit fluidisé

Ces deux régions ont été modélisées par un réacteur piston (lit fluidisé) avec un décalage d'axe (effet de la conversion à l'injecteur) de sorte que la conversion de l'hydrocarbure était calculée par les équations suivantes :

$$X_i = X_{i,\,Injector} + X_{i,\,Fluidized\ Bed} \tag{3.1}$$

$$X_i = 100\left(1 - e^{-k'\left(Z_j + b_i\right)}\right) \tag{3.2}$$

$$k' = \frac{A k_0}{v} e^{-E_A/RT} = k_0' e^{-E_A/RT} \tag{3.3}$$

Le paramètre Z_j correspond à la position où le mélange entre l'air et l'hydrocarbure survient dans le lit fluidisé et où les réactions d'oxydation débutent. Afin d'évaluer Z_j pour une combustion par des injections séparées, le jet à l'extrémité de l'injecteur a été caractérisé par la profondeur de pénétration calculée au moyen de six corrélations différentes (Zenz 1968, Benjelloun et al. 1995, Shen et al. 1990, Shakhova 1968, Merry 1971, Hong et al. 1997, Okhotskii 2001, Penyazkov 2005).

3.4 MODÉLISATION DE LA COMBUTION DANS LA ZONE DE DÉSENGAGEMENT

Afin de représenter la combustion dans la zone de désengagement d'un lit fluidisé, un modèle utilisant une microcinétique de réaction en phases gazeuses a été développé. Tel que mentionné dans la revue de littérature, la cinétique de combustion du propane subit une transition d'un mécanisme à faible température ($T < 600$ K) à un mécanisme à température intermédiaire ($T > 650$ K). Ces deux régimes sont séparés par une région à coefficient de température négatif (600 – 650 K). La production de flammes froides a été observée à température faible et intermédiaire. La création de flammes froide est associée à un changement d'agent principal de réaction radicalaire en chaîne des hydroperoxydes au peroxyde d'hydrogène (Ranzi et al. 1994, Wilk et al. 1986).

Les expériences effectuées lors de cette recherche utilisaient des températures intermédiaires où la réaction radicalaire principale serait la dissociation du peroxyde d'hydrogène en deux radicaux d'hydroxyle (Ranzi et al. 1994, Wilk et al. 1986). Afin de modéliser le cinétique de combustion, six mécanismes de microcinétique bien établis dans la littérature scientifique ont été utilisés et comparés: le mécanisme de Dagaut et al. (1987), Marinov et al. (1998), San Diego (2010), GRI version 3 (2010), Sung et al. (1998) et Qin et al. (2000).

Le modèle de Dagaut et al. (1987) (50 espèces chimiques et 274 réactions élémentaires) a été validé au moyen de résultats expérimentaux obtenus dans un réacteur auto-agité par jets gazeux pour un large spectre de coefficients d'équivalence (0.15-4) et de températures (900-1200 K). Le modèle de Marinov et al. (1998) (126 espèces chimiques et 638 réactions élémentaires) a démontré une bonne concordance avec des résultats expérimentaux d'oxydation de NO et d'hydrocarbures dans un réacteur piston atmosphérique et une plage de températures de 600 à 1100 K. Ce mécanisme inclut la cinétique de combustion de l'hydrogène, le méthane, l'éthylène, l'éthane, le propane et l'éthanol. Le mécanisme de San Diego (2010) (46 espèces chimiques et 235 réactions élémentaires), la troisième version du mécanisme GRI (2010) (53 espèces chimiques et 325 réactions élémentaires), le mécanisme de Sung et al. (1998) (92 espèces

chimiques et 621 réactions élémentaires) et le modèle de Qin et al. (2000) (70 espèces chimiques et 463 réactions élémentaires) ont également été utilisés. Ces quatre modèles ont été comparés à des résultats expérimentaux (temps d'induction, vitesses de flamme et gradients axiaux d'espèces chimiques) obtenus à des températures supérieures à celles utilisées lors des expériences de cette thèse. Toutefois, ces mécanismes contiennent les réactions élémentaires pour décrire la combustion à températures faibles et intermédiaires.

L'hydrodynamique de la phase gazeuse dans la zone de désengagement a été modélisée au moyen d'un réacteur piston. Les profils de température mesurés expérimentalement en régime permanent on été utilisés dans le modèle réactionnel et les équations ont été résolues à l'aide du logiciel ChemKin 4.1. Les mécanismes de microcinétique ne tenaient pas compte des réactions en phase hétérogène qui auraient pu avoir lieu à la surface des particules solides.

Deux séries de simulations ont été effectuées. Dans la première série, la zone de désengagement a été modélisée par un réacteur piston. La composition chimique de la phase gazeuse a, quant à elle, été mesurée à la surface du lit fluidisé et a été utilisée comme condition frontière. Dans la seconde série de simulations, un second réacteur piston a été ajouté, en amont, afin de simuler les réactions ayant lieu dans la région du lit fluidisé de solides et la production d'agents de réaction radicalaire. La composition chimique parfaitement mélangée à l'extrémité de l'injecteur a été utilisée en tant que condition frontière à l'entrée du réacteur piston simulant le lit fluidisé de solides. De plus, le temps de résidence moyen du gaz a été ajusté individuellement afin d'obtenir la conversion adéquate dans le lit fluidisé. La mixture, à la sortie du premier réacteur piston, (lit fluidisé) était ensuite injectée à l'entrée du second (zone de désengagement).

3.5 DÉVELOPMENT D'UNE MÉTHODE POUR LA MESURE SIMULTANÉE DE LA FRACTION DE SOLIDES ET DE LA COMPOSITION CHIMIQUE DE LA PHASE GAZEUSE

Des expériences ont été effectuées avec un FT-IR (modèle Excalibur 3100™ de Varian) équipé d'un détecteur à haute sensibilité tellurure de mercure-cadmium (TMC) refroidi à l'azote liquide. Dans une première série de tests, le FT-IR a été utilisé avec une cellule de mesure placée dans un

compartiment à échantillons tel qu'illustré dans la Figure 3-3. Le rayon infrarouge venant de l'interféromètre était transmis à travers la cellule de mesure. Le spectre d'absorbance résultant était mesuré par le détecteur TMC. Avant chaque expérience, le signal de fond était mesuré en purgeant la cellule de mesure avec de l'air et en prenant la moyenne de 20 spectres. Ensuite, un système gaz/solide était simulé dans la cellule de mesure en injectant une mixture de 1.8 vol% C_3H_8 + 98.2 vol% air et en plaçant une toile métallique dans la trajectoire du rayon infrarouge incident (épaisseur de 1 mm et 16% de surface ouverte).

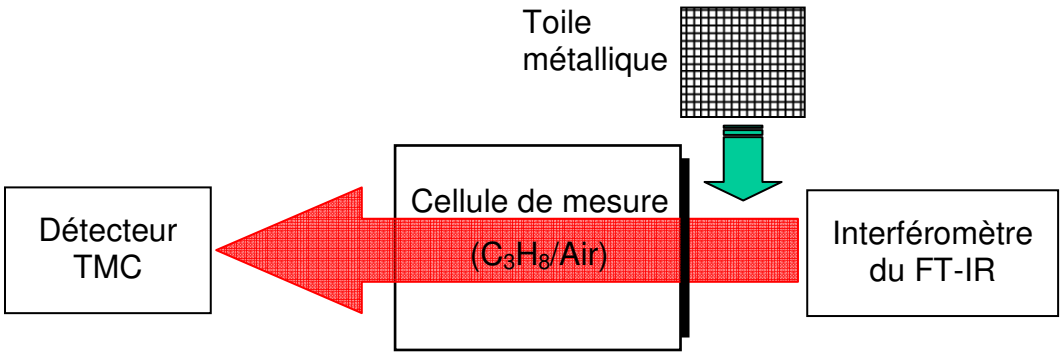

Figure 3-3: Spectromètre FT-IR

Une seconde série d'expériences a été réalisée avec une sonde à fibres-optiques pour l'infrarouge moyen. Des mesures in-situ de composition chimique gazeuse et de fraction volumétrique de solides ont été accomplies à l'intérieur d'un écoulement gaz/solide de CH_4/N_2 et de particules de sable de silice (d_p = 290 µm). Une illustration de l'appareil expérimental est présentée dans la Figure 3-4. La sonde était composée de deux fibres-optiques de silice fluorée (une fibre émettrice et une fibre réceptrice) avec une ouverture numérique de 0.2 et un diamètre de cœur de 600 µm. La sonde à fibres-optiques était connectée au FT-IR au moyen d'un Fibremate™ de la compagnie Harrick. Un miroir plan plaqué d'or était positionné perpendiculairement à une distance de 5 mm de l'extrémité de la sonde. Le miroir réfléchissait le rayon IR incident vers la fibre-optique réceptrice, ce qui produisait un volume de mesure entre la sonde et le miroir tel que coloré en gris dans la figure 3-4. Les expériences ont été effectuées en premier lieu par la mesure du signal de fond – une mixture de CH_4/N_2 était injectée dans le volume de mesure et un spectre de fond, constitué de la moyenne de 20 spectres individuels, était mesuré. Ensuite, le volume de mesure

était purgé avec de l'air tandis que l'entonnoir était rempli de particules de sable afin d'initier un écoulement de solides. Les spectres d'absorbance ont été enregistrés à une fréquence de 4.5 Hz (résolution temporelle de 0.22 s) et la fraction molaire de méthane a été mesurée simultanément à la fraction de solides. Le taux d'écoulement de particules solides a été varié en modifiant le diamètre de la gorge de l'entonnoir. La fraction de solides correspondante à chacune des diamètres de gorge ont ensuite été mesurée au moyen d'une sonde à fibre-optique conventionnelle. Quatre différentes fractions de solides ont été utilisées: 0, 0.015, 0.038 et 0.097. De plus, quatre mixtures différentes de CH_4/N_2 ont été injectées à partir de cylindres de gaz calibrés. Ces mixtures étaient caractérisées par des fractions volumétriques de méthane de 0, 0.1, 3.25 et 10.1 vol% dans l'air ou l'azote.

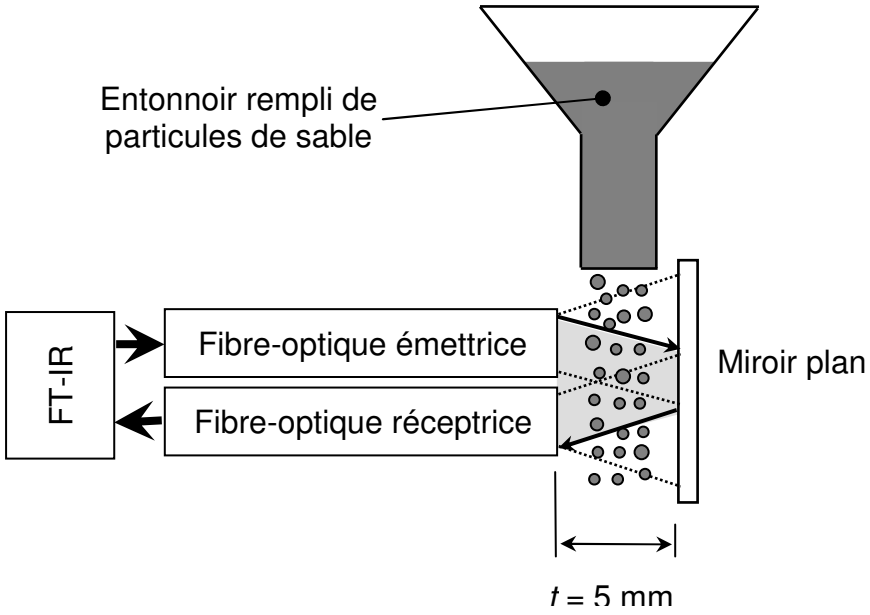

Figure 3-4: Appareil expérimental avec sonde à fibres-optiques infrarouges

Des expériences de traceur gazeux ont également été effectuées dans le petit réacteur à lit fluidisé (5 cm D.I.) illustré dans la figure 3-5. La sonde à fibres-optiques a été utilisée afin de mesurer la fraction volumétrique de traceur dans les phases bulle et émulsion. Le lit de solides était composé de particules FCC ($U_{mf} = 2.5$ mm/s and $U_{mb} = 2.7$ mm/s, $d_p = 83$ μm et 14% de fines ($d_p \leq 44$ μm)) et il était fluidisé avec un écoulement d'azote d'une vitesse de 2.6 mm/s. Le lit

fluidisé en expansion avait une hauteur de 12.5 cm et la sonde à fibre-optique était insérée dans le lit à une hauteur de 7 cm au-dessus du distributeur. Un miroir était positionné perpendiculairement à l'extrémité de la sonde. Les bulles de gaz étaient produites dans le volume de mesure de la sonde à fibres-optiques en injectant une mixture de 10.1 % CH_4 + 89.9% N_2 au moyen d'un injecteur orienté vers le bas. La mixture de CH_4/N_2 était injectée avec un débit de 10 mL/s par l'ouverture manuelle d'une valve pendant approximativement 0.5 s et à un intervalle d'environ 11 secondes.

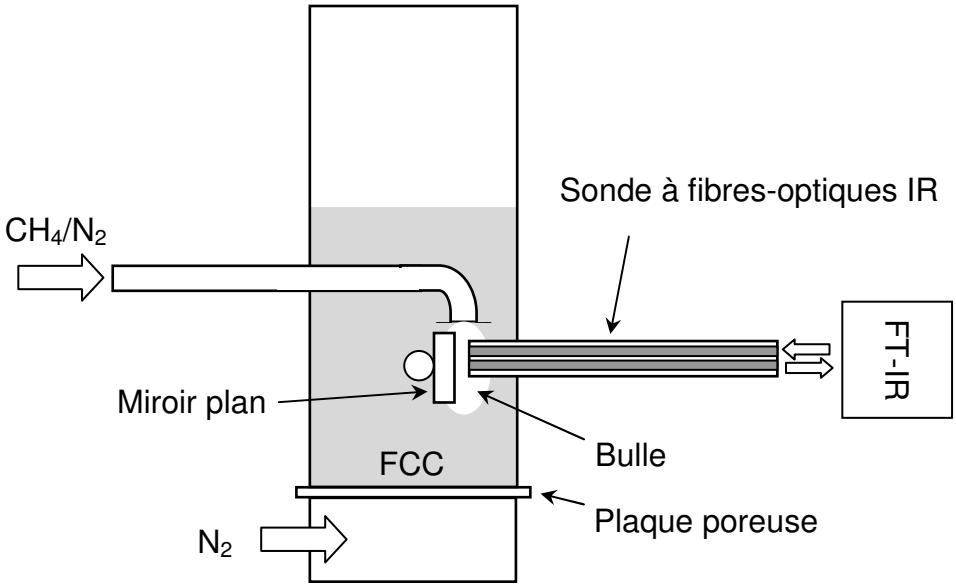

Figure 3-5: Réacteur à lit fluidisé

CHAPITRE 4 COMBUSTION EN LIT FLUIDISÉ DES N-ALKANES C1-C4

Cet article a été soumis au journal *Fuel*.

4.1 PRÉSENTATION DE L'ARTICLE

L'objectif de cet article est d'étudier la combustion des n-alcanes C_1-C_4 dans un lit fluidisé de solides inertes. Les températures nécessaires à la conversion complète des alcanes C_1-C_4 dans la région du lit fluidisé (températures critiques de transition) ont été mesurées. De plus, une cinétique de réaction globale et de premier ordre est mesurée pour chacun des alcanes. Finalement, un pour prédire la conversion dans la région de l'injecteur et la région du lit fluidisé sont proposés.

Les résultats mettent en évidence des similitudes entre la combustion des n-alcanes C_2-C_4: ils sont caractérisés par les mêmes températures critiques de transitions T_1 (température du lit fluidisé en-dessous de laquelle la combustion se produit essentiellement dans la zone de désengagement) et T_2 (température du lit fluidisé au-delà de laquelle la combustion se produit entièrement au niveau du distributeur). De plus, la cinétique des n-alcanes C_2-C_4 peut être décrite par une seule expression de type Arrhénius. Dans le cas du méthane, les taux de combustion observés sont significativement plus lent de sorte que les températures critiques de transition sont plus élevées et la cinétique de combustion plus lente.

L'article propose deux modèles réacteur piston en séries afin de prédire la conversion dans le lit fluidisé: un modèle pour la région de l'injecteur et un modèle pour le lit fluidisé. Les résultats démontrent qu'une hausse de la température du lit augmente la conversion au niveau de l'injecteur, tandis qu'une élévation de la vitesse d'injection décroît la conversion. La conversion à proximité de l'injecteur est modélisée par un réacteur piston dont la longueur est corrélée à la température par une expression de type Arrhénius, de façon similaire au temps d'induction d'une mixture inflammable homogène. L'effet inhibiteur de la vitesse d'injection est également inclus dans cette corrélation.

FLUIDIZED BED COMBUSTION OF C_1-C_4 N-ALKANES

Jean-Philippe Laviolette, Gregory S. Patience, Jamal Chaouki

(Soumis à Fuel, 2010)

4.2 FLUIDIZED BED COMBUSTION OF C1-C4 N-ALKANES

4.2.1 Abstract

The non-premixed combustion of C_1 to C_4 n-alkanes with air was investigated inside a bubbling fluidized bed of inert sand particles at intermediate temperatures: $923\ K \leq T_B \leq 1123\ K$. For ethane, propane and n-butane, combustion occurred mainly in the freeboard region at bed temperatures below $T_1 = 923$ K. On the other hand, complete conversion occurred within 0.2 m of the injector at: $T_2 = 1073$ K. For methane, the measured values of T_1 and T_2 were significantly higher at 1023 K and above 1123 K, respectively. The fluidized bed combustion was accurately modeled with first-order global kinetics and two one-phase PFR models in series: one PFR to model the region close to the injector and another to represent the main fluidized bed body. The measured global reaction rates for C_2 to C_4 n-alkanes were characterized by a uniform Arrhenius expression, while the global reaction rate for methane was significantly slower. Reactions in the injector region either led to significant conversion in that zone or an autoignition delay inside the main fluidized bed body. The conversion in the injector region increased with rising fluidized bed temperature and decreased with increasing jet velocity. To account for the promoting and inhibiting effects, an analogy was made with the concept of induction time: the PFR length (b_i) of the injector region was correlated to the fluidized bed temperature and jet velocity using an Arrhenius expression.

Keywords: combustion, fluidized bed, methane, propane, ethane, n-butane and non-premixed

4.2.2 Introduction

In the context of increasingly more severe environmental regulations due to global warming, new fluidized bed processes are currently under development to produce energy and chemical products from biomass and natural gas feedstocks. Combustion is inherent to many of these processes, which include selective oxidation of alkanes, biomass gasification, combustion of non-conventional feedstocks (biomass and co-firing) and many more. Combustion may involve many hydrocarbons present in the feedstock or produced from thermal cracking during the reaction. A good knowledge of the combustion process and the operating conditions necessary for complete combustion in the fluidized bed region is essential for process design and safety during operation, startup and shutdown.

The combustion of methane, LPG and propane in fluidized beds of inert particles has been the subject of several studies in premixed [1-10] and non-premixed modes [11-16]. Fluidized bed temperature has been reported as a key parameter that determines in-bed fuel conversion: the combustion front moves towards the distributor as the fluidized bed temperature is increased. At low fluidized bed temperature, the combustion is first initiated in the freeboard region. Increasing the temperature moves the combustion front to the bubbles bursting at the upper surface of the bed, then to bubbles igniting in the bed and finally to small bubbles where ignition occurs practically at the level of the distributor and the process appears flameless [7, 9]. While some studies have suggested that combustion occurs predominantly inside the bubble phase as opposed to the emulsion phase [9], methane and propane combustion have been reported in fixed beds of sand particles at temperatures above 1023 K and 973 K, respectively [1, 17].

Two critical transition temperatures have been defined for fluidized bed combustion in inert particles. Below the lower critical temperature (T_1), combustion only occurs above the bed surface. Between T_1 and the upper critical temperature (T_2), combustion begins to move inside the bubbles within the bed. Finally, above T_2, combustion takes place entirely within the bed and close to the distributor. For methane combustion in inert sand particles, the values of T_1 and T_2 reported in the literature range between 823-1018 K and 1133-1250 K, respectively [18]. For

propane, T_2 was measured in a shallow bed ($H_B \approx 0.1$ m) of sand particles as 1123 K [2, 9]. Investigations on the fluidized bed combustion of other alkanes in inert particles are scarce.

Fluidized bed combustion can be estimated from a reaction model that combines the gas/solids hydrodynamics and the reaction kinetics. Several gas-phase hydrodynamics models of varying complexity have been proposed in the literature [18]. Hydrocarbon conversion in fluidized beds has been shown to vary from plug flow to back-mixed flow depending on the fluidization conditions and the reaction. A recent gas tracer study by Lorences et al. [19] showed that the gas-phase hydrodynamics is very close to plug flow when $U_g \leq 6\ U_{mf}$.

The mass transfer rate at the distributor is greater than inside the fluidized bed main body [18]. For fast reactions, such as combustion, significant conversion can occur in the injector tip surroundings. Therefore, the region near the injector and the main fluidized bed body require two different gas-phase hydrodynamic models. For a downward-facing sparger, counterflow ignition studies should yield some insights into the parameters affecting conversion at the injector tip [20-22]. These studies show that the ignitability and conversion decreases with decreasing temperature and increasing strain rate (counterflow gas velocities). The latter can be explained by the fact that the ignition of hydrocarbons involves intermediate species whose lifetimes may be similar to the characteristic time scales of mass and heat transfer. To characterize the injector region, one-phase and two-phase models have been proposed in the literature [18].

Several microkinetic and first-order global kinetics schemes are available in the literature for gas-phase systems [5, 6, 23]. Gas-phase microkinetic models have also been modified to account for the "quenching" effect of solids particles on the free radicals [17, 24]. Microkinetic reaction networks are complex but essential to simulate the production of intermediate species. However, in fuel lean conditions, the parent hydrocarbon conversion inside a fluidized bed has been shown to be accurately represented by a first order reaction [17, 25, 26]. Global gas-phase kinetics have been proposed for methane, but they are scarce in the literature for ethane and higher alkanes (C_2+) [23].

It may be possible to express the first-order kinetics or conversion of C_2+ alkanes in terms of a single expression or correlation. Studies have reported similarities between the combustion chemistry of n-alkanes: their combustion rate is controlled by the same main chain branching path, which can be summarized by the following elementary reactions at intermediate temperatures (~ 850 K to 1200 K) [27-30]:

$$H + O_2 + M \rightarrow HO_2 + M \quad (1)$$

$$RH + HO_2 \rightarrow R + H_2O_2 \quad (2)$$

$$H_2O_2 + M \rightarrow OH + OH + M \quad (3)$$

In the above equations, RH is an alkane, R is an alkyl radical and M is a third body. Saxena *et al*. [29] have demonstrated that the high temperature induction time of propane and higher alkanes can be accurately estimated by employing rate parameters of elementary steps (2) to (4).

$$HO_2 + HO_2 \rightarrow H_2O_2 + O_2 \quad (4)$$

In fact, the induction time of C_2-C_5 n-alkanes measured in shock tubes shows a similar dependence on temperature, pressure and mixture composition such that it may be calculated from a single correlation with an uniform activation energy [27-28]. The previous studies show that at a similar stoichiometry, temperature and pressure, the induction time decreases as C_2H_6 < n-C_4H_{10} < C_3H_8 [27, 28, 31]. Methane, on the other hand, has been observed to yield significantly higher induction times, which can be explained by the production of a methyl radical in equation (2), which recombines to form ethane, resulting in chain termination. If the combustion chemistry and induction time correlations among C_2+ n-alkanes show such similarities, a parallel may also be made between their global reaction kinetics and conversion.

In the present study, the non-premixed combustion of methane, ethane, propane and n-butane was studied in a fluidized bed of sand particles at temperatures ranging from 923 K to 1123 K. The flow of each hydrocarbon was adjusted to obtain a constant heat release rate. Lower and upper critical bed temperatures (T_1 and T_2) were measured for each hydrocarbon. Furthermore, a simple

reaction model with first-order reaction kinetics was developed and compared to the experimental results. The first-order kinetic parameters were measured for each n-alkane and compared.

4.2.3 Experimental

The experiments were performed in the fluidized bed reactor shown in Figure 4.1. The region of the fluidized bed of solids had an inner diameter of 0.2 m and a height of approximately 1.0 m. Inert sand particles (d_p = 290 μm and U_{mf} = 0.08 m/s) were used as the bed material. The bed was fluidized with air, injected through the distributor, and the hydrocarbon fuels (methane, ethane, propane and n-butane) were injected through a downward-facing sparger with the tip located at a distance of 0.1 m above the distributor. Prior to each experiment, the fluidized bed reactor was heated to the desired temperature with a natural gas burner connected to the windbox. Heavy vacuum gas oil (HVGO) was also injected through the sparger to accelerate the heating process. Once the bed temperature had reached the desired value, the HVGO injection and the natural gas burner were stopped and the fluidized bed was heated for about 1 hour with propane to burn any HVGO residues.

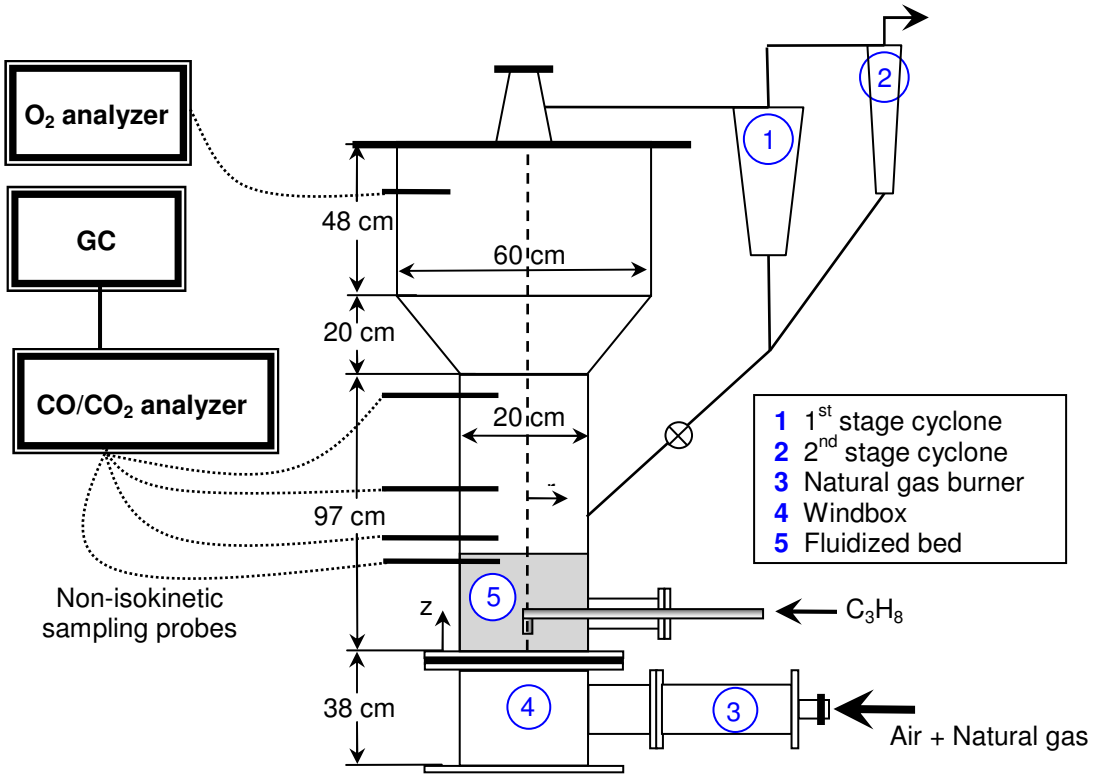

Figure 4-1: Fluidized bed reactor

The experiments were conducted at a superficial gas velocity of 0.4 m/s and at five bed temperatures: 923 K, 973 K, 1023 K, 1073 K and 1123 K. The temperature was measured at 9 different axial positions with thermocouples. Gas was sampled at six axial and five radial positions. The sampled gas was analyzed by a Siemens Ultramat™ CO/CO_2 analyzer and a Varian CP-4900™ micro-GC connected in series to measure the volume fraction of the following species: H_2, CH_4, C_2H_4, C_2H_6, C_3H_8, n-C_4H_{10}, O_2, N_2, CO and CO_2. At each axial position, a cross-sectional average (surface area weighted) of species volume fraction was calculated. Gas was also sampled in the disengagement region and the oxygen volume fraction was recorded by an oxygen analyzer. The mixed-cup volume fraction at the injector tip was adjusted for each hydrocarbon to obtain a heat release rate of 3.8 kW (calculated from the lower heating value). For methane, ethane, propane and n-butane, the corresponding mixed-cup volume fractions were 5.1%, 2.5%, 1.9% and 1.3%, respectively.

4.2.4 Results and discussion

4.2.4.1 Critical transition fluidized bed temperatures

Lower (T_1) and upper (T_2) critical transition bed temperatures were measured for methane, ethane, propane and n-butane.

4.2.4.2 Ethane, propane and n-butane

Figure 4.2a shows the axial profile of conversion for ethane, propane and n-butane inside the fluidized bed reactor at a bed temperature of 923 K. The corresponding axial profile of CO_2 volume fraction is presented in Figure 4.2b. The expanded bed height was 0.55 m and it is shown on both figures as a dashed line. At 923 K, ethane, propane and n-butane conversion was insignificant inside the fluidized bed: conversion fluctuated between 0-4%, 0-18% and 10-27% for ethane, propane and n-butane, respectively. Furthermore, the CO_2 volume fractions in the fluidized bed remained low at approximately 0.7%. Combustion occurred mainly at the bed surface and inside the freeboard as conversion reached 92%, 93% and 96% at 0.2 m above the

bed surface (Z = 0.75 m) for ethane, propane and n-butane, respectively. This was accompanied by a significant increased in the CO_2 volume fraction, which reached approximately 5.5% for all alkanes. Complete conversion was obtained at Z = 0.97 m.

As the bed temperature was increased to 973 K, the combustion front moved upstream inside the fluidized bed for ethane, propane and n-butane. Figures 4.2c and 4.2d show the axial profile of conversion and CO_2: combustion was initiated within 0.15 m (Z = 0.25 m) of the injector tip where conversion was 24%, 57% and 61% for ethane, propane and n-butane, respectively. Conversion increased with height in the fluidized bed and reached 60%, 79% and 84% at 0.1 m below the bed surface (Z = 0.46 m) for ethane, propane and n-butane. The unconverted hydrocarbons burned inside the freeboard region and complete conversion was observed at 0.2 m above the bed surface (Z = 0.75 m). The combustion in the fluidized bed and freeboard regions was accompanied by a corresponding increase in the CO_2 volume fraction, which reached approximately 3.8% at 0.1 m below the fluidized bed surface (Z = 0.46 m) and 6.0% in the freeboard region at Z = 0.75 m (complete combustion).

Figures 4.2(e) and 4.2(f) show the axial profile of CO_2 and conversion for the three n-alkanes as the bed temperature was increased further to 1023 K. Near complete fuel conversion occurred in the fluidized bed as conversion reached 95%, 95% and 98% for ethane, propane and n-butane, respectively, only 0.36 m (Z = 0.46 m) downstream of the injector. At that position, the CO_2 volume fraction reached about 6.0%, which indicated that complete combustion was nearly achieved. Complete conversion was observed 0.2 m over the bed surface (Z = 0.75 m). Rising the bed temperature by 50 K to 1073 K resulted in 99% conversion within 0.25 m of the sparger tip (Z = 0.35 m) for all three alkanes.

These results demonstrate that the fluidized bed combustion of the C_2-C_4 alkanes is characterized by similar critical bed temperatures. At a bed temperature of 923 K, combustion occurred primarily in the freeboard region for C_2 to C_4 n-alkanes: this was defined as the lower critical temperature (T_1). Furthermore, complete combustion occurred in the fluidized bed region and within 0.25 m of the sparger tip at 1073 K, which was defined as the upper critical temperature

(T_2). This is indicative of similar temperature dependence for C_2 to C_4 n-alkane fluidized bed combustion and similar global activation energies.

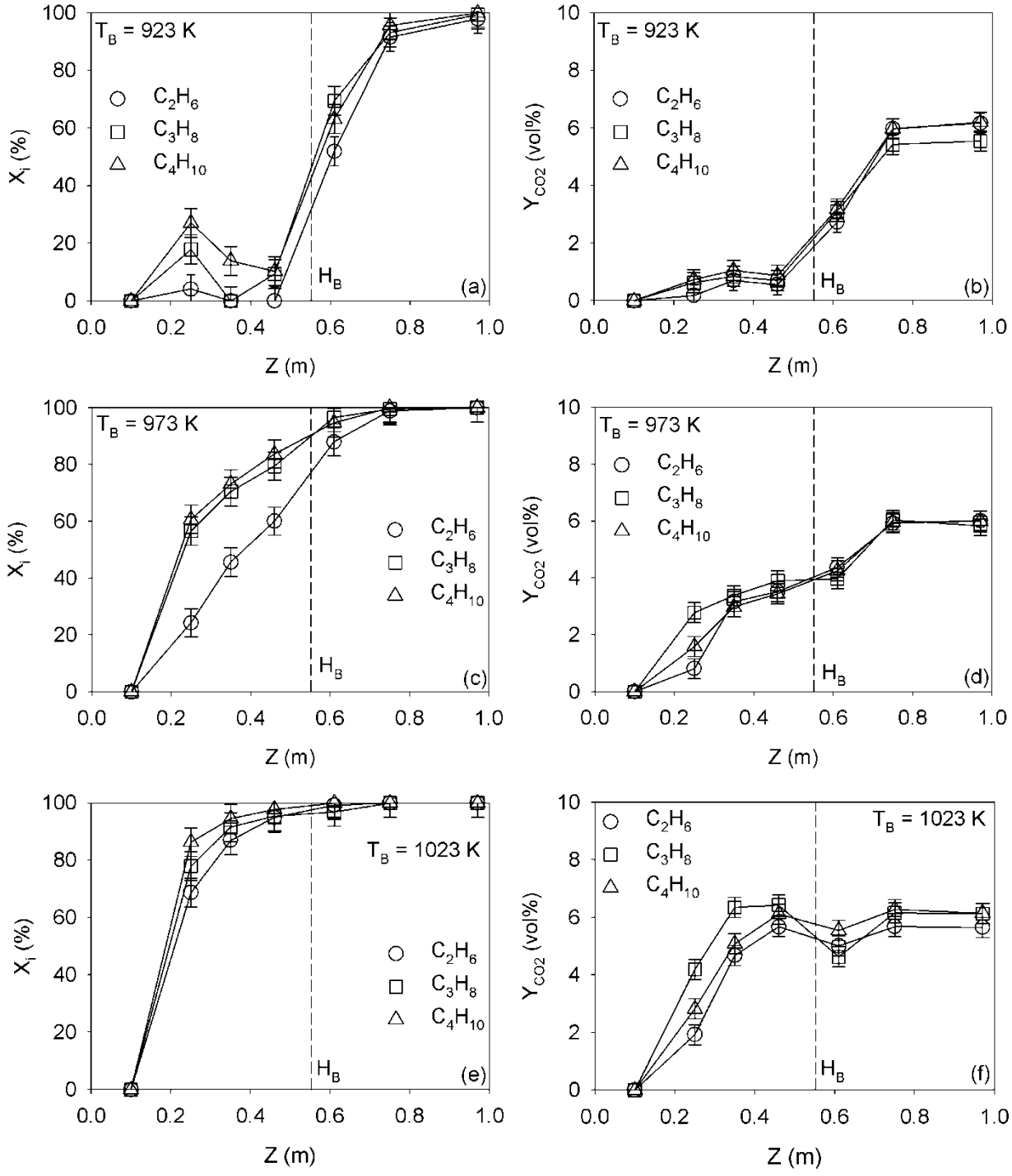

Figure 4-2: Conversion and Y_{CO2} axial profiles at 923 K, 973 K and 1023 K

The measured T_2 is lower than the value of 1123 K previously reported for propane [2, 9]. However, this discrepancy may be explained by the fact that conversion was not measured at a bed temperature of 1073 K – experiments were performed at bed temperatures of 1023 K and 1123 K [2, 9].

4.2.4.3 Methane

Compared to ethane, propane and n-butane, methane fluidized bed combustion was initiated at significantly higher bed temperatures. Figure 4.3 shows the axial profile of methane conversion at 973 K, 1023, 1073 and 1123 K. At a bed temperature of 973 K, no methane conversion was measured in the fluidized bed (0% at Z = 0.46 m) and combustion occurred entirely in the freeboard region: methane conversion increased from 37% at 0.06 m above the bed surface (Z = 0.61 m) to 99% at Z = 0.97 m, respectively.

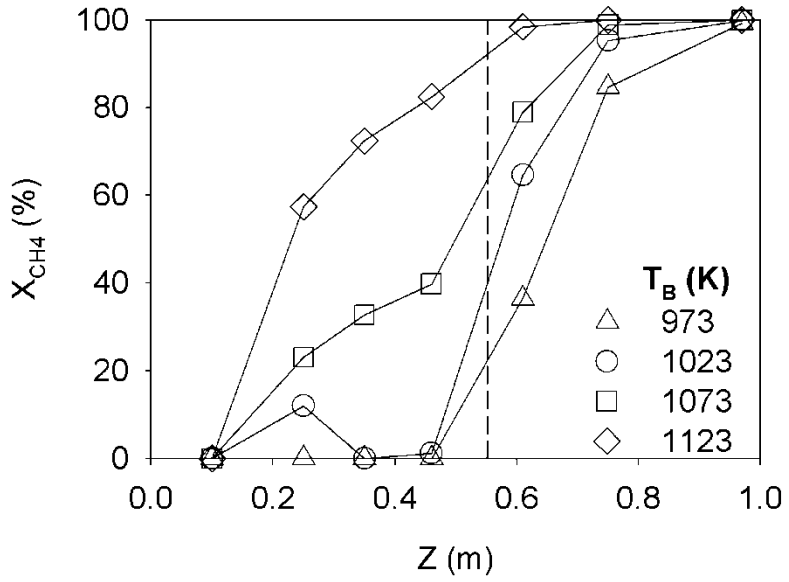

Figure 4-3: X_{CH4} axial profiles at various fluidized bed temperatures

As the temperature was increased to 1023 K, the methane in-bed conversion was low – the measured conversion fluctuated between 0% and 12%. Combustion mainly occurred at the bed

surface – conversion increased to 64% at 0.06 m above the bed surface (Z = 0.61 m). This was accompanied by a significant increase in the volume fraction of CO_2 in the freeboard. Complete methane conversion was observed in the freeboard region at Z = 0.97 m.

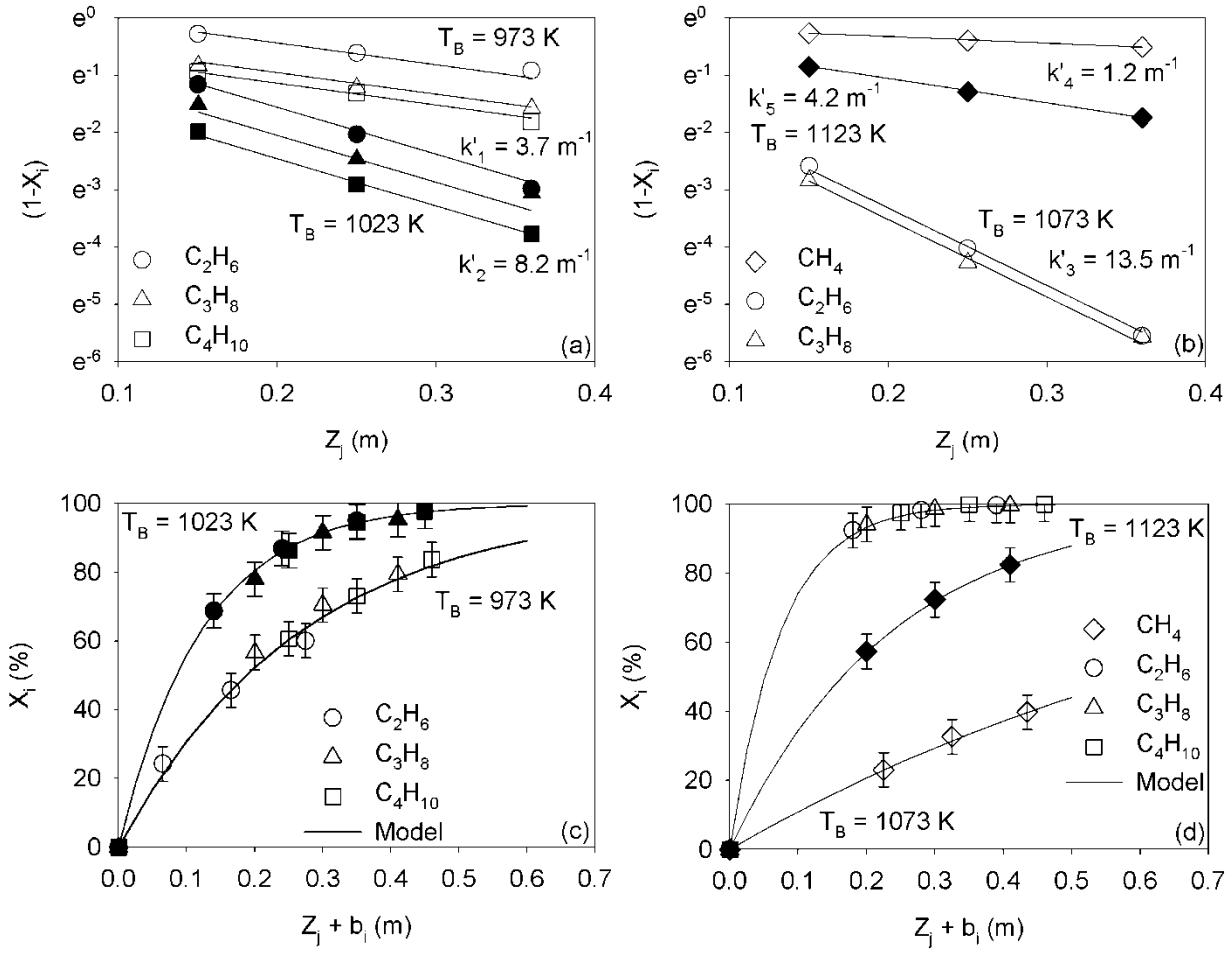

Figure 4-4: Comparison between the model and experiments at T_B = 973, 1023,1073 and 1123 K

The bed temperature was risen by 50 K to 1073 K and significant in-bed conversion was observed: conversion reached 23% at a distance of 0.15 m downstream of the sparger (Z = 0.25 m) and increased to 40% at 0.09 m below the bed surface (Z = 0.46 m). The unconverted methane burned in the freeboard and complete conversion was recorded at Z = 0.97 m.

The bed temperature was increased further to 1123 K and methane conversion increased to 83% at 0.1 m below the bed surface (Z = 0.46 m). The unconverted methane burned inside the freeboard region and conversion reached 98% only 0.06 m above the bed surface (Z = 0.61 m).

Fluidized bed combustion required significantly higher bed temperatures compared to ethane, propane and n-butane. Methane conversion occurred essentially in the freeboard region for bed temperatures below 1023 K, which was defined as the lower critical temperature (T_1). This value of T_1 is in the range of previous observations [18]. Furthermore, complete in-bed conversion of methane required bed temperatures above 1123 K and this agrees with the reported T_2 values in the scientific literature [18]. The measured lower and upper critical bed temperatures for methane, ethane, propane and n-butane are listed in Table 4.1.

Table 4.1: Measured T_1 and T_2 for C_1 to C_4 n-alkanes

n-Alkane	**T_1 (K)**	**T_2 (K)**
CH_4	1023	> 1123
C_2H_6	923	1073
C_3H_8	923	1073
n-C_4H_{10}	923	1073

4.2.4.4 C_1-C_4 n-alkanes global reaction rates

A simple one-phase reaction model was developed to predict the in-bed conversion of methane, ethane, propane and n-butane. The fluidized bed gas-phase hydrodynamics was modeled as a plug flow reactor (PFR) and first-order kinetics was used. The fluidized bed reactor was separated in two separate zones: (1) the injector region (high gas/gas and gas/solid mixing near

the sparger tip) and (2) the main fluidized bed body. The hydrocarbon conversion was calculated from equations (4.5) to (4.7):

$$X_i = X_{i,\,Injector} + X_{i,\,Fluidized\ Bed} \tag{4.5}$$

$$X_i = 100\left(1 - e^{-k'\left(Z_j + b_i\right)}\right) \tag{4.6}$$

$$k' = \frac{A k_0}{v} e^{-E_A/RT} = k_0' e^{-E_A/RT} \tag{4.7}$$

The parameter Z_j corresponds to the position where the fuel/air mixing occurs and where the free radical build-up is initiated. To determine Z_j, the flow pattern at the injector tip was characterized by calculating the jet penetration depth using six correlations [32-37]. Jet penetration depth correlations for downward injectors are scarce in the literature. However, previous observations have shown that the jet penetration depth is similar for horizontal and downwards jets [38]. Table 4.2 lists the jet penetration depths calculated from three correlations: the obtained values were small and comprised between 0.0 m and 0.034 m. Three correlations yielded negative jet penetration depths, which may be explained by the fact that the present operating conditions are outside the validity range of the correlations [31-33]. The three correlations are not included in Table 4.2. Since the calculated jet penetration depths were small, $Z_j = 0.0$ m was taken as the injector tip position (Z = 0.1 m).

Figure 4.4a shows the in-bed conversion of ethane, propane and n-butane as a function of Z_j on a natural logarithmic scale for two bed temperatures: 973 K and 1023 K. A linear relationship is observed between the ordinate [$\ln(1-X_i)$] and Z_j, which indicates that the model agrees well with the experimental results. The slope of the curve represents the first order reaction rate (k'): the same reaction rate was measured for ethane, propane and n-butane. For bed temperatures of 973 K and 1023 K, k' was measured as 3.7 m^{-1} and 8.2 m^{-1}, respectively. Therefore, the temperature dependence of the reaction rate was uniform for C_2 to C_4 n-alkanes, which implies that the activation energy (E_A) was also the same.

Similar observations were made at higher bed temperatures. Figure 4.4b shows the in-bed conversion of methane, ethane and propane as a function of Z_j on a natural logarithmic scale for

two bed temperatures: 1073 K and 1123 K. The first-order global reaction rate for ethane and propane was measured as 13.5 m^{-1} at 1073 K. N-butane conversion reached 100% and could therefore not be included in Figure 4.4b. For methane, however, the reaction rate was significantly lower compared to C_2-C_4 n-alkanes: k' rose from 1.2 m^{-1} to 4.2 m^{-1} as the bed temperatures was increased from 1073 K to 1123 K.

Table 4.2: Jet penetration depth correlations

Correlation	**Jet penetration (cm)**				**Orientation**	**Ref.**
	CH_4	**C_2H_6**	**C_3H_8**	**C_4H_{10}**		
$\frac{L_j}{D_j} = 7.8\left(\frac{\rho_j}{\rho_p}\right)\frac{U_j}{(gD_j)^{1/2}}$	0.06	0.06	0.06	0.06	Horizontal	[32]
$\frac{L_j}{D_j} = 5.52\left[\frac{\rho_j U_j^2}{(\rho_p - \rho_g)gD_j}\right]^{0.27}$	3.4	2.8	2.6	2.4	Horizontal	[33]
$L_j = \frac{Q_n}{2w}\left(\frac{\rho_g}{\rho_b}\right)^{1/2}$	1	0.7	0.6	0.4	Downward	[34]

The global reaction rates can be expressed in the Arrhenius form:

$$k'_{CH4} = \left(1.99\times10^{12}\right)e^{-251008/RT} \qquad \text{(R = 8.314 J/mol.K)} \tag{4.8}$$

$$k'_{C2H6} = k'_{C3H8} = k'_{C4H10} = \left(2.59\times10^{7}\right)e^{-127300/RT} \tag{4.9}$$

The reaction rate constant and the activation energy for methane were calculated from the reactions rates measured at bed temperatures of 1073 K and 1123 K. On the other hand, the parameters for ethane, propane and n-butane were calculated from the reaction rates at 973 K and 1023 K. Equation (4.9) overpredicts the global reaction rate at 1073 K and yields 16.4 m^{-1} compared to the measured value of 13.5 m^{-1}. This discrepancy can be explained by the fact that the in-bed conversions were very high at this temperature (in the order of 93% to 100%). At these

high conversions, a variation of 1.0% in the measured value greatly affects the measured slope in Figure 4.4b. The precision in the conversion measurements was estimated as ±5% absolute from the variations in repeated measurements.

The fact that ethane, propane and n-butane have the same global kinetics is consistent with previous studies, which have shown that the induction times of C_2 and higher alkanes are of similar magnitude and are governed by the same temperature dependence or activation energy [27-28]. Methane is also known to be significantly less reactive than higher n-alkanes [28, 30].

4.2.4.5 Contribution from the injector region

The region close to the injector is modeled as a separate PFR and the parameter b_i of equation (4.7) represents its contribution to the overall fluidized bed conversion. A positive value for b_i means that combustion occurred in the injector region. On the other hand, a negative value for b_i implies that autoignition did not occur in the injector region and occurred in the main fluidized bed body only after an induction delay. Therefore, the parameter b_i is analogous to an induction distance as it increases with decreasing induction delay.

Table 4.3: Parameter b_i at the different bed temperatures (T_B)

n-Alkane	**Parameter b_i (m) for various T_B (K)**			
	973	1023	1073	1123
CH_4	N/A	N/A	-0.075	0.05
C_2H_6	-0.085	-0.020	0.010	N/A
C_3H_8	0.050	0.050	0.06	N/A
n-C_4H_{10}	0.100	0.100	0.100	N/A

The values for b_i were determined such that the model would fit with the experimental data. Table 4.3 lists the values of b_i for C_1-C_4 n-alkanes for all tested fluidized bed temperatures. For methane and ethane, b_i decreased with temperature, which is consistent with previous induction time studies where induction time decreased with increasing temperature. For methane, b_i increased from -0.075 m at 1073 K to 0.05 m at 1123 K. For ethane, b_i increased from -0.085 m at 973 K to 0.01 m at 1073 K. For propane and n-butane, b_i remained approximately constant at 0.05 m and 0.1 m, respectively.

Figures 4.4c and 4.4d compare the measured and predicted conversion of C_1 to C_4 n-alkanes for fluidized bed temperatures of 973 K to 1123 K: the agreement between the model and the experimental results is good.

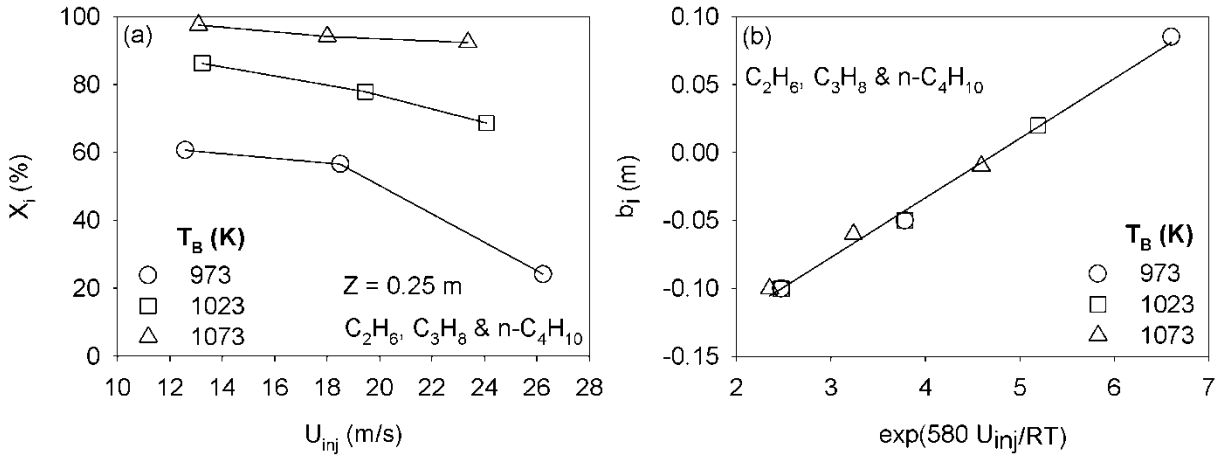

Figure 4-5: Conversion in the injector region

To better understand the observed trends in the values of b_i in Table 4.3, Figure 4.5a shows the conversion (X_i) measured 0.15 m (Z = 0.25 m) above the injector tip as a function of fluidized bed temperature (T_B) and fuel injection velocity (U_j) for C_2H_6, C_3H_8 and n-C_4H_{10}. Note that the injection velocity at the sparger tip varied from 23-24 m/s, 18-19 m/s and 12-13 m/s for C_2H_6, C_3H_8 and n-C_4H_{10}, respectively. For a specific bed temperature, the lowest conversion was obtained with ethane, followed by propane and n-butane. However, these hydrocarbons share similar kinetics as demonstrated earlier and autoignition temperature measured in non-premixed

counterflow experiments have been shown to increase as $C_2H_6 < n\text{-}C_4H_{10} < C_3H_8$ [20-22, 27, 28, 30]. Therefore, this strongly suggests that the decrease in conversion for ethane is due to the increased injection velocity and strain rate, which quench intermediate species and free radicals near the injector. It is also observed from Figure 4.5a that the reduction in conversion due to an increase in fuel injection velocity decreases with rising bed temperature. At higher temperatures, the reaction rates may become so fast that they remain relatively unaffected by the enhanced mixing near the sparger tip.

Since the parameter b_i is analogous to an induction distance, it was attempted to produce a correlation of b_i based on the Arrhenius equation. Induction time has been shown in several studies to be well correlated to temperature through an Arrhenius-type expression. Similarly to fluidized bed temperature, it was assumed that the fuel injection velocity at the sparger had an exponential effect on b_i:

b_i = (Average distance travelled by the gas in injector region) – (induction distance) (4.10)

$$b_i \propto t_j \frac{U_g}{(1-\varepsilon)} - \tau \frac{U_g}{(1-\varepsilon)} \tag{4.11}$$

$$b_i = 0.2083 - 0.0438\, e^{582U_{inj}/RT_B} \tag{4.12}$$

Figure 4.5b shows the parameter b_i as a function of $exp\left(580U_{inj}/RT\right)$: the correlations is very good at reproducing the experimental trend.

As shown in equation (4.11), the parameter b_i is proportional to the average gas residence time in the injector region (t_j) and the mixture induction time (τ) through the interstitial gas velocity. It seems reasonable to believe that the autoignition in the non-premixed hydrocarbon/air mixture is governed by the induction time at the stoichiometry concentration. In fact, the hydrocarbon/air interface at the sparger should be characterized by a wide range of equivalence ratios and

autoignition should be determined by the conditions that are most reactive. The average fluidized bed solids fraction (1-ε) can be estimated from the pressure drop across the bed (5.5 kPa), the solids density (ρ_p = 2650 kg/m^3) and the bed height (H_B = 0.55 m): (1-ε) = 0.39. Using this value of solids fraction results in an average gas residence at the injector (t_j) of 0.200 s and an induction time that decreased from 0.160 s to 0.140 s for propane (U_j = 18 m/s) as the bed temperature was increased from 973 K to 1073 K. In comparison, the low-temperature induction time correlation of Penyazkov *et al.* [39] yields lower values of 0.033 s at 973 K and 0.012 s at 1073 K for a stoichiometric propane/air mixture. The lower values of Penyazkov *et al.* [39] may be explained by the fact that the measurements were performed on a homogeneous mixture in a different apparatus (shock tube): a non-premixed mixture and strain rates increase induction time in the present study.

4.2.5 Conclusions

The non-premixed combustion of methane, ethane, propane and n-butane with air was investigated in a fluidized bed of inert sand particles. The bed temperature was varied between 923 K and 1123 K while the superficial gas velocity was kept constant at 0.4 m/s. Critical transition bed temperatures (T_1 and T_2) were measured for each fuel. For ethane, propane and n-butane, combustion occurred mainly in the freeboard region at bed temperatures below T_1 = 923 K (650^{o}C). On the other hand, complete conversion occurred within 0.2 m of the injector at: T_2 = 1073 K. For methane, the measured values of T_1 and T_2 were significantly higher at 1023 K and above 1123 K, respectively.

The fluidized bed combustion was accurately modeled with first-order global kinetics and two one-phase PFR models in series: one PFR to model the region close to the injector and another to represent the main fluidized bed body. The global reaction rates of C_2 to C_4 n-alkanes were evaluated and found to be characterized by a uniform Arrhenius expression. On the other hand, the methane global reaction rate was significantly slower with a higher activation energy.

The reaction model for the injector region either increased conversion near the sparger tip or delayed autoignition inside the main fluidized bed body. The conversion in the injector region increased with rising fluidized bed temperature and decreased with increasing jet velocity (strain rate). To account for the promoting and inhibiting effects in the sparger region, an analogy was made with the concept of induction time: the PFR length (b_i) was varied as a function of the fluidized bed temperature and jet velocity. The PFR length was correlated to these two parameters using an Arrhenius expression, similarly to induction time correlations.

4.2.6 Nomenclature

A Cross-sectional area (m^2)

b_i Parameter in equation (7) for i^{th} species (m)

D_j Injector nozzle diameter (m)

E_A Activation energy (J)

g Gravitational constant (9.81 m/s^2)

H_B Fluidized bed height (m)

k_0 First-order reaction rate constant (m^{-1})

L_j Jet penetration length (m)

Q_n Jet volumetric flow rate at 0^oC & 101.3 kPa (litres)

R Universal gas contant (8.314 J/Kmol)

r Radial position (m)

t_j Average gas residence time in injector region (s)

T Temperature (K)

T_B Fluidized bed temperature (K)

T_1 Lower critical temperature (K)

T_2 Upper critical temperature (K)

U_j Gas injection velocity at the sparger tip (m/s)

U_{mf} Minimum fluidization velocity (m/s)

U_g Superficial gas velocity (m/s)

v Volumetric flow rate (m^3/s)

w Nozzle thickness (cm)

X_i Conversion of i^{th} species (%)

Y_i Volume fraction of i_{th} species (vol%)

Z Axial position above the distributor (m)

Z_j Axial position above the injector tip (m)

Greek letters

ε Average void fraction in fluidized bed

ρ_b Fluidized bed density (kg/m^3)

ρ_g Fluidizing gas density (kg/m^3)

ρ_j Gas density at injector nozzle (kg/m^3)

ρ_p Particle density (kg/m^3)

τ Induction time (s)

4.2.7 References

[1] Hesketh RP, Davidson JF. Combustion of methane and propane in an incipiently fluidized bed. Combust Flame **1991**;85:449-467.

[2] Van der Vaart DR. Freeboard ignition of premixed hydrocarbon gas in a fluidized bed. Combust Flame **1988**;71:35-39.

[3] Van der Vaart DR. The chemistry of premixed hydrocarbon/air combustion in a fluidized bed. Fuel **1988**;67:1003-1007.

[4] Friedman J, Li H. Natural gas combustion in a fluidized bed heat-treating furnace. Combustion Sci Technol **2005**; 177; 2211-2241.

[5] Dounit S, Hemati M, Andreux R. Modelling and experimental validation of a fluidized-bed reactor freeboard region: application to natural gas combustion. Chem Eng J **2008**; 140; 457-465.

[6] Pre P, Hemati M, Marchand B. Study on natural gas combustion in fluidized beds: modelling and experimental validation. Chem Eng Sci **1998**; 53 (16); 2871-2883.

[7] Zukowski W. A simple model for explosive combustion of premixed natural gas with air in a bubbling fluidized of inert sand. *Combust Flame* **2003**; 134; 399-409.

[8] Baron J, Bulewicz EM, Zukowski W, Kandefer S, Pilawska M. Combustion of hydrocarbon fuels in a bubbling fluidized bed. Combust Flame **2002**; 128; 410-421.

[9] Dennis JS, Hayhurst AN, Mackley IG. The ignition and combustion of propane/air mixtures in a fluidised bed. 19th Symp. (Intl.) on Combust. 1982; 1205-1212.

[10] Srinivasan RA, Sriramulu S, Kulasekaran S, Agarwal PK. Mathematical modeling of fluidized bed combustion-2: combustion of gases. Fuel **1998**; 77; 1033-1049.

[11] Mabrouk R, Chaouki J, Laviolette J-P, Patience GS. On natural gas combustion in a fluidized bed. *Proc. 9th Conference on Circulating Fluidized Beds*, Hamburg, Germany, **2008**.

[12] Ross DP, Yan HM, Zhang DK. An experimental study of propane combustion in a fluidized-bed gasifier. Combust Flame **2001**; 124; 156-164.

[13] Sotudeh-Gharebaagh R. Combustion of natural gas in a turbulent fluidized bed reactor. *PhD Thesis*, Ecole Polytechnique, Montreal, Canada, **1998**.

[14] Singh B, Rigby GR, Callcott TG. Combustion of gaseous fuels in a fluidised bed. *Fluidised Combustion Conference*, Paper C5, London, **1975**.

[15] Stubington JF, Davidson JF. Gas-phase combustion in fluidized beds. AIChE Journal **1981**; 27 (1); 59-65.

[16] Sotudeh-Gharebaagh R, Chaouki J. Investigation of highly exothermic reactions in a turbulent fluidized bed reactor. Energy & Fuels **2007**; 21; 2230-2237.

[17] Sotudeh-Gharebagh R, Chaouki J. The heterogeneous and homogeneous combustion of methane over inert particles. Can J Chem Eng **2003**; 81; 1182-1191.

[18] Laviolette J-P, Sotudeh-Gharebagh R, Mabrouk R, Patience GS, Chaouki J. In A. Agarwal (ed.)Handbook of Combustion (vol.5), Wiley **2010**.

[19] Lorences M, Laviolette J-P. Fluid bad gas RTD: effect of fines and internals. *Powder Technol* **2006**; 168 (1); 1-9.

[20] Humer S, Seiser R, Seshadri K. Non-premixed and premixed extinction and autoignition of C_2H_4, C_2H_6, C_3H_6 and C_3H_8. *P Combust Inst.* **2002**; 29; 1597-1604.

[21] Fotache CG, Wang H, Law CK. Ignition of ethane, propane, and butane in counterflow jets of cold fuel versus hot air under variable pressures. *Combust Flame.* **1999**; 117; 777-794.

[22] Jomaas G, Zheng XL, Zhu DL, Law CK. Experimental determination of counterflow ignition temperatures and laminar flame speeds of C_2-C_3 hydrocarbons at atmospheric and elevated pressures. *P Combust Inst.* **2005**; 30; 193-200.

[23] Ross DP, Yan H-M, Zhang D-K. Modelling of a laboratory-scale bubbling fluidised-bed gasifier with feeds of both char and propane. *Fuel* **2004**; 83; 1979-1990.

[24] Jeng R-S, Altwicker ER, Morgan III MM, Wilk RD. Propane combustion in a spouted bed combustor II: a modeling study in the bed region. *Combustion Science and Technol* **2001**; 170; 119-149.

[25] Foka M, Chaouki J, Guy C, Klvana D. Natural gas combustion in a catalytic turbulent fluidized bed. *Chem. Eng. Sci.* **1994**; 49 (24A); 4269-4276.

[26] Chaouki J, Klvana D, Guy C. Selective and complete catalytic oxidation of natural gas in turbulent fluidized beds. *Korean J. Chem. Eng.* **1999**; 16 (4); 494-500.

[27] Horning DC, Davidson DF, Hanson RK. Study of the high-temperature autoignition of n-alkane/O_2/Arixtures. *Journal of Propulsion and Power* **2002**; 18 (2); 363.

[28] Burcat A, Scheller K, Lifshitz A. Shock-tube investigation of comparative ignition delay times for C_1-C_5 alkanes. *Combust Flame* **1971**; 16; 29-33.

[29] Saxena P, Peters N, Williams FA. An analytical approximation for high-temperature autoignition times of higher alkanes. *Combust Flame* **2007**; 149; 79-90.

[30] Westbrook, CK. Chemical kinetics of hydrocarbon ignition in practical combustion systems. Proc Combust Inst **2000**; 28; 1563-1577.

[31] Lamoureux N, Paillard C-E, Vaslier V. Low hydrocarbon mixtures ignition delay times investigation behind reflected shock waves. *Shock Waves* **2002**; 11; 309-322.

[32] Zenz FA, Bubble formation and grid design, IChemE Symposium Series **1968**; 30; 136–139.

[33] Benjelloun F, Liegeois R, Vanderschuren J. Penetration length of horizontal gas jets into atmospheric fluidized beds, in: J.F. Large, C. Laguerie (Eds.), Fluidization VIII: Proceedings of the Eighth Engineering Foundation Conference on Fluidization, Amer Inst of Chemical Engineers, **1995**, 239–246.

[34]Shen Z, Briens CL, Kwauk M, Bergougnou MA. Study of a downward gas jet in a two-dimensional fluidized bed. Can J Chem Eng **1990**; 68; 534-540.

[35] Shakhova NA, Discharge of turbulent jets into a fluidized bed, Journal of Engineering Physics and Thermophysics **1968**; 14 (1); 32–36.

[36] Merry JMD, Penetration of a horizontal gas jet into a fluidised bed, Trans Inst Chem Eng **1971**; 49 (4); 189–195.

[37] Hong R, Li H, Li H, Wang Y. Studies on the inclined jet penetration length in a gas–solid fluidized bed, Powder Technol **1997**; 92; 205–212.

[38] Okhotskii VB. Depth of penetration of a gas jet into a granular medium. Theor Found Chem Eng **2001**; 35(2): 199-200.

[39] Penyazkov OG, Ragotner KA, Dean AJ, Varatharajan B. Autoignition of propane-air mixtures behind reflected shock waves. Proc Combust Inst **2005**; 30: 1941-1947.

CHAPITRE 5 COMBUSTION DU PROPANE DANS LA ZONE DE DÉSENGAGEMENT D'UN LIT FLUIDISÉ

Cet article a été soumis au journal Fuel.

5.1 PRÉSENTATION DE L'ARTICLE

L'objectif de cet article est d'étudier la combustion du propane dans la zone de désengagement d'un réacteur à lit fluidisé. Des expériences sont menées avec une faible vitesse superficielle de gaz afin de minimiser l'emportement de solides en aval du lit fluidisé. Durant les expériences, le flux de solides, la composition chimique de la phase gazeuse et la température sont mesurés simultanément avec une sonde à prélèvement non-isocinétique et des thermocouples.

Les profiles axiaux de fractions volumétriques de propane sont comparés aux prédictions de six modèles de microcinétique pour la combustion homogène en phase gazeuse. Les résultats démontrent que les modèles surestiment le temps d'induction dans la zone de désengagement et sous-estiment le taux de combustion. Or, ceci suggère que des radicaux libres dans la région du lit fluidisé peuvent être entraînés en aval où ils accélèrent les réactions de combustion dans la zone de désengagement.

GAS-PHASE PROPANE COMBUSTION IN THE FREEBOARD OF A FLUIDIZED BED

Jean-Philippe Laviolette, Gregory S. Patience, Concetta La Marca, Jamal Chaouki

(Submitted to Fuel, 2010)

5.2 GAS-PHASE COMBUSTION IN THE FREEBOARD OF A FLUIDIZED BED

Propane combustion experiments were conducted in the freeboard of a fluidized bed of sand particles at temperatures between 818 K and 923 K and at superficial gas velocity twice the minimum fluidization velocity. The freeboard region was characterized by simultaneous measurements of solids flux, chemical composition, temperature and pressure. Autoignition was only recorded within 0.06 m of the bed surface at temperatures greater than 833 K. Propane conversion predicted by six different microkinetic mechanistic models were compared to the experimental measurements: all six models underestimated the reaction rate above the bed surface. However, accounting for the production of H_2O_2 during in-bed combustion significantly increased the calculated reaction rates and resulted in a better agreement between predicted and measured propane conversion.

5.2.1 Introduction

Gas-phase homogenous combustion is a major constraint in attaining high yields, particularly selectivity, in processes involving heterogeneous catalysis and specially as applied to partial oxidation reactions. Together with product yield losses, combustion represents a significant safety hazard in the case of reactions involving molecular oxygen and hydrocarbons. Chemical processes requiring molecular oxygen are widespread in the industry. Also, new processes are currently under development for chemicals production and power generation in the context of increasing oil prices and global warming: selective oxidation of alkanes, biomass gasification, and combustion of non-conventional feedstocks, for example. Fluidized bed reactors are currently being developed for several of these processes due to their high heat transfer characteristics.

In order to increase productivity, fluidized bed processes may operate within the explosion envelope while feeding the oxidant and hydrocarbon separately into the bed. This can be achieved due to the ability of the solids phase to suppress the homogeneous reactions (combustion) and at the same time promote selective heterogeneous reactions. However, due to operational constraints, the processes may be operated under conditions of partial conversion. In the case of selective oxidation reactions, for example, the selectivity has been shown to decrease at high conversion due to the increase in the rate of product decomposition [1-4]. Therefore, downstream of the bed – in the freeboard, cyclones and associated piping – the effluent gas phase composition is potentially explosive, characterized by high hydrocarbon and oxygen concentrations, elevated temperatures and an insufficient solids volume fraction to quench non-selective homogeneous reactions [5-6]. Minimizing the risk of gas-phase combustion-deflagration in these regions remains an important design issue.

Several explosion criteria, such as explosion limits, autoignition temperatures and induction time correlations [7-17] have been published in the scientific literature for gas-phase homogeneous systems. Hesketh *et al*. [18] showed that induction time correlations can be adequate to predict ignition delays above a fixed bed with $T_B \leq 973$ K and with negligible combustion in the bed. However, extrapolating these correlations to fluidized bed reactors introduces uncertainties since the entrained solid particles inhibit gas-phase reactions downstream of the fluidized bed. Furthermore, the axial and radial distribution of solids above the bed surface is non-homogeneous: solids entrainment decreases exponentially from the bed surface until it reaches a steady value above the transport disengagement height [19-20]. Together with heterogeneous solids distribution, axial and radial temperature gradients may exist in the freeboard region as well as species concentration gradients. Finally, partial reactant conversion in the fluidized bed region produces reaction intermediates and free radicals that may influence the reaction kinetics in the freeboard region.

To accurately predict induction time and the rate of combustion of a hydrocarbon/oxygen mixture in the freeboard for a wide range of operating conditions, a combustion model that combines the gas/solids hydrodynamics, reaction microkinetics, temperature gradient and correct initial

boundary condition must be developed. Steady state freeboard reaction models have been developed by De Lasa *et al.* [21], Chen *et al*. [22], Walsh *et al*. [23], Sotudeh-Gharebagh *et al*. [24], Dounit *et al.* [25], and Hartman *et al*. [26] for various reactions. However, these models have relied on global kinetic mechanisms, and were unable to model the free radical chemistry and induction time. Furthermore, they used correlations to estimate solids volume fraction, which may introduce significant errors.

Elementary step level free-radical kinetics models are necessary to characterize induction time and to account for the effect of intermediate products on reaction times. Several homogeneous gas-phase microkinetic models for propane oxidation are available in the literature for the low ($T < 600$ K) [27], intermediate (650-1000K) [28-29] and high temperature ($T > 1000$ K) regions [30-33]. Some of these models have been previously modified to account for the quenching effect of solid particles on free radicals [34-35]. A gas-phase microkinetic model was previously used by Hutchenson *et al*. [4] to predict the oxygen conversion in the freeboard of a lab-scale fluidized bed (0.128 m I.D.) of vanadyl pyrophosphate (VPP) catalyst during n-butane selective oxidation. The calculated conversions were compared to experimental measurements: the predicted conversions were significantly lower than the measured values. Two possible explanations were given for this discrepancy: (1) some important heterogeneous/homogeneous reactions may not have been included in the model and that (2) the production of free radicals in the bed was not taken into account. However, this study relied on a limited characterization of the freeboard region: temperature and species volume fractions were measured at one position such that the freeboard was assumed to be perfectly mixed.

The reaction model should be better validated with experimental data of hydrocarbon combustion in the freeboard of a fluidized bed if the parameters that affect the reaction are carefully characterized, namely the mixture composition, solids volume fraction and temperature. Furthermore, since these parameters are coupled, they should be measured simultaneously in the freeboard, even though this task is very challenging.

In the present study, non-premixed propane fluidized bed combustion experiments were conducted in a pilot-scale reactor (I.D. = 0.2 m) at low bed temperatures (818 K $\leq T_B \leq$ 923 K), which resulted in low in-bed conversion and autoignition in the freeboard region. Sand particles (d_p = 290 μm) and a low superficial gas velocity of 0.17 m/s ($U_g = 2.1 \times U_{mf}$) were used for all experiments to limit solid entrainment into the freeboard region. The steady-state combustion process in the freeboard region was characterized by simultaneous measurements of solids entrainment flux, chemical composition, pressure and temperature. A gas-phase reaction model with elementary step level free-radical kinetics was developed and compared to the experimental data. Six well-established microkinetic models from the literature were used [28-33].

5.2.2 Experimental

The experiments were conducted in a fluidized bed reactor with an inner diameter of 0.2 m in the bed and freeboard regions. Sand particles (Geldart group B, $\rho_s = 2650$ kg/m^3, d_p = 290 μm and U_{mf} = 0.08 m/s) were used as the bed material and air was the fluidizing media. Propane was injected separately through a downward-facing sparger whose tip was located at 0.1 m above the distributor. For all experiments, a low superficial gas velocity of 0.17 m/s ($U_g = 2.1 \times U_{mf}$) and low bed temperatures (818 K $\leq T_B \leq$ 923 K) were used. The fluidized bed surface and freeboard region were characterized by simultaneous measurements of solids entrainment flux, chemical composition and temperature. Solids and gas were sampled simultaneously from the reactor using a non-isokinetic probe. The solids flux was measured from the mass of the solids samples and the gas was analyzed with a gas chromatograph and a CO/CO_2 analyzer for the following chemical species: C_3H_8, C_3H_6, C_2H_6, C_2H_4, CH_4, CO, CO_2, N_2, O_2 and H_2. Temperature was measured with 10 thermocouples positioned along the reactor's length.

5.2.3 Kinetic modeling in the freeboard

A gas-phase reaction model with elementary step level free-radical kinetics was developed and compared to the experimental data. Propane is known to undergo a transition from a low temperature reaction regime (T < 600 K) to an intermediate reaction regime (T > 650 K)

separated by a negative temperature coefficient regime (600 - 650 K). Cool flames have been observed to occur in the low and transition temperature regimes, the latter being attributed to a change in the main chain branching agent from hydroperoxides to hydrogen peroxide [36-37].

The present laboratory experiments were performed with freeboard temperatures located in the intermediate temperature region, where the main chain branching reaction is thought to be the dissociation of hydrogen peroxide into two hydroxyl radicals [36-37]. To model the kinetics, six well-established microkinetic reaction schemes from the literature were used and compared: the mechanisms of Dagaut *et al*. [29], Marinov *et al*. [28], San Diego [32], GRI release 3 [33], Sung *et al*. [31] and Qin *et al*. [30].

The model of Dagaut *et al*. [29] (50 species and 274 elementary reactions) has been validated with propane oxidation experiments in a jet-stirred reactor for a wide range of equivalence ratios (0.15 - 4) and temperatures (900 - 1200 K)., The model of Marinov *et al*. [28] (126 species and 638 elementary reactions) has demonstrated good agreement with NO and hydrocarbon oxidation experiments in an atmospheric flow reactor and a temperature range of 600 to 1100 K. This kinetic scheme includes the flame chemistry for hydrogen, methane, ethylene, ethane, propane and ethanol. The San Diego mechanism [32] (46 species and 235 reactions), the third release of the GRI mechanism [33] (53 species and 325 reactions), the model of Sung *et al*. [31] (92 species and 621 reactions) and the model of Qin *et al*. [30] (70 species and 463 reactions) were also used. These four models have been compared to experimental data (induction times, flame speeds and species axial gradients) obtained at higher temperatures than those used in the present investigation. However, these models contain the reaction steps for the intermediate temperature reaction regime.

The gas-phase hydrodynamics in the freeboard were modeled as an ideal plug flow reactor (PFR). The steady-state temperature profiles that were measured experimentally were used in the model and the simulations were run with the ChemKin 4.1 software. The kinetic schemes excluded heterogeneous reactions steps that could have occurred at the surface of the solid particles.

Two sets of simulations were performed. In the first set, the freeboard region was modelled as a plug flow reactor and the mixture composition measured at the bed surface served as the inlet boundary condition. In the second set of simulations, a second PFR was added upstream of the freeboard PFR to model the fluidized bed and the production of free radicals and branching agents in that region. The mixed-cup mixture composition at the sparger tip was considered as the inlet boundary condition of the fluid bed PFR and the gas residence time was adjusted individually for each model to obtain the correct in-bed conversion. The mixture at the exit of the fluid bed PFR was fed to the inlet of the freeboard PFR.

5.2.4 Results and discussion

The first part of this investigation consisted of conducting propane fluidized bed combustion experiments at low bed temperatures and low superficial gas velocity to observe freeboard combustion with low solids entrainment.

5.2.4.1 Freeboard combustion experimental results

During the experiments, upward solids flux and propane volume fraction were measured simultaneously at several axial and radial positions. The local solids entrainment flux varied with radial position – the upward flux reached a maximum at the reactor centerline and decreased close to the wall. Figure 5.1 shows the axial profile of the solids entrainment flux (G_{SU}) cross-sectional average for two bed temperatures (T_B): 853 K and 923 K. The entrainment flux decreased exponentially with height (Z) from an asymptote located at a height of 0.29 m above the distributor (Z = 0). The asymptote position was defined as the bed surface and the beginning of the freeboard region [20] and this was also confirmed by pressure measurements: pressure decreased in the fluidized bed and reached a constant value a few centimetres upstream of Z = 0.29 m. Solids entrainment flux decreased exponentially to zero at Z = 0.4 m and the transport disengagement height (TDH) was therefore 0.11 m for both bed temperatures. The bed temperature did not have a significant effect on the bed height and TDH in the tested range.

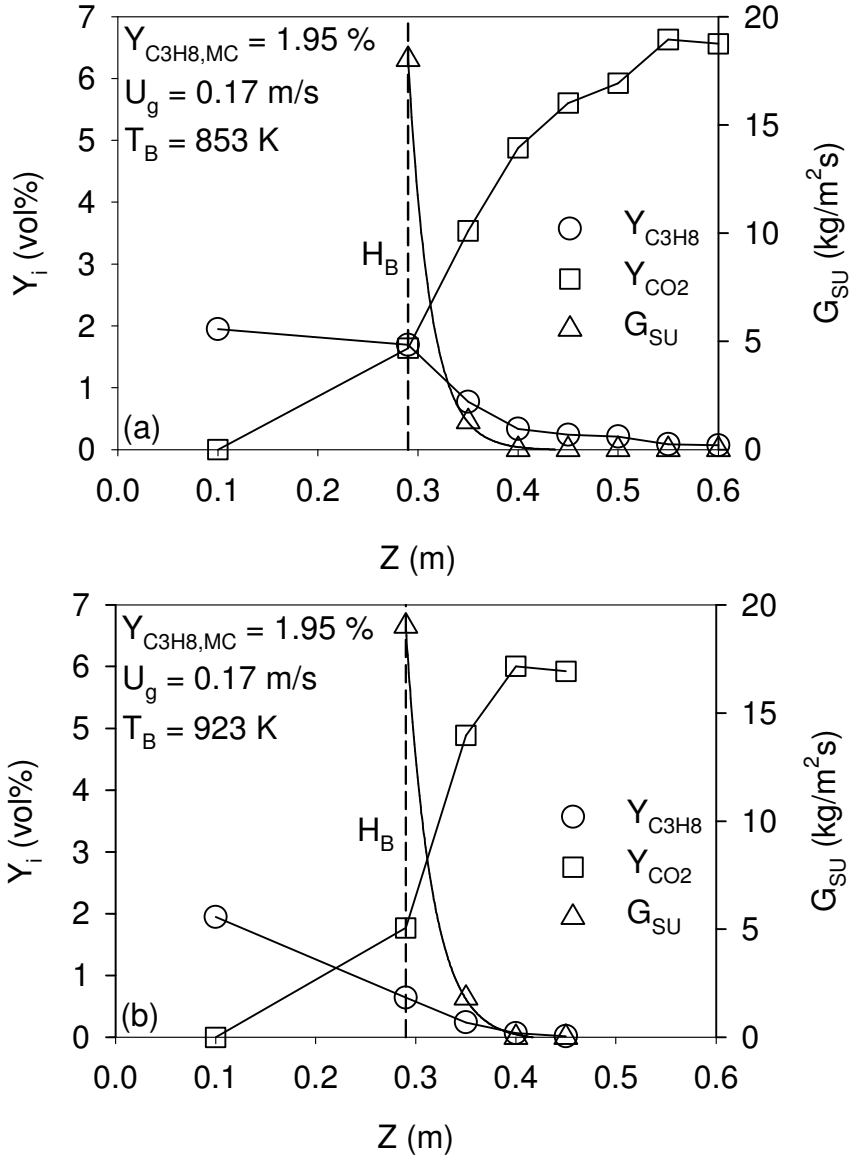

Figure 5-1: Y_{C3H8} and G_{SU} axial profiles in the freeboard region

Figure 5.1 also shows the axial profile of propane and carbon dioxide volume fractions (Y_i) for the two bed temperatures. A radial profile of propane volume fraction was observed at the bed surface (Z = 0.29 m) – propane volume fraction reached a maximum of 3.1 % at the centerline and decreased to 1.35 % at a distance of 0.02 m from the wall at a bed temperature of 853 K. A cross-sectional average of Y_{C3H8} is therefore presented for Z = 0.29 m in Figure 1. However,

above the bed surface (Z > 0.29 m), Y_{C3H8} was uniform across the reactor radius, which indicated that the freeboard was well-mixed radially at all axial positions.

As shown in Figure 5.1, the propane conversion inside the bed of solids increased with rising bed temperature. For an inlet mixed-cup propane volume fraction ($Y_{C3H8,MC}$) of 1.95 vol% at the sparger tip, the propane volume fraction decreased to 1.69 vol% (X_{C3H8} = 13.1 %) and 0.64 vol% (X_{C3H8} = 67.1 %) at the bed surface for bed temperatures of 853 K and 932 K, respectively. The in-bed combustion of propane was accompanied by an increase in the CO_2 volume fraction from 0 % at the sparger to 0.95% and 2.00% at the bed surface for bed temperatures of 853K and 923K, respectively. The low in-bed conversion measurements are consistent with previous studies that indicate that propane combustion is triggered near the bed surface and in the bubble phase at these low bed temperatures [5-6].

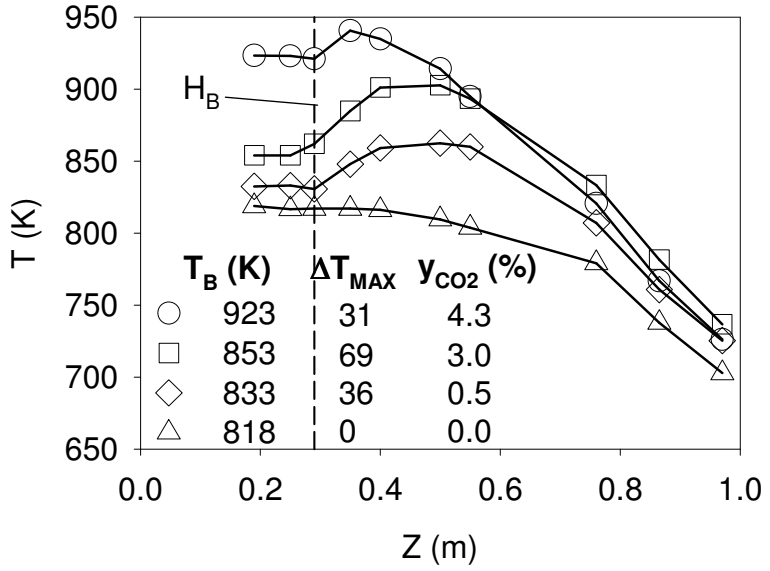

Figure 5-2: Axial temperature profile inside the fluidized bed and freeboard regions

Propane combustion continued downstream of the bed surface, in the freeboard, as shown in Figure 5.1. Propane conversion increased further at both temperatures just 0.06 m above the bed surface. Propane volume fraction decreased from 1.69 vol% (X_{C3H8} = 13.1%) to 0.77 vol%

(X_{C3H8} = 60.3%) and from 0.64 vol% (X_{C3H8} = 67.1%) to 0.24 vol% (X_{C3H8} = 87.7%) for a bed temperature of 853 K and 923 K, respectively. For both bed temperatures, propane combustion continued downstream until nearly all the propane was consumed. At T_B = 853 K, the propane volume fraction declined to 0.03% (X_{C3H8} = 96.6%) at a distance of 0.31 m above the bed surface (Z = 0.6 m). However, at the higher bed temperature, the propane combustion process reached completion within 0.16 m of the bed surface where Y_{C3H8} was measured as 0.02 % (X_{C3H8} = 99.1 %). Propane combustion was accompanied by an increase in Y_{CO2}, which reached about 6% for both bed temperatures when all the propane was consumed. It is interesting to note that most of the propane combustion occurred within 0.11 m of the bed surface and in the presence of solid particles, which have been shown to inhibit gas-phase reactions.

Propane combustion produced a significant temperature increase in the freeboard. Figure 5.2 shows the steady state axial temperature profile for five bed temperatures (T_B): 923, 853, 833 and 818 K. Propane combustion in the reactor was observed at three of these bed temperatures of 923 K, 853 K and 833 K. At T_B = 818 K, the fluid bed and freeboard temperatures were insufficient to trigger autoignition. When propane combustion occurred in the reactor, the bed temperature remained approximately constant due to the low in-bed propane conversion and the high concentration of solid particles, which are characterized by a high thermal capacity. On the other hand, the temperature increased significantly in the freeboard and above T_B at several axial positions. Figure 5.2 also includes the maximum temperature increase recorded (ΔT_{MAX}) and the CO_2 volume fraction (Y_{CO2}) measured 0.06 m above the bed surface. The maximum temperature increase recorded in the freeboard during propane combustion was significantly lower than the temperature calculated for a constant pressure adiabatic case. For example, at T_B = 853 K, a maximum temperature increase of 69 K was measured compared to a temperature increase of 968 K for constant pressure adiabatic combustion. This discrepancy can be explained by heat losses at the reactor walls, by the presence of solids in the freeboard and by the fact that the combustion process occurred over a distance of at least 0.1 m. The ΔT_{MAX} measured in the freeboard increased as the bed temperature decreased from 923 K to 853 K due to a decline in in-bed propane conversion and a higher propane breakthrough in the freeboard. At bed temperatures of 923 K and 853 K, propane combustion reached completion close to the bed as shown in Figure 5.1 and as indicated by the high Y_{CO2} measured at Z_F = 0.06 m shown in Figure 5.2.

However, when the bed temperature was decreased to 833 K, combustion in the fluid bed and freeboard was observed occasionally – the fluid bed and freeboard temperature approached the threshold value at which induction time was too high and autoignition did not occur. Figure 5.2 shows the temperature profile in the reactor for $T_B = 833$ K when combustion was observed. At $T_B = 833$ K, the measured ΔT_{MAX} decreased due to an incomplete propane combustion in the freeboard as indicated by a Y_{CO2} of only 0.5 % at a distance of 0.06 m above the bed surface.

At $T_B = 818$ K, combustion in the fluidized bed and freeboard was never observed: no temperature increase and no CO_2 were detected in the freeboard. The temperature in the freeboard reached a maximum at the bed and decreased with height due to heat losses at the reactor walls. It is interesting to note that for all cases where combustion was observed in the freeboard ($T_B = 923$ K, 853 K and 833 K), the onset of combustion always occurred close to the bed and within 0.06 m of its surface. It is possible that combustion was triggered immediately at the surface. This study was limited by the distance the between the bed surface and the first sampling probe (0.06 m).

One series of measurements was performed at $T_B = 853$ K during propane combustion to check for radial temperature gradients. The thermocouples were moved along the reactor radius from the centreline to the reactor wall and the freeboard temperature was observed to be uniform across the freeboard radius, which suggested that the gas was well mixed radially.

5.2.4.2 Freeboard combustion modelling

A gas-phase reaction model was developed to predict induction time and the reaction rate of propane inside the freeboard region.

5.2.4.2.1 Considering only the freeboard

The first modeling attempt consisted of using experimentally measured axial temperature profiles (shown in Figure 5.2) in a plug flow reactor model for the freeboard portion of the reactor.

Preliminary gas tracer experiments were performed in the freeboard and at ambient temperature for $Z_F \geq 0.16$ m: the gas-phase hydrodynamics was found to be plug flow in that region. The stable species composition measured by the GC at the bed surface was used as the inlet boundary condition for the freeboard and six kinetic models were used and compared.

Figure 5.3(a) shows the experimental and predicted axial profiles of propane volume fraction (Y_{C3H8}) in the freeboard for a bed temperature of 853 K obtained with the 6 microkinetic reaction schemes. In Figure 5.3(a), $Z_F = 0$ m corresponds to the bed surface (Z = 0.29 m). All six reaction mechanisms predict lower propane reaction rates compared to the experimental observations. The GRI model [33] predicts no propane combustion in the freeboard at all. The San Diego model [32] (SD), the model of Dagaut *et al*. [29] (D), the model of Sung *et al*. [31] (S) and the model of Qin *et al*. [30] (Q) predict no propane consumption at a distance of 0.06 m above the bed surface while the experimental data showed a 54% decrease in propane volume fraction (from $Y_{C3H8} = 1.69\%$ at the bed surface to $Y_{C3H8} = 0.77\%$ at $Z_F = 0.06$ m. At $Z_F = 0.31$ m, these four microkinetic models yield propane volume fractions that ranged from 1.20% (SD) to 0.69% (Q) compared to the experimental measurement of 0.07%. The microkinetic scheme of Marinov *et al*. [28] (M) fit the experimental data the best, predicting a faster propane reaction rate inside the freeboard and a propane molar fraction of 0.20% at $Z_F = 0.31$ m.

A similar discrepancy between the experimental and predicted propane reaction rates was observed at a bed temperature of 923 K. Figure 5.4(a) shows the measured and predicted axial profiles of propane volume fraction in the freeboard obtained with the six microkinetics reaction schemes. The GRI model predict an onset of combustion at a distance of about 0.15 m above the bed surface and a rapid consumption of propane within 0.10 m, however this trend does not fit the experimental data very well. The other five reaction mechanisms predict an onset or propane combustion within 0.06 m of the bed surface, however the propane reaction rate is underestimated in all cases. At $Z_F = 0.16$ m, the San Diego model [32] (SD) and the models of Dagaut *et al*. [29] (D), Sung *et al*. [31] (S), Qin *et al*. [30] (Q) and Marinov *et al*. [28] (M) predict propane volume fractions of 0.41%, 0.44%, 0.28%, 0.23% and 0.1%, respectively. These values

are higher than the measured value of 0.02%. Again, the model of Marinov *et al*. [28] (M) fitted the experimental data the best.

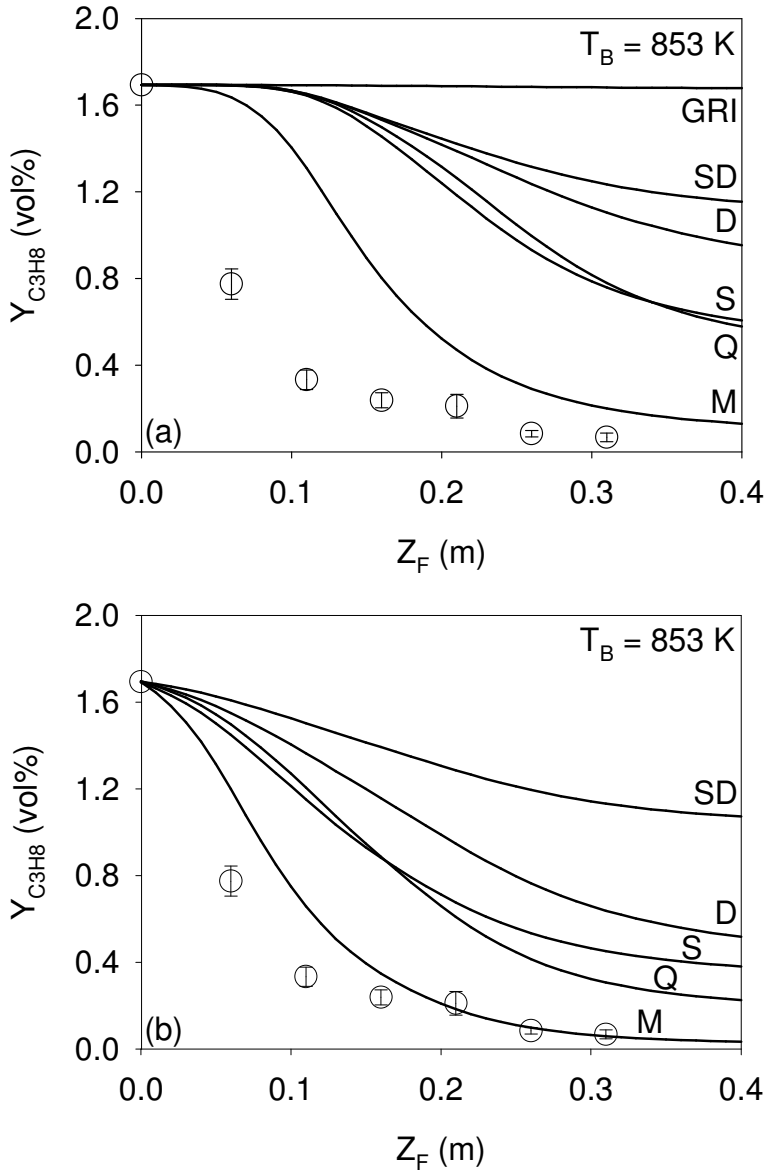

Figure 5-3: Experimental and predicted Y_{C3H8} axial profiles for T_B = 853 K and U_g = 0.17 m/s: (a) 1 PFR (freeboard) & (b) 2 PFRs in series (fluidized bed + freeboard)

(O: Experimental data, SD: San Diego [32], D: Dagaut *et al*. [29], S: Sung *et al*. [31], Q: Qin *et al*. [30], M: Marinov *et al*. [28])

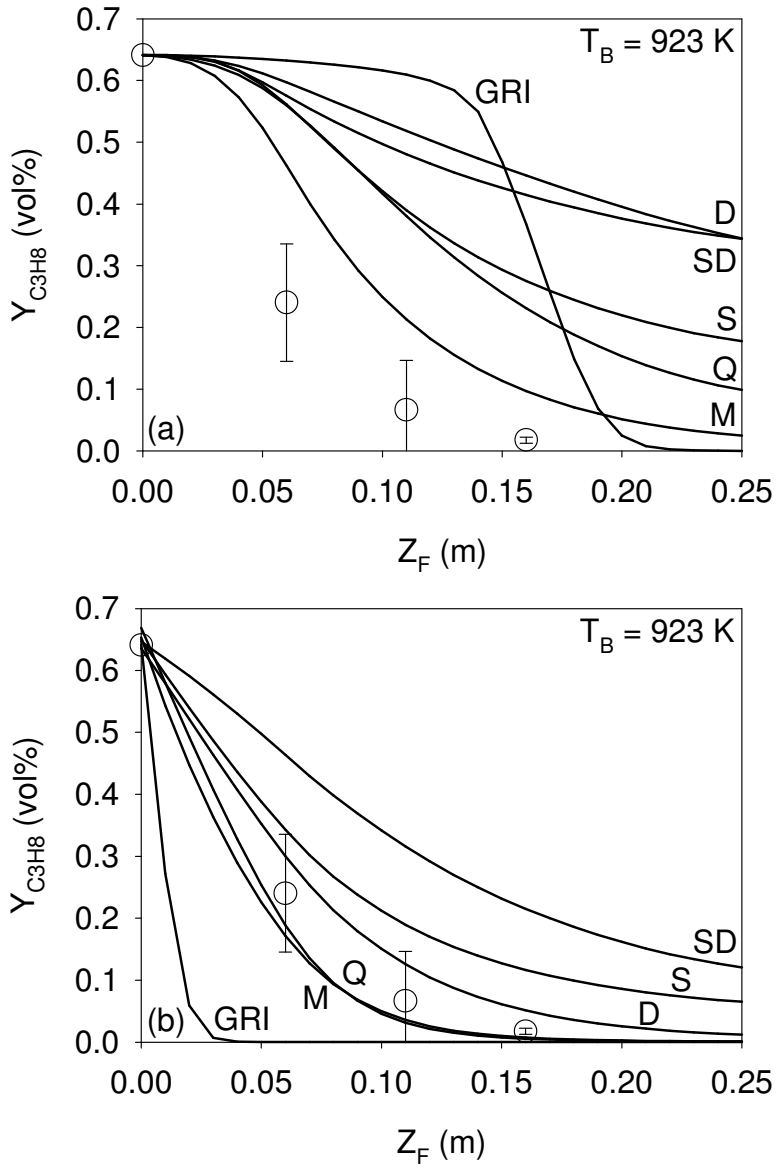

Figure 5-4: Experimental and predicted Y_{C3H8} axial profiles for T_B = 923 K and U_g = 0.17 m/s:

(a) 1 PFR (freeboard) & (b) 2 PFRs in series (fluidized bed + freeboard)

(O: Experimental data, SD: San Diego [32], D: Dagaut *et al*. [29], S: Sung *et al*. [31],

Q: Qin *et al*. [30], M: Marinov *et al*. [28])

The discrepancy between the predicted and measured Y_{C3H8} axial profiles could be due to: (1) the absence of important gas-phase reactions in the models, (2) the production of free radicals and intermediates upstream of the bed surface and/or (3) gas backmixing in the freeboard.

The possibility that important gas-phase reactions may not be included in the reaction model motivated the use of six different well established microkinetic schemes. These models contain state of the art chemistry networks. Furthermore, the models of Dagaut *et al*. [29] and Marinov *et al*. [28] have been validated at conditions (temperature, pressure and composition) similar to the ones used in the present study.

Since in-bed conversion was observed at the bed temperatures of 853 K and 923 K, free radicals and intermediates were produced upstream of the freeboard. These species may have been transported in sufficient amount into the freeboard to accelerate the reaction.

5.2.4.2.2 Accounting for upstream conversion

To model the in-bed conversion, one plug flow reactor was added upstream of the freeboard. It has been previously shown by Lorences *et al*. [38] that the gas-phase hydrodynamics in fluidized beds are very close to plug flow when $U_g \leq 6 \times U_{mf}$. The mixed-cup propane/air composition at the sparger tip was used as the inlet boundary conditions and the temperature was assumed constant at the bed temperature. This first reactor residence time was adjusted to match measured propane composition at the fluidized bed/freeboard interface. Therefore, the initial condition for the second reactor modeling the freeboard contained reactive intermediates produced in the first reactor.

Figure 5.3(b) shows the experimental and predicted Y_{C3H8} obtained with the six microkinetic mechanisms for a bed temperature of 853 K. With the GRI mechanism, a long induction time and no propane combustion was obtained within 0.4 m of the bed surface (not shown in Figure 5.3(b)). On the other hand, with the other five kinetic schemes, the onset of combustion

occurred earlier and immediately at the freeboard inlet. Furthermore, the reaction rate of propane and the total amount of propane consumed in the freeboard increased such that the calculated Y_{C3H8} axial profiles yielded a better fit of the experimental data. At $Z_F = 0.31$ m, the predicted Y_{C3H8} ranged from 1.13% (SD) to 0.06% (M) compared to the experimental measurement of 0.07%. The mechanism of Marinov *et al*. [28] yielded the best fit of the experimental data.

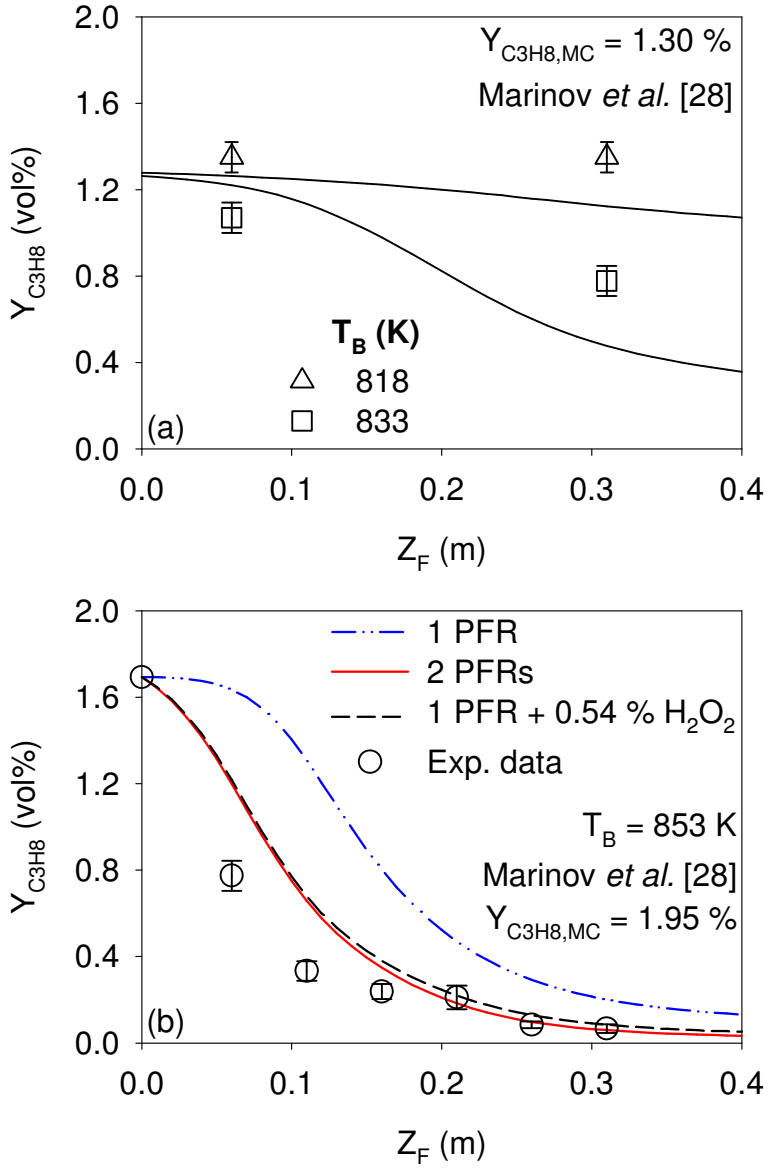

Figure 5-5: Performance of the mechanism of Marinov *et al*. [28] at low T_B (818 K and 830 K) and with the addition of H_2O_2

The addition of a PFR upstream of the freeboard also accelerated the propane combustion in the freeboard at a bed temperature of 923 K as shown in Figure 5.4(b). The 6 kinetic mechanisms predicted an onset of combustion at the bed surface ($Z_F = 0.0$ m) and faster propane combustion rates in the freeboard compared to Figure 5.4(a), which yielded a better fit between the calculated and experimental Y_{C3H8} axial profiles. At $Z_F = 0.16$, the predicted Y_{C3H8} ranged between 0.22% (SD) and 0.00% (GRI) compared to the measured value of 0.02%. The mechanisms of Marinov *et al*. [28] (M) and Qin *et al*. [30] gave the best fit of the experimental data.

The validity of the six microkinetic schemes can also be evaluated by comparing the gas residence time necessary in the fluidized bed (PFR) model to obtain the correct propane in-bed conversion with experimental value. The actual average gas residence time inside the fluidized bed can be estimated from the bed height (0.29 m), the superficial gas velocity at the bed temperature (0.17 m/s) the void fraction inside the bed. Furthermore, the void fraction can be calculated from the pressure drop across the bed (2.6 kPa), the solids density (2650 kg/m^{3}s) and the bed height (0.29 m). The average gas residence time inside the fluidized bed was estimated as of 1.1 s.

Table 5.1 lists the gas residence time in the fluidized bed (PFR) model that was necessary to obtain the correct propane conversion at the freeboard inlet for each microkinetic scheme. The GRI mechanism required gas residence times that were significantly higher than the estimated value, particularly at $T_B = 853$ K. The other mechanisms required gas residence time that were on the same order as the experimental value.

The propane freeboard conversion predicted by the mechanism of Marinov *et al*. [28] (M) also agreed well with measurements at bed temperatures of 818 K and 830 K. Figure 5.5(a) shows the experimental and predicted Y_{C3H8} axial profiles at these conditions. At $T_B = 833$ K, partial propane combustion occurred in the freeboard, which produced a significant temperature increase, as previously discussed and shown in Figure 5.2. On the other hand, a bed temperature

of 818 K did not produce combustion in the freeboard region. Marinov *et al*. [28] fits the experimental data well as combustion was predicted at T_B = 833 K. Furthermore, very little propane consumption was predicted at T_B = 818 K in agreement with the experiments. These simulations were performed by taking into account the in-bed conversion in the fluidized bed region. Furthermore, a fluid bed gas residence time of 1.2 second was used, which corresponds to the residence time used for the simulation at T_B = 853 K (see Table 5.1). The good agreement between the model of Marinov *et al*. [28] and the present experimental results may be explained by: (1) a higher number of species and elementary reactions that better reproduce the reaction and (2) the fact that the model was validated for conditions (pressure, temperature and mixture compositions) similar to the ones tested in the present study.

Table 5.1: Average gas residence time in fluidized bed

Microkinetic mechanism	**Details**	**τ_B (s)**	
		T_B = 853 K	**T_B = 923 K**
Dagaut *et al.* [29] (D)	50 species 274 elementary reactions	2.3	1.4
GRI v3 [33] (GRI)	53 species 325 elementary reactions	16.1	3.3
Marinov *et al*. [28] (M)	126 species 638 elementary reactions	1.2	0.6
Sung *et al*. [31] (S)	92 species 621 elementary reactions	1.9	1.0
San Diego [32] (SD)	46 species 235 elementary reactions	2.9	2.2
Qin *et al*. [30] (Q)	70 species 463 elementary reactions	2.2	1.0

A set of simulations were performed in order to identify the chemical species and/or free radicals produced in the fluid bed that were responsible for accelerating combustion in the freeboard:

chemical species were removed one-by-one from the inlet of the second PFR modeling the freeboard. Using this procedure, the reactive intermediates that had no influence on the freeboard combustion were gradually eliminated. Figure 5.5(b) shows the experimental and predicted axial profiles of Y_{C3H8} in the freeboard by the model of Marinov *et al*. [28] for the cases where:

1) Only the freeboard was modeled and in-bed combustion was not accounted for (1 PFR).
2) The fluidized bed was modeled with one PFR and the gas residence time was adjusted to obtain the correct in-bed propane conversion at the fluidized bed/freeboard interface. The inlet boundary condition of the second PFR (freeboard) contained all the reactive intermediates produced by the microkinetic models in the first reactor.
3) Only the freeboard was modeled and the H_2O_2 produced in the fluidized bed model of point (2) above was introduced at the freeboard inlet along with the propane/oxygen mixture.

Figure 5.5(b) shows that hydrogen peroxide produced upstream of the bed surface could account for most of the increased reaction rate in the freeboard. This was the case for all six microkinetic models used in this study. Hydrogen peroxide is known to be the main chain branching agent in the tested temperature range. These results suggest that the production of hydrogen peroxide in the fluidized bed region may promote combustion reactions in the freeboard for partial in-bed conversion conditions.

5.2.4.2.3 Gas backmixing in the freeboard

During the induction period, the initial hydrocarbon decomposition produces free radicals and intermediates that promote the overall reaction. In free radical systems, it is therefore possible that gas backmixing may lead to lower induction times and higher conversion rates compared to an ideal plug flow reactor. To characterize the freeboard region, a series of gas tracer experiments was conducted at ambient temperature over the bed surface at $Z_F \geq 0.16$ m: the gas-phase hydrodynamics was found to be plug flow. However, gas backmixing may occur closer to the bed surface and especially in the transport disengagement height (TDH) where solid particles are present (0.11 m – as shown in Figure 5.1). To investigate the effect of backmixing on propane conversion in the TDH, the latter was modeled as one perfectly mixed reactor: a lower conversion was obtained compared to the case of a plug flow reactor with all microkinetic

models. These results suggest that backmixing in the freeboard could not explain the discrepancy between predicted and measured Y_{C3H8} axial profiles.

5.2.5 Conclusions

Propane combustion experiments were performed in the freeboard region of a fluidized bed of inert sand particles at low bed temperatures ($818\ K \leq T_B \leq 923\ K$) and low gas superficial velocity ($U_g = 2.1 \times U_{mf}$). The freeboard region was characterized by simultaneous measurements of solids flux, chemical composition, temperature and pressure. Experiments showed that combustion in the freeboard occurred within 0.06 m of the bed surface for $T_B \geq 833$ K. In-bed conversion decreased with declining bed temperature and freeboard combustion resulted in a significant temperature increase. A reaction model was developed to predict propane induction time and reaction in the freeboard region. Six different gas-phase propane combustion microkinetic mechanisms were used and the predicted Y_{C3H8} axial profiles were compared to the experimental measurement – all six mechanisms predicted lower reaction rates compared to the experimental results. The models also predicted the production of H_2O_2 during the partial oxidation and decomposition of propane upstream of the freeboard, which is known as the main chain branching agent in the considered temperature range. The introduction of hydrogen peroxide at the inlet of the freeboard region in the simulations significantly accelerated the propane combustion rates and resulted in a better agreement between predicted and measured Y_{C3H8} axial profiles. These results suggest that autoignition and gas-phase combustion in the freeboard region can be promoted by the production of free radicals during reactions in the fluidized bed region. The model of Marinov *et al*. [28] yielded the best quantitative agreement with the experimental results among the considered microkinetic schemes.

5.2.6 Nomenclature

d_P	average particle size (μm)
G_{SU}	solids upward flux or entrainment flux (kg/m^2s)
r	radial position (m)

R	reaction radius (0.2 m)
τ_B	average gas residence time in fluidized bed (s)
T	temperature (K)
T_B	fluidized bed temperature (K)
U_g	superficial gas velocity (m/s)
U_{mf}	minimum fluidization velocity (m/s)
Y_i	volume fraction of species i (vol%)
Z	axial position (m)
Z_F	axial position in the freeboard (m)

5.2.7 References

[1]Botella P, López Nieto JM, Solsona B. Selective oxidation of propene to acrolein on Mo-Te mixed oxides catalysts prepared from ammonium telluromolybdates. J Mol Catal A-Chem 2002;184:335-347.

[2]Lorences MJ, Patience GS, Cenni R, Diez F, Coca J. VPO transient lattice oxygen contribution. Catal Today 2006; 112:45-48.

[3]Malleswara Rao TV, Deo G. Ethane and Propane Oxidation over Supported V2O5/TiO2 Catalysts: Analysis of Kinetic Parameters. Ind Eng Chem Res 2007;46:70-79.

[4]Hutchenson KW, La Marca C, Patience GS, Laviolette J-P, Bockrath RE. Parametric study of butane oxidation in a circulating fluidized bed reactor. Submitted to Appl Catal A-Gen 2009.

[5]Van der Vaart DR. The chemistry of premixed hydrocarbon/air combustion in a fluidized bed. Fuel 1988;67:1003-1007.

[6]Van der Vaart DR. Freeboard ignition of premixed hydrocarbon gas in a fluidized bed. Combust Flame 1988;71:35-39.

[7]Brokaw RS, Jackson JL. Effect of temperature, pressure, and composition on ignition delays for propane flames. P 5th Combust Inst 1955:563-569.

[8]Chang CJ, Thompson AL, Winship RD. Ignition delay of propane in air between 725-880^{o}C under isothermal conditions. P 7th Combust Inst 1959:431-435.

[9]Burcat A, Lifshitz A. Shock-tube investigation of ignition in propane-oxygen-argon mixtures. P Combust Inst 1971: 745-755.

[10]Burcat A, Scheller K, Lifshitz A. Shock-tube investigation of comparative ignition delay times for C1-C5 alkanes. Combust Flame 1971;16:29-33.

[11]Cathonnet M, Boettner JC, James H. Experimental study and numerical modeling of high temperature oxidation of propane and n-butane. P 18th Combust Inst 1981:903-913.

[12]Kin K, Soo Shin K. Shock tube and modeling study of the ignition of propane. Bull Korean Chem Soc 2001;22(3):303-307.

[13]Penyazkov OG, Ragotner KA, Dean AJ, Varatharajan B. Autoignition of propane-air mixtures behind reflected shock waves. P Combust Inst 2005;30:1941-1947.

[14]Horning DC, Davidson DF, Hanson RK. Study of the high-temperature autoignition of n-alkane/O2/Ar mixtures. J Propul Power 2002;18(2):363-371.

[15]Zhukov VP, Sechenov VA, Starikovskii. Autoignition of a lean propane-air mixture at high pressures. Kinet Catal 2005;46(3):319-327.

[16]Freeman G, Lefebvre AH. Spontaneous ignition characteristics of gaseous hydrocarbon-air mixtures. Combust Flame 1984;58:153-162.

[17]Cadman P, Thomas GO, Butler P. The auto-ignition of propane at intermediate temperature and high pressures. Phys Chem Chem Phys 2000;2:5411-5419.

[18]Hesketh RP, Davidson JF. Combustion of methane and propane in an incipiently fluidized bed. Combust Flame 1991;85:449-467.

[19]Wen CY, Chen LH. Fluidized bed freeboard phenomena: entrainment and elutriation. AIChE J 1982;28(1):117-128.

[20]Kunii D, Levenspiel O. Entrainment of solids from fluidized beds I.Hold-up of solids in the freeboard II.Operation of fast fluidized bed. Powder Technol 1990;61:193-206.

[21]De Lasa HI, Grace JR. The influence of the freeboard region in a fluidized bed catalytic cracking regenerator. AIChE J 1979;25(6):984-991.

[22]Chen LH, Wen CY. Model of solid gas reaction phenomena in the fluidized bed freeboard. AiChEJ 1982;28(6):1019-1027.

[23]Walsh PM, Chaung TZ, Dutta A, Beér JM, Srofim AF. Particle entrainment and nitric oxide reduction in the freeboard of a fluidized coal combustor. ACS Fuels Volumes 1982;27(1):243-261.

[24]Sotudeh-Gharebagh R, Mostoufi N. Simulation of a catalytic turbulent fluidized bed reactor using the sequential modular approach. Fuel Process Technol 2003;85:189-200.

[25]Dounit S, Hemati M, Andreux R. Modeling and experimental validation of a fluidized-bed reactor freeboard region: application to natural gas combustion. Chem Eng J 2008;140:457-465.

[26]Hartman M, Trnk O, Pohořelý, Svoboda K. High-temperature reaction in the freeboard region above a bubbling fluidized bed. Ind Eng Chem Res 2010;XX:XX.

[27]Buda F, Glaude PA, Battin-Leclerc F, Porter R, Hughes KJ, Griffiths JF. Use of detailed kinetic mechanisms for the prediction of autoignitions. J Loss Prevent Proc 2006;19:227-232.

[28]Marinov NM, Pitz WJ, Westbrook CK, Hori M, Matsunaga N. An experimental and kinetic calculation of the promotion effect of hydrocarbons on the NO-NO2 conversion in a flow reactor. P Combust Inst 1998;27: 389-396.

[29]Dagaut P, Cathonnet M, Boettner JC, Gaillard F. Kinetic oxidation of propane oxidation. Combust Sci Technol 1987;56:23-63.

[30]Qin Z, Lissianski VV, Yang H, Gardiner Jr WC, Davis SG, Wang H, Combustion chemistry of propane: a case study of detailed reaction mechanism optimization. P Combust Inst 2000; 28:1663–1669.

[31]Sung CJ, Li B, Law CK, Wang H. Structure and sooting limits in counterflow methane/air and propane/air diffusion flames from 1 to 5 atmospheres, 27th Symp (Intl) Combust. 1998:1523-1530.

[32]Chemical-Kinetic Mechanisms for Combustion Applications, San Diego Mechanism web page, Mechanical and Aerospace Engineering (Combustion Research), University of California at San Diego. (http://maeweb.ucsd.edu/~combustion/cermech/)

[33]Smith GP, Golden DM, Frenklach M, Moriarty NW, Eiteneer B, Goldenberg M, Bowman CT, Hanson RK, Song S, Gardiner Jr WC, Lissianski VV, Qin Z. http://www.me.berkeley.edu/gri_mech/

[34]Jeng R-H, Altwicker ER, Morgan III MM, Wilk RD. Propane combustion in a spouted bed combustor II: a modeling study in the bed region. Combust Sci Technol 2001;170:119-149.

[35]Sotudeh-Gharebagh R, Chaouki J. The heterogeneous and homogeneous combustion of methane over inert particles. Can J Chem Eng 2003;81:1182-1191.

[36]Ranzi E, Faravelli T, Gaffuri P, Pennati GC, Sogaro A. A wide range modeling study of propane and n-butane oxidation. Combust Sci Technol 1994;100:299-330.

[37]Wilk RD, Cernansky NP, Cohen RS. The oxidation of propane at low and transition temperatures. Combust Sci Technol 1986;49:41-78.

[38]Lorences M, Laviolette J-P. Fluid bad gas RTD: effect of fines and internals. Powder Technol 2006; 168 (1): 1-9.

CHAPITRE 6 NOUVELLE MÉTHODE DE SPECTROSCOPIE POUR LA MESURE SIMULTANÉE ET QUANTITATIVE DE LA COMPOSITION CHIMIQUE DE LA PHASE GAZEUSE ET DE LA FRACTION DE SOLIDES

Cet article a été accepté par *AIChE journal* en 2010. L'article est présentement publié en ligne. Un brevet sur la méthode de mesure décrite dans cet article a été déposé aux États-Unis. La confirmation du dépôt du brevet est présentée à l'annexe 9.

6.1 PRÉSENTATION DE L'ARTICLE

L'objectif de cet article est de développer une nouvelle méthode spectroscopique pour la mesure simultanée et quantitative de la fraction de solides et de la composition chimique de la phase gazeuse. La méthode est utilisée avec une sonde à fibres optiques infrarouges afin d'effectuer des mesures in situ et en ligne dans des systèmes gaz/solides. Les résultats démontrent que les valeurs d'absorbance résultantes de la fraction de solides et de la composition chimique sont additives. Des mesures instantanées sont effectuées à une fréquence atteignant 4.5 Hz avec une précision considérable (erreur relative maximale d'environ 5% sur les mesures moyennées dans le temps). Des mesures sont effectuées dans un lit fluidisé afin de mesurer la fraction volumétrique d'un traceur gazeux dans la phase bulle et la phase émulsion.

SIMULTANEOUS QUANTITATIVE MEASUREMENT OF GASEOUS SPECIES COMPOSITION AND SOLIDS VOLUME FRACTION IN A GAS/SOLID FLOW

Jean-Philippe Laviolette, Gregory S. Patience and Jamal Chaouki

(Published in AIChE Journal, 2010)

6.2 SIMULTANEOUS QUANTITATIVE MEASUREMENT OF GASEOUS SPECIES COMPOSITION AND SOLIDS VOLUME FRACTION IN A GAS/SOLID FLOW

A novel spectroscopic method was developed to measure quantitatively and simultaneously solids volume fraction (1-ε) and gaseous species composition (Y_i) in a gas/solid system. The method was comprised of an FT-IR coupled to a fibre-optic probe that could perform real-time and in-situ measurements of absorbance. The effect of (1-ε) and Y_i on the absorbance spectra were additive and could be independently calibrated. Experiments were conducted with alkane/nitrogen mixtures and two types of particles: sand and FCC. Fuel mole fractions and (1-ε) were varied between 1.8 - 10.1 mol% and 0 - 0.45, respectively. The relative errors for Y_i time-averaged measurements were below 6% and the error increased significantly with decreasing beam intensity. A proof of concept for a novel application in fluidized beds was also completed: the fibre-optic probe was used to measure the molar fraction of a tracer gas inside the emulsion and bubble phases during gas tracer experiments.

6.2.1 Introduction

Multiphase processes are common to many industries: petrochemical, chemical, pharmaceutical, energy, food, pulp and paper, etc. They are also present throughout the process chain: energy generation (combustors), transformation (gasifiers, chemical reactors, mixers and dryers), purification/separation (cyclones and precipitators) and waste disposal (chimneys). System characterization through the measurement of species composition and solids volume fraction is critical for process control, optimization and trouble-shooting in the industries and laboratories. It is also essential for the development of hydrodynamic (gas/liquid/solid) and kinetic models.

Chemical species composition and solid volume fraction are currently measured independently with two different techniques.

Several non-invasive and invasive techniques have been developed to measure solids volume fraction in two- and three-phase systems. Invasive techniques involve the insertion of probes to measure the local capacitance [1, 2, 3], conductivity [4, 5, 6], fluorescence [7], forward-scattering [8] or back-scattering of light in the medium [2, 9, 10, 11]. The solids volume fraction is derived from the measurement, which can be made in-situ and in real-time. In liquid/solid or gas/liquid/solid systems, the slurry phase can also be sampled with special probes to measure the liquid and solids volume fraction [7, 12]. Non-invasive techniques include tomography [13, 14, 15, 16], densitometry [11] and the analysis of ultrasonic wave distortions [17]. These techniques produce time- or space-averaged maps solids volume fraction in multiphase systems with varying resolution.

Species concentrations in the gas or liquid phases can be analyzed continuously or intermittently [12] with analytical instruments (chromatograph, spectrometer, etc.) via sampling. Furthermore, in the context of the U.S. Food and Drug Administration (FDA) process analytical technology (PAT) initiative, several publications have reported the development of infrared applications for the measurement of chemical species composition in multiphase samples [18, 19]. Similar applications have also been developed for the in-situ monitoring of reactions at the surface of catalysts [20, 21]. These systems function in transmission and diffuse reflectance modes (on the solid surface) and can measure species composition the continuous phases (liquid and gas) as well as characterizing qualitatively the chemical composition of the discrete phase (solid particles and liquid droplets) [22, 23, 24, 25, 26]. All these techniques measure species concentrations in the continuous phase as a spatial average between the different regions of varying solids volume fractions (bubble and emulsion phases in fluidized bed, for example).

A technique that measures species composition and solids volume fraction simultaneously yields much more information into multiphase processes since solids volume fraction and species concentrations are dependent parameters. These two parameters are coupled through the reaction

kinetics and the hydrodynamics. During reaction, solids volume fraction influences chemical reactions through heterogeneous catalytic and/or inhibitive effects as well as through the thermal balance. Furthermore, at the hydrodynamic level, multiphase systems are often characterized by different regions of varying void fraction and the species composition in these regions are fundamental to the process characterization. For example, bubbling and turbulent gas/solid fluidized beds are characterized by a dense phase (emulsion) and a dilute phase (bubbles). Bubbles cause gas by-passing that lowers the process yield. The simultaneous measurement of solids volume fraction and gaseous species composition discriminates between the reactants in the dilute and dense phases and this measurement can hardly be made with existing methods.

Infrared (IR) spectroscopy offers a great potential for the simultaneous measurement of solids volume fraction and gaseous species composition. IR spectroscopic applications in multiphase systems are affected by the solid phase characteristics. The solids volume fraction and particle size have been shown to influence the interaction between the light and the solids, which affect the path length of the IR beam and the effective sample size [20, 23]. An increase in particle size has been reported to decrease the fraction of scattered light and to increase penetration depth of light into the solid particles, resulting in increased absorbance and an upward shift of the absorbance baseline in diffuse reflectance spectroscopy [23]. Therefore, current IR spectroscopic applications in multiphase system rely on the uniformity of the solid samples with time (between measurements). This is achieved by performing the spectral acquisition in immobile samples such as solid tablets [25, 27, 28, 29, 30]. On the other hand, measurements in dynamic systems (fluidized beds or mixers, for example) require shutdown prior to the spectral acquisition [31, 32], the synchronization of the spectral acquisition to a specific vessel position [33] or measurement in regions of high solids density [34]. Non-intrusive NIR monitoring of powder blend homogeneity has also been conducted in symmetrical mixers to ensure the temporal uniformity of the solids volume fraction when complete mixing is reached [35]. Finally, mathematical treatments of the spectra, such as the derivative treatment, are often used to minimize the effects of baseline shifts due to changes in the solid phase properties [23]. However, multiphase systems are generally characterized by solids volume fractions that are heterogeneous in space and time. Therefore, the in-situ and real-time measurement of species concentrations in the different regions of a multiphase system requires the simultaneous determination of solids

volume fraction. The measurement volume can be made independent of the solid properties by inclining the emitting and receiving fibres to form a convergent scheme [36]. This principle can be applied to an IR fibre-optic probe to measure species concentrations.

In multiphase systems, the movement of powders makes spectroscopy measurements and interpretation more complex. The measured absorbance spectra are influenced by variations in the solids volume fraction and the average distance from the sample to the probe. When samples are moving, different parts of the spectrum may also be influenced to a varying degree by local heterogeneities (different material components). The effects of moving particles on Fourier-Transform spectroscopy have been investigated by De Paepe *et al*. [37], Berntsson *et al.* [38] and Andersson *et al*. [39]. It was shown that the movement of the particles produced artefacts on the measured spectrum at certain wavenumbers that depended on the timescale of the spectral scan compared to the rate of movement of the particles. The wavenumber at which the artefact appeared increased with increasing modulation frequencies such that the effects of moving particles could be completely eliminated at the wavenumbers of interest with a sufficiently high modulation frequency.

In the present study, a novel spectroscopic method was developed for the simultaneous and quantitative measurement of gaseous species composition (Y_i) and solids volume fraction ($1-\varepsilon$). Experiments were conducted using near- and mid-IR Fourier transform transmission spectroscopy (6000-1000 cm^{-1}). A fibre-optic probe was constructed to perform in-situ and real-time measurements in a gas/solid flow of methane/nitrogen and silica sand particles (d_p = 290 μm). Absorbance spectra were recorded at a frequency of 4.5 Hz for a period of 75 seconds and both Y_i and ($1-\varepsilon$) were evaluated from each spectrum. Methane molar fractions in nitrogen were measured over a range of 0-10.1 vol%. Furthermore, the solids volume fraction was varied between 0-0.1. The fibre-optic probe was also used inside a fluidized bed of FCC catalyst during gas tracer experiments to measure the tracer (CH_4) molar fraction inside the bubble and emulsion phases (($1-\varepsilon$) = 0.45).

6.2.2 Experimental

Experiments were conducted with an FT-IR (Varian Excalibur series 3100) equipped with a high sensitivity mercury-cadmium-telluride (MCT) detector cooled with liquid nitrogen. In a first series of tests, the FT-IR was used with a gas flow cell located in its sample compartment as shown in Figure 6.1. The IR beam coming from the interferometer was transmitted through the gas flow cell and the absorbance spectrum was measured by the MCT detector. Prior to each experiment, a background spectrum was measured by flushing the gas flow cell with air and by co-adding 20 spectra. Then, a gas/solid system was simulated in the FT-IR sample compartment by injecting a mixture containing 1.8 vol% C_3H_8 in air inside the gas flow cell and by placing a metal mesh (open area ratio of 16% and thickness of 1 mm) in the path of the IR beam.

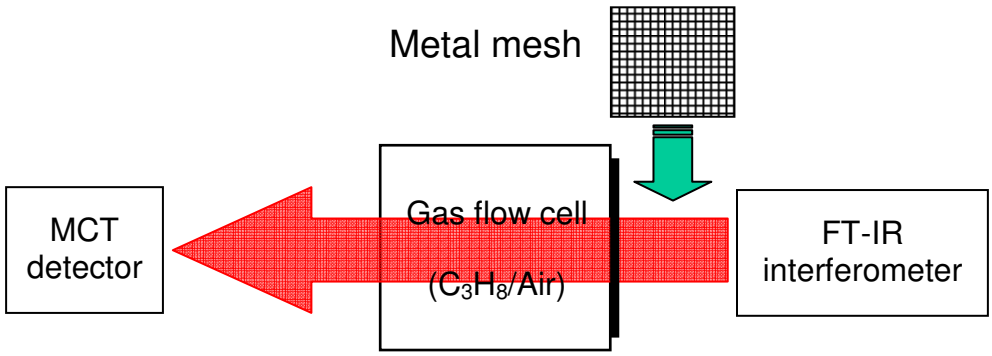

Figure 6-1: FT-IR apparatus

A second series of experiments were performed with a mid-IR fibre-optic probe. In-situ measurements of gaseous species composition and solids volume fraction were conducted inside a gas/solid flow of CH_4/N_2 mixtures and silica sand particles (d_p = 290 µm). A schematic of the apparatus is shown in Figure 2. The probe was composed of two parallel fluoride glass fibre-optics (an emitting and a receiving fibre-optic) with a numerical aperture of 0.2 and a core diameter of 600 µm. The fibre-optic probe was connected to the FT-IR with a Harrick Fibremate™. A planar gold-coated mirror was positioned perpendicularly to the probe tip at a distance of 5 mm. The mirror reflected the emitted IR beam to the receiving fibre-optic, which resulted in a measurement volume between the probe tip and the mirror as shown in grey on Figure 6.2. Experiments were conducted by first measuring a background spectrum - a CH_4/N_2

mixture was injected inside the measurement and a background spectrum was obtained from the co-addition of 20 spectra. Then, the measurement volume was flushed with air and the funnel was filled with sand particles to initiate a flow of solids. Absorbance spectra were measured at a frequency of 4.5 Hz (temporal resolution of 0.22 s) and the methane molar fraction was measured simultaneously to the solids volume fraction. The flow of solid particles was varied by changing the diameter of the funnel diameter at its throat. The corresponding solids volume fraction for each throat diameter was measured with a conventional back-scattering fibre-optic probe between the IR probe and the mirror. Four solids volume fractions were used: 0, 0.015, 0.038 and 0.097. Furthermore, four different CH_4/N_2 compositions were injected from calibrated gas cylinder in the measurement volume: 0, 0.1, 3.25 and 10.1 vol%.

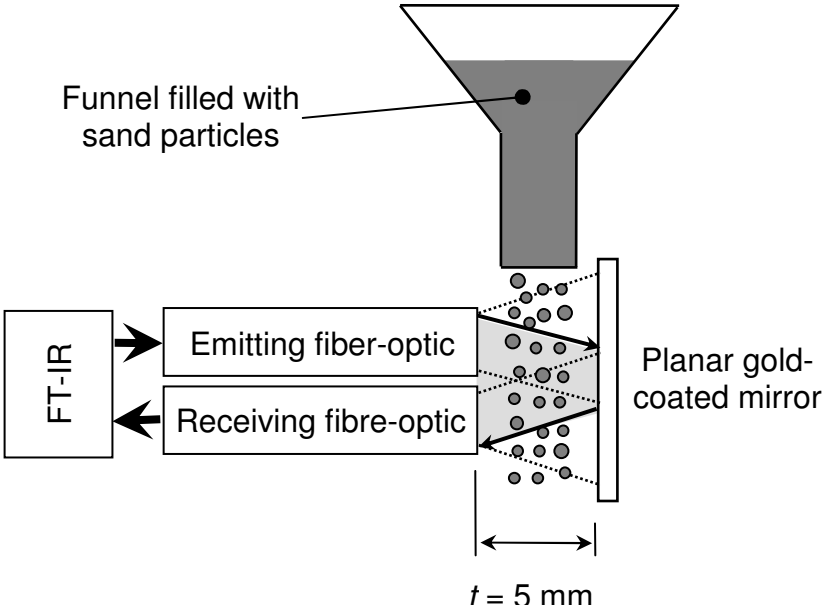

Figure 6-2: Fibre-optic probe apparatus

Gas tracer experiments were also conducted in a small scale fluidized bed reactor (I.D. = 5 cm) illustrated in Figure 6.3 and the fibre-optic probe was used to measure the tracer molar fraction inside the bubble and emulsion phases. The reactor was filled with FCC particles (d_p = 83 μm and 14% fines ($d_p \leq 44$ μm)) and was fluidized with nitrogen at a superficial gas velocity of 2.6 mm/s (U_{mf} = 2.5 mm/s and U_{mb} = 2.7 mm/s). The expanded bed height was 12.5 cm and the fibre-optic probe was inserted in the bed at a height of 7 cm. A mirror was positioned

perpendicularly at the probe tip and gas bubbles were produced in the fibre-optic probe measurement volume by injecting a mixture containing 10.1% CH_4 + 89.9% N_2 through a downward facing sparger. The CH_4/N_2 mixture was injected at a flow rate of 10 mL/s by manually opening a toggle valve for roughly 0.5 s at an interval of approximately 11 seconds.

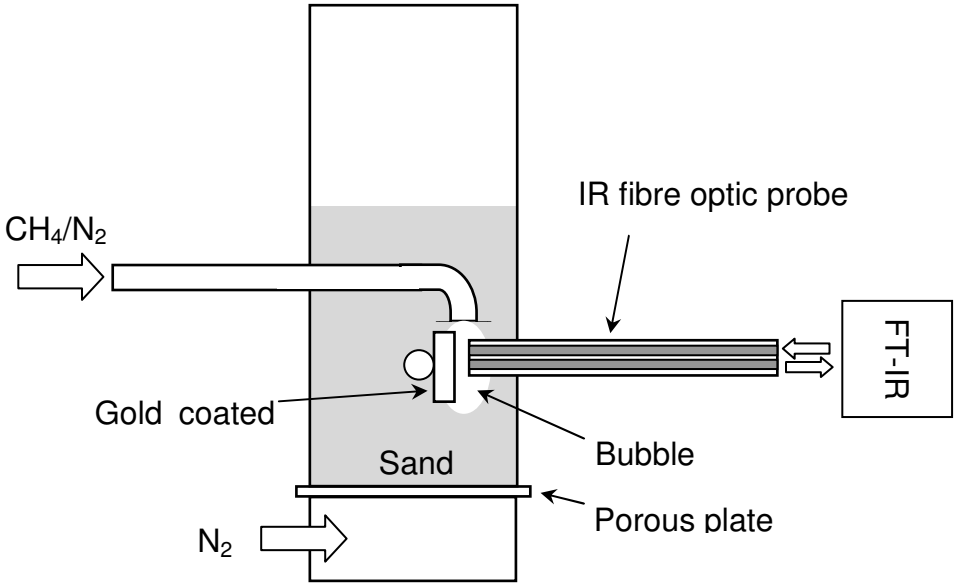

Figure 6-3: Fluidized bed reactor

6.2.3 Results and discussion

During transmission spectroscopy in a gas/solid sample, both solid particles and gaseous species contribute to the absorbance spectrum according to equation (6.1): the total absorbance at wavelength λ has a contribution from the solids volume fraction and from the gaseous species composition. Solid particles reduce the incident beam intensity by absorption, reflection and diffusion. Solids can also influence the path length and sample volume such that the absorbance due to the chemical species is a function of solids volume fraction.

$$A_{Total,\lambda} = A_{(1-\varepsilon),\lambda} + A_{Y_i,\lambda}\left[fn(1-\varepsilon)\right] \tag{6.1}$$

In the specific case of transmission spectroscopy where the effect of solids fraction on path length and sample volume can be neglected, equation (6.1) can be simplified to:

$$A_{Total,\,\lambda} = A_{(1-\varepsilon),\,\lambda} + A_{Y_i,\,\lambda} \tag{6.2}$$

Equation (6.2) is valid when the reflected or diffused beam intensity measured is negligible compared to the transmitted light intensity. In equation (6.2), the effects of solids volume fraction and gaseous species composition on the absorbance spectrum are independent. Therefore, the effect of $(1-\varepsilon)$ and Y_i can be calibrated independently.

6.2.3.1 Experiments with the FT-IR

A first series of experiments were conducted with the FT-IR of Figure 6.1. A background spectrum of air was taken and 4 absorbance spectra were subsequently measured for the following conditions:

- Air and $(1-\varepsilon) = 0$ (Figure 6.4a)
- Air and $(1-\varepsilon) = 0.84$ (Figure 6.4b)
- 1.8% C_3H_8 + 98.2% air and $(1-\varepsilon) = 0$ (Figure 6.4c)
- 1.8% C_3H_8 + 98.2% air and $(1-\varepsilon) = 0.84$ (Figure 6.4d)

Figure 6.4a shows the absorbance spectrum of air, which corresponded to the background absorbance spectrum and resulted in a baseline of zero absorbance. Two calibration absorbance spectra were measured to independently evaluate the effect of the propane molar fraction and the solids volume fraction. The absorbance spectrum for air and a solids volume fraction of 0.84 is shown in Figure 6.4b - the baseline absorbance increased almost uniformly across the spectrum from to 0 to a higher absorbance. The average baseline absorbance was 0.77 in the region of 3436.90-3427.98 cm^{-1}. This specific range of wavenumbers (3436.90-3427.98 cm^{-1}) was chosen to evaluate the average baseline absorbance since it was characterized by a good signal-to-noise ratio and since it was not absorbed by propane. The second calibration spectrum was obtained by

injecting a mixture of 1.8% C_3H_8 in air inside the gas flow cell and by removing the metal mesh from the sample compartment. The injection of C_3H_8 resulted in the formation of two absorbance peaks at 2967.96 and 1471.68 cm^{-1}, as illustrated in Figure 6.4c. The average peak height of the tallest peak (at 2967.96 cm^{-1}) was measured as 0.92 in the region of 2969.65-2966.27 cm^{-1}.

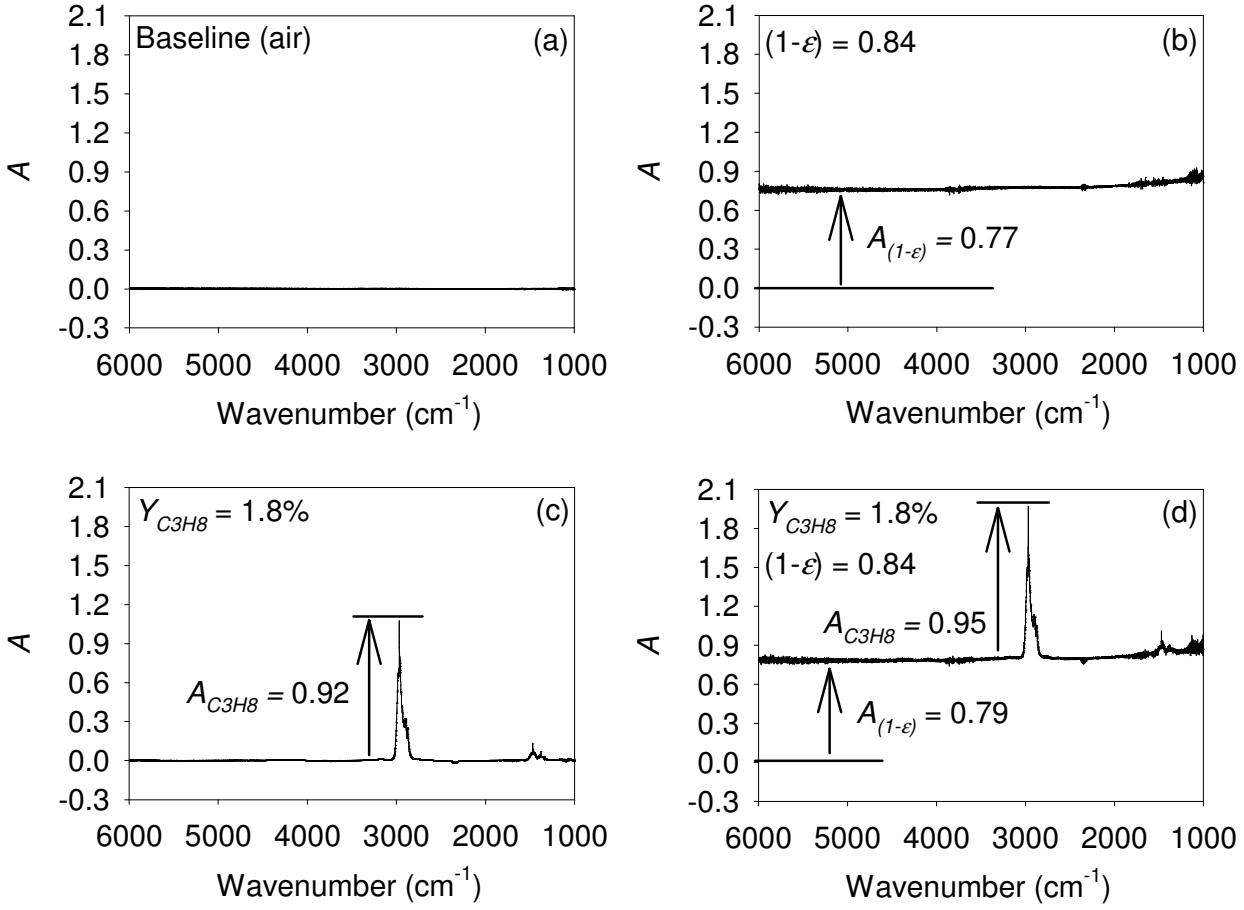

Figure 6-4: Simultaneous measurement of Y_{C3H8} and (1-ε)

Finally, the propane concentration and the solids volume fraction were measured simultaneously. The mixture of 1.8% C_3H_8 was injected inside the gas flow cell and the metal mesh was inserted inside the sample compartment. The resulting absorbance spectrum corresponded to the addition of both calibration spectra as observed in Figure 6.4d: the baseline absorbance was 0.79 (compared to 0.77) and the average C_3H_8 peak height above the baseline was 0.95 (compared to

0.92). Therefore, the propane concentration and solids volume fraction were measured simultaneously with a relative error of approximately 3% if a linear relation between absorbance and the two parameters is assumed. Equation (6.2) was valid in that particular case since the metal mesh had no appreciable influence on the path length of the IR beam – the path length was defined by the width of the sample compartment.

6.2.3.2 Experiments with the fibre-optic probe

A fibre-optic probe was built to conduct in-situ measurements of solids volume fraction and species concentrations inside a flow of silica sand particles. Using the fibre-optic probe resulted in a significant loss in IR beam intensity, which occurred most likely at the probe tip. However, some signal loss probably occurred at the FT-IR/probe interface (Harrick Fibremate™) as well. Designing a system to yield a sufficiently intense transmitted IR beam was a challenge. The first fibre-optic probe prototype was built with two fibre-optics with a core diameter of 300 μm and no IR signal was ever measured by the FT-IR. The feasibility of using a more powerful external IR source was examined, but the coupling of the IR beam with the FT-IR interferometer proved to be particularly complex and yielded a significant risk of reducing the IR beam intensity below that of the internal FT-IR source. The installation of an external source was therefore abandoned. The construction of a new probe with core diameters of 600 μm and a complete re-alignment of the FT-IR increased the transmitted IR beam intensity sufficiently to perform the current experiments.

Another means of increasing the IR signal intensity consisted of installing a more sensitive detector. Indium antimonide (InSb) detectors can offer higher signal-to-noise ratios compared to MCT detectors at the wavenumbers of interest in the present study and an InSb detector was therefore tested. However, the selected InSb detector functioned at relatively low modulation frequencies (5-10 kHz) compared to the MCT detector (5-80 kHz) and this proved to be problematic in gas/solid systems where particles are moving. Particle movement produced artefacts (noise) in the interferograms and absorbance spectra and an initial analysis was performed to eliminate the artefacts from the wavenumbers of interest.

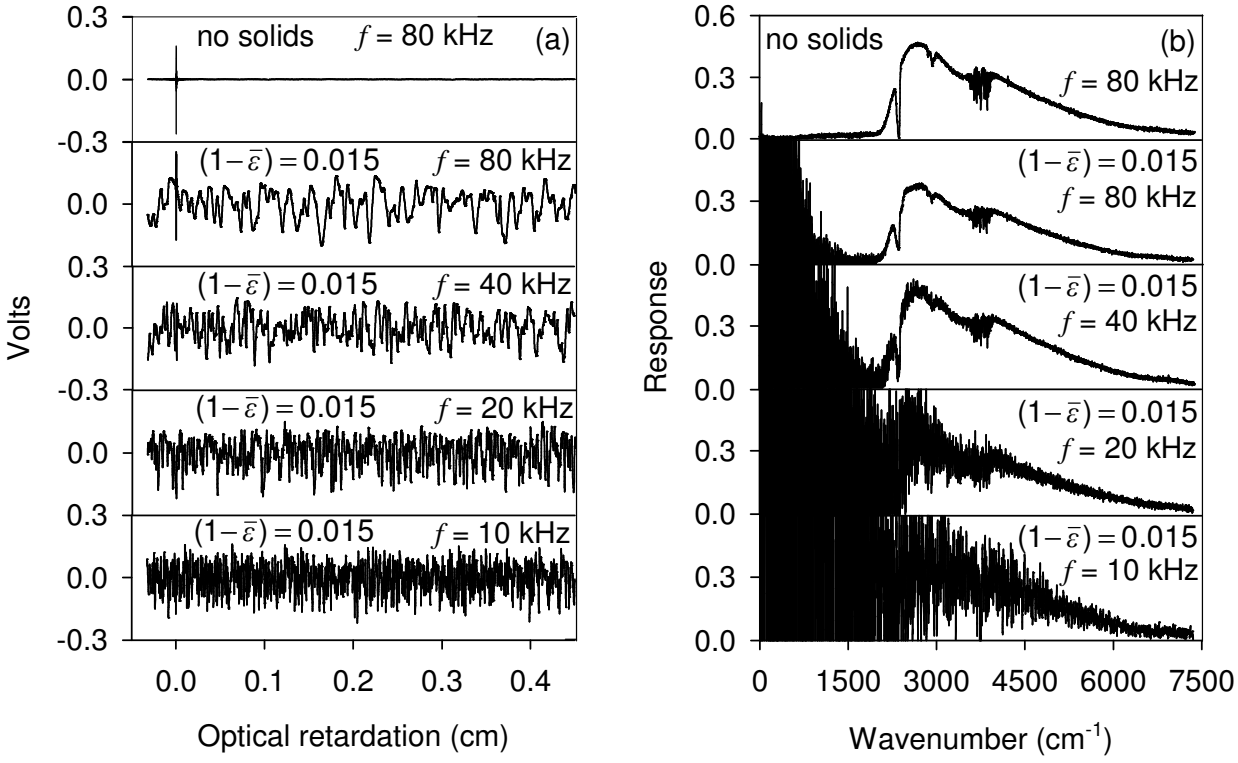

Figure 6-5: Effect of particle movement:

(a) typical interferograms for moving particles [(1- $\bar{\varepsilon}$) = 0.015];

(b) corresponding single-beam spectra

6.2.3.2.1 Effect of particle movement

Figure 6.5(a) shows typical interferograms measured with the fibre-optic probe in air at different modulation frequencies and two solids volume fractions. In the absence of solid particles, the interferogram was characterized by a centreburst at an optical retardation of 0 cm and a signal decay at higher retardation. With a flow of solids in the probe measurement volume that corresponded to a time-average solids volume fraction (1- $\bar{\varepsilon}$) of 0.015, fluctuations in the signal appeared. The number of fluctuations decreased as the modulation frequency (*f*) was increased from 10 to 80 kHz. Figure 6.5(b) shows the corresponding single-beam spectra. In the absence of solid particles, the spectrum was characterized by a reasonably high signal-to-noise ratio (S/N) over the entire spectrum. However, with a flow of solids and (1- $\bar{\varepsilon}$) = 0.015, noise was observed

in the regions of low wavenumber (high wavelength and low frequency). The noise was produced by temporal variations in transmitted IR beam intensity due to heterogeneities in the gas/solid flow. As the modulation frequency was increased from 10 to 80 kHz, the noise moved to lower wavenumbers (higher wavelengths and lower frequencies). The modulation frequency corresponds to the number of displacements of 632.8 nm (equal to the laser wavelength) the moving mirror makes in 1 second in the interferometer. As the mirror speed was increased, a growing number of wavenumbers were modulated to frequencies that were significantly higher than the frequency at which the moving silica particles changed the transmitted IR beam intensity. At high wavenumbers (high frequency), the signal amplitude remained largely unaffected by the movement of particles. At a modulation frequency of 80 kHz, the artefacts were outside the wavenumber range of interest (2700-3300 cm^{-1}) and all experiments were therefore performed with this setting. Tests were also performed at higher solids volume fractions with no significant effect on the location of the fluctuations observed in the spectra.

6.2.3.2.2 Simultaneous measurement of methane concentration and solids volume fraction

The fibre-optic probe was used to measure in-situ absorbance spectra across the flow of sand particles. IR spectroscopy is based on the ratio of the background and the measured spectra. Experimentally, it was simpler to measure a background spectrum with a mixture of CH_4/N_2 (without solid particles) and conduct the experiments with a flow of particles in air such that negative CH_4 absorbance peaks were obtained. However, the methane molar fractions are reported as positive values in the present document. The results were unaffected by this procedure since the IR path length and measurement volume were independent of the solids volume fraction. When the mirror was removed from the tip of the probe, the signal amplitude measured by the MCT detector was zero. Therefore, the IR beam collected by the receiving fibre-optic did not have any contribution from diffuse reflectance on the solids surface and the probe measurement volume was only defined by the mirror position. Furthermore, the effects of methane concentration and solids volume fraction on the absorbance spectrum were independent.

A calibration was first performed with the fibre-optic probe to evaluate the effect of methane molar fraction and solids volume fraction on the absorbance spectrum. The effect of methane

molar fraction (Y_{CH4}) was calibrated with four mixtures containing 0, 0.1, 3.25 and 10.1 vol% of methane in nitrogen. The apex of the methane peak (A_{CH4}) was located at a wavenumber of 3017.63 cm^{-1} and its average absorbance was measured in the region of 3018.96-3016.86 cm^{-1}. The average absorbance in the region of 3018.96-3016.86 cm^{-1} is shown as a function of methane molar fraction in Figure 6.6(a). The relationship between absorbance and Y_{CH4} was non-linear, but such a deviation from the Beer Law is common in infrared spectroscopy [40].

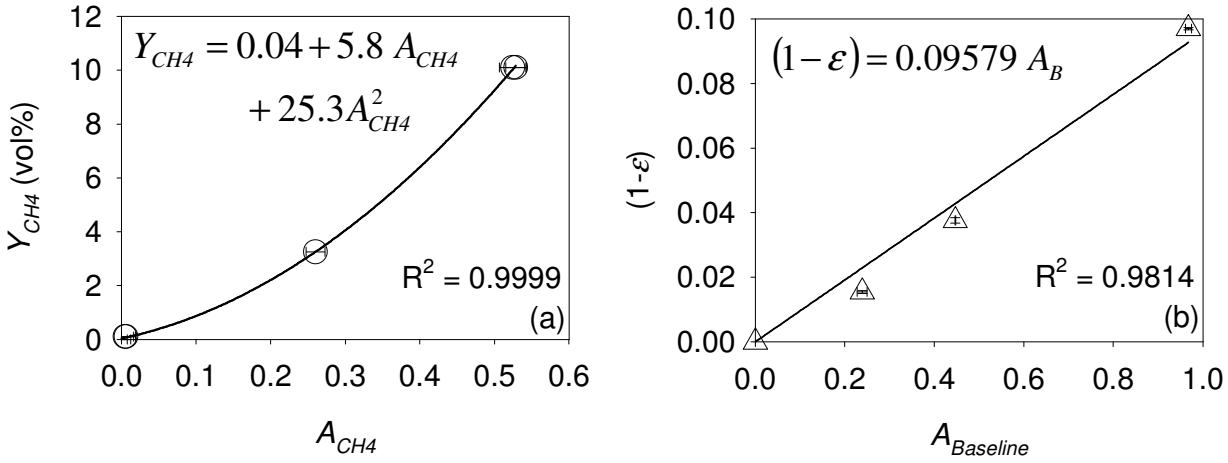

Figure 6-6: Probe calibration

The effect of solids volume fraction was calibrated by varying the solids flow in the fibre-optic measurement volume. Four solids volume fractions were used (0, 0.015, 0.038 and 0.097) and the average baseline absorbance ($A_{(1-\varepsilon)}$) was measured in the regions of 2997.73-2992.04, 3036.70-3030.72 and 3045.87-3040.39 cm^{-1} during 75 seconds at a frequency of 4.5 Hz. This range of wavenumbers was chosen to evaluate the average baseline absorbance since it was characterized by a good signal-to-noise ratio and since it was not absorbed by methane. Figure 6.7 shows the history of the baseline absorbance for three solid flows that corresponded to time-averaged solids volume fractions of 0, 0.015 and 0.097. The measured absorbance fluctuated due to heterogeneities in the flow of solids. The average baseline absorbance is shown in Figure 6.6(b) as a function of solids volume fraction and the relationship is close to linear. Cutolo *et al.* [8] previously reported a linear relationship between absorbance and solids volume fractions. In the present case, solids volume fraction was measured by a conventional back-scattering fibre-optic

probe with a different measurement volume compared to the IR fibre-optic probe. Since the solids volume fraction was not completely constant across the flow of sand particles produced by the funnel, this may explain the observed deviation from the linear relationship.

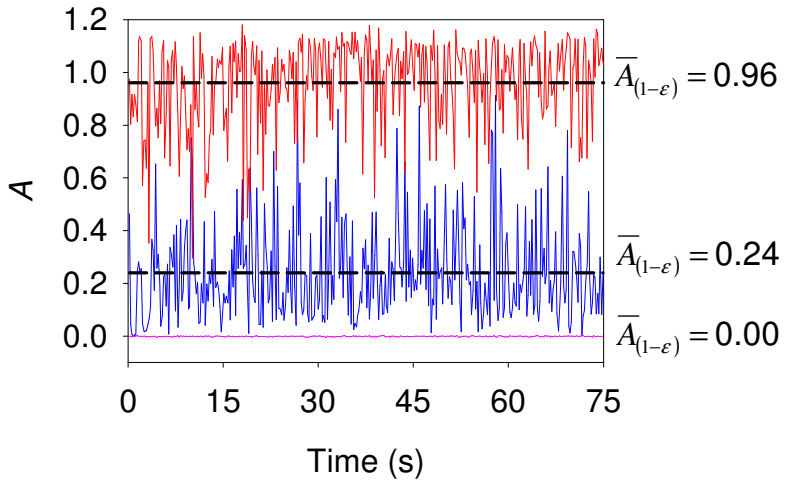

Figure 6-7: Solids volume fraction measurement

Finally, the methane concentration and the solids volume fraction were simultaneously measured in the system. A background spectrum was first taken with a mixture containing 3.25% CH_4 in nitrogen. Then, a flow of sand particles that corresponded to a time-averaged solids volume fraction of 0.015 was initiated in air. Absorbance spectra were measured in real-time for 75 seconds and at a frequency of 4.5 Hz (temporal resolution of 0.22 second). Figure 6.8(a) shows the average baseline absorbance ($A_{(1-\varepsilon)}$) and average methane peak absorbance (A_{CH4}) as a function of time for run #2 (Table 1). Both $A_{(1-\varepsilon)}$ and A_{CH4} fluctuated with time around time-averaged values of 0.26 and 0.19, respectively. The calibrations (Figure 6.6) were used to calculate the instantaneous methane molar fraction (Y_{CH4}) and solids volume fraction ($1-\varepsilon$) at each time interval. Figure 6.8(b) shows the calculated Y_{CH4} and ($1-\varepsilon$) as a function of time: both measurements fluctuated, but the time-averaged values were very close to the real values: 3.24% (compared to the real value of 3.25%) and 0.019 (compared to the real value of 0.015).

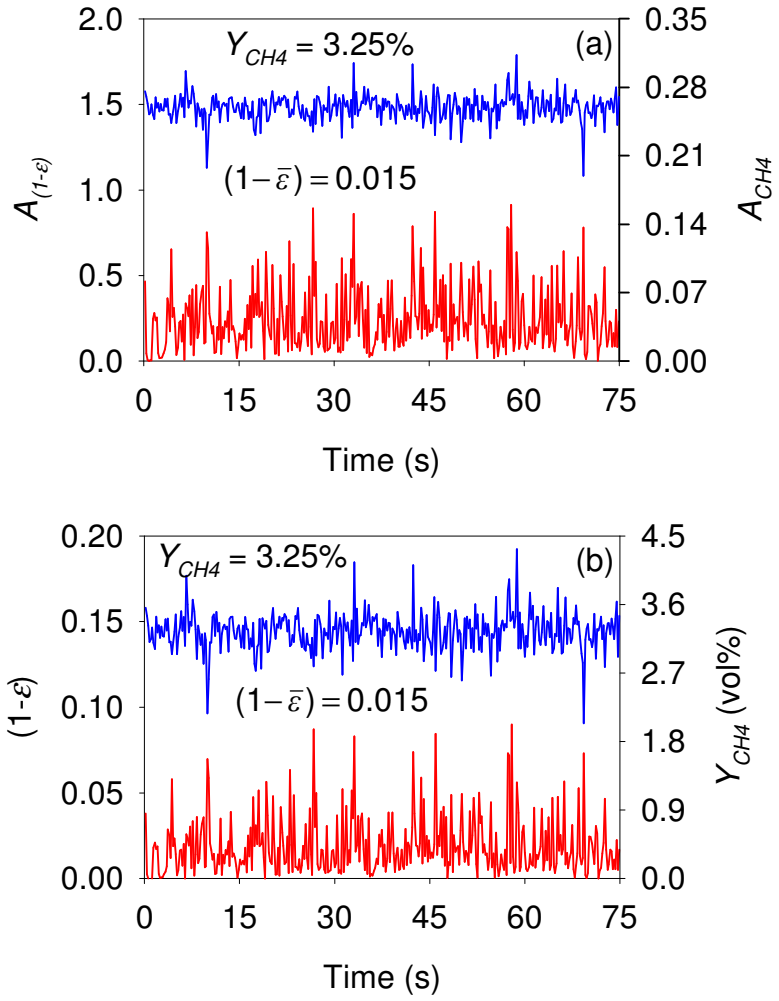

Figure 6-8: Simultaneous measurement of (1-ε) and Y_{CH4}

Figure 6.9 shows the measured methane molar fraction as a function of time and four horizontal lines represent the 5% and 10% relative deviation from the real value (3.25% CH_4). A majority of data points (55%) were within 5% of the real value. Furthermore, 87% of data points had a relative error of 10% or less.

Table 6.1 lists the experiments where solids volume fraction and methane concentration were measured simultaneously. The methane molar fractions and solids volume fractions fed to the system are listed for each run as well as the measured time-averaged values obtained from the

absorbance spectra. The measured time-averaged solids volume fraction (1-$\bar{\varepsilon}$) and methane molar fraction ($\overline{Y}_{CH4}$) were all very close to the real values: the maximum relative error on the measured $\overline{Y}_{CH4}$ was 5.8% (run #9). Table 6.1 also shows the percentage of data points that had a relative error in the measured $\overline{Y}_{CH4}$ of 5% and 10% or less – this percentage decreased with increasing solids volume fraction. Increasing the solids volume fraction decreased the accuracy of the real-time and time-averaged Y_{CH4} measurements.

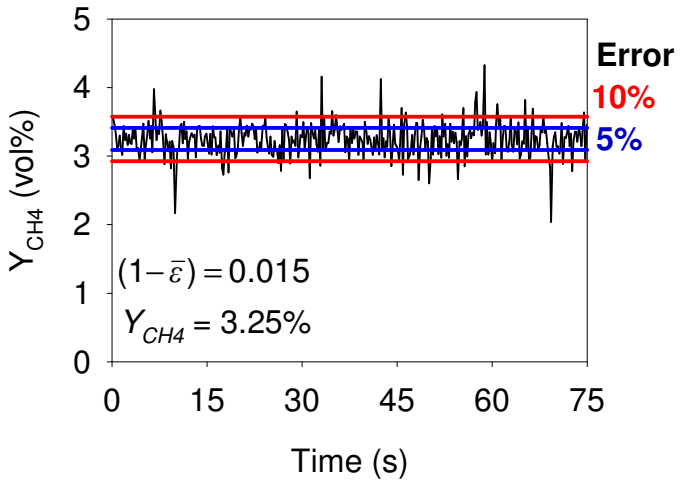

Figure 6-9: Error on instantaneous Y_{CH4} measurement

6.2.3.2.3 Effects of the transmitted IR beam intensity on the Y_i measurement error

As the solids volume fraction increased, the intensity of the transmitted IR beam decreased and the signal-to-noise ratio (S/N) of the FT-IR decreased accordingly. Figure 6.10a was obtained by taking a background spectrum of a mixture of 3.25% CH_4 in nitrogen and measuring the absorbance spectra of air with two time-averaged solids volume fractions (0 and 0.015). Figure 6.10a shows that a time-averaged solids volume fraction of 0.015 resulted in a significantly lower S/N and the fluctuations of the baseline were of the same order as the methane peak (located at 3017.63 cm^{-1}).

The intensity of the IR beam is a concern with fibre-optic probes since their use significantly reduces the effective IR signal. Figure 6.10b shows the single beam spectrum of the FT-IR and the fibre-optic probe for air and $(1-\varepsilon) = 0$: the IR signal intensity was reduced by a factor of approximately 288 when the fibre-optic probe was installed. Note that the sensitivity of the MCT detector had to be increased by a factor of 16 with the fibre-optic probe.

Table 6.1: Simultaneous measurement of Y_{CH4} and $(1-\varepsilon)$

Run	Fed to system		Measurements			
	$\overline{Y_{CH4}}$ (%)	$\overline{(1-\varepsilon)}$	$\overline{Y_{CH4}}$ (%)	$\overline{(1-\varepsilon)}$	Percentage (%) of Y_{CH4} measurements within a relative error of	
					± 5%	± 10%
1	3.25	0.015	3.31	0.019	54	83
2	3.25	0.015	3.24	0.019	55	87
3	10.1	0.015	10.09	0.02	83	98
4	10.1	0.015	10.20	0.018	82	98
5	3.25	0.038	3.31	0.039	38	70
6	3.25	0.038	3.41	0.037	37	63
7	10.1	0.038	10.05	0.041	61	86
8	10.1	0.038	9.95	0.04	63	87
9	3.25	0.097	3.44	0.097	18	31
10	10.1	0.097	10.06	0.098	30	55

For each experimental run listed in Table 6.1, the variance (σ) of the methane molar fraction measurements was calculated. Figure 6.11 shows the variance as a function of time-average solids volume fraction and methane molar fraction: increasing the solids volume fraction greatly increased the variance. This strongly suggests that the accuracy of the fibre-optic probe

measurements can be improved by increasing the IR beam intensity. This could be achieved by using a fibre-optic bundle, optimizing the signal transmission at the probe tip and at the FT-IR/fibre-optic probe interface (Harrick Fibremate™). The effect of decreasing S/N could also be minimized by improving the curve smoothing technique to evaluate the baseline absorbance.

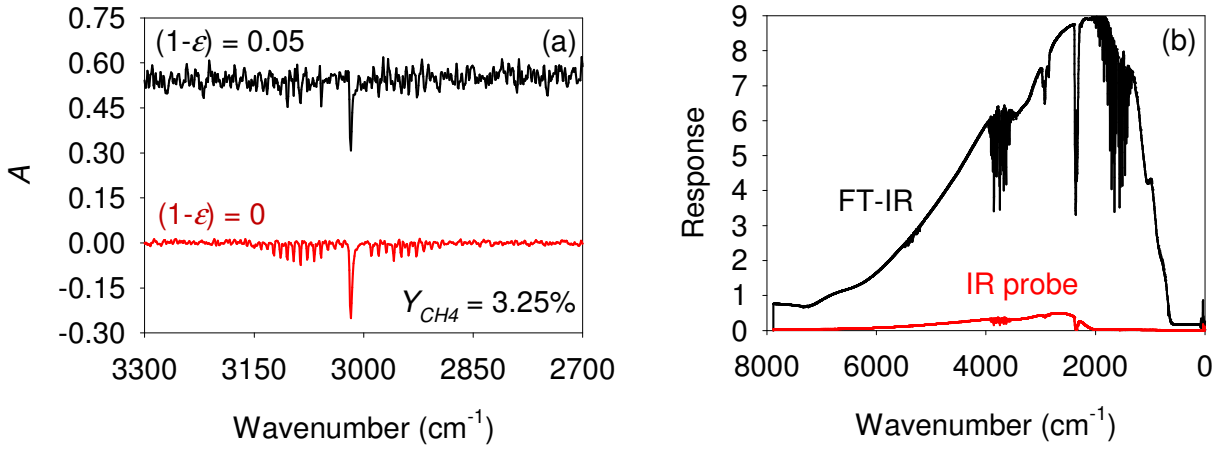

Figure 6-10: Sources of error on Y_{CH4} measurement

6.2.3.2.4 Real-time and time-averaged Y_i measurements

Real-time Y_{CH4} measurements were characterized by greater errors than the time-averaged values. For example, Figure 6.9 shows instantaneous Y_{CH4} measurements with relative errors of more than 10% while the error on the time-averaged Y_{CH4} measurement (Table 6.1 - run #2) was less than 1%. Furthermore, the maximum relative error on the time-averaged Y_{CH4} measurements was 5.8% (run #9). Applied to a multiphase reactor, the present method could measure precisely the time-averaged chemical species composition inside the regions of relatively low solids volume fractions. The technique can also be more sensitive to lower $(1-\varepsilon)$ and Y_i measurements by increasing the IR beam path length (t). Since an average species composition between the dense and dilute phases can be measured by using a sampling probe and analysing the samples, the chemical composition in the dense phase could be calculated by subtracting the dilute phase composition from the average (dilute and dense phases) composition.

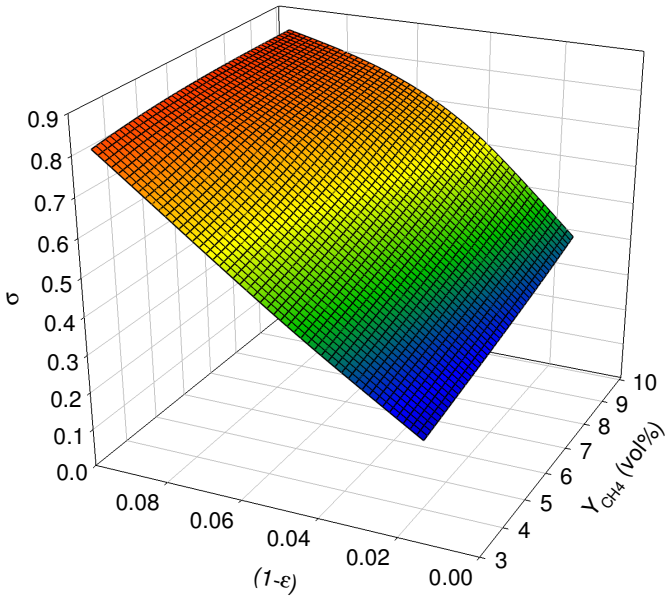

Figure 6-11: Effect of (1-ε) and Y_{CH4} on the variance of Y_{CH4}

6.2.4 Application in fluidized beds - chemical composition measurement in the bubble phase

Gas tracer experiments were conducted in a fluidized bed and the fibre-optic probe was used with the spectroscopic method to measure the molar fraction of a CH_4 tracer inside the bubble and emulsion phases. A bed of FCC particles was incipiently fluidized with nitrogen and bubbles were produced at the tip of the fibre-optic probe by the injection of a nitrogen/methane mixture (10.1% CH_4) through a sparger. Figure 6.12 shows the history of solids volume fraction and methane molar fraction measured by the fibre-optic probe during a typical experiment: the solids volume fraction was 0.45 in the emulsion phase and decreased significantly to 0.05-0 when gas bubbles of CH_4/N_2 were injected at intervals of approximately 11 seconds. The measured methane volume fraction in the emulsion phase fluctuated significantly (5% to -5%) due to the low intensity of the transmitted IR beam and the resulting low S/N. Figure 6.13(a) shows a typical absorbance spectrum measured in the emulsion phase: the low intensity of reflected signal

resulted in a high absorbance throughout the spectrum. However, the time-average methane molar fraction was measured accurately as 0.0% (100% nitrogen).

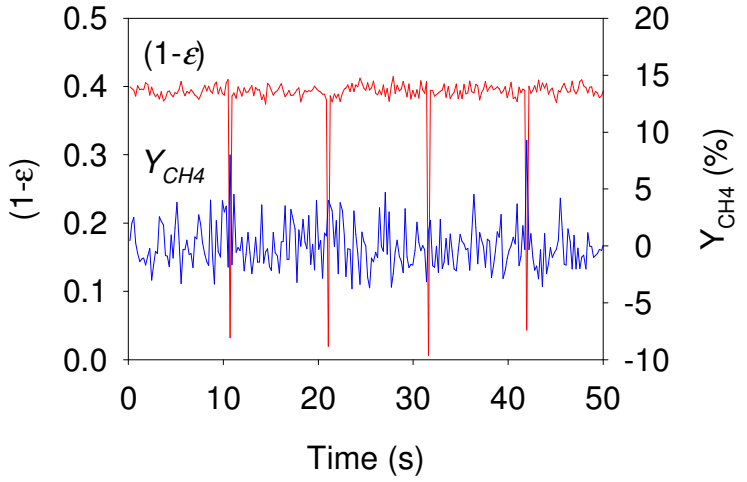

Figure 6-12: Simultaneous measurement of Y_{CH4} and (1-ε) in the fluidized bed

Figure 6.13(b) shows an absorbance spectrum measured inside a bubble: a methane peak was observed at 3017.63 cm^{-1}. However, the injection of bubbles produced gas/solids movement, which caused noise in most recorded absorbance spectra: 5 spectra out of the 27 measured in the bubble phase were sufficiently clear to make a measurement of Y_{CH4}. Figure 6.13(c) shows a typical absorbance spectrum where noise was observed and the methane peak was indistinguishable. This noise could be eliminated in the wavelengths of interest by using a FT-IR with a higher modulation frequency.

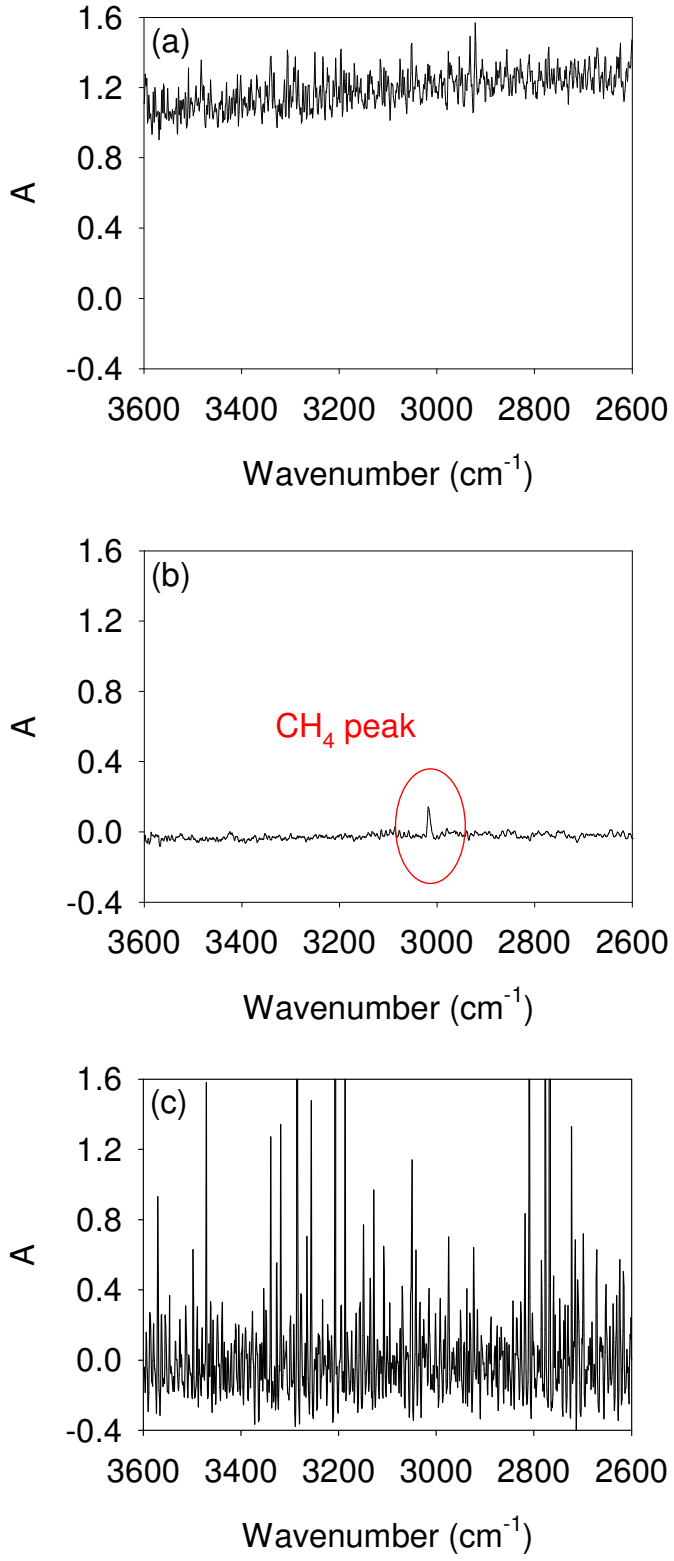

Figure 6-13: Absorbance spectra in fluidized bed

The average peak height measured in the bubble phase corresponded to a methane molar fraction of 5% compared to the injected 10.1% CH_4 in nitrogen. This discrepancy may be due to mixing at the injector tip between the gas injected through the sparger and the fluidizing gas. Furthermore, the small number of clear spectra that were measured in the bubble phase could also explain the low value of Y_{CH4} measured since time-average measurements were more accurate than instantaneous measurements. During the present study, the measured absorbance spectra had to be exported and analyzed manually, which greatly reduced the number of spectra that could be considered to measure Y_{CH4} in the bubble phase. However, these results clearly show that the developed spectroscopic method with a fibre-optic probe can measure the gas composition in the bubble phase.

6.2.5 Limitations of the technique and future work

This measurement technique is limited by the modulation frequency of the spectrometer: the modulation frequency needs to be sufficiently high to avoid noise in the absorbance spectrum due to movement in the gas/solid system. The FT-IR used in the present study was purchased in 2001 and new models are currently available with significantly higher modulation frequencies.

Another limitation of the technique is the IR beam intensity transmitted in the fibre-optic probe, which needs to be as high as possible in order to maximize the signal-to-noise ratio. This is critical if instantaneous measurements are required. On the other hand, time-averaged measurements have been shown in the present study to be much more accurate with lower IR beam intensity. The IR beam intensity can be increased by using a fibre-optic bundle, using a more sensitive detector, using a more powerful IR source, optimizing the signal transmission at the probe tip and at the FT-IR/fibre-optic probe interface (Harrick Fibremate™). More recent models of FT-IR also propose higher IR signal intensity compared to the equipment used in the present study.

The fibre-optic probe used in this study is limited to ambient temperature applications: fluoride glass fibre-optics used can be exposed to temperatures below 150°C. However, fibre-optic probes have been developed with plastic fibre-optics for temperatures up to 1000°C [41]. Therefore, it is reasonable to assume that the measurement technique could be used to perform in-situ measurements in high temperature multiphase systems with an adequately designed fibre-optic probe.

6.2.6 Conclusions

A novel spectroscopic method was developed to measure quantitatively and simultaneously solids volume fraction ($1-\varepsilon$) and gaseous species composition (Y_i) in a gas/solid system. The method was comprised of an FT-IR coupled to a fibre-optic probe that could perform real-time and in-situ measurements of absorbance. The effect of solids volume fraction and gaseous chemical composition on the absorbance spectra were additive and could be independently calibrated. Experiments were conducted with methane/nitrogen and propane/nitrogen mixtures and two types of particles: sand and FCC. Fuel mole fraction and solids volume fraction were varied between 1.8 - 10.1 mol% and 0 - 0.45, respectively. The relative errors for the time-averaged measurements of gaseous species mole fraction were below 6% and the error increased significantly with decreasing beam intensity. The fibre-optic probe was also used in a fluidized bed to measure the molar fraction of a gas tracer inside the emulsion and bubble phases during gas tracer experiments.

The results strongly suggest that the accuracy of instantaneous fibre-optic probe measurements could be significantly improved by increasing the IR beam intensity. This could be achieved by using a fibre-optic bundle, using a more sensitive detector, using a more powerful IR source, optimizing the signal transmission at the probe tip and at the FT-IR/fibre-optic probe interface (Harrick Fibremate™). New FT-IR models also propose significantly higher IR signal intensity compared to the equipment used in the present study. The effect of decreasing signal-to-noise ratio could also be minimized by improving the curve smoothing technique to evaluate the baseline absorbance.

More measurements need to be performed in gas/solid systems at ambient and high temperatures to fully demonstrate the possibilities of this measurement method. High modulation frequencies from newer models of FT-IR should help resolve the problem of noise in the absorbance spectra caused by gas/solid movement. In theory, this method could also be used for liquid/solid, gas/liquid, liquid/liquid and gas/liquid/solid systems. However, work has to be performed in order to identify the limitations in these specific systems.

6.2.7 Acknowledgment

The authors are grateful to the Natural Sciences and Engineering Research Council of Canada (NSERC) for their financial support. The authors would also like to thank IRphotonics for their assistance in the fibre-optic probe construction.

6.2.8 Nomenclature

A Absorbance

d_p Average particle size (μm)

f Modulation frequency (kHz)

t Distance between probe tip and mirror (mm)

Y_i Molar fraction of specie i (vol%)

Greek symbols

$(1-\varepsilon)$ Solids volume fraction

λ Wavelength (μm)

σ Variance

6.2.9 References

[1]Werther J, Molerus O. The local structure of gas fluidized beds – I. A statistically based measuring system. *International Journal of Multiphase Flow*. 1973; 1 (1): 103-122.

[2]Yates JG, Simons SRJ. Experimental methods in fluidization research. *International Journal of Multiphase Flow*. 1994; 20: 297-330.

[3]Hage B, Werther J. The guarded capacitance probe – A tool for the measurement of solids flow patterns in a laboratory and industrial fluidized bed. *Powder Technology*. 1997; 93 (3): 235-245.

[4]Begovich J, Watson JS. An electroconductivity technique for the measurement of axial variation of hold-ups in three-phase fluidized beds. *AIChE Journal*. 1978; 24 (2): 351-354.

[5]Uribe-Salas A, Gomez CO, Finch JA. A conductivity technique for gas and solids holdup determination in three-phase reactors. *Chemical Engineering Science*. 1994; 49 (1): 1-10.

[6]Liu M, Wang T, Yu W, Wang J. An electrical conductivity probe method for measuring the local solid holdup in a slurry system. *Chemical Engineering Journal.* 2007; 132: 37-46.

[7]Huizenga P, Meijer R, Kuipers JAM, van Swaaij WPM. Fluoroptic solids holdup measurements in slurry systems. *AIChE Journal.* 1998; 44 (4): 982-988.

[8]Cutolo A, Rendina I, Arena U, Marzocchella A, Massimilla L. Optoelectronic technique for the characterization of high concentration gas-solid suspension. *Applied Optics* 1990, 29 (9), pp. 1317-1322.

[9]Ishida M, Tanaka H. Optical probe to detect both bubbles and suspended particles in a three-phase fluidized bed. *Journal of Chemical Engineering of Japan.* 1982; 15 (5): 389-391.

[10]Hu T, Yu B, Wang Y. Holdups and models of three phase fluidized beds. In: Ostergaard K, Sorensen A. *Fluidization V*. New York: Engineering Foundation, 1986: 353.

[11]Esmaeili B, Chaouki J, Dubois C. An evaluation of the solid hold-up distribution in a fluidized bed of nanoparticles using radioactive densitometry and fibre optics. *Canadian Journal of Chemical Engineering.* 2008; 86: 543-552.

[12]Gandhi B, Prakash A, Bergougnou MA. Hydrodynamic behaviour of slurry column at high solids concentrations. *Powder Technology*. 1999; 103 (2): 80-94.

[13]Chaouki J, Larachi F, Duduković MP. Noninvasive tomographic and velocimetric monitoring of multiphase flows. *Industrial & Engineering Chemistry Research*. 1997; 36 (11): 4476-4503.

[14]Pugsley T, Tanfara H, Malcus S, Cui H, Chaouki J, Winters C. Verification of fluidized bed electrical capacitance tomography measurements with a fibre optic probe. *Chemical Engineering Science*. 2003; 58 (17): 3923-3934.

[15]Marashdeh Q, Fan LS, Du B, Warsito W. Electrical capacitance tomography – A perspective. *Industrial & Engineering Chemistry Research.* 2008; 47 (10): 3708-3719.

[16]Razzak SA, Barghi S, Zhu JX, Mi Y. Phase holdup measurements in a gas-liquid-solid circulating fluidized bed (GLSCFB) riser using electrical resistance tomography and optical fibre probe. *Chemical Engineering Journal*. 2009; 147: 210-218.

[17]Uchida S, Okamura S, Katsumata T. Measurement of longitudinal distribution of solids holdup in a three-phase fluidized bed by ultrasonic technique. *Canadian Journal of Chemical Engineering*. 1989; 67: 166-169.

[18]Luypaert J, Massart DL, Vander Heyden Y. Near-infrared spectroscopy applications in pharmaceutical analysis. *Talanta*. 2007; 72 (3): 865-883.

[19]Swarbrick B. Process analytical technology: a strategy for keeping manufacturing viable in Australia. *Vibrational Spectroscopy.* 2007; 44: 171-178.

[20]Armaroli T, Bécue T, Gautier S. Diffuse reflection infrared spectroscopy (drifts) : application to the in situ analysis of catalysts. *Oil & Gas Science and Technology*. 2004 ; 59 (2): 215-237.

[21]Kondo JN, Yang S, Zhu Q, Inagaki S, Domen K. In situ infrared study of n-heptane isomerization over Pt/H-beta zeolites. *Journal of Catalysis.* 2007; 248 (1): 53-59.

[22]Corveleyn S, Vandenbossche GMR, Remon JP. Near-infrared (NIR) monitoring of H_2O_2 vapor concentration during vapour hydrogen peroxide (VHP) sterilisation. *Pharmaceutical Research*. 1997; 14 (3): 294-298.

[23]Rantanen J, Räsänen E, Tenhunen J, Känsäkoski M, Mannermaa J-P, Yliruusi J. In-line moisture measurement during granulation with a four-wavelength near infrared sensor: an

evaluation of particle size and binder effects. *European Journal of Pharmaceutics and Biopharmaceutics*. 2000a; 50 (2): 271-276.

[24]Rantanen J, Antikainen O, Mannermaa J-P, Yliruusi J. Use of the near-infrared reflectance method for measurement of moisture content during granulation. *Pharmaceutical Development and Technology*. 2000; 5 (2): 209-217.

[25]Cogdill RP, Anderson CA, Delgado M, Chisholm R, Bolton R, Herkert T, Afnan AM, Drennen III JK. Process analytical technology case study part I: feasibility studies for quantitative near-infrared method development. *AAPS PharmSciTech*. 2005; 6 (2): E273-E283.

[26]Triadaphillou S, Martin E, Montague G, Norden A, Jeffkins P, Stimpson S. Fermentation process tracking through enhanced spectral calibration modeling. *Biotechnology and Bioengineering*. 2007; 97 (3): 554-567.

[27]Andersson M, Josefson M, Langkilde FW, Wahlund K-G. Monitoring of a film coating process for tablets using near infrared reflectance spectrometry. *Journal of Pharmaceutical and Biomedical Analysis*. 1999; 20: 27-37.

[28]Kirsch JD, Drennen JK. Determination of film-coated tablet parameters by near-infrared spectroscopy. *Journal of Pharmaceutical and Biomedical Analysis*. 1995; 13: 1273-1281.

[29]Kirsch JD, Drennen JK. Near-infrared spectroscopic monitoring of the film coating process. *Pharmaceutical Research*. 1996; 13 (2): 234-237.

[30]Abrahamsson C, Johansson J, Andersson-Engels S, Svanberg S, Folestad S. Time-resolved NIR spectroscopy for quantitative analysis of intact pharmaceutical tablets. *Analytical Chemistry*. 2005; 77 (4): 1055-1059.

[31]Hailey PA, Doherty P, Tapsell P, Oliver T, Aldridge PK. Automated system for the on-line monitoring or powder blending processes using near-infrared spectroscopy part I. system development and control. *Journal of Pharmaceutical and Biomedical Analysis*. 1996; 14 (5): 551-559.

[32]Sonja Sekulic S, Wakeman J, Doherty P, Hailey PA. Automated system for the on-line monitoring of powder blending processes using near-infrared spectroscopy: Part II. Qualitative approaches to blend evaluation *Journal of Pharmaceutical and Biomedical Analysis*. 1998; 17: 1285-1309.

[33]Sonja Sekulic S, Ward HW, Brannegan DR, Stanley ED, Evans CL, Sciavolino ST, Hailey PA, Aldridge PK. On-line monitoring of powder blend homogeneity by near-infrared spectroscopy. *Analytical Chemistry*. 1996; 68: 509-513.

[34]Frake P, Greenhalgh D, Grierson SM, Hempenstall JM, Rudd DR. Process control and end-point determination of a fluid bed granulation by application of near infra-red spectroscopy. *International Journal of Pharmaceutics*. 1997; 151 (1): 75-80.

[35]Bellamy LJ, Nordon A, Littlejohn D. Real-time monitoring of powder mixing in a convective blender using non-invasive reflectance NIR spectrometry. *The Analyst*. 2008; 133: 58-64.

[36]Cui H, Mostoufi N, Chaouki J. Comparison of measurement techniques of local particle concentration for gas-solid fluidization. In: Kwauk M, Li J, Yang W-C. *Fluidization X*. New York: Engineering Foundation, 2001: 779-786.

[37]De Paepe ATG, Dyke JM, Hendra PJ, Langkilde FW. Rotating samples in FT-RAMAN spectrometers. *Spectrochimica Acta Part A*. 1997; 53: 2261-2266.

[38]Berntsson O, Danielsson L-G, Folestad S. Characterization of diffuse reflectance fiber probe sampling on moving solids using a Fourier transform near-infrared spectrometer. *Analytical Chimica Acta.* 2001; 431: 125-131.

[39]Andersson M, Svensson O, Folestad S, Josefson M, Wahlund K-G. NIR spectroscopy on moving solids using a scanning grating spectrometer – impact on multivariate process analysis. *Chemometrics and Intelligent Laboratory Systems*. 2005; 75: 1-11.

[40]Skoog DA, Holler FJ, Crouch SR. Principles of Instrumental Analysis (6th edition). Brooks Cole. 2006.

[41]Cui H, Sauriol P, Chaouki J. High temperature fluidized bed reactor: measurements, hydrodynamics and simulation. Chemical Engineering Science. 2003; 58: 1071-1077.

CHAPITRE 7 DISCUSSION GÉNÉRALE

Afin d'éviter la combustion dans la zone de désengagement, il est important que la conversion des réactifs soit la plus élevée possible dans la région de lit fluidisé de solides afin d'éviter la formation d'une mixture inflammable en aval. La température du lit fluidisé est un des paramètres clé qui détermine le taux de conversion dans cette région. Le premier article de cette thèse (chapitre 4) a mesuré expérimentalement les températures critiques de transitions T_1 (température du lit fluidisé en-dessous de laquelle le front de combustion est situé dans la zone de désengagement) et T_2 (température au-dessus de laquelle la combustion se produit à quelques centimètres du point d'injection).

Les résultats démontrent qu'une température de lit de 1073 K (T_2) est suffisante pour que la combustion des n-alkanes C_2-C_4 se produise entièrement dans le lit et à quelques centimètres du point d'injection. Si la température est diminuée en dessous de 923 K (T_1), le front de combustion se trouvera au-dessus de la surface du lit fluidisé. Pour le méthane, ces températures sont significativement plus élevées avec $T_1 = 1023$ K et $T_2 > 1123$ K.

Ces températures critiques pourraient varier si les conditions d'opérations changent. Par exemple, une vitesse de fluidisation plus élevée diminuerait le temps de résidence du gaz. D'un autre côté, le taux de transfert de masse entre les phases bulle et émulsion augmenterait avec un changement de régime de fluidisation (bullage à turbulent, par exemple) et pourrait favoriser une combustion rapide. En conséquence, les températures critiques mesurées dans cette étude devraient, a priori, constituer une bonne indication pour un large éventail de conditions de fluidisation. Toutefois, il serait intéressant d'effectuer des mesures similaires à des vitesses superficielles plus élevées.

La cinétique de réaction globale a également été mesurée pour le méthane, l'éthane, le propane et le n-butane. Cette mesure a été effectuée an assumant que l'hydrodynamique de la phase gazeuse était bien caractérisée par deux réacteurs pistons en série: un réacteur piston pour la région de l'injecteur et un autre pour la région développée du lit fluidisé. La validité de cette hypothèque semble confirmée par les observations de Lorences et al. (2006) et aussi par la bonne

concordance du modèle de combustion développé dans cette étude avec les données expérimentales. La cinétique de combustion mesurée pour l'éthane, le propane et le n-butane pouvait être exprimée par une seule expression de type Arrhenius. Toutefois, il faut noter que la cinétique est peut-être légèrement différente, mais à l'intérieur de la marge d'erreur des mesures. Cette similitude entre les cinétiques de réactions est possiblement due à des agents de réactions radicalaires en chaîne similaires entre les n-alcanes C_2-C_4. Pour le méthane, la cinétique de combustion mesurée était significativement plus lente. Il faut noter que le transfert de masse n'était pas limitant lors de ces expériences. Dans un tel cas, l'énergie d'activation aurait été proche de zéro puisque que les coefficients de diffusion augmentent à peu près linéairement en fonction d'une hausse de température.

À proximité de l'injecteur, le taux de transfert de matière est significativement plus élevé comparativement au lit fluidisé. Les résultats expérimentaux ont démontré que les conditions dans la région de l'injecteur et dans le lit fluidisé peuvent produire une conversion élevée à proximité de l'injecteur ou un délai d'autoallumage dans la région du lit fluidisé. La conversion mesurée près de l'injecteur augmentait avec une hausse de la température du lit et diminuait avec un accroissement de la vitesse du jet à l'extrémité de l'injecteur. L'effet inhibiteur de la vitesse d'injection sur les réactions de combustion a également été observé lors d'études sur l'auto-allumage dans des écoulements à contre-courant (Fotache et al. 1999, Jomaas et al. 2005, Humer et al. 2002). Afin d'inclure les effets promoteur et inhibitifs de la région de l'injecteur, un parallèle a été effectué avec le concept de temps d'induction: la longueur du réacteur piston caractérisant la zone de l'injecteur a été corrélée à la température du lit fluidisé et de la vitesse d'injection avec une expression de type Arrhenius. Une telle expression peut prédire de manière précise le temps d'induction d'une mixture inflammable dans un système homogène. Le modèle de réaction démontre une bonne concordance avec les résultats expérimentaux.

Lorsque des contraintes opératoires limitent la conversion des réactifs dans la région du lit fluidisé, il est important d'évaluer le risque d'auto-allumage et de réactions dans la zone de désengagement. Le deuxième article de cette thèse (chapitre 5) constitue une étude expérimentale sur la combustion du propane dans la zone de désengagement. Lors de ces expériences, la vitesse

du gaz de fluidisation était maintenue près de la vitesse minimale de fluidisation afin de minimiser l'emportement de solides en aval du lit de solides. Des profils axiaux de fractions volumétriques de propane ont été mesurés à la surface d'un lit fluidisé et dans la zone de désengagement. La température du lit fluidisé était maintenue faible (818 K - 923 K) afin que la combustion de propane s'effectue essentiellement dans la zone de désengagement. Les mesures ont été effectuées après que l'opération du réacteur ait atteint un régime permanent. Il est intéressant de noter que l'auto-allumage de la mixture inflammable de propane/air se produisait toujours à la surface du lit fluidisé et jamais en aval. Ceci peut être expliqué par le fait que la température dans la région de désengagement atteignait sa valeur maximale à la surface du lit fluidisé lorsque l'injection du propane débutait. Sinon, cela peut mettre en évidence un couplage entre la zone de réaction du lit fluidisé et celle de la zone de désengagement – la réaction se produisant dans le lit fluidisé se poursuivait dans la zone de désengagement.

Les résultats expérimentaux ont été comparés à un modèle de réaction utilisant un mécanisme de microcinétique pour un système homogène en phase gazeuse. La microcinétique est essentielle afin de reproduire la production de radicaux libres qui précède l'autoallumage. Six mécanismes distincts de microcinétique ont été utilisés et comparés. Les résultats suggèrent que les agents de réactions radicalaires en chaîne produits dans le lit fluidisé peuvent être entraînés dans la zone de désengagement où ils accélèrent la combustion. Dans le présent, les modèles suggèrent que du peroxyde d'hydrogène est l'agent de réaction radicalaire principale, ce qui est également affirmer dans la littérature scientifique pour les températures utilisées.

Lors des expériences sur la combustion dans le lit fluidisé (chapitre 4) et dans la zone de désengagement (chapitre 5), la caractérisation des régions de faibles fractions de solides a été très ardue sinon impossible. Afin de caractériser la zone de désengagement, une mesure simultanée de flux de particules et de composition chimique a été effectuée à l'aide d'une sonde à prélèvement non-isocinétique. Or, la mesure était moyennée dans le temps puisque les mesures instantanées étaient impossibles avec cette méthode. De plus, il n'est pas simple de convertir une mesure de flux de solides en fraction de solides afin de considérer l'effet des particules sur la cinétique. Ces expériences auraient grandement bénéficiés d'une méthode de mesure simultanée de la fraction

de solides et de la composition chimique de la phase gazeuse. Dans la région du lit fluidisé, la caractérisation des réactions se produisant la région à proximité de l'injecteur et dans la phase bulle aurait nécessitée une technique similaire.

Dans le chapitre 6, une méthode de mesure spectroscopique permettant la mesure simultanée de la fraction de solides et de la composition chimique de la phase gazeuse a été développée. En mode transmission, les résultats ont démontré que l'absorbance produite par des solides en suspension et celle produite par une composition chimique sont additives. Ainsi, cette caractéristique rend possible la mesure simultanée de ces deux paramètres en mesurant des spectres d'absorbance. Or, ceci ne serait probablement pas valable en mode diffusion diffuse puisque le volume de mesure dépendrait de la fraction de solides.

La méthode spectroscopique a été utilisée avec une sonde à fibres optiques infrarouges afin d'effectuer des mesures en ligne (fréquence de mesure de 4.5 Hz) et in situ dans un écoulement gaz/solide et un lit fluidisé. Des mesures d'une grande précision ont été effectuées avec une erreur relative généralement de moins de 5% sur la composition chimique. Également, la méthode a été utilisé avec succès pour mesurer la fraction volumétrique d'un traceur dans la phase bulle d'une lit fluidisé gaz/solide.

Les résultats démontrent que la méthode est limitée par deux paramètres:

- L'intensité du rayon infrarouge transmis dans l'échantillon et récolté par le détecteur du spectromètre.
- La vitesse de mouvement des solides et la fréquence de modulation du spectromètre.

L'intensité du signal mesuré par le spectromètre et le ratio signal sur bruit (S/N) décroissait en fonction de la diminution du signal infrarouge. Un signal faible augmentait l'erreur sur les mesures instantanées. L'erreur relative sur la mesure pouvait toutefois être significativement

diminuée en-dessous de 5% si une moyenne temporelle des mesures instantanées était effectuée. L'intensité du rayon infrarouge pourrait être accrue en:

- Augmentant l'intensité de la source infrarouge
- Optimisant le transfert du rayon infrarouge à l'interface spectromètre/sonde à fibres-optiques
- Optimisant le transfert du rayon infrarouge l'extrémité de la sonde
- Augmentant la sensibilité du détecteur

De nouveaux modèles de FT-IR sont caractérisés par des rayons infrarouge plus puissants. De plus, un plus grand nombre de fibres optiques ou des fibres plus grosses pourraient être utilisé. Donc, il y a des avenues possibles afin d'augmenter l'intensité du signal infrarouge.

Le mouvement des particules solides produisait du bruit dans le spectre d'absorbance mesuré. Afin d'effectuer des mesures dans des systèmes multiphasiques, les résultats du chapitre 6 démontrent que la fréquence de modulation doit être suffisamment élevée afin de déplacer le bruit aux basses fréquences et à l'extérieur des longueurs d'ondes d'intérêts. Lors des présentes expériences, la fréquence de modulation était suffisamment élevée afin d'éliminer le bruit. Toutefois, pour des applications où la vitesse des particules solides serait plus élevée, de nouveaux modèles de FT-IR offrent présentement des fréquences de modulation supérieures aux 80 kHz utilisés dans cette étude.

La sonde infrarouge développée ne peut résister à des températures au-delà d'environ 150^{o}C. Toutefois, des sondes à fibres-optiques ont été conçues afin de résister à des températures atteignant 1000^{o}C (Cui et al. 2003).

CONCLUSION

L'objectif principal de cette thèse était de développer des outils de modélisation et de caractérisation des phénomènes de réactions homogènes en phases gazeuses dans les réacteurs à lit fluidisé.

Dans la première partie de ce travail, la combustion en lit fluidisé du méthane, éthane, propane et n-butane avec de l'air a été étudiée en mode d'injection séparée. Un lit fluidisé de particules inertes de sables a été opéré dans le régime à bulle et à des températures intermédiaires : $923\ K \leq T_B \leq 1123\ K$. Pour l'éthane, le propane et le n-butane, la combustion avait lieu principalement dans la région de désengagement lorsque la température du lit fluidisé était inférieure à $T_1 = 923$ K. D'un autre côté, la combustion se produisant entièrement à l'intérieur d'une distance de 0.2 m de l'injecteur lorsque la température du lit était supérieure à $T_2 = 1073$ K. Pour le méthane, les valeurs de T_1 et T_2 étaient significativement plus élevées avec des mesures respectives de 1023 K et 1123 K. La combustion dans le lit fluidisé a été modélisée avec précision à l'aide d'une cinétique globale de première ordre et une modèle hydrodynamique composé de deux réacteurs pistons en séries : un qui caractérisait la région près de l'injecteur et un autre pour la région de lit fluidisé en aval. La cinétique globale de réaction a été mesurée pour chacun des hydrocarbures. Pour les n-alcanes C_2 à C_4, la cinétique globale était caractérisé par une seule expression de type Arrhenius, alors que la cinétique du méthane était significativement plus lente. Les propriétés de la région de l'injecteur causaient soit une conversion importante dans cette région, soit un délai d'auto-allumage dans le lit fluidisé. La conversion des réactifs près de l'injecteur augmentait avec une hausse de la température du lit fluidisé et diminuait avec une hausse de la vitesse d'injection du gaz à l'extrémité de l'injecteur. Afin de prendre ce phénomène en compte dans le modèle de réaction, une analogie a été effectuée avec le concept de temps d'induction. Ainsi, la longueur du réacteur piston caractérisant la région de l'injection a été corrélée à la température du lit fluidisé et la vitesse d'injection avec une expression de type Arrhenius.

Dans la seconde partie de cette thèse, la combustion du propane dans la zone de désengagement d'un lit fluidisé de sable a été étudiée. La température du lit fluidisé a été maintenue faible entre 818 K et 923 K afin que la combustion se produise essentiellement en aval du lit fluidisé. De plus, une vitesse superficielle de gaz deux fois supérieure à la vitesse minimale de fluidisation a été utilisée pour minimiser l'emportement des solides. Durant les expériences, la zone de désengagement a été caractérisée par des mesures simultanées de flux de solides, de composition chimique de la phase gazeuse, de température et de pression. L'auto-allumage de la mixture propane/air a été observé à seulement 0.06 m de la surface du lit pour des températures de lit fluidisé supérieures à 833 K. Six mécanismes de microcinétique ont été utilisés afin de reproduire le profil axial de conversion du propane: tous les modèles ont sous-estimé le taux de réaction dans la zone de désengagement. Or, lorsque le modèle considérait le H_2O_2 produit lors de la combustion dans le lit fluidisé, la vitesse de réaction calculée dans la zone de désengagement étaient significativement plus élevée et menait à une meilleure concordance entre le modèle et les résultats expérimentaux.

La troisième partie de ce travail relate le développement d'une nouvelle méthode spectroscopique pour la mesure quantitative et simultané de la fraction de solides ($1-\varepsilon$) et de la composition chimique dans la phase gazeuse (Y_i) dans un système gaz/solide. La méthode a été utilisée avec un FT-IR connecté à une sonde à fibres-optiques à laquelle des mesures en temps réel et in situ ont été effectuées. L'effet de ($1-\varepsilon$) et Y_i sur le spectre d'absorbance mesuré étaient additifs et pouvaient être calibrés de manière indépendante. Des mesures ont été effectuées avec des mixtures alkane/azote et deux types de particules: du sable et du catalyseur FCC. La fraction volumétrique de l'hydrocarbure et ($1-\varepsilon$) ont été variées entre des valeurs respectives de 1.8 - 10.1 mol% et 0 - 0.45. Les erreurs relatives sur la mesure de Y_i étaient toujours inférieures à 6% and l'erreur augmentait avec une baisse de l'intensité du rayon infrarouge. Une preuve de concept a été effectuée dans un lit fluidisé: la sonde à fibres-optiques a été utilisée pour mesurer la fraction volumétrique d'un traceur gazeux dans la phase bulle et émulsion.

Les résultats ont également démontré que la méthode est limitée par deux paramètres:

- L'intensité du rayon infrarouge transmis dans l'échantillon et récolté par le détecteur du spectromètre.
- La vitesse de mouvement des solides et la fréquence de modulation du spectromètre.

Un signal infrarouge faible augmente l'erreur sur les mesures instantanées. L'erreur relative sur la mesure peut toutefois être significativement diminuée en-dessous de 5% si une moyenne temporelle est effectuée. L'intensité du rayon infrarouge pourrait être accrue en:

- Augmentant l'intensité de la source IR
- Optimisant le transfert du rayon IR à l'interface spectromètre/sonde à fibres-optiques
- Optimisant le transfert du rayon IR l'extrémité de la sonde
- Augmentant la sensibilité du détecteur

Le mouvement des particules solides produit du bruit dans le spectre d'absorbance mesuré de sorte que la fréquence de modulation doit être suffisamment élevée afin de déplacer le bruit vers les basses fréquences à l'extérieur des longueurs d'ondes d'intérêts.

BIBLIOGRAPHIE

Abrahamsson C., Johansson J., Andersson-Engels S., Svanberg S., Folestad S. (2005). Time-resolved NIR spectroscopy for quantitative analysis of intact pharmaceutical tablets. Analytical Chemistry, 77(4), 1055-1059.

Andersson M., Josefson M., Langkilde F.W., Wahlund K.G.. (1999) Monitoring of a film coating process for tablets using near infrared reflectance spectrometry. Journal of Pharmaceutical and Biomedical Analysis, 20, 27-37.

Andersson M., Svensson O., Folestad S., Josefson M., Wahlund K.G.. (2005). NIR spectroscopy on moving solids using a scanning grating spectrometer – impact on multivariate process analysis. Chemometrics and Intelligent Laboratory Systems, 75, 1-11.

Armaroli T., Bécue T., Gautier S. (2004). Diffuse reflection infrared spectroscopy (drifts) : application to the in situ analysis of catalysts. Oil & Gas Science and Technology, 59(2), 215-237.

Baron J., Bulewicz E.M., Zukowski W., Kandefer S., Pilawska M.. (2002). Combustion of hydrocarbon fuels in a bubbling fluidized bed. Combustion and Flame, 128, 410-421.

Begovich J., Watson J.S.(1978). An electroconductivity technique for the measurement of axial variation of hold-ups in three-phase fluidized beds. AIChE Journal, 24 (2): 351-354.

Bellamy L.J., Nordon A., Littlejohn D. (2008). Real-time monitoring of powder mixing in a convective blender using non-invasive reflectance NIR spectrometry. The Analyst, 133, 58-64.

Benjelloun F., Liegeois R., Vanderschuren J. (1995). Penetration length of horizontal gas jets into atmospheric fluidized beds. In J.F. Large, C. Laguerie, *Fluidization VIII: Proceedings of the Eighth Engineering Foundation Conference on Fluidization* (American Institute of Chemical Engineers, 239–246). New York: Engineering Foundation.

Berntsson O., Danielsson L.G., Folestad S. (2001). Characterization of diffuse reflectance fiber probe sampling on moving solids using a Fourier transform near-infrared spectrometer. Analytical Chimica Acta, 431, 125-131.

Botella P., López Nieto J.M., Solsona B. (2002). Selective oxidation of propene to acrolein on Mo-Te mixed oxides catalysts prepared from ammonium telluromolybdates. Journal of Molecular Catalysis A:Chemical, 184, 335-347.

Brokaw R.S., Jackson J.L. (1955). Effect of temperature, pressure, and composition on ignition delays for propane flames. *The 5th International Symposium on Combustion*, (563-569). New York: Reihold.

Buda F., Glaude P.A., Battin-Leclerc F., Porter R., Hughes K.J., Griffiths J.F. (2006). Use of detailed kinetic mechanisms for the prediction of autoignitions, Journal of Loss Prevention in the Process Industries, 19, 227-232.

Burcat A., Scheller K., Lifshitz A. (1971). Shock-tube investigation of comparative ignition delay times for C_1-C_5 alkanes. Combustion and Flame, 16, 29-33.

Burcat A., Lifshitz A. (1971). Shock-tube investigation of ignition in propane-oxygen-argon mixtures. Proceedings of the Combustion Institute, 745-755.

Burcat A., Scheller K., Lifshitz A. (1971). Shock-tube investigation of comparative ignition delay times for C1-C5 alkanes. Combustion and Flame, 16, 29-33.

Cadman P., Thomas G.O., Butler P.. (2000). The auto-ignition of propane at intermediate temperature and high pressures. Physical Chemistry Chemical Physics, 2, 5411-5419.

Cathonnet M., Boettner J.C., James H. (1981). Experimental study and numerical modeling of high temperature oxidation of propane and n-butane. *Proceedings of the 18th Symposium of the Combustion Institute*, (18, 903-913). Pittsburgh: The Combustion Institute.

Chang C.J., Thompson A.L., Winship R.D. (1959). Ignition delay of propane in air between 725-880^{o}C under isothermal conditions. *Proceedings of the 7h Symposium of the Combustion Institute*, (431-435). Pittsburgh: The Combustion Institute.

Chaouki J., Klvana D., Guy C.. (1999). Selective and complete catalytic oxidation of natural gas in turbulent fluidized beds. Korean Journal of Chemical Engineering, 16(4), 494-500.

Chaouki J., Larachi F., Duduković M.P. (1997). Noninvasive tomographic and velocimetric monitoring of multiphase flows. Industrial & Engineering Chemistry Research, 36(11), 4476-4503.

Chen L.H., Wen C.Y. (1982). Model of solid gas reaction phenomena in the fluidized bed freeboard. AIChE Journal, 28(6), 1019-1027.

Cogdill R.P., Anderson C.A., Delgado M., Chisholm R., Bolton R., Herkert T., Afnan A.M., Drennen III J.K. (2005). Process analytical technology case study part I: feasibility studies for quantitative near-infrared method development. AAPS PharmSciTech, 6(2), E273-E283.

Corveleyn S., Vandenbossche G.M.R., Remon J.P. (1997). Near-infrared (NIR) monitoring of H_2O_2 vapor concentration during vapour hydrogen peroxide (VHP) sterilisation. Pharmaceutical Research, 14(3), 294-298.

Cui H., Mostoufi N., Chaouki J. (2001). Comparison of measurement techniques of local particle concentration for gas-solid fluidization. In Kwauk M., Li J., Yang W.C. *Fluidization X*. (779-786). New York: Engineering Foundation.

Cui H., Sauriol P., Chaouki J. (2003). High temperature fluidized bed reactor: measurements, hydrodynamics and simulation. Chemical Engineering Science, 58, 1071-1077.

Cutolo A., Rendina I., Arena U., Marzocchella A., Massimilla L. (1990). Optoelectronic technique for the characterization of high concentration gas-solid suspension. Applied Optics, 29 (9), 1317-1322.

Dagaut P., Cathonnet M., Boettner J.C., Gaillard F. (1987). Kinetic oxidation of propane oxidation. Combustion Science and Technology, 56, 23-63.

De Lasa H.I., Grace J.R. (1979). The influence of the freeboard region in a fluidized bed catalytic cracking regenerator. American Institute of Chemical Engeneers Journal, 25(6), 984-991.

Dennis J.S., Hayhurst A.N., Mackley I.G. (1982). The ignition and combustion of propane/air mixtures in a fluidised bed. *The 19th International Symposium on Combustion*, (1205-1212). Pittsburgh: The Combustion Institute.

De Paepe A.T.G., Dyke J.M., Hendra P.J., Langkilde F.W. (1997). Rotating samples in FT-RAMAN spectrometers. Spectrochimica Acta Part A, 53, 2261-2266.

Dounit S., Hemati M., Andreux R. (2008). Modelling and experimental validation of a fluidized-bed reactor freeboard region: application to natural gas combustion. Chemical Engineering Journal, 140, 457-465.

Esmaeili B., Chaouki J., Dubois C. (2008). An evaluation of the solid hold-up distribution in a fluidized bed of nanoparticles using radioactive densitometry and fibre optics. Canadian Journal of Chemical Engineering, 86, 543-552.

Foka M., Chaouki J., Guy C., Klvana D. (1994). Natural gas combustion in a catalytic turbulent fluidized bed. Chemical Engineering Science, 49(24A), 4269-4276.

Fotache C.G., Wang H., Law C.K. (1999). Ignition of ethane, propane, and butane in counterflow jets of cold fuel versus hot air under variable pressures. Combustion and Flame, 117, 777-794.

Frake P., Greenhalgh D., Grierson S.M., Hempenstall J.M., Rudd D.R. (1997). Process control and end-point determination of a fluid bed granulation by application of near infra-red spectroscopy. International Journal of Pharmaceutics, 151(1), 75-80.

Freeman G., Lefebvre A.H. (1984). Spontaneous ignition characteristics of gaseous hydrocarbon-air mixtures. Combustion and Flame, 58, 153-162.

Friedman J., Li H. (2005). Natural gas combustion in a fluidized bed heat-treating furnace. Combustion Science and Technology, 177, 2211-2241.

Gandhi B., Prakash A., Bergougnou M.A. (1999). Hydrodynamic behaviour of slurry column at high solids concentrations. Powder Technology, 103(2), 80-94.

Hage B., Werther J. (1997). The guarded capacitance probe – A tool for the measurement of solids flow patterns in a laboratory and industrial fluidized bed. Powder Technology, 93(3), 235-245.

Hailey P.A., Doherty P., Tapsell P., Oliver T., Aldridge P.K. (1996). Automated system for the on-line monitoring or powder blending processes using near-infrared spectroscopy part I. system development and control. Journal of Pharmaceutical and Biomedical Analysis, 14(5), 551-559.

Hartman M., Trnk O., Pohořelý M., Svoboda K.(2010). High-temperature reaction in the freeboard region above a bubbling fluidized bed. Industrial & Engineering Chemistry Research, 49(6), 2672–2680.

Hesketh R.P., Davidson J.F. (1991). Combustion of methane and propane in an incipiently fluidized bed. Combustion and Flame, 85, 449-467.

Hong R., Li H., Li H., Wang Y. (1997). Studies on the inclined jet penetration length in a gas–solid fluidized bed, Powder Technology, 205–212.

Horning D.C., Davidson D.F., Hanson R.K. (2002). Study of the high-temperature autoignition of n-alkane/O_2/Arixtures. Journal of Propulsion and Power, 18(2), 363-371.

Hu T., Yu B., Wang Y. (1986). Holdups and models of three phase fluidized beds. In Ostergaard K., Sorensen A. *Fluidization V*. (353). New York: Engineering Foundation.

Huizenga P., Meijer R., Kuipers J.A.M., Van Swaaij W.P.M. (1998). Fluoroptic solids holdup measurements in slurry systems. AIChE Journal, 44 (4), 982-988.

Humer S., Seiser R., Seshadri K. (2002). Non-premixed and premixed extinction and autoignition of C_2H_4, C_2H_6, C_3H_6 and C_3H_8. Proceedings of the Combustion Institute, 29, 1597-1604.

Hutchenson K.W., La Marca C., Patience G.S., Laviolette J.P., Bockrath R.E. (2010). Parametric study of butane oxidation in a circulating fluidized bed reactor. Catalysis A: General, 376(1-2), 91-103.

Ishida M., Tanaka H. (1982). Optical probe to detect both bubbles and suspended particles in a three-phase fluidized bed. Journal of Chemical Engineering of Japan, 15(5), 389-391.

Jeng R.S., Altwicker E.R., Morgan III M.M., Wilk R.D. (2001). Propane combustion in a spouted bed combustor II: a modeling study in the bed region. Combustion Science and Technology, 170, 119-149.

Jomaas G., Zheng X.L., Zhu D.L., Law C.K. (2005). Experimental determination of counterflow ignition temperatures and laminar flame speeds of C_2-C_3 hydrocarbons at atmospheric and elevated pressures. Proceedings of the Combustion Institute, 30, 193-200.

Kin K., Soo Shin K. (2001). Shock tube and modeling study of the ignition of propane. Bulletin of the Korean Chemical Society, 22(3), 303-307.

Kirsch J.D., Drennen J.K. (1995). Determination of film-coated tablet parameters by near-infrared spectroscopy. Journal of Pharmaceutical and Biomedical Analysis, 13, 1273-1281.

Kirsch J.D., Drennen J.K. (1996). Near-infrared spectroscopic monitoring of the film coating process. Pharmaceutical Research, 13(2), 234-237.

Kondo J.N., Yang S., Zhu Q., Inagaki S., Domen K. (2007). In situ infrared study of n-heptane isomerization over Pt/H-beta zeolites. Journal of Catalysis, 248(1), 53-59.

Kunii D., Levenspiel O. (1990). Entrainment of solids from fluidized beds I.Hold-up of solids in the freeboard II.Operation of fast fluidized bed. Powder Technology, 61, 193-206.

Lamoureux N., Paillard C.E., Vaslier V. (2002). Low hydrocarbon mixtures ignition delay times investigation behind reflected shock waves. Shock Waves, 11, 309-322.

Laviolette J.P., Sotudeh-Gharebagh R., Mabrouk R., Patience G.S., Chaouki J. (2010) Fluidized bed combustion of methane and other hydrocarbons. In Agarwal A. *Handbook of Combustion* (vol.5), Weinheim: Wiley.

Liu M., Wang T., Yu W., Wang J. (2007). An electrical conductivity probe method for measuring the local solid holdup in a slurry system. Chemical Engineering Journal, 132, 37-46.

Lorences M., Laviolette J.P. (2006). Fluid bad gas RTD: effect of fines and internals. Powder Technology, 168(1), 1-9.

Lorences M.J., Patience G.S., Cenni R., Diez F., Coca J.. (2006a). VPO transient lattice oxygen contribution. Catalysis Today, 112, 45-48.

Luypaert J., Massart D.L., Vander Heyden Y. (2007). Near-infrared spectroscopy applications in pharmaceutical analysis. Talanta, 72(3), 865-883.

Mabrouk R., Chaouki J., Laviolette J.P., Patience G.S. (2008). On natural gas combustion in a fluidized bed. *Proceedings of the 9th Conference on Circulating Fluidized Beds*, Hamburg, Germany.

Malleswara Rao T.V., Deo G. (2007). Ethane and Propane Oxidation over Supported V2O5/TiO2 Catalysts: Analysis of Kinetic Parameters. Industrial & Engineering Chemistry Research, 46, 70-79.

Marashdeh Q., Fan L.S., Du B., Warsito W. (2008). Electrical capacitance tomography – A perspective. Industrial & Engineering Chemistry Research, 47(10), 3708-3719.

Marinov N.M., Pitz W.J, Westbrook C.K., Hori M., Matsunaga N. (1998). An experimental and kinetic calculation of the promotion effect of hydrocarbons on the NO-NO2 conversion in a flow reactor. Proceedings of the Combustion Institute, 27, 389-396.

Merry J.M.D. (1971). Penetration of a horizontal gas jet into a fluidised bed. Transactions of the Institution of Chemical Engineers, 49(4), 189–195.

Okhotskii V.B. (2001). Depth of penetration of a gas jet into a granular medium. Theoretical Foundations of Chemical Engineering, 35(2), 199-200.

Penyazkov O.G, Ragotner K.A., Dean A.J., Varatharajan B. (2005). Autoignition of propane-air mixtures behind reflected shock waves. Proceedings of the Combustion Institute, 30, 1941-1947.

Pre P., Hemati M., Marchand B. (1998). Study on natural gas combustion in fluidized beds: modelling and experimental validation. Chemical Engineering Science, 53(16), 2871-2883.

Pugsley T., Tanfara H., Malcus S., Cui H., Chaouki J., Winters C. (2003). Verification of fluidized bed electrical capacitance tomography measurements with a fibre optic probe. Chemical Engineering Science, 58(17), 3923-3934.

Qin Z., Lissianski V.V., Yang H., Gardiner Jr. W.C., Davis S.G., Wang H. (2000). Combustion chemistry of propane: a case study of detailed reaction mechanism optimization. Proceedings of the Combustion Institute, 28, 1663–1669.

Rantanen J. Antikainen O. Mannermaa J.P., Yliruusi J. (2000). Use of the near-infrared reflectance method for measurement of moisture content during granulation. Pharmaceutical Development and Technology, 5(2), 209-217.

Rantanen J., Räsänen E., Tenhunen J., Känsäkoski M., Mannermaa J.P., Yliruusi J.(2000a). In-line moisture measurement during granulation with a four-wavelength near infrared sensor: an evaluation of particle size and binder effects. European Journal of Pharmaceutics and Biopharmaceutics, 50(2), 271-276.

Ranzi E., Faravelli T., Gaffuri P., Pennati G.C., Sogaro A. (1994). A wide range modeling study of propane and n-butane oxidation. Combustion Science and Technology, 100, 299-330.

Razzak S.A., Barghi S., Zhu J.X., Mi Y. (2009) Phase holdup measurements in a gas-liquid-solid circulating fluidized bed (GLSCFB) riser using electrical resistance tomography and optical fibre probe. Chemical Engineering Journal, 147, 210-218.

Reinhardt, B., Cordonnier, A., Florent, P. (1999). Use of an isokinetic sampling propane. Results in a cyclone. Powder Technology, 101, 81-90.

Rhodes, M..J., Laussmann, P. (1992). A simple non-isokinetic sampling probe for dense suspensions. Powder Technology, 70, 141-151.

Ross D.P., Yan H.M., Zhang D.K. (2001). An experimental study of propane combustion in a fluidized-bed gasifier. Combustion and Flame, 124, 156-164.

Ross D.P., Yan H.M., Zhang D.K. (2004). Modelling of a laboratory-scale bubbling fluidised-bed gasifier with feeds of both char and propane. Fuel, 83, 1979-1990.

Saxena P., Peters N., Williams F.A. (2007). An analytical approximation for high-temperature autoignition times of higher alkanes. Combustion and Flame, 149, 79-90.

Shakhova N.A. (1968). Discharge of turbulent jets into a fluidized bed, Journal of Engineering Physics and Thermophysics, 14 (1), 32–36.

Shen Z., Briens C.L., Kwauk M., Bergougnou M.A. (1990). Study of a downward gas jet in a two-dimensional fluidized bed. Canadian Journal of Chemical Engineering, 68, 534-540.

Singh B., Rigby G.R., Callcott T.G. (1975). Combustion of gaseous fuels in a fluidised bed. *Fluidised Combustion Conference*. London: Paper C5.

Skoog D.A., Holler F.J., Crouch S.R.(2006) Principles of Instrumental Analysis (6th edition). Belmont: Brooks Cole.

Smith G.P., Golden D.M., Frenklach M., Moriarty N.W., Eiteneer B., Goldenberg M., Bowman C.T., Hanson R.K., Song S., Gardiner Jr. W.C., Lissianski V.V., Qin Z. http://www.me.berkeley.edu/gri_mech/

Sonja Sekulic S., Wakeman J., Doherty P., Hailey P.A. (1998) Automated system for the on-line monitoring of powder blending processes using near-infrared spectroscopy: Part II. Qualitative approaches to blend evaluation Journal of Pharmaceutical and Biomedical Analysis, 17, 1285-1309.

Sonja Sekulic S., Ward H.W., Brannegan D.R., Stanley E.D., Evans C.L., Sciavolino S.T., Hailey P.A., Aldridge P.K. (1996). On-line monitoring of powder blend homogeneity by near-infrared spectroscopy. Analytical Chemistry, 68, 509-513.

Sotudeh-Gharebaagh R. (1998). *Combustion of natural gas in a turbulent fluidized bed reactor*. PhD Thesis, École Polytechnique, Montréal, Québec, Canada.

Sotudeh-Gharebagh R., Chaouki J. (2003). The heterogeneous and homogeneous combustion of methane over inert particles. Canadian Journal Chemical Engineering , 81, 1182-1191.

Sotudeh-Gharebaagh R., Chaouki J. (2007). Investigation of highly exothermic reactions in a turbulent fluidized bed reactor. Energy & Fuels, 21, 2230-2237.

Sotudeh-Gharebagh R., Mostoufi N. (2003). Simulation of a catalytic turbulent fluidized bed reactor using the sequential modular approach. Fuel Processing Technology, 85, 189-200.

Srinivasan R.A., Sriramulu S., Kulasekaran S., Agarwal P.K. (1998). Mathematical modeling of fluidized bed combustion-2: combustion of gases. Fuel, 77, 1033-1049.

Stubington J.F., Davidson J.F. (1981). Gas-phase combustion in fluidized beds. AIChE Journal, 27 (1), 59-65.

Sung C.J., Li B., Law C.K., Wang H. (1998). Structure and sooting limits in counterflow methane/air and propane/air diffusion flames from 1 to 5 atmospheres, *The 27th International Symposium of Combustion*, (1523-1530). Pittsburgh: The Combustion Institute.

Swarbrick B. (2007). Process analytical technology: a strategy for keeping manufacturing viable in Australia. Vibrational Spectroscopy, 44, 171-178.

Triadaphillou S., Martin E., Montague G., Norden A., Jeffkins P., Stimpson S. (2007) Fermentation process tracking through enhanced spectral calibration modeling. Biotechnology and Bioengineering, 97(3), 554-567.

Uchida S., Okamura S., Katsumata T. (1989) Measurement of longitudinal distribution of solids holdup in a three-phase fluidized bed by ultrasonic technique. Canadian Journal of Chemical Engineering, 67, 166-169.

Uribe-Salas A., Gomez C.O., Finch J.A. (1994). A conductivity technique for gas and solids holdup determination in three-phase reactors. Chemical Engineering Science, 49(1), 1-10.

Van der Vaart D.R. (1988). Freeboard ignition of premixed hydrocarbon gas in a fluidized bed. Combustion and Flame, 71, 35-39.

Van der Vaart D.R. (1988a). The chemistry of premixed hydrocarbon/air combustion in a fluidized bed. Fuel, 67, 1003-1007.

Van der Meer, E.H., Thorpe, R.B. & Davidson, J.F. (2000). Flow patterns in the square cross-section riser of a circulating fluidized bed and the effect of riser exit design. Chemical Engineering Science, 55, 4079-4099.

Walsh P.M., Chaung T.Z., Dutta A., Beér J.M., Srofim A.F. (1982). Particle entrainment and nitric oxide reduction in the freeboard of a fluidized coal combustor. ACS Fuels Volumes, 27(1), 243-261.

Wen C.Y., Chen L.H. (1982). Fluidized bed freeboard phenomena: entrainment and elutriation. AIChE Journal, 28(1), 117-128.

Werther J., Molerus O. (1973). The local structure of gas fluidized beds – I. A statistically based measuring system. International Journal of Multiphase Flow, 1(1), 103-122.

Westbrook, C.K. (2000). Chemical kinetics of hydrocarbon ignition in practical combustion systems. Proceedings of the Combustion Institute, 28, 1563-1577.

Wilk R.D., Cernansky N.P., Cohen R.S. (1986). The oxidation of propane at low and transition temperatures. Combustion Science and Technology, 49, 41-78.

Yates J.G., Simons S.R.J. (1994) Experimental methods in fluidization research. International Journal of Multiphase Flow, 20, 297-330.

Zenz F.A. (1968). Bubble formation and grid design, IChemE Symposium Series, 30, 136–139.

Zhukov V.P., Sechenov V.A. Starikovskii. (2005). Autoignition of a lean propane-air mixture at high pressures. Kinet Catal, 46(3), 319-327.

Zukowski W. (2003). A simple model for explosive combustion of premixed natural gas with air in a bubbling fluidized of inert sand. Combustion and Flame, 134, 399-409.

Chemical-Kinetic Mechanisms for Combustion Applications, San Diego Mechanism web page, Mechanical and Aerospace Engineering (Combustion Research), University of California at San Diego. (http://maeweb.ucsd.edu/~combustion/cermech/)

ANNEXE 1 – ARTICLE PRESENTÉE À LA CONFÉRENCE CHEMCON 2006 (INDE)

Propane-oxygen induction time measurement in the freeboard of a fluidized bed – Freeboard characterization

Jean-Philippe Laviolette[1a], Julia Duchastel-Légaré[a], Gregory S. Patience[a], Concetta La Marca[b] and Jamal Chaouki[a]

[a]*Department of Chemical Engineering, Ecole Polytechnique, Montreal, Quebec,Canada*

[b]*DuPont Engineering Research and Technology, Wilmington, DE, USA*

ABSTRACT

In the present study, the gas and solids hydrodynamics were characterized inside the freeboard and disengagement sections of a pilot scale fluidized bed using gas RTD and a fibre-optics probe for two superficial velocities: U_g = 0.2 and 0.6 m/s. Experiments were performed at ambient temperature and vanadyl pyrophosphate catalyst (Geldart group A) was used as the bed material. Results showed that the hydrodynamic regime inside the freeboard was close to plug flow for both velocities. However, the diverging area leading to the disengagement region produced large scale fluctuations in the Gas RTD at low velocity, which disappeared at higher velocity. Furthermore, the fibre-optic probe showed that the solids concentration was approximately constant along the radius of the reactor and decreased with increasing height as well as decreasing superficial velocity.

INTRODUCTION

The direct oxidative conversion of lower alkanes to oxygenated products is undergoing intense research due to their lower costs compared to olefins. Propane to acrylic acid is one such process and several kinetic studies [1] have indicated that high oxygen (15-70%) and low propane (2-3%) concentrations favour the selective reaction. Furthermore, while propane conversion increases with temperature, reaction

---

[1] *Present address: Department of Chemical Engineering, Ecole Polytechnique, C.P. 6079, succ. Centre-Ville, Montreal (Quebec), Canada, H3C 3A7 (jean-philippe.laviolette@polymtl.ca)*

temperatures above approximately 450^{o}C were reported to result in a loss of selectivity. Under these conditions, the risk of homogeneous gas-phase auto-ignition represents a safety concern. In fluidized bed reactors, explosive mixtures may be avoided by feeding oxygen and hydrocarbons to the bed separately. However, under partial conversion conditions, the catalyst concentration in the freeboard region is insufficient to quench free radicals and thus gas phase auto-ignition becomes an important safety hazard. The risk of auto-ignition in the freeboard, cyclones and downstream piping must be quantified for design purposes.

Induction time – the time in which a hydrocarbon-oxygen mixture auto-ignites – is one essential design parameter. Propane-oxygen induction time measurements can be found throughout the literature [2]. However, agreement between these studies is generally lacking and the discrepancy most likely is due to the strong relationship between the induction time and the experimental conditions as well as vessel geometry. Consequently, there remains a need to develop generalized relationships between propane-oxygen induction time, process conditions, solids concentration and reactor geometry at different scales. Previous studies have shown that induction time varies with temperature (T), pressure (P), mixture composition, solids concentration (C_S) and vessel characteristics but extrapolating these tendencies to a fluidized bed introduces uncertainties. Induction time studies have been performed in several types of vessels (static vessels, flow reactors, shock tubes and high compression machines), but never in fluidized beds.

Induction times also are likely dependant upon the gas hydrodynamics. Previous studies performed in flow reactors were at high turbulent flow regimes such that perfect radial mixing was assumed. Chang *et al*. [3] observed no significant variations as the Reynolds number was varied from 2000 to 14000. However, if induction time is to be measured in a fluidized bed under realistic operating conditions, the flow regime may be closer to laminar and the gas-phase hydrodynamics may have two essential effects. First, it may affect the induction time directly since the mass transfer will determine the mixture to wall heat transfer, which may prevent thermal run-away. Secondly, it may give rise to radial gradients that will render the contribution of the different physical parameters (T, P, C_S, etc) difficult to assess. In the end, this potentially can lead to significant uncertainties in the induction time correlation. Hence, the gas-phase hydrodynamics must be characterized before proceeding to the measurement of induction time.

Solids concentration is another factor which has been shown to affect induction time. In a fluidized bed operating at velocities above the minimum bubbling velocity, bubbles form at the distributor and rise through the bed. As the bubbles reach the bed surface and collapse, particles are dispersed into the freeboard and disengagement regions. The effect of solids has never been quantified in induction time

measurement studies nor included in correlations. Furthermore, radial gradients in solids concentrations will lead to uncertainties in the system characterization. It is therefore essential to characterize the solids hydrodynamics inside the freeboard and disengagement regions.

In order to relate the position of auto-ignition (detectable with a thermocouple) to the induction time, the average mixture residence time must be measured at the different radial and axial locations inside the reactor. This can easily be done with gas RTD studies. In prior studies, gas RTD experiments have been mostly performed inside the bed of solids [4]. In comparison, the gas hydrodynamics freeboard and disengagement regions should be simpler due to the absence of bubbles, but it is complicated by the presence of a diverging area. In fact, the effect of a disengagement region on gas RTD not been previously reported.

In the present study, experiments were performed in order to characterize the gas and solids hydrodynamics inside the freeboard (I.D. = 20 cm) and disengagement (I.D. = 60 cm) regions of a fluidized bed reactor at ambient temperature and with equilibrated VPO (Geldart A) as the bed material. Gas RTD studies were performed to determine the flow regime of the gas above the bed. RTD was also used to map the average gas residence time at different positions (axial and radial) inside the two regions of interest. Lastly, a fibre-optic probe was used to quantify the variation of solids concentration with radial and axial positions inside the freeboard.

EXPERIMENTAL APPARATUS

The experiments were conducted in a fluidized bed as shown in Figure 1. The bed and freeboard regions had an inner diameter of 20 cm, while the disengagement section had an inner diameter of 60 cm. The experimental procedure consisted of first fluidizing the solids with air at ambient temperature for all experiments. In the RTD studies, propane was used as the tracer and was injected as a step function into the fluidizing air stream upstream of the windbox. Preliminary tests showed that the tracer mixed perfectly before reaching the windbox. The RTD curves for different radial and axial positions were then obtained through in-line sampling and analysis with an FT-IR unit with a recording speed of 2 Hz. The tracer was injected via the opening of a solenoid four-way valve which was triggered by the FT-IR unit. This resulted in a variability of the measured average gas residence time that was below 0.8 s in the freeboard region. Furthermore, the volumetric sampling rate was set at 5 mL/s which represented less than 1% of the total flow inside the reactor and minimized the perturbations on the system.

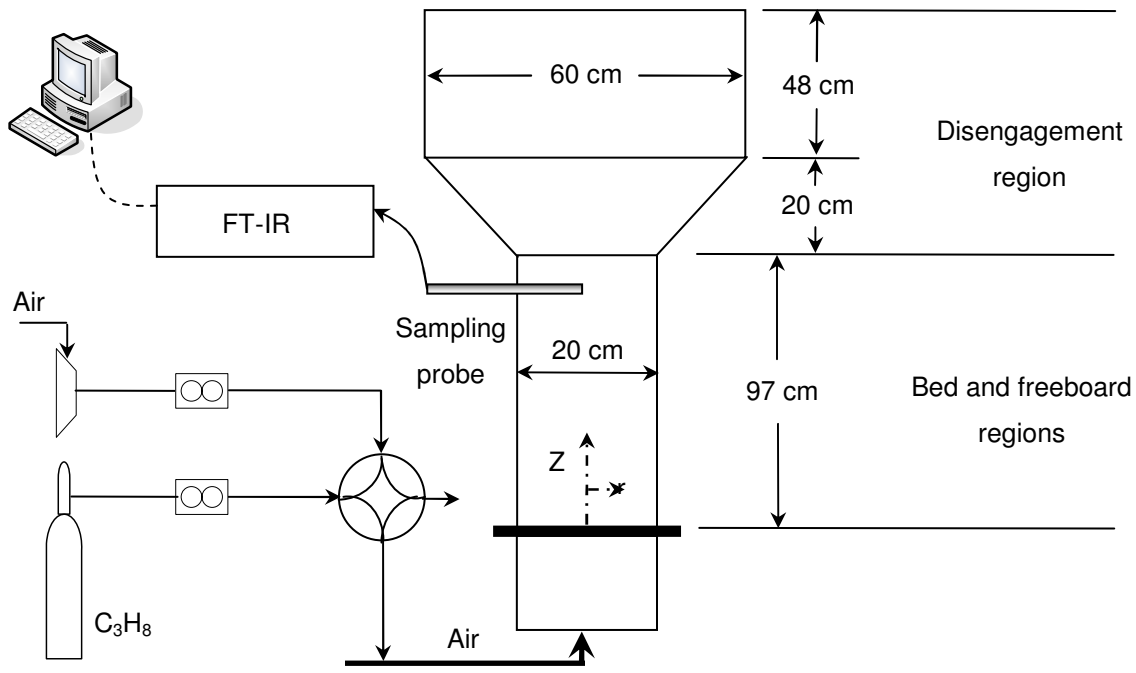

Figure 1: Experimental apparatus

To quantify the solids concentration into the freeboard region, a fibre-optics probe was used. Essentially, the probe consisted of 4 emitting and 4 receiving fibre-optics with a 1mm thick window at the tip such that the fibre-optic output was linearly proportional to the solids concentrations. A PV-4A particle velocity analyzer (Institute or Process Engineering, Chinese Academy of Sciences) was used as a light source and to (record time series of instantaneous local voidage at various axial and radial positions. To ensure the validity and the repeatability of the sampled signals, five series of 33 000 data points were collected at a sampling rate of 2 kHz for every position.

RESULTS AND DISCUSSION

The freeboard region begins at the bed surface and it is continuously moving due to bubble bursting. The bubbles also entrain solids into the freeboard resulting in a vertical gradient of solids concentration. Consequently, the bed surface gets diffused and does not constitute a well defined line.

Solids concentration

The bed surface can be more accurately defined by measuring pressure records. Figure 2 shows the measured pressure profile inside the reactor for two superficial velocities as well as the calculated values given by a modified Kato and Wen model [5]. Since the pressure drop is proportional to the void fraction,

we can assume that the freeboard region begins where the pressure reaches a plateau and the solids fraction is low. Hence, at U_g = 0.6 m/s, it is observed from the experimental data and the model that the bed surface is located somewhere between 35 and 45 cm. Also, at U_g = 0.16 m/s, the bed surface is located slightly lower at around 35 cm.

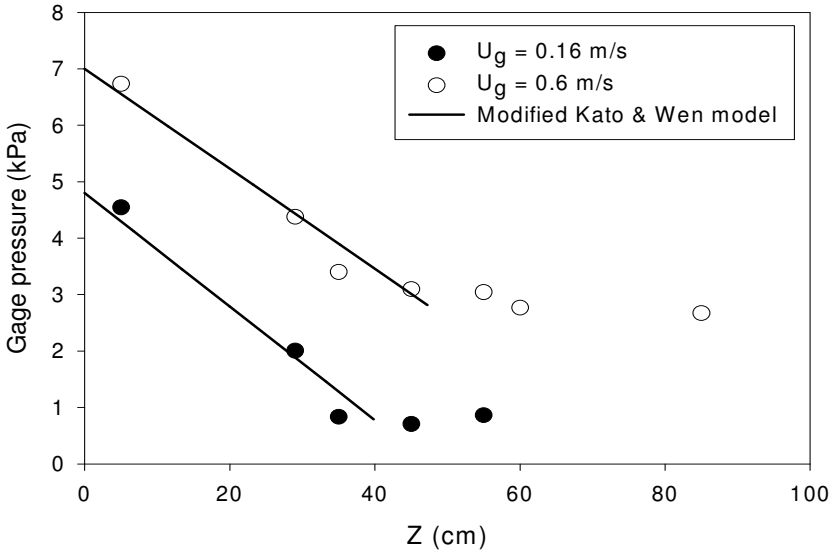

Figure 2: Axial pressure profile in the fluidized bed reactor

A fibre-optic probe was used to quantify the variation of solids fraction (1-ε) with axial and radial positions and the results are shown in Figures 3 and 4. Hence, Figure 3 shows that the solids concentration was approximately invariant with radial position. Furthermore, we note from Figure 4 that the radially averaged solids concentration remained constant near the bed surface and then decreased with increasing axial position and decreasing superficial velocity. Near the bed, the bubble bursting phenomenon governs the solids entrainment, which results in a region of high solids fraction. However, as Z increases, the amount of solids ejected by the bubbles decreases and the gas superficial velocity gradually becomes a more important factor in entrainment. The experimental data was compared to the results reported by Morooka *et al*. [6] for FCC catalyst (d_p = 66 μm) at U_g = 0.15 and 0.5 m/s. The results of Morooka *et al*. [6] show that the exponential decrease of (1-ε) with Z was valid only at a certain height (approximately 75 cm) above the bed surface. Our results agree fairly well with their data.

Gas-phase hydrodynamics in the freeboard and disengagement regions

To characterize the gas-phase hydrodynamics we used gas RTD with step function gas injection. Therefore, the first derivative of the experimental data (F(t) curve) was taken to obtain the E(t) curve. Hence, Figure 5 shows the E(t) curve inside the freeboard for U_g = 0.2 m/s (a) and 0.6 m/s (b) at three

radial positions. It is seen that the curves for each of the three different radial positions are indistinguishable and have a nearly Gaussian shape. Therefore, the gas was well mixed radially. This was observed at all positions inside the freeboard.

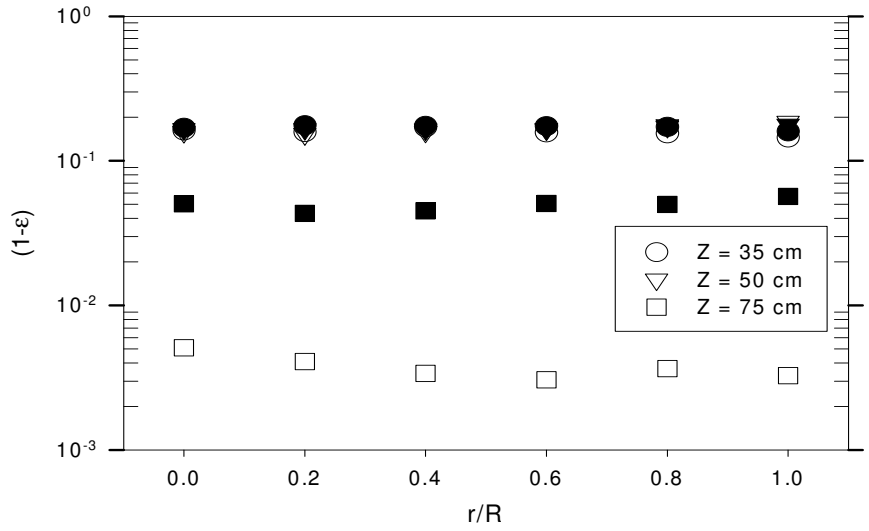

Figure 3: Solids volume fraction w.r.t. axial and radial positions

(Filled symbols [U_g = 0.6 m/s] and empty symbols [U_g = 0.16 m/s])

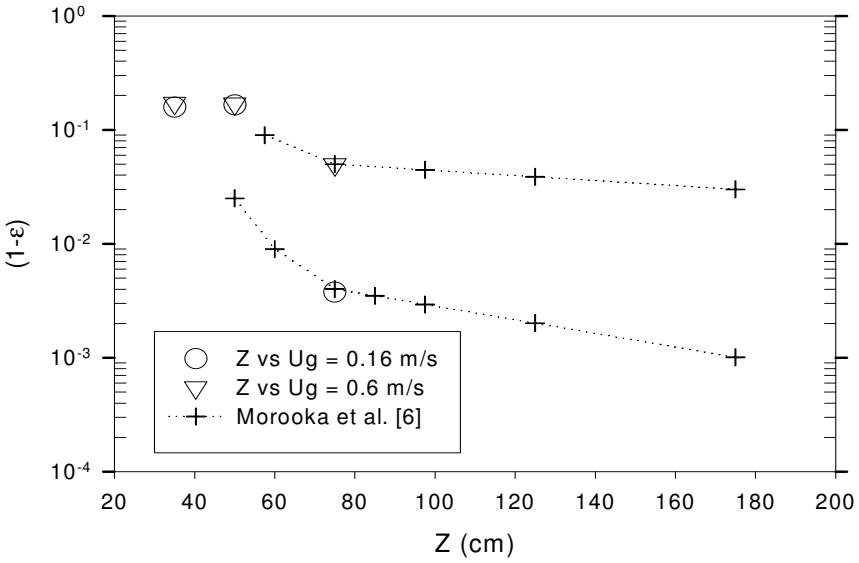

Figure 4: Average solids fraction w.r.t. to axial position

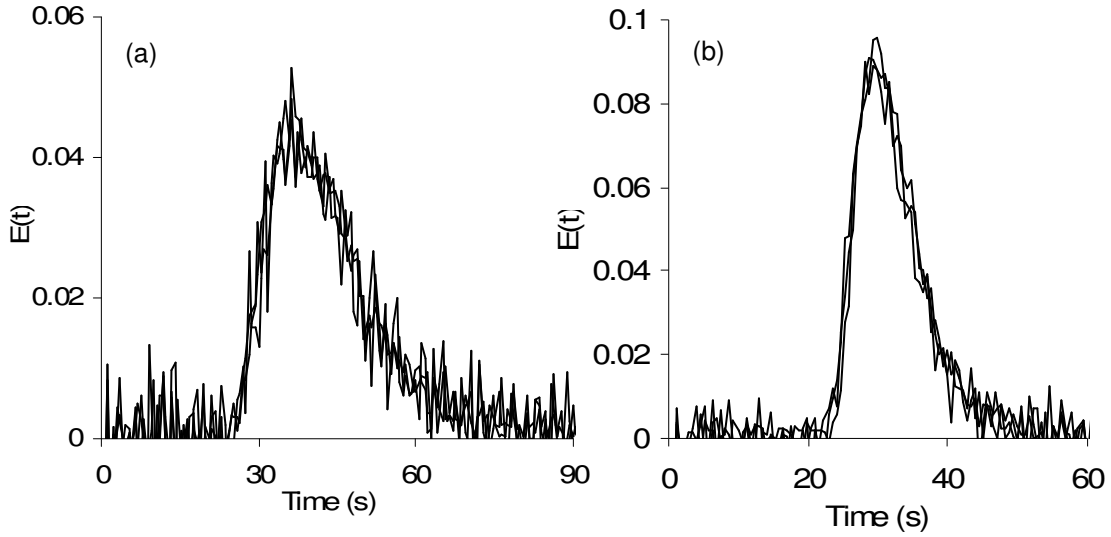

Figure 5: E(t) curve in the freeboard at Z = 96 cm and for: (a) U_g = 0.6 m/s and (b) U_g = 0.2 m/s taken at r/R = 0, 0.5, 1.

However, inside the disengagement region and at U_g = 0.2 m/s, the E(t) curve deformed as shown in Figure 6 which was obtained at the centreline at two axial positions. As the superficial velocity was increased to 0.6 m/s, the E(t) curve retained its Gaussian shape as observed from Figure 7. At low velocity and inside the freeboard, the flow regime is close to turbulent flow with a Reynolds number (Re) of 2750, which is near the commonly used threshold of 3000. However, in the disengagement region, due to an increase in diameter (3×) and a decrease in U_g (÷9 by assuming rapid expansion of the gas), the Re is divided by a factor of three and the flow becomes laminar. Therefore, there are most likely large scale mixing patterns that form inside the disengagement section and deforms the tracer front. However, at U_g = 0.6 m/s, the flow is highly turbulent inside the reactor with Re = 8250 and it approaches plug flow. Table 1 lists the first (t_{mean}) and second (σ^2) moments of the E(t) curve for different axial positions inside the freeboard and disengagement regions. Note that the reported values have been averaged over the entire section of the reactor. In essence, Table 1 shows that the variance does not change significantly with height inside the freeboard, which further supports the conclusion that the hydrodynamics in that region is close to plug flow. This is also true for U_g = 0.6 m/s inside the disengagement region.

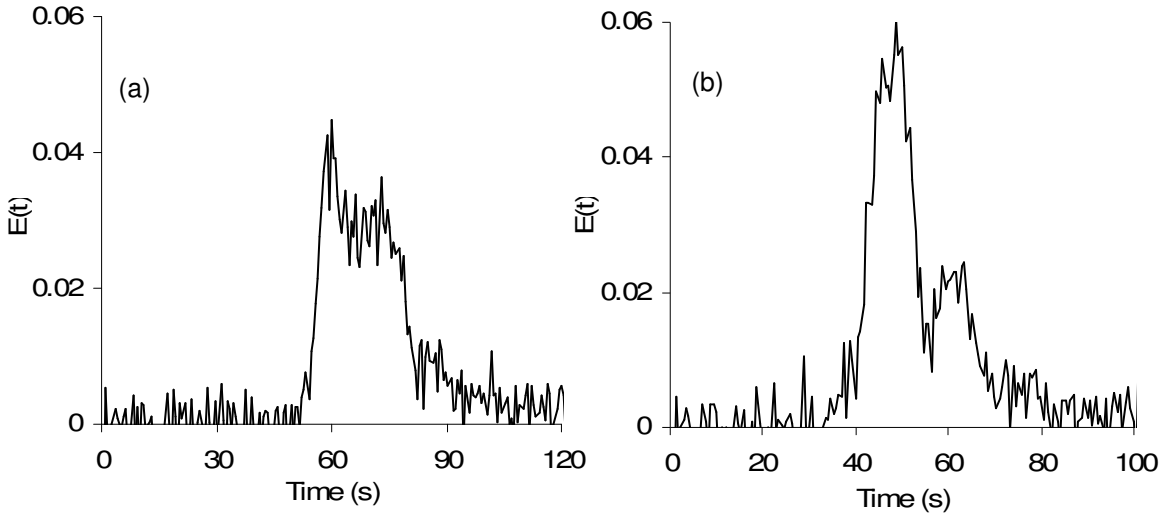

Figure 6: E(t) curve for U_g = 0.2 m/s and for: (a) Z = 122 cm and (b) Z = 152 cm at the centreline (r/R = 0)

Table 1: Properties of the E(t) curves and n-CSTRs model parameters

Z (cm)	U_g (cm/s)	σ^2 (s^2)	t_{mean} (s)	$(t_{mean}-t)_{max}$ (s)
45	20	85.8	42.1	0.2
96	20	90.5	43.4	0.8
122	20	88.9	51.9	1.6
152	20	103.3	70.4	3.8
96	60	22	31.9	0.4
122	60	20.3	31.2	0.8
152	60	20.7	34.6	0.6

In order to relate the position of ignition to the induction time, the average residence time of the gas must be measured. Furthermore, the fifth column reports the maximum absolute variation. It is shown that inside the freeboard and disengagement (at U_g = 0.6 m/s only) regions, the variation reaches a maximum of 0.8 seconds. On the other hand, the variation increased significantly at U_g = 0.2 m/s inside the

disengagement region due to the large scale mixing patterns. This larger variation will lead to higher uncertainties in the induction time measurements.

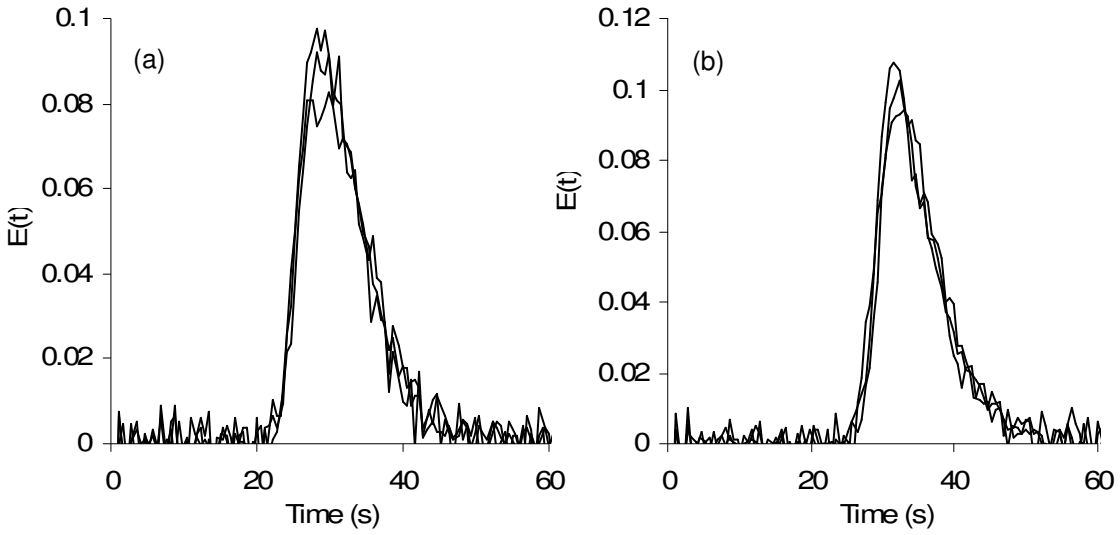

Figure 7: E(t) curve for U_g = 0.6 m/s and for: (a) Z = 122 cm and (b) Z = 152 cm taken at r/R = 0, 0.5, 1.

CONCLUSIONS

In the present study, the solids and gas hydrodynamics were characterized. First, it was shown with fibre-optic probe measurements that the solids concentration remained approximately constant with radial position and with axial position close to the bed surface. As the axial position was increased, the solids fraction decreased with both increasing height and decreasing superficial velocity. Furthermore, gas RTD experiments showed that the hydrodynamic regime inside the freeboard was close to plug flow at U_g = 0.2 and 0.6 m/s velocities. However, the diverging area leading to the disengagement region produced perturbations on the E(t) curve at low velocity which were likely due to large scale eddies in the flow since the Reynolds number was inside the laminar range. At higher gas velocity (U_g = 0.6 m/s), the flow approached plug flow again inside the disengagement region.

REFERENCES

[1] Landi, G., Lisi, L. and Volta, J.-C. “Oxidation of propane to acrylic acid over vanadyl pyrophosphate: modifications of the structural and acid properties during the precursor activation and their relationship with catalytic performance”, *Journal of Molecular Catalysis A: Chemical*, 222, 2004, P. 175-181.

[2] Herzler, J., Jerig, L. and Roth, P. “Shock-tube study of the ignition of propane at intermediate temperatures and high pressures”, *Combustion Science and Technology*, 176, 2004, P. 1627-1637.

[3] Chang, C.J., Thompson, A.L. and Winship, R.D. “Ignition delay of propane in air between 725-800^{o}C under isothermal conditions”, 7th International Symposium on Combustion (1958, London). *Proceedings*. The Combustion Institute, editor. Pittsburgh. Combustion Institute, 1958. P. 431-435.

[4] Lorences, M.J., Laviolette, J.-P., Patience, G.S., Alonso, M. and Diez, F.V. “Fluid bed gas RTD: Effect of fines and internals”, *Powder Technology*, 168, 2006, P. 1-9.

[5] Kato, K., Wen,C. Y*.,* "Bubble assemblage model for fluidised bed catalytic reactor" , *Chemical Engineering Science*, 24, 1969, P. 1351-1369.

[6] Morooka, S., Kawazuishi, K. and Kato, Y. “Holdup and flow pattern of solid particles in freeboard of gas-solid fluidized bed with fine particles”, *Powder Technology*, 26, 1980, P. 75-82.

ANNEXE 2 – ARTICLE PRESENTÉE À LA CONFÉRENCE IFSA 2008

Gas-phase combustion in the freeboard of a fluidized bed

Jean-Philippe Laviolette, Gregory S. Patience and Jamal Chaouki

Ecole Polytechnique, Montréal, Canada

Keywords: fluidized bed, propane, combustion, freeboard, non-isokinetic sampling, solids flux

ABSTRACT

Propane was injected inside a high temperature fluidized bed through a sparger and the freeboard region was characterized using pressure, solids flux, species volume fraction and temperature measurements during freeboard combustion. Solids flux and species volume fractions were measured simultaneously using a non-isokinetic probe. A decrease in propane and oxygen as well as an increase in temperature was observed in the freeboard. The solids flux measurements showed a net upward flow at the centre of the reactor and a net downward flow near the wall. Furthermore, the solids entrainment was found to decrease exponentially with height from the bed surface. The measured entrainment at the bed surface was significantly higher than predicted by the correlation of Wen *et al.* [1]: 17.6 kg/m^{2}s compared to 8.18×10^{-4} kg/m^{2}s. Pressure and solids flux measurements were also used to locate the fluidized bed surface. Solids flux measurements were more precise than pressure to determine bed height. The location of the bed surface was taken as the inflection point of the entrainment curve. Finally, the temperature profile corresponding to the measured solids flux and species volume fractions was determined using a series of thermocouples positioned along the length of the reactor.

INTRODUCTION

Many industrial catalytic processes involve simultaneous heterogeneous and homogeneous reaction pathways. Homogeneous reactions generally result in yield lost of the desired compound, but they may also represent a significant safety hazard in the case of fast and highly

exothermic reactions such as those involving oxygen and hydrocarbons. Chemical processes with oxygen and hydrocarbons are widespread in the industry. Furthermore, new processes are currently under development in the context of oil price fluctuations and global warming: selective oxidation of alkanes, combustion of cheaper feedstock for heating and catalyst regeneration, biomass gasification, etc. Fluidized bed reactors are currently being developed for a variety of these processes. In order to maximize productivity, they may operate within the explosion limits while feeding the oxidant and hydrocarbon separately into the bed – through spargers. This is possible due to the ability of the solids phase to suppress the homogeneous reactions (combustion) and at the same time promote selective heterogeneous reactions.

Due to operational constraints, these processes may operate under partial conversion conditions. For example, selectivity generally declines at high conversion in selective oxidation processes due to an increase in the rate of series reactions [2, 3, 4]. The implications for fluid bed is that downstream of the solids – in the freeboard, cyclones and associated piping – the effluent gas phase composition is potentially explosive – high hydrocarbon and oxygen concentrations, elevated temperature with an insufficient solids volume fraction to quench non-selective homogeneous reactions [5, 6]. Minimizing the risk of gas-phase combustion-deflagration in these regions remains an important design issue.

The threshold conditions leading to autoignition (self-initiated homogeneous combustion) must be known to minimize the safety hazards not only during standard operation but also during start-up as well as emergency shut down conditions. Several explosion criteria (explosion limits, autoignition temperature and induction times [6]) measured in homogeneous gas-phase systems as well as gas-phase kinetic models are available in the scientific literature [7]. However, extrapolating these tendencies to a fluidized bed reactor introduces uncertainties since the entrained solid particles affect the gas-phase reactions downstream of the fluidized bed. Furthermore, fluidized beds are non-homogeneous systems - solids entrainment decreases exponentially from the bed surface to the transport disengagement height [1]. Also, an axial temperature gradient may exist in the freeboard region as well as species concentration gradients depending on the hydrodynamics.

To accurately predict gas-phase combustion in the freeboard of a fluidized bed for a wide range of operational conditions, a freeboard combustion model that combines the gas/solids hydrodynamics and the reaction kinetics must be developed. This model needs to integrate through the axial gradient of solids fraction and temperature that characterize the freeboard as well as accounting for the effects of solids on the reaction kinetics. Models of the reaction in the freeboard of fluidized beds have been previously proposed by Chen *et al.* [8] Dounit *et al.* [9] and Dounit *et al.* [10]. These models used entrainment models that include a correlation for the entrainment at the bed surface such as the model of Wen *et al.* [1]. However, the solids entrainment at the bed surface was extrapolated from experimental data measured several centimetres downstream of the bed surface (sometimes more than 50 centimetres). Therefore, the existing entrainment models may yield significant errors near the bed surface and better accuracy would be obtained by directly measuring solids fraction.

The species volume fractions and solids fraction measured in the freeboard are two dependent parameters since the reaction kinetics varies with solids fraction. The ability of sand particles to inhibit homogeneous reactions and to delay autoignition has been shown by Hesketh *et al*. [6]. Solids entrainment has been previously measured using non-isokinetic probes [11, 12, 13]. The measured solids flux using such probes has been found to be constant for a range of sampling rates such that the probe does not necessarily have to be at the isokinetic condition. Also, solids fraction has been measured using fibre-optic probes [14, 15] and capacity probes [15]. With these techniques, solids fraction/entrainment is measured independently of species volume fractions.

In the present study, propane was injected inside a high temperature fluidized bed through a downward facing sparger and the freeboard region was characterized using pressure, solids flux, species volume fraction and temperature measurements during freeboard combustion. The fluidized bed temperature, superficial velocity and propane/air ratio were adjusted to obtain propane combustion in the freeboard. Solids flux and species volume fractions were measured simultaneously using a non-isokinetic probe. The temperature profile in the freeboard was monitored using eight thermocouples.

EXPERIMENTAL SETUP & CONDITIONS

The experiments were conducted in the fluidized bed reactor of Figure 1. The bed and freeboard regions had an inner diameter of 20 cm, while the disengagement section had an inner diameter of 60 cm. For all experiments, sand particles (Geldart group B – ρ_s = 2650 kg/m^3, d_p = 250 µm) were used as the bed material and air was the fluidizing media. The experimental procedure first consisted of adjusting the superficial gas velocity to 24 cm/s (at 650°C). The fluidized bed was then heated to 680°C with the natural gas burner upstream of the windbox and by injecting heavy vacuum gas oil (HVGO) through the sparger. When the bed temperature reached 680°C, the burner and HVGO injection were stopped and propane was injected through the sparger for 30 minutes to burn HVGO residues.

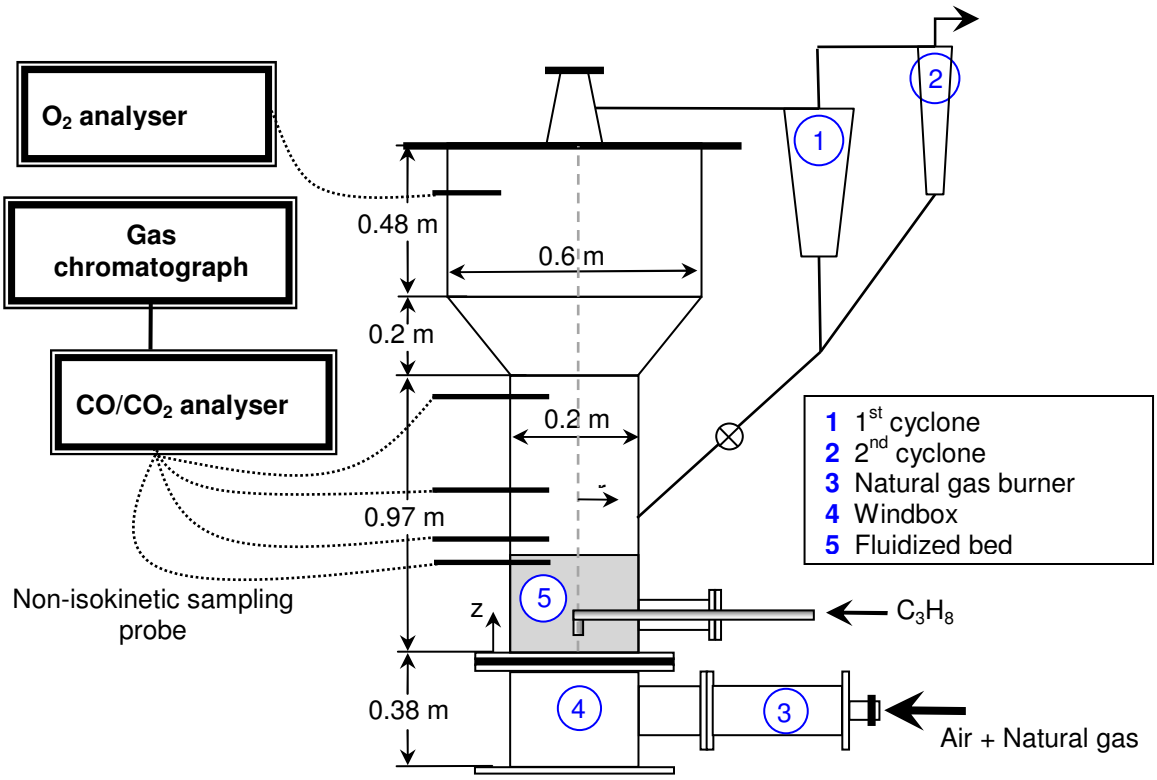

Figure 1: Fluidized bed reactor

The propane was then turned off and the fluidized bed cooled down until the bed temperature reached 645°C. Propane was then injected through the downward sparger to obtain a mixed-cup

volume fraction of 2 vol% in air. A non-isokinetic probe was used to sample gas and solids simultaneous from 5 axial and 6 radial positions. The sampling system is shown in Figure 2 and consisted of a 4.1 mm I.D. probe bent at a 90^o at its tip. The sampled gas/solid stream first went through a 250 mL container that lowered the sampled gas velocity and caused the separation of the solid particles from the gas. The gas was analyzed by a Siemens Ultramat CO/CO_2 analyzer and a Varian CP-4900 micro-GC that measured the following species: O_2, H_2, CH_4, C_2H_4, C_2H_6, C_3H_6, C_3H_8, CO, CO_2 and N_2. Solids flux was calculated from the mass of the sampled solids and the sampling time:

$$G_{SU,D} = \frac{m}{A.t} \tag{1}$$

The cross-sectional area at the probe's tip was 0.66 cm^2. The upward (G_{SU}) and downward (G_{SD}) solid fluxes were measured by orienting the probe tip downward and upward, respectively. The sampling flow rate was controlled using a rotameter connected to a vacuum line. During the sampling time, the bed temperature increased to 650ºC.

Gas was also sampled in the disengagement region (z = 147 cm) and analyzed with an oxygen analyzer (Siemens Oxymat 6.1). The results from the GC, CO/CO_2 analyzer and oxygen analyzer were compared and used in a molar balance to confirm the validity of the measured species volume fractions. The temperature along the reactor was monitored using 8 thermocouples located along the length of the reactor. The sparger consisted of a 4.1 mm I.D. tube pointing downward at the bed centreline. The sparger tip was located at a height of 9.8 cm above the distributor.

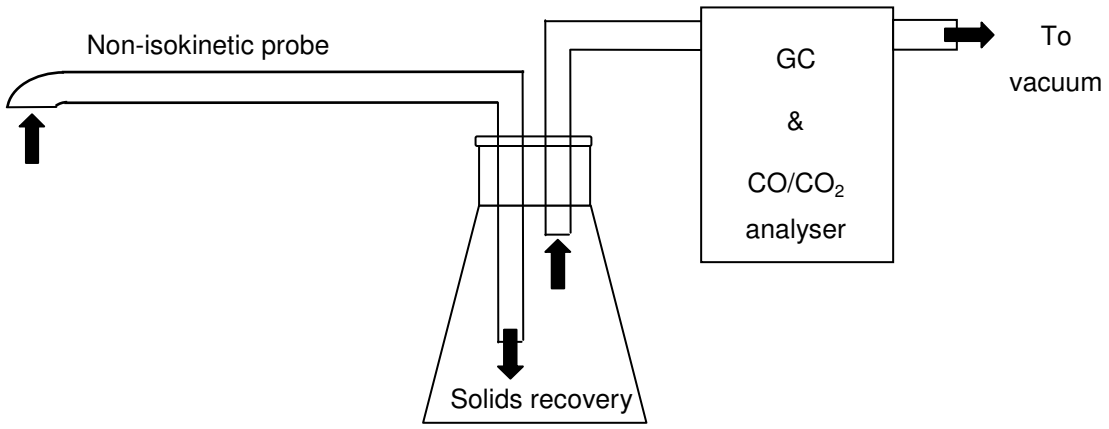

Figure 2: Schematic of sampling system

RESULTS AND DISCUSSION

The reaction rate of propane combustion in the freeboard of a fluid bed depends on species volume fractions, temperature and solids fraction. They are dependent parameters and should ideally be measured simultaneously.

Simultaneous sampling of gas and solids

A non-isokinetic sampling probe was used to measure the species volume fractions and the solids flux simultaneously. From the superficial gas velocity (U_g = 24 cm/s) and the probe cross-sectional area, the sampling rate required to obtain a gas velocity of 24 cm/s at the probe tip was 310 mL/min. However, a preliminary set of experiments was conducted to determine the effect of gas sampling rate on the solids flux. The sampling probe was positioned near the bed at z = 29 cm and the upward solids flux (G_{SU}) was measured at three radial positions: r = 0 (centre), 4 and 8 cm. The gas sampling rate was varied from 232 mL/min to 580 mL/min. These experiments were conducted at a bed temperature of 650ºC and with propane freeboard combustion. Upward solids flux as a function of gas sampling rate is shown in Figure 3(a): the measured solids flux was almost independent of sampling rate in the range of 270 - 470 mL/min. Therefore, it was not necessary to have sampling that was precisely iso-kinetic and a sampling rate of 425 mL/min was used for all experiments.

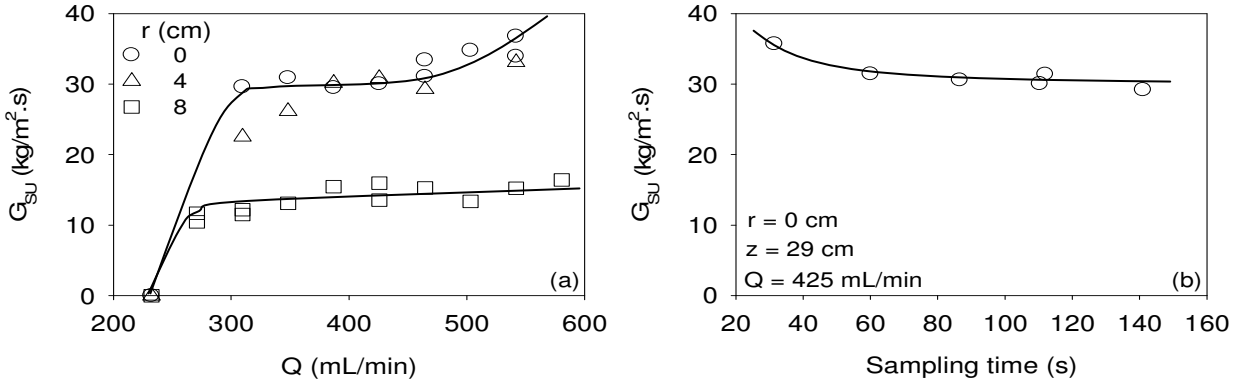

Figure 3: The isokinetic condition

Experiments were also conducted to determine the effect of sampling time on the measured solids flux. Figure 3(b) shows the measured upward solids flux at the centreline as a function of sampling time. The solids flux decreased by 14% (from 35.7 kg/m^{2}s to 31.4 kg/m^{2}s) as the sampling time was increased from 31 to 60 seconds. After 60 seconds, the measured solids flux remained more constant with sampling time: it decreased by 7.0 % (from 31.4 kg/m^{2}s to 29.2 kg/m^{2}s) as the sampling time was increased to 141 seconds. This decrease in measured solids flux was most probably due to the fact that the mass of sampled solids represented a significant fraction of the total bed: 275 g was sampled after 141 seconds, which represented 3.3 % of the total mass of the bed (8.3 kg). These results suggest that a minimum sampling time of 60 seconds was required to reach a permanent condition.

The gas sampled with the non-isokinetic sampling probes was sent to the CO/CO_2 analyzer and the GC for analysis. Figure 4 shows the measured CO_2 species fractions at the centreline (r = 0 cm), z = 87 cm and with Q = 425 mL/min as a function of sampling time. A sampling time of only 20 seconds was required for a representative measurement of the species volume fractions inside the reactor.

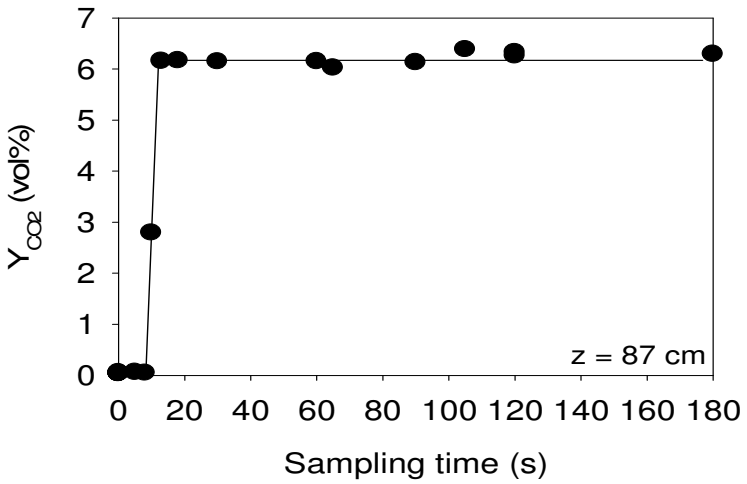

Figure 4: Sampling time impact

Solids flux in the freeboard

Upward (G_{SU}) and downward (G_{SD}) solid fluxes were measured at 5 axial positions and 6 radial positions. The radial profiles of solids flux are shown in Figure 5(a) for three axial positions: 29, 35 and 45 cm above distributor. The upward (empty symbols) and downward (filled symbols) solids fluxes reached a maximum at reactor centreline and decreased closer to the wall. The measurements were averaged over the fluid bed cross-section. At z = 29 cm, the upward and downward solids fluxes were 17.6 kg/m^{2}s and 19.0 kg/m^{2}s, respectively (difference of 1.4 kg/m^{2}s). At z = 35 cm, the upward solids flux was 4.7 kg/m^{2}s and the downward solids flux was 3.0 kg/m^{2}s (difference of 1.7 kg/m^{2}s). At z = 45 cm, the upward and downward solids flux were both zero.

The radial profiles of net solids flux (G_S) are shown in Figure 5(b) for three axial positions: there was a net upward of solids at the centre of the reactor. Near the wall, there was a net downward flow of solids. This agrees well with the literature [16, 17, 18].

Table 1 compares the upward solids flux of the present study with the values measured by Large *et al.* [19] with silica sand ($d_p > 250$ µm) at ambient temperature and $U_g = 30$ cm/s.

Large *et al.* [19] measured solids entrainment 50 cm above the fluid bed and used extrapolation to estimate the entrainment at the surface. Wen *et al.* [1] used these results to develop a correlation for the entrainment at the bed surface. It can be seen from Table 1 that using the correlation of Wen *et al.* [1] to estimate the entrainment at the bed surface yield a significant error: the present study measured 17.6 kg/m^{2}s and the correlation estimated 8.18×10^{-4} kg/m^{2}s. Furthermore, the measurements of Large *et al.* [19] were one order of magnitude smaller than the values obtained in the present study. This difference can be explained by the extrapolation, which resulted in significant errors.

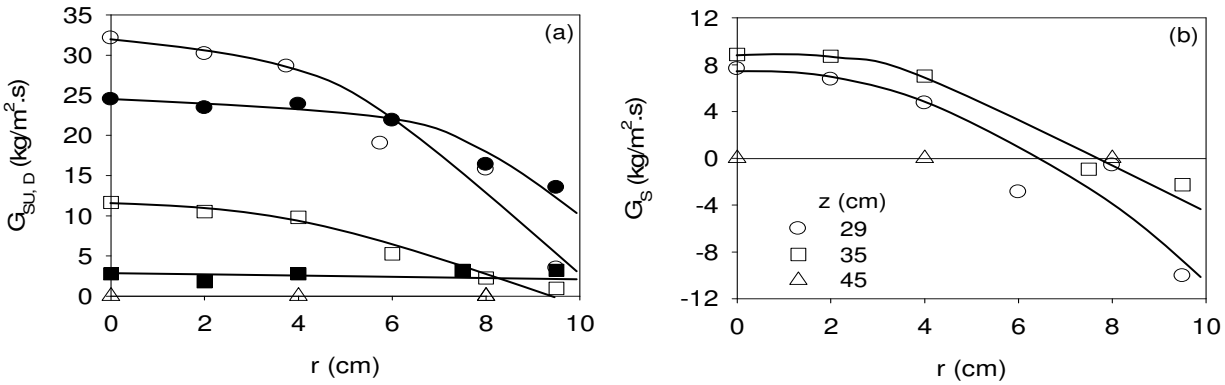

Figure 5: Solids flux radial profile

Defining the location of the bed surface

The freeboard region begins at the fluidized bed surface. Bubbles form at the distributor, rise rapidly through the bed and collapse at its surface releasing solid particle upward. The bubble dynamics result in successive expansion and collapse of the fluidized bed. Depending on the gas superficial velocity, solids entrainment can be significant and the bed surface can be diffuse.

In the present study, a time-average position of the bed surface was determined by pressure and solids flux measurements. During the experiments, the static pressure was continually measured at 4 axial positions at the wall and the time-averaged value was calculated. Figure 6 shows the time-averaged static pressure inside the reactor. The pressure decreased significantly from

2.6 kPa to 0.3 kPa from z = 5 to 25 cm. These results suggest that these two probes were inside the fluidized bed where the high solids fraction results in a significant hydrostatic pressure. In the freeboard where the solids fraction is much lower, pressure remained constant at 0.1 kPa from z = 35 to 77 cm. Therefore the pressure profile indicates that the bed surface was located between z = 25 and 35 cm.

Table 1: Entrainment at the bed surface

Solids type	**U_g (cm/s)**	**d_p (μm)**	**T_b (°C)**	**G_{SUo} (kg/m^{2}s)**	**Reference**
Silica sand	24	250	650	17.6	This work
Silica sand	24	250	650	8.18×10^{-4}	Correlation - Wen *et al.* [1]
Silica sand	30	130	Ambient	2.2-3	Experimental data – Large *et al.* [19]
Silica sand	20	130	Ambient	10^{-2}	

The measurements of upward solids flux (or entrainment flux) were also used to determine the bed surface position. Entrainment flux was measured at 5 axial positions (z = 29, 35, 46, 56 and 88 cm) and 6 radial positions (r = 0, 2, 4, 6, 8, 10 cm). Figure 6 shows the cross-sectional average of entrainment flux as a function of axial position. The entrainment flux reached 17.6 kg/m^{2}s at a height of 29 cm and then decreased exponentially to 4.7 kg/m^{2}s at z = 35 cm and zero at z = 46 cm. If the inflection point of the solid flux curve is taken as the bed surface as proposed by Kunii *et al.* [20], the bed surface was located at z = 29 cm. This agrees well with the pressure measurements. These results show that the position of the bed surface can be determined more precisely with solids flux measurements compared to pressure measurements.

Species volume fraction in the freeboard

The species volume fractions were measured simultaneously to the solids flux at several positions inside the freeboard. Figure 7 shows the radial profile of gaseous species at four axial positions inside the freeboard. At the bed surface (z = 29 cm), there was a radial profile of propane volume fraction – propane volume fraction decreased from 0.9 vol% at the centerline to 0.4 vol% at 5 mm from the wall. At z = 35 cm, the radial profile was more uniform with an average volume fraction of 0.3 vol%.

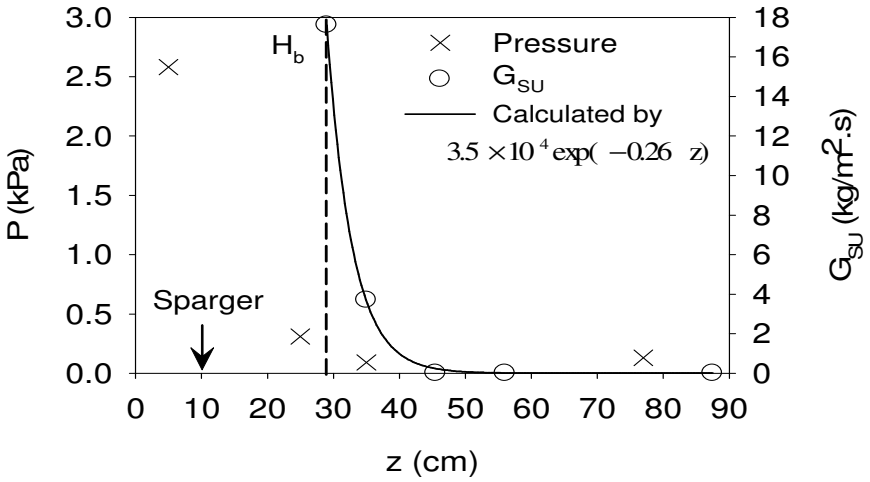

Figure 6: Defining the bed height

The radial profile of oxygen in the freeboard is shown in Figure 7(b). The oxygen radial profile was approximately flat throughout the freeboard.

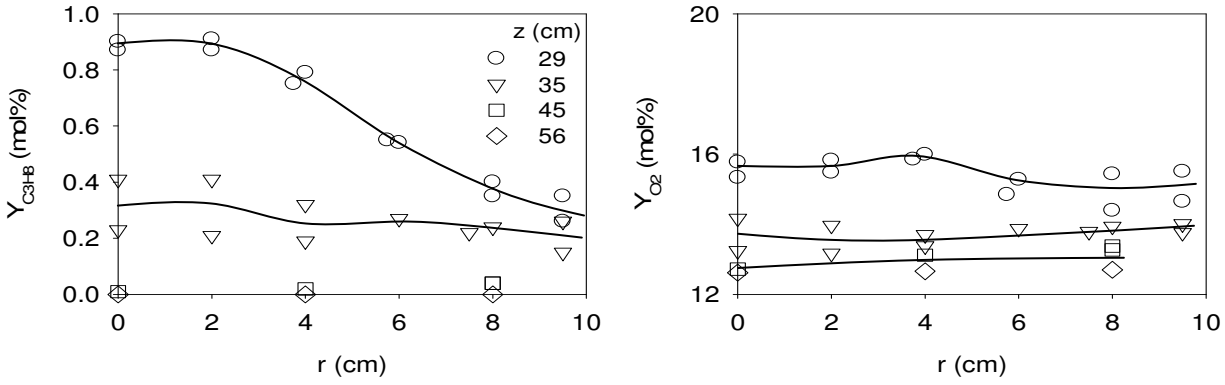

Figure 7: Species radial profile at bed surface

Freeboard combustion

As the unconverted propane entered the freeboard, high temperatures combined to low solids fraction resulted in propane combustion. Figures 8(a) and 8(b) show the axial profiles of C_3H_8, CO, O_2 and CO_2 inside the fluidized bed reactor – propane conversion inside the fluid bed reached 71% as propane decreased from 1.77 vol% (mixed-cup) at the inlet to 0.51 vol% at the bed surface (z = 29 cm). In the freeboard, the remaining propane reacted with oxygen to form CO_2 and complete combustion was obtained at z = 56 cm.

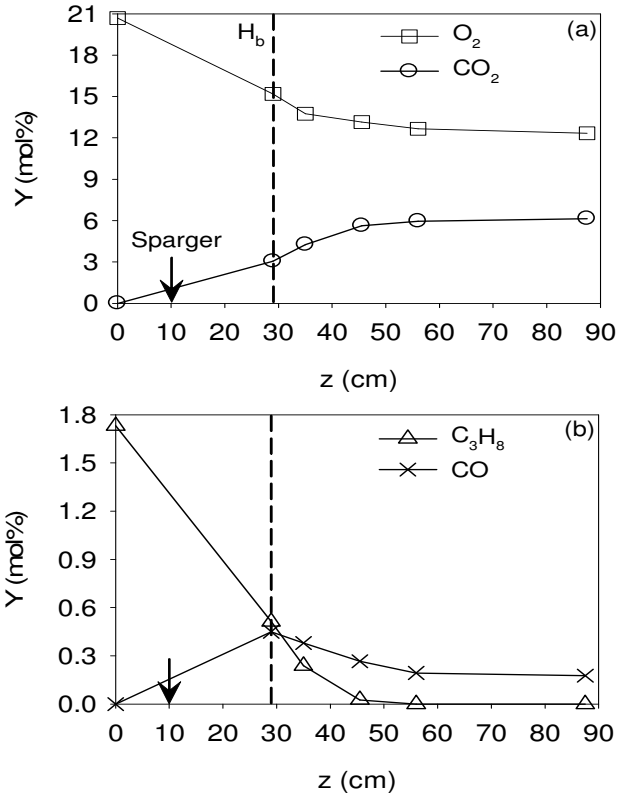

Figure 8: Freeboard combustion

Temperature profile

Measuring the axial temperature profile inside the fluid bed reactor that corresponds to the measured solids flux and species volume at each sample point is a difficult task unless the system

reaches steady. The temperature profile inside the freeboard was monitored with eight thermocouples positioned along the length of the reactor. Two thermocouples were located inside the fluidized bed and six in the freeboard. Figure 9 shows the axial temperature profiles just prior to propane injection (t = 0 s) and after injection when one sample point was done (t ≈ 170 s). After injection, the temperature inside the fluidized bed and freeboard increased with time due to the exothermicity of the combustion reaction. Between each sample points, the propane was stopped to allow the fluidized bed and freeboard to cool down. During combustion, a maximum temperature increase of 33ºC was measured inside the freeboard. Using the chemical composition of the gas measured at the bed surface (z = 29 cm) and assuming adiabatic constant pressure combustion, the theoretical temperature increase is calculated as 546ºC from the CEA equilibrium code [21].

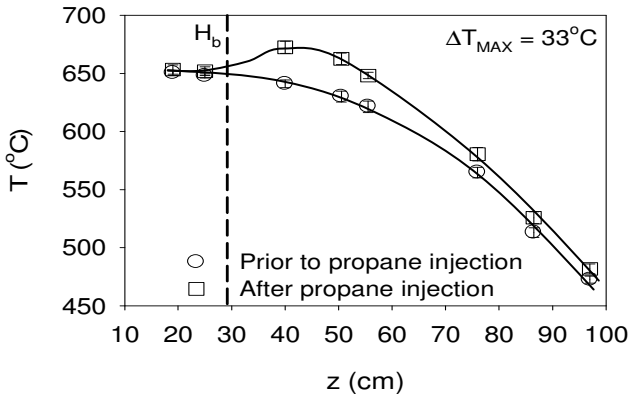

Figure 9: Axial temperature profile

Figure 9 shows the variation in the axial temperature profiles (before and after propane injection) for the entire experimental run (time required to sample from all axial and radial positions) - the maximum temperature variation was ± 5ºC.

It was seen earlier from Figure 4 that only 20 seconds of sampling time was required to measure species volume fractions. Figure 10 shows the temperature history at all sample points following the injection of propane at t = 0 s. After the sampling time of approximately 170 s, the temperature inside the reactor increased by a maximum of 2ºC within 20 seconds. Therefore, the

measured reactor temperature profile "after propane injection" corresponds to the measured solids flux and species volume fractions.

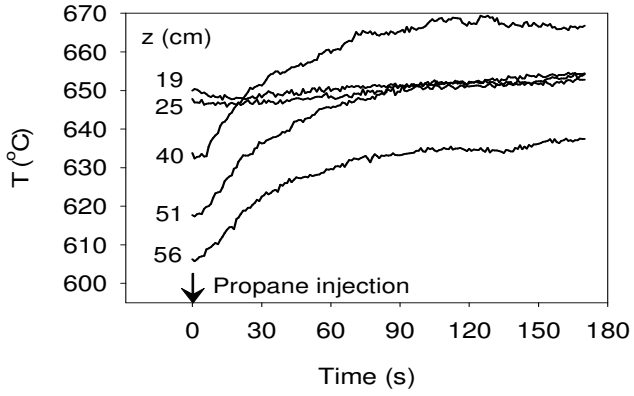

Figure 10: Temperature history

CONCLUSIONS

In the present study, propane was injected inside a high temperature fluidized bed through a downward facing sparger and the freeboard region was characterized using pressure, solids flux, species volume fraction and temperature measurements during freeboard combustion. The combustion in the fluidized bed and freeboard was confirmed by a decrease in oxygen and propane as well as a temperature increase in the reactor. Solids flux and species volume fractions were measured simultaneously using a non-isokinetic probe. The measurements showed a net upward flow of solids at the centre of the reactor and a net downward flow near the wall. Furthermore, the upward solids flux was found to decrease exponentially with height from the bed surface. The measured entrainment at the bed surface was found to be significantly higher than predicted by the correlation of Wen *et al.* [1]: 17.6 kg/m^{2}s compared to 8.18×10^{-4} kg/m^{2}s. Pressure and solids flux measurements were also used to locate the fluidized bed surface. Solids flux measurements were found to be more precise than pressure to determine bed height. The location of the bed surface was taken as the inflection point of the entrainment curve. Finally, the temperature profile corresponding to the measured solids flux and species volume fractions was determined using a series of thermocouples positioned along the length of the reactor.

NOMENCLATURE

A	Cross-sectional area at the tip of the sampling probe (m^2)
d_p	Average particle size (μm)
G_S	Net solids flux ($kg/m^2.s$)
G_{SD}	Downward solids flux ($kg/m^2.s$)
G_{SU}	Upward solids flux ($kg/m^2.s$)
H_b	Bed height (cm)
m	Mass of sampled solids (kg)
r	Radial position (cm)
t	Time (s)
T	Temperature (ºC)
T_b	Fluidized bed temperature (ºC)
Q	Sampling rate (mL/min)
Y	Molar fraction (mol%)
z	Axial position (cm)

REFERENCES

1. Wen, C.Y. & Chen, L.H. 1982. Fluidized bed freeboard phenomena: entrainment and elutriation. *AIChE J.* 28 (1): 117-128.
2. Malleswara Rao, T.V. & Deo, G. 2007. Ethane and propane oxidation over supported V_2O_5/TiO_2 catalysts: analysis of kinetic parameters. *Ind. Eng. Chem. Res.* 46 (1): 70-79
3. Patience, G.S. & Lorences, M.J. 2006. VPO transient oxidation kinetics. *Int. J. Chem. React. Eng.* 4 (A22).

4. Botella, P., Lopez Nieto, J.M. & Solsona, B. 2002. Selective oxidation of propene to acrolein on Mo-Te mixed oxides catalyst prepared from ammonium telluromolybdates. *J. Mol. Catal. A-Chem.* 184: 335-347.
5. Van der Vaart, D.R. 1988. Freeboard ignition of premixed hydrocarbon gas in a fluidised bed. *Fuel*, 67: 1003-1007.
6. Hesketh, R.P. & Davidson, J.F. 1991. Combustion of methane and propane in an incipiently fluidized bed. *Combust. Flame*. 85: 449-467.
7. Marinov, N.M., Pitz, W.J., Westbrook, C.K., Vincitore, A.M., Castaldi, M.J., Senkan, S.M. and Melius, C.F. 1998. Aromatic and polycyclic aromatic hydrocarbon formation in a laminar premixed *n*-Butane flame. *Combust. Flame.* 114 (1-2): 192-213.
8. Chen, L.H. & Wen, C.Y. 1982. Model of solid gas reaction phenomena in the fluidized bed freeboard. *AIChE J.* 28 (6): 1019-1027.
9. Dounit, S., Hemati, M. & Steinmetz, D. 2001. Natural gas combustion in fluidized bed reactors between 600 and 850ºC: experimental study and modelling of the freeboard. *Powder Technol.* 120: 49-54.
10. Dounit, S., Hemati, M. & Andreux, R. 2008. Modelling and experimental validation of a fluidized-bed reactor freeboard region: Application to natural gas combustion. *Chem. Eng. J.* 140: 457-465.
11. Rhodes, M.J. & Laussmann, P. 1992. A simple non-isokinetic sampling probe for dense suspensions. *Powder Technol.* 70: 141-151.
12. Reinhardt, B., Cordonnier, A. & Florent, P. 1999. Use of an isokinetic sampling propane. Results in a cyclone. *Powder Technol.* 101: 81-90.
13. Van der Meer, E.H., Thorpe, R.B. & Davidson, J.F. 2000. Flow patterns in the square cross-section riser of a circulating fluidized bed and the effect of riser exit design. *Chem. Eng. Sci.* 55: 4079-4099.
14. Morooka S., Kawazuishi, K. & Kato, Y. 1980. Holdup and flow pattern of solids particles in freeboard of gas-solid fluidized bed with fine particles. *Powder Technol.* 26: 75-82.
15. Werther, J. 1999. Measurement techniques in fluidized beds. *Powder Technol.* 102: 15-36.
16. Aguillón, J., Shakourzadeh, K. & Guigon, P. 1995. Comparative study of non-isokinetic sampling probes for solids flux measurement in circulating fluidized beds. *Powder Technol.* 83: 79-84.

17. Van Breugel, J.W., Stein, J.J.M. & de Vries, R.J. 1970. Isokinetic sampling in a dense gas-solids stream. *Proc. Instn. Mech. Engrs.* 184: 18-23.
18. Rhodes, M.J., Laussmann, P., Villain, F. & Geldart, D. 1988. Measurement of radial and axial solids flux variations in the riser of a circulating fluidized bed. *In* Basu, P. & Large, J.F. (eds) *Circulating Fluidized Bed Technology II*: 155-164. Oxford: Pergamon Press.
19. Large J.F., Martinie, Y. & Bergougnou, M.A. 1977. Interpretative model for entrainment in a large gas-fluidized bed. *J. Powders Bulk Solids Technol.* 1: 15-21.
20. Kunii, D. & Levenspiel, O. 1991. *Fluidization Engineering*. 2nd edition. Boston, MA: Butterworth-Heinemann.
21. Gordon S. & McBride, B.J. 1994. Computer program for calculation of complex chemical equilibrium compositions and applications. *NASA RP-1311*.

ANNEXE 3 – ARTICLE PRÉSENTÉ À LA CONFÉRENCE FBC 2009 (CHINE)

GAS-PHASE COMBUSTION IN THE FREEBOARD OF A FLUIDIZED BED – FREEBOARD CHARACTERIZATION

Jean-Philippe Laviolette, Gregory S. Patience and Jamal Chaouki

Department of Chemical Engineering, Ecole Polytechnique, Montréal, Canada

Abstract: The prediction of propane autoignition in the freeboard of a fluidized bed is complicated by the presence of solids, intermediate products and non-homogeneities (solids, temperature and species gradients) that should be accounted for in a reaction model. However, the simultaneous characterization of these parameters during combustion is very challenging. An experimental study of propane combustion inside the freeboard (I.D. = 0.2 m) of a fluidized bed of sand (d_p = 290 μm) was performed at a low superficial gas velocity (U_g = 0.24 m/s). Propane was injected inside the fluidized bed (T_{Bed} = 650ºC) through a downward-facing sparger. Also, solids flux and species volume fractions were measured using a non-isokinetic sampling probe. The results showed an exponential decrease with height of the upward solids flux (G_{SU}) – G_{SU} was zero at 0.17 m above the bed surface, which was taken as the inflection point of the G_{SU} curve. G_{SUo} measurements were significantly higher than the values given by the correlation of Wen *et al.* (1982). The bed surface (boundary condition) and freeboard were characterized by measuring pressure, solids flux, species volume fractions and temperature at several radial and axial positions. During the experiments, the fluidized bed achieved a pseudo steady-state operation that ensured that the measured temperature profile corresponded to the solids flux and species fractions. Partial propane combustion in the fluidized bed (71%) produced CO and cracking species that were transported in the freeboard. Complete combustion occurred within 0.15 m of the bed surface and the propane induction time in the freeboard (< 0.25 s) was on the same order as the values given by three induction time correlations for homogeneous systems.

Keywords: propane, freeboard, induction time, non-isokinetic sampling, combustion

INTRODUCTION

Homogeneous reactions generally result in yield lost of the desired compound, but they may also represent a significant safety hazard in the case of fast and highly exothermic reactions such as those involving oxygen and hydrocarbons. Chemical processes with oxygen and hydrocarbons are widespread in the industry and new processes are currently under development in the context of oil price fluctuations and global warming: selective oxidation of alkanes, combustion of cheaper feedstock for heating and catalyst regeneration, biomass gasification, etc. Fluidized bed reactors are currently being developed for a variety of these processes. In order to maximize productivity, they may operate within the explosion limits while feeding the oxidant and hydrocarbon separately into the bed – through spargers. This is possible due to the ability of the solids phase to suppress the homogeneous reactions (combustion) and at the same time promote selective heterogeneous reactions. However, downstream of the solids – in the freeboard, cyclones and associated piping – the effluent gas phase composition is potentially explosive – high hydrocarbon and oxygen concentrations, elevated temperature with an insufficient solids volume fraction to quench non-selective homogeneous reactions (Van der Vaart, 1988; Hesketh *et al.,* 1991). Minimizing the risk of gas-phase combustion-deflagration in these regions remains an important design issue.

Several explosion criteria (explosion limits, autoignition temperature and induction times (Hesketh *et al.,* 1991)) measured in homogeneous gas-phase systems as well as gas-phase kinetic models are available in the scientific literature (Marinov *et al.*, 1998). Nevertheless, extrapolating these tendencies to a fluidized bed reactor introduces uncertainties since the entrained solid particles affect the gas-phase reactions downstream of the fluidized bed. Furthermore, fluidized beds are non-homogeneous systems - solids entrainment decreases exponentially from the bed surface to the transport disengagement height (Wen *et al*., 1982). Also, an axial temperature gradient may exist in the freeboard region as well as species concentration gradients depending on the hydrodynamics.

To accurately predict gas-phase combustion in the freeboard of a fluidized bed for a wide range of operational conditions, a freeboard combustion model that combines the gas/solids hydrodynamics and the reaction kinetics must be developed. This model needs to integrate through the axial gradient of solids fraction and temperature that characterize the freeboard as well as accounting for the effects of solids on the reaction kinetics. Furthermore, the model should account for the partial combustion and cracking

product originating from the fluidized bed. On the other hand, the simultaneous characterization of solids fraction, species concentration, temperature and pressure in the bed and freevoard during combustion is very challenging.

Freeboard reaction models have been previously proposed by Chen *et al.* (1982), Dounit *et al.* (2001) and Dounit *et al.* (2008). To estimate solids entrainment, the correlation of Wen *et al.* (1982) was used, which is based on the extrapolation of data measured several centimetres downstream of the bed surface (sometimes more than 0.5 m). Consequently, the existing entrainment models may yield significant errors near the bed surface and better accuracy would be obtained by directly measuring solids fraction. Also, the location of the bed surface (beginning of the freeboard region) and its corresponding boundary condition (solids fraction/flux, species fractions, temperature and pressure) need to be clearly defined.

In the present study, propane was injected inside a high temperature fluidized bed through a downward facing sparger and the freeboard region was characterized by simultaneously measuring pressure, solids flux, species volume fraction and temperature during freeboard combustion. Solids flux and species volume fractions were measured using a non-isokinetic probe. The temperature profile in the freeboard was monitored using eight thermocouples.

EXPERIMENTAL APPARATUS

The experiments were conducted in the fluidized bed reactor of Figure 1. The bed and freeboard regions had an inner diameter of 20 cm. For all experiments, sand particles (Geldart group B, ρ_s = 2650 kg/m^3 and d_p = 290 μm) were used as the bed material and air was the fluidizing media. The experimental procedure first consisted of adjusting the superficial gas velocity to 0.24 m/s (at 650^{o}C). The fluidized bed was then heated with the natural gas burner upstream of the windbox and by injecting heavy vacuum gas oil (HVGO) through the sparger. When the bed temperature reached 680^{o}C, the burner and HVGO injection were stopped and propane was injected through the sparger for 30 minutes to burn HVGO residues.

The propane was turned off and the fluidized bed cooled down until the bed temperature reached 645^{o}C. Propane was then injected through the downward sparger to obtain a mixed-cup volume fraction of 2 vol% in air. A non-isokinetic probe was used to sample gas and solids simultaneous from 5 axial and 6 radial positions. The sampling system consisted of a 4.1 mm I.D. probe bent at a 90^o at its tip. The

sampled gas/solid stream first went through a 250 mL container that lowered the sampled gas velocity and caused the separation of the solid particles from the gas. The gas was analyzed by a Siemens Ultramat CO/CO_2 analyzer and a Varian CP-4900 micro-GC that measured the following species: O_2, H_2, CH_4, C_2H_4, C_2H_6, C_3H_6, C_3H_8, CO, CO_2 and N_2. Solids flux was calculated from the mass of the sampled solids and the sampling time.

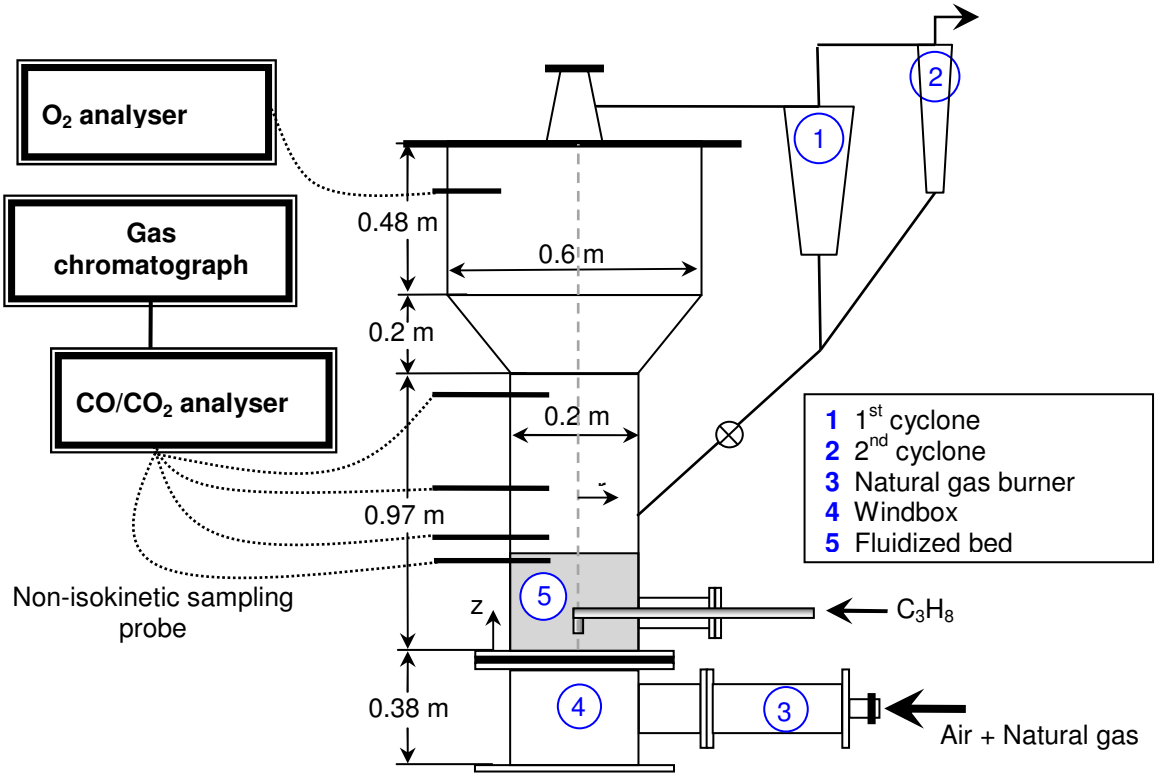

Fig. 1: Fluidized bed reactor

The upward (G_{SU}) and downward (G_{SD}) solid fluxes were measured by orienting the probe tip downward and upward, respectively. The sampling flow rate was controlled using a rotameter connected to a vacuum line. Gas was also continuously sampled in the disengagement region (z = 1.47 m) and analyzed with an oxygen analyzer (Siemens Oxymat 6.1). The results from the GC, CO/CO_2 analyzer and oxygen analyzer were compared and used in a molar balance to confirm the validity of the measured species volume fractions. The temperature along the reactor was monitored using 8 thermocouples located along the length of the reactor. The sparger consisted of a 4.1 mm I.D. tube pointing downward at the bed centreline. The sparger tip was located at a height of 0.098 m above the distributor.

RESULTS AND DISCUSSION

The reaction rate of propane combustion in the freeboard of a fluid bed depends on species volume fractions, temperature and solids fraction. They are dependent parameters and should be measured simultaneously.

Freeboard characterization

Simultaneous sampling of gas and solids

A non-isokinetic sampling probe was used to measure the species volume fractions and the solids flux simultaneously. A preliminary set of experiments showed that the measured solids flux was almost independent of sampling rate in the range of 270 - 470 mL/min. Therefore, it was not necessary to have sampling that was precisely iso-kinetic and a sampling rate of 425 mL/min was used for all experiments. Results also showed that a minimum sampling time of 60 seconds was required to reach a permanent condition. The gas sampled with the non-isokinetic sampling probes was sent to the CO/CO_2 analyzer and the GC for analysis. A sampling time of only 20 seconds was required for a representative measurement of the species volume fractions inside the reactor.

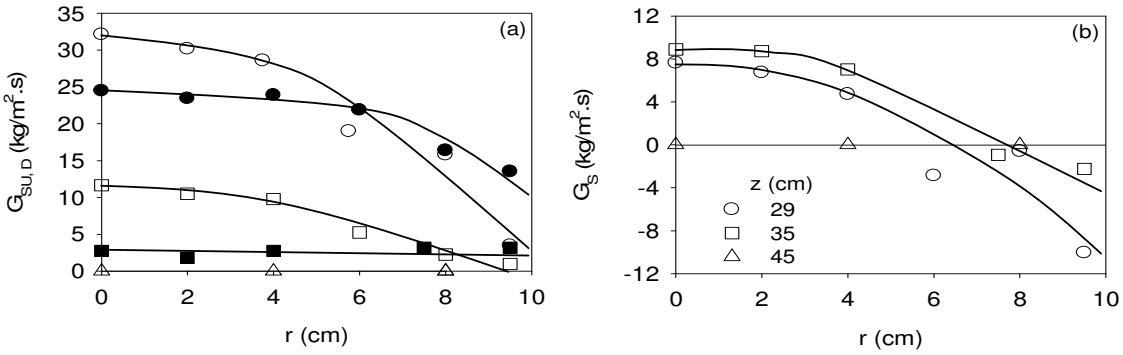

Fig. 2: Solids flux radial profile

Solids flux in the freeboard

Upward (G_{SU}) and downward (G_{SD}) solid fluxes were measured at 5 axial positions and 6 radial positions. The radial profiles of solids flux are shown in Figure 2(a) for three axial positions: 0.29, 0.35 and 0.45 m above the distributor. The upward (empty symbols) and downward (filled symbols) solids fluxes reached a maximum at the reactor centreline and decreased closer to the wall. The measurements were averaged over the fluid bed cross-section. At Z = 0.29 m, the upward and downward solids fluxes were 17.6 kg/m^{2}s and 19.0 kg/m^{2}s, respectively (difference of 1.4 kg/m^{2}s). At Z = 0.35 m, the upward solids flux was

4.7 kg/m^{2}s and the downward solids flux was 3.0 kg/m^{2}s (difference of 1.7 kg/m^{2}s). At Z = 0.45 m, the upward and downward solids flux were both zero. The radial profiles of net solids flux (G_S) are shown in Figure 2(b) for three axial positions: there was a net upward of solids at the centre of the reactor. Near the wall, there was a net downward flow of solids. This agrees well with the literature (Aguillón *et al.,* 1995; Van Breugel *et al.,* 1970; Rhodes *et al.,* 1988).

At each axial position, the measurements were averaged over the fluidized bed cross-section. Figure 3(a) compares the upward solids flux of the present study with the values given by the correlation of Wen *et al.* (1982). The correlation of Wen *et al.* (1982) underestimated G_{SU} at the bed surface: the present study measured 17.6 kg/m^{2}s and the correlation estimated 8.18×10^{-4} kg/m^{2}s. Wen *et al.* (1982) derived the correlation by extrapolating measurements of Large *et al.* (1977) made at 0.50 m above the bed surface, which may explain the observed discrepancy.

Defining the bed surface

In the present study, a time-average position of the bed surface was determined by pressure and solids flux measurements. Figure 3(b) shows the time-averaged static pressure measured at 4 axial positions at the wall and the cross-sectional mean of G_{SU} measured at 5 axial positions and 6 radial positions. The pressure decreased significantly in the bed from 2.6 kPa to 0.3 kPa (Z = 0.05 to 0.25 m) and remained constant at 0.1 kPa (Z = 0.35 to 0.77 m) in the freeboard. This indicates that the bed surface was located between Z = 0.25 and 0.35 m.

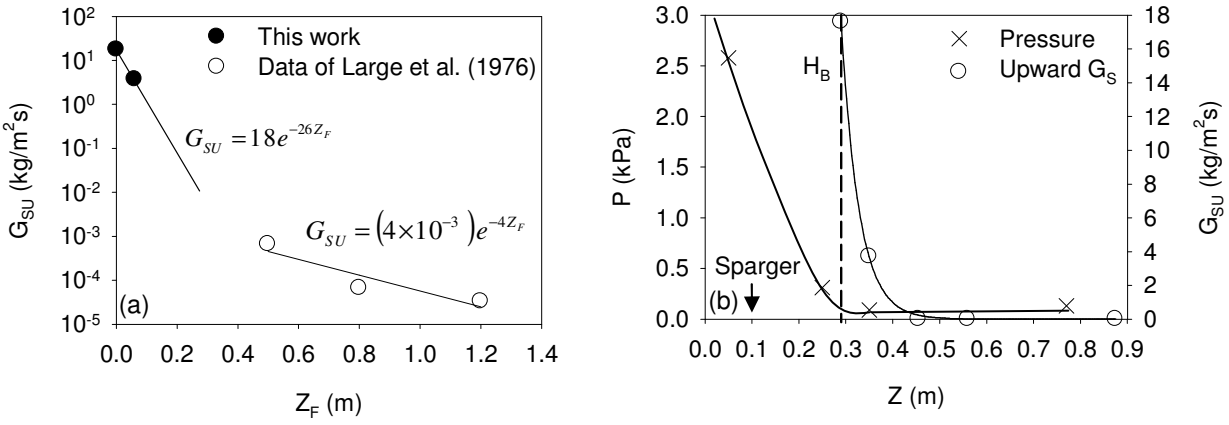

Fig. 3: Upward solids flux and pressure measurements

The upward solids flux reached 17.6 kg/m^{2}s at a height of 0.29 m and then decreased exponentially to 4.7 kg/m^{2}s at Z = 0.35 m and zero at Z = 0.46 m. If the inflection point of the solid flux curve is taken as the bed surface as proposed by Kunii et al. (1991), the bed height (H_B) was 0.29 m. This agrees well with the pressure measurements.

Temperature profile

The temperature profile inside the freeboard was monitored with eight thermocouples positioned along the length of the reactor. Two thermocouples were located inside the fluidized bed and six in the freeboard. Figure 4(a) shows the axial temperature profiles just prior to propane injection (t = 0 s) and after injection when one sample point was done (t ≈ 170 s). After injection, the temperature inside the fluidized bed and freeboard increased with time due to the exothermicity of the combustion reactions. Between each sample points, the propane was stopped to cool down the fluidized bed and freeboard. During combustion, a maximum temperature increase of 33ºC was observed inside the freeboard. Using the chemical composition of the gas measured at the bed surface (z = 0.29 m) and assuming adiabatic constant pressure combustion, the theoretical temperature increase is calculated as 546ºC from the CEA equilibrium code (Gordon *et al.,* 1994). The temperature in the freeboard reached a maximum of 670ºC during the experiments.

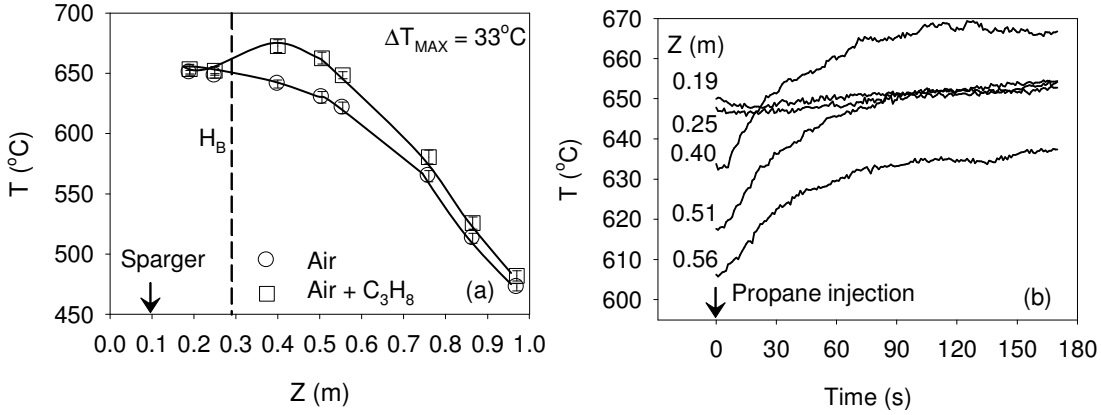

Fig. 4: Freeboard temperature profile

Figure 4(b) shows the temperature history of 5 thermocouples in the freeboard following the injection of propane at t = 0 s. After the sampling time of approximately 170 s, the temperature inside the reactor increased by a maximum of 2ºC within 20 seconds, which was the required sampling time for a representative measurement of the species volume fractions inside the reactor. Therefore, the measured

solids flux and species volume fractions corresponded to the temperature profile with an uncertainty of ±2ºC.

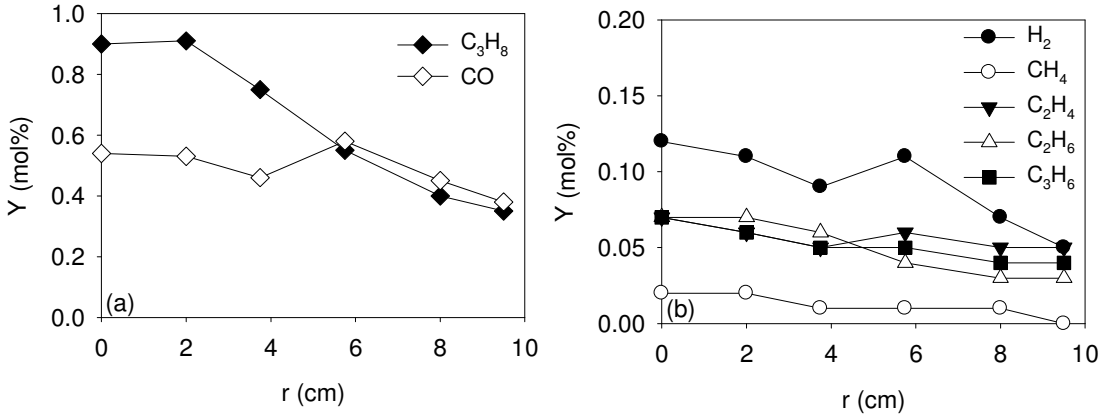

Figure 5: Species at the bed surface

Species at the bed surface

Partial combustion of C_3H_8 inside the fluidized bed produced CO and CO_2. Furthermore, the high temperature resulted in C_3H_8 cracking. Figures 5(a) and 5(b) shows the volume fractions of C_3H_8, CO, H_2, CH_4, C_2H_4, C_2H_6 and C_3H_6 at the bed surface (Z = 0.29 cm). The volume fraction of C_3H_8 decreased from 0.9% at the centreline to 0.4% at 5 mm from the wall. The volume fractions of CO, H_2, CH_4, C_2H_4, C_2H_6 and C_3H_6 were approximately constant throughout the reactor radius at 0.45%, 0.07%, 0.01%, 0.06%, 0.04% and 0.04%, respectively.

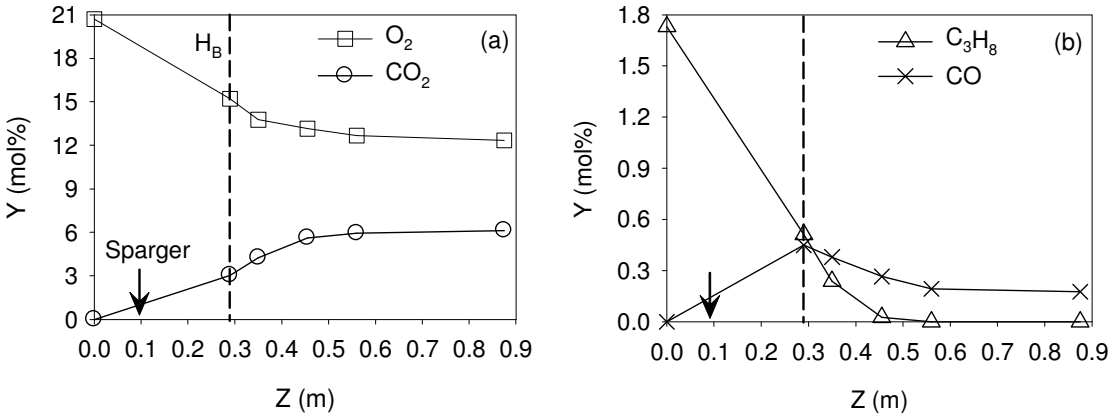

Figure 6: Freeboard combustion

Freeboard combustion

Figures 6(a) and 6(b) show the axial profiles (cross-sectional average) of C_3H_8, CO, O_2 and CO_2 inside the fluidized bed reactor – propane conversion inside the fluid bed reached 71% as propane decreased from 1.77 vol% (mixed-cup) at the inlet to 0.51 vol% at the bed surface (Z = 0.29 m). In the freeboard, the remaining propane reacted with oxygen to form CO_2 and complete combustion was obtained at Z = 0.56 m (17 cm above the bed surface).

Table 1 compares the measured induction time with the values from three propane induction time correlations for homogeneous systems that are available in the scientific literature. The induction time is given for the bed temperature (650ºC) and the maximum temperature observed inside the freeboard (670ºC). Also, the C_3H_8 and O_2 at the bed surface were used. In the present work, the measured induction time was below 0.25 s, which was the gas residence time between the bed surface (Z = 0.29 m) and the next sampling point (Z = 0.35 m). Between these two sampling positions, a 53% decrease in propane was observed. The measured induction time was on the same order as the values given by the correlations.

Table 1: Induction time data

τ (s)		**Reference**
650ºC	670ºC	
0.28	0.18	Burcat *et al.,* 1971
0.07	0.06	Penyazkov *et al*., 2005
0.68	0.33	Kim *et al.*, 2001
< 0.25		This work

CONCLUSIONS

An experimental study of propane combustion inside the freeboard (I.D. = 0.2 m) of a fluidized bed of sand (d_p = 290 μm) was performed at low superficial gas velocity (U_g = 0.24 m/s). Propane was injected

inside the fluidized bed (T_{Bed} = 650ºC) through a downward-facing sparger. Solids flux and species volume fractions were measured using a non-isokinetic sampling probe. The results showed an exponential decrease with height of the upward solids flux (G_{SU}) – G_{SU} was zero at 0.17 m above the bed surface, which was taken as the inflection point of the G_{SU} curve. G_{SUo} measurements were significantly higher than the values given by the correlation of Wen *et al.* (1982). The bed surface (boundary condition) and freeboard were characterized by measuring pressure, solids flux, species volume fractions and temperature at several radial and axial positions. During the experiments, the fluidized bed achieved a pseudo steady-state operation that ensured that the measured temperature profile corresponded to the solids flux and species fractions. Partial propane combustion in the fluidized bed (71%) produced CO and cracking species that were transported in the freeboard. Complete combustion occurred within 0.15 m of the bed surface and the propane induction time in the freeboard (< 0.25 s) was on the same order as the values given by three induction time correlations for homogeneous systems.

References

Aguillón, J., Shakourzadeh, K., Guigon, P.: Powder Technol. 83 (1995), pp. 79-84.

Botella, P., Lopez Nieto, J.M., Solsona, B.: J. Mol. Catal. A-Chem. 184 (2002), pp. 335-347.

Burcat, A., Lifshitz, A.: Proceedings of the 13th International Symposium on Combustion, Combustion Institute (1971), pp. 745-755.

Chen, L.H.,Wen, C.Y.: AIChE J. 28 (6) (1982), pp. 1019-1027.

Dounit, S., Hemati, M., Steinmetz, D.: Powder Technol. 120 (2001), pp. 49-54.

Dounit, S., Hemati, M., Andreux, R. Chem. Eng. J. 140 (2008), pp. 457-465.

Gordon S., McBride, B.J.: Computer program for calculation of complex chemical equilibrium compositions and applications. NASA RP-1311 (1994).

Hesketh, R.P., Davidson, J.F.: Combust. Flame 85 (1991), pp. 449-467.

Kunii, D., Levenspiel, O.: Fluidization Engineering, Butterworth-Heinemann, 1991.

Kim, K., Soo Shin, K.: Bull. Korean Chem. Soc. 22 (3) (2001), pp. 303-307.

Large J.F., Martinie, Y., Bergougnou, M.A.: J. Powders Bulk Solids Technol. 1 (1977), pp. 15-21.

Malleswara Rao, T.V., Deo, G.: Ind. Eng. Chem. Res. 46 (1) (2007), pp. 70-79.

Marinov, N.M., Pitz, W.J., Westbrook, C.K., Vincitore, A.M., Castaldi, M.J., Senkan, S.M., Melius, C.F.: Combust. Flame. 114 (1-2) (1998), pp. 192-213.

Morooka S., Kawazuishi, K., Kato, Y.: Powder Technol. 26 (1980), pp. 75-82.

Patience, G.S., Lorences, M.J.: Int. J. Chem. React. Eng. 4 (A22) (2006).

Penyazkov, O.G., Ragotner, K.A., Dean, A.J., Varatharajan, B.: Proceedings of the Combustion Institute, Elsevier Inc. (2005) pp. 1941-1947.

Reinhardt, B., Cordonnier, A., Florent, P.: Powder Technol. 101 (1999), pp. 81-90.

Rhodes, M.J., Laussmann, P., Villain, F., Geldart, D.: Circulating Fluidized Bed Technology II (Basu, P., Large, J.F. (eds)), Pergamon Press Oxford (1988), pp. 155-164.

Rhodes, M.J., Laussmann, P.: Powder Technol. 70 (1992), pp. 141-151.

Van Breugel, J.W., Stein, J.J.M., de Vries, R.J.: Proc. Instn. Mech. Engrs. 184 (1970), pp. 18-23.

Van der Vaart, D.R.: Fuel 67 (1988), pp. 1003-1007.

Van der Meer, E.H., Thorpe, R.B., Davidson, J.F.: Chem. Eng. Sci. 55 (2000), pp. 4079-4099.

Wen, C.Y., Chen, L.H.: AIChE J. 28 (1) (1982), pp. 117-128.

Werther, J.: Powder Technol. 102 (1999), pp. 15-36.

Notation

Symbols

d_p	average particle size	μm
G_S	solids flux	kg/m^2s
r	radial position	cm
t	time	s
T	temperature	ºC
U_g	superficial gas velocity	cm/s
Z	axial position	m

Greek letters

τ	induction time	s

Subscripts

Bed	fluidized bed
D	downwards
F	freeboard
g	gas phase
o	fluidized bed surface
s	solid phase
U	upwards

ANNEXE 4 – ARTICLE PRESENTÉ À LA CONFÉRENCE WCCE8 2009 (MONTRÉAL, CANADA)

GAS-PHASE COMBUSTION IN THE FREEBOARD OF A FLUIDIZED BED

Jean-Philippe Laviolette, Gregory S. Patience and Jamal Chaouki

Ecole Polytechnique, Montréal, Canada

Department of Chemical Engineering

Abstract: The prediction of propane autoignition in the freeboard of a fluidized bed is complicated by the presence of solids, intermediate products and non-homogeneities (solids, temperature and species gradients). An experimental and modeling study of propane combustion inside a fluidized bed and the freeboard (I.D. = 20 cm) was performed. Propane was injected inside a bubbling fluidized bed (T_{Bed} = 650ºC and U_g = 24 cm/s) of sand particles (d_p = 290 μm) through a downward-facing sparger. The combustion process in the bed and freeboard was characterized by measuring pressure, solids flux, species volume fractions and temperature at several radial and axial positions. The results were compared to a homogeneous microkinetic model and induction time correlations from the literature. The results showed that the upward solids flux (G_{SU}) decreased exponentially with height and the bed surface was defined as the inflection point. G_{SU} measurements were significantly higher than the values given by the correlation of Wen *et al.* (1982). G_S was zero at a distance of 15 cm above the bed and the combustion was complete within 27 cm. The measured induction time was on the same order as the values given by three induction time correlations. However, reaction rates from a homogeneous microkinetic model were significantly lower than the experimental values.

Keywords: fluidized bed, propane, combustion, freeboard, non-isokinetic sampling, solids flux, induction time, microkinetic modelling

1. INTRODUCTION

Homogeneous reactions generally result in yield lost of the desired compound, but they may also represent a significant safety hazard in the case of fast and highly exothermic reactions such as those involving oxygen and hydrocarbons. Chemical processes with oxygen and hydrocarbons are widespread in the industry and new processes are currently under development in the context of oil price fluctuations and global warming: selective oxidation of alkanes, combustion of cheaper feedstock for heating and catalyst regeneration, biomass gasification, etc. Fluidized bed reactors are currently being developed for a variety of these processes. In order to maximize productivity, they may operate within the explosion limits while feeding the oxidant and hydrocarbon separately into the bed – through spargers. This is possible due to the ability of the solids phase to suppress the homogeneous reactions (combustion) and at the same time promote selective heterogeneous reactions. However, downstream of the solids – in the freeboard, cyclones and associated piping – the effluent gas phase composition is potentially explosive – high hydrocarbon and oxygen concentrations, elevated temperature with an insufficient solids volume fraction to quench non-selective homogeneous reactions (Van der Vaart, 1988; Hesketh *et al.,* 1991). Minimizing the risk of gas-phase combustion-deflagration in these regions remains an important design issue.

Several explosion criteria (explosion limits, autoignition temperature and induction times (Hesketh *et al.,* 1991)) measured in homogeneous gas-phase systems as well as gas-phase kinetic models are available in the scientific literature (Marinov *et al.*, 1998). However, extrapolating these tendencies to a fluidized bed reactor introduces uncertainties since the entrained solid particles affect the gas-phase reactions downstream of the fluidized bed. Furthermore, fluidized beds are non-homogeneous systems - solids entrainment decreases exponentially from the bed surface to the transport disengagement height (Wen *et al*., 1982). Also, an axial temperature gradient may exist in the freeboard region as well as species concentration gradients depending on the hydrodynamics.

To accurately predict gas-phase combustion in the freeboard of a fluidized bed for a wide range of operational conditions, a freeboard combustion model that combines the gas/solids hydrodynamics and the reaction kinetics must be developed. This model needs to integrate through the axial gradient of solids fraction and temperature that characterize the freeboard as well as accounting for the effects of solids on the reaction kinetics. Models of the reaction in the freeboard of fluidized beds have been previously proposed by Chen *et al.* (1982), Dounit *et al.* (2001) and Dounit *et al.* (2008). These models used entrainment models that include a correlation for the entrainment at the bed surface such as the model of Wen *et al.* (1982). However, the solids entrainment at the bed surface was extrapolated from experimental data measured several centimetres downstream of the bed surface (sometimes more than 50 centimetres). Therefore, the existing entrainment models may yield significant errors near the bed surface and better accuracy would be obtained by directly measuring solids fraction.

In the present study, propane was injected inside a high temperature fluidized bed through a downward facing sparger and the freeboard region was characterized using pressure, solids flux, species volume fraction and

temperature measurements during freeboard combustion. The fluidized bed temperature, superficial velocity and propane/air ratio were adjusted to obtain propane combustion in the freeboard. Solids flux and species volume fractions were measured simultaneously using a non-isokinetic probe. The temperature profile in the freeboard was monitored using eight thermocouples.

2. EXPERIMENTAL APPARATUS

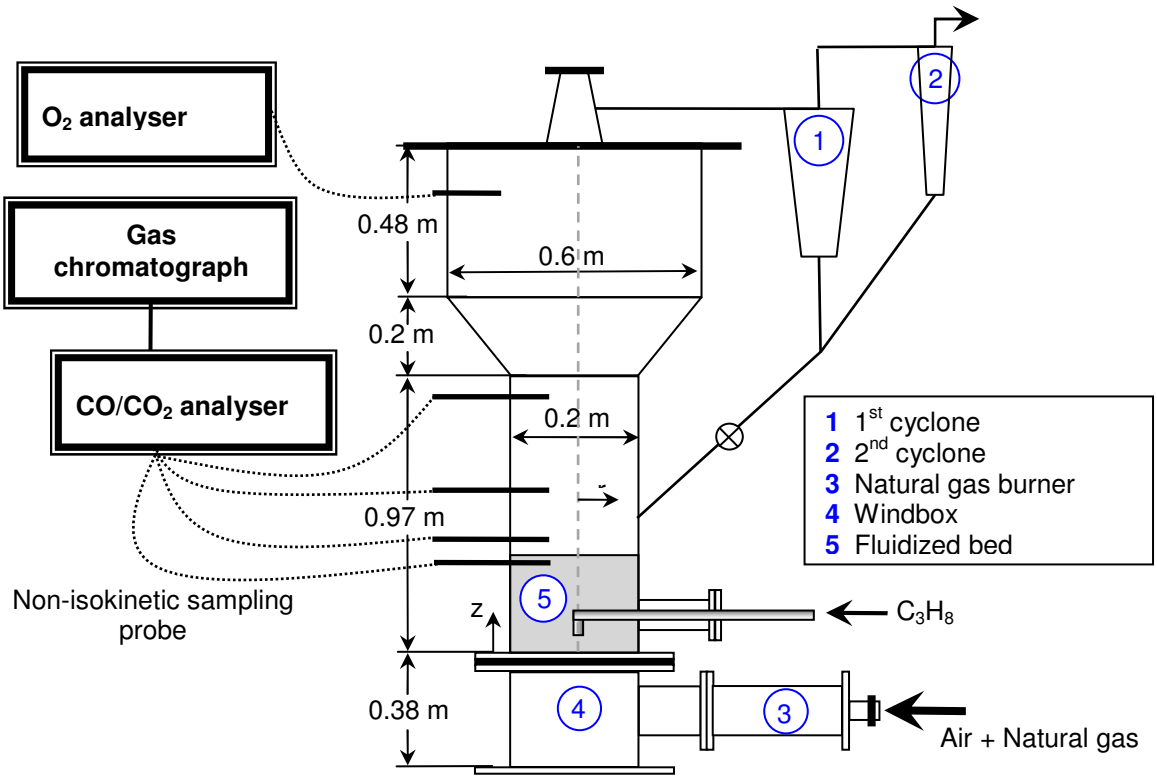

Fig. 1: Fluidized bed reactor

The experiments were conducted in the fluidized bed reactor of Figure 1. The bed and freeboard regions had an inner diameter of 20 cm. For all experiments, sand particles (Geldart group B ρ_s = 2650 kg/m^3, d_p = 290 μm) were used as the bed material and air was the fluidizing media. The experimental procedure first consisted of adjusting the superficial gas velocity to 24 cm/s (at 650°C). The fluidized bed was then heated with the natural gas burner upstream of the windbox and by injecting heavy vacuum gas oil (HVGO) through the sparger. When the bed temperature reached 680°C, the burner and HVGO injection were stopped and propane was injected through the sparger for 30 minutes to burn HVGO residues.

The propane was turned off and the fluidized bed cooled down until the bed temperature reached 645°C. Propane was then injected through the downward sparger to obtain a mixed-cup volume fraction of 2 vol% in air. A non-isokinetic probe was used to sample gas and solids simultaneous from 5 axial and 6 radial positions. The sampling system consisted of a 4.1 mm I.D. probe bent at a 90° at its tip. The sampled gas/solid stream first went through a 250 mL container that lowered the sampled gas velocity and caused the separation of the solid particles from the gas. The gas was analyzed by a Siemens Ultramat CO/CO_2 analyzer and a Varian CP-4900 micro-GC that measured the following species: O_2, H_2, CH_4, C_2H_4, C_2H_6, C_3H_6, C_3H_8, CO, CO_2 and N_2. Solids flux was calculated from the mass of the sampled solids and the sampling time:

The upward (G_{SU}) and downward (G_{SD}) solid fluxes were measured by orienting the probe tip downward and upward, respectively. The sampling flow rate was controlled using a rotameter connected to a vacuum line. Gas was also continuously sampled in the disengagement region (z = 147 cm) and analyzed with an oxygen analyzer (Siemens Oxymat 6.1). The results from the GC, CO/CO_2 analyzer and oxygen analyzer were compared and used in a molar balance to confirm the validity of the measured species volume fractions. The temperature along the reactor was monitored using 8 thermocouples located along the length of the reactor. The sparger consisted of a 4.1 mm I.D. tube pointing downward at the bed centreline. The sparger tip was located at a height of 9.8 cm above the distributor.

3. RESULTS AND DISCUSSION

The reaction rate of propane combustion in the freeboard of a fluid bed depends on species volume fractions, temperature and solids fraction. They are dependent parameters and should ideally be measured simultaneously.

3.1 Simultaneous sampling of gas and solids

A non-isokinetic sampling probe was used to measure the species volume fractions and the solids flux simultaneously. A preliminary set of experiments showed that the measured solids flux was almost independent of sampling rate in the range of 270 - 470 mL/min. Therefore, it was not necessary to have sampling that was precisely iso-kinetic and a sampling rate of 425 mL/min was used for all experiments. Results also showed that a minimum sampling time of 60 seconds was required to reach a permanent condition. The gas sampled with the non-isokinetic sampling probes was sent to the CO/CO_2 analyzer and the GC for analysis. A sampling time of only 20 seconds was required for a representative measurement of the species volume fractions inside the reactor.

3.2 Solids flux in the freeboard

Upward (G_{SU}) and downward (G_{SD}) solid fluxes were measured at 5 axial positions and 6 radial positions. At each axial position, the measurements were averaged over the fluidized bed cross-section. The radial profiles of net solids flux (G_S) showed a net upward of solids at the centre of the reactor. Near the wall, there was a net downward flow of solids. This agrees well with the literature (Aguillón *et al.,* 1995; Van Breugel *et al.,* 1970; Rhodes *et al.,* 1988).

Figure 2 compares the upward solids flux of the present study with the values given by the correlation of Wen *et al.* (1982). Figure 2 shows that the correlation of Wen *et al.* (1982) underestimates G_{SU} at the bed surface: the present study measured 17.6 kg/m^{2}s and the correlation estimated 8.18×10^{-4} kg/m^{2}s. Wen *et al.* (1982) derived the correlation by extrapolating measurements of Large *et al.* (1977) made at 50 cm above the bed surface, which may explain the observed discrepancy.

3.3 Defining the bed surface

In the present study, a time-average position of the bed surface was determined by pressure and solids flux measurements. Figure 3 shows the time-averaged static pressure measured at 4 axial positions at the wall and the cross-sectional mean of entrainment flux measured at 5 axial positions and 6 radial positions. The pressure decreased significantly in the bed from 2.6 kPa to 0.3 kPa (Z = 5 to 25 cm) and remained constant at 0.1 kPa (Z = 35 to 77 cm) in the freeboard. This indicates that the bed surface was located between Z = 25 and 35 cm.

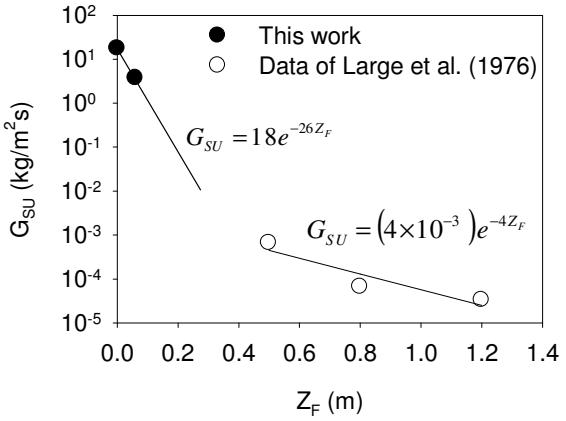

Fig. 2: Upward solid flux

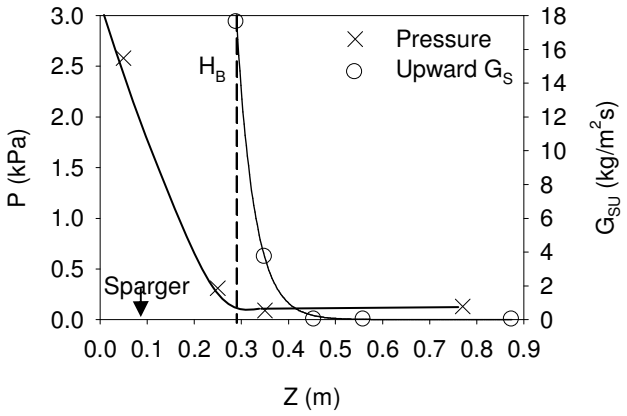

Fig. 3: Bed height

The entrainment flux reached 17.6 kg/m^{2}s at a height of 29 cm and then decreased exponentially to 4.7 kg/m^{2}s at Z = 35 cm and zero at Z = 46 cm. If the inflection point of the solid flux curve is taken as the bed surface as proposed by Kunii *et al.* (1991), the bed height (H_B) was 29 cm. This agrees well with the pressure measurements.

3.4 Temperature profile

The temperature profile inside the freeboard was monitored with eight thermocouples positioned along the length of the reactor. Two thermocouples were located inside the fluidized bed and six in the freeboard. Figure 4(a) shows the axial temperature profiles just prior to propane injection (t = 0 s) and after injection when one sample point was done (t ≈ 170 s). After injection, the temperature inside the fluidized bed and freeboard increased with time due to the exothermicity of the combustion reactions. Between each sample points, the propane was stopped to allow the fluidized bed and freeboard to cool down. During combustion, a maximum temperature increase of 33ºC was measured inside the freeboard. Using the chemical composition of the gas measured at the bed surface (z = 29 cm) and assuming adiabatic constant pressure combustion, the theoretical temperature increase is calculated as 546ºC from the CEA equilibrium code (Gordon *et al.,* 1994).

Figure 4(b) shows the temperature history at all sample points following the injection of propane at t = 0 s. After the sampling time of approximately 170 s, the temperature inside the reactor increased by a maximum of 2ºC within 20 seconds (required sampling time to measure species with GC and Ultramat). Therefore, the reactor temperature profile corresponds to the measured solids flux and species volume fractions.

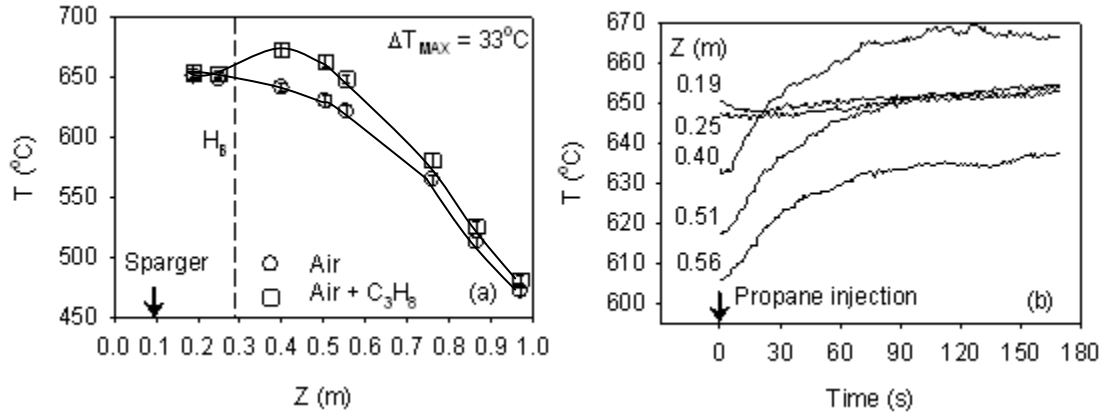

Fig. 4: Freeboard temperature profile

3.5 Species fraction in the freeboard and freeboard combustion

The results showed a radial profile of species volume fraction at the bed surface (z = 29 cm) – propane volume fraction decreased from 0.9 vol% at the centerline to 0.4 vol% at 5 mm from the wall. At z = 35 cm, the radial profile was more uniform with an average volume fraction of 0.3 vol%. Figures 5(a) and 5(b) show the axial profiles (cross-sectional average) of C_3H_8, CO, O_2 and CO_2 inside the fluidized bed reactor – propane conversion inside the fluid bed reached 71% as propane decreased from 1.77 vol% (mixed-cup) at the inlet to 0.51 vol% at the bed surface (z = 29 cm). In the freeboard, the remaining propane reacted with oxygen to form CO_2 and complete combustion was obtained at z = 56 cm.

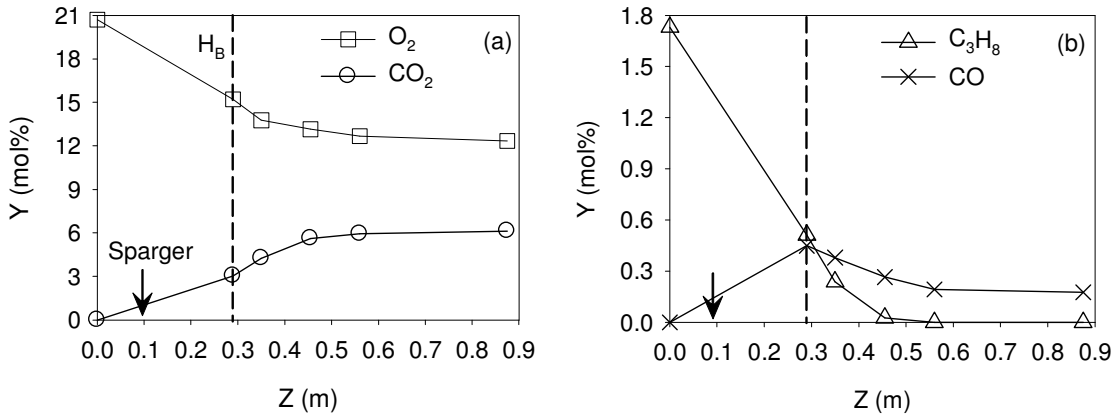

Fig. 5: Freeboard combustion

Table 1 compares the measured induction time with the values given by three correlations available in the scientific literature – the measured induction time is on the order of the values given by the correlations.

TABLE 1 Induction time data

T (ºC)	τ (s)	Reference
-	< 0.25	This work
650	0.28	Burcat *et al.,* 1971
650	0.07	Penyazkov *et al*., 2005
650	0.68	Kim *et al.*, 2001

4. MODELLING

A homogeneous microkinetic model (Marinov *et al.*, 1998) was used to model the freeboard combustion. The gas-phase hydrodynamics was modeled as plug flow. Figure 6 compares the modelling and experimental results – the model underestimates the combustion rates. This may be explained by the presence of free radicals that come from partial combustion in the fluidized bed.

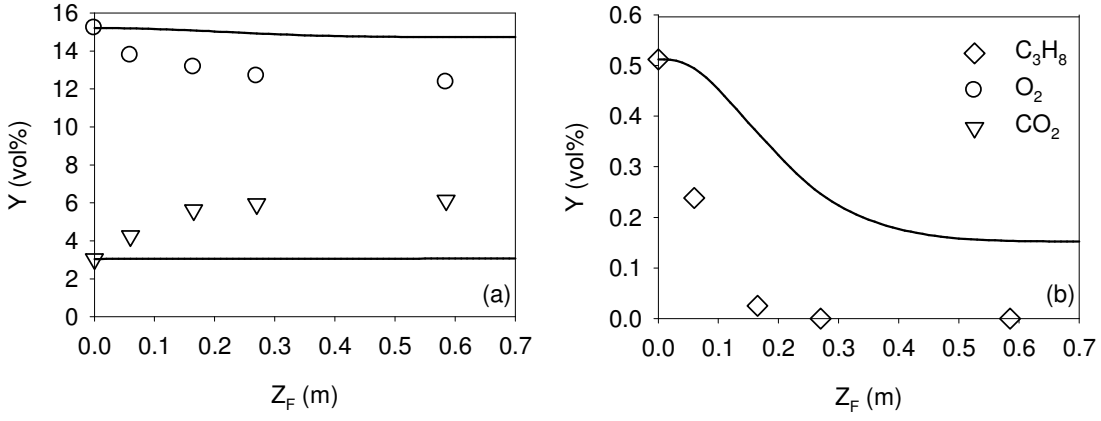

Fig. 6: Modelling results

5. CONCLUSIONS

In the present study, the combustion of propane in the freeboard of a fluidized bed was studied by injecting propane inside a high temperature fluidized bed through a downward facing sparger. The freeboard region was characterized using pressure, solids flux, species volume fraction and temperature measurements during combustion. The combustion in the fluidized bed and freeboard was confirmed by a decrease in oxygen and propane as well as a temperature increase in the reactor. Solids flux and species volume fractions were measured simultaneously using a non-isokinetic probe. The measurements showed a net upward flow of solids at the centre of the reactor and a net downward flow near the wall. Furthermore, the upward solids flux was found to decrease exponentially with height from the bed surface. The measured entrainment at the bed surface was found to be significantly higher than predicted by the correlation of Wen *et al.* (1982): 17.6 kg/m^2s compared to 8.18×10^{-4} kg/m^2s. Pressure and solids flux measurements were also used to locate the fluidized bed surface. Solids flux measurements were found to be more precise than pressure to determine bed height. The location of the bed surface was taken as the inflection point of the entrainment curve. The temperature profile corresponding to the measured solids flux and species volume fractions was determined using a series of thermocouples positioned along the length of the reactor.

REFERENCES

Aguillón, J., Shakourzadeh, K. and P. Guigon (1995) Comparative study of non-isokinetic sampling probes for solids flux measurement in circulating fluidized beds. *Powder Technol.* 83, 79-84.

Botella, P., Lopez Nieto, J.M. and B. Solsona (2002). Selective oxidation of propene to acrolein on Mo-Te mixed oxides catalyst prepared from ammonium telluromolybdates. *J. Mol. Catal. A-Chem.* 184, 335-347.

Burcat, A. and A. Lifshitz (1971) Shock-tube investigattion of ignition in propane-oxygen-argon mixtures. In: Proceedings of the 13th International Symposium on Combustion, 745-755, Combustion Institute, Pittsburgh.

Chen, L.H. and C.Y. Wen (1982) Model of solid gas reaction phenomena in the fluidized bed freeboard. *AIChE J.* 28, 6, 1019-1027.

Dounit, S., Hemati, M. and D. Steinmetz (2001). Natural gas combustion in fluidized bed reactors between 600 and 850ºC: experimental study and modelling of the freeboard. *Powder Technol.* 120, 49-54.

Dounit, S., Hemati, M. and R. Andreux (2008). Modelling and experimental validation of a fluidized-bed reactor freeboard region: Application to natural gas combustion. *Chem. Eng. J.* 140, 457-465.

Gordon S. and B.J. McBride (1994). Computer program for calculation of complex chemical equilibrium compositions and applications. *NASA RP-1311*.

Hesketh, R.P. and J.F. Davidson (1991). Combustion of methane and propane in an incipiently fluidized bed. *Combust. Flame*. 85, 449-467.

Kunii, D. and O. Levenspiel (1991). *Fluidization Engineering*. 2nd edition. Boston, MA: Butterworth-Heinemann.

Kim, K. and K. Soo Shin (2001). Shock tube and modeling study of the ignition of propane. Bull. Korean Chem. Soc. 22, 3, 303-307.

Large J.F., Martinie, Y. and M.A. Bergougnou (1977). Interpretative model for entrainment in a large gas-fluidized bed. *J. Powders Bulk Solids Technol.* 1, 15-21.

Malleswara Rao, T.V. and G. Deo (2007). Ethane and propane oxidation over supported V_2O_5/TiO_2 catalysts: analysis of kinetic parameters. *Ind. Eng. Chem. Res.* 46, 1, 70-79.

Marinov, N.M., Pitz, W.J., Westbrook, C.K., Vincitore, A.M., Castaldi, M.J., Senkan, S.M. and C.F. Melius (1998). Aromatic and polycyclic aromatic hydrocarbon formation in a laminar premixed *n*-Butane flame. *Combust. Flame.* 114, 1-2, 192-213.

Morooka S., Kawazuishi, K. and Y. Kato (1980). Holdup and flow pattern of solids particles in freeboard of gas-solid fluidized bed with fine particles. *Powder Technol.* 26, 75-82.

Patience, G.S. and M.J. Lorences (2006). VPO transient oxidation kinetics. *Int. J. Chem. React. Eng,* 4, A22.

Penyazkov, O.G., Ragotner, K.A., Dean, A.J. and B. Varatharajan (2005). Autoignition of propane-air mixtures behind reflected shock waves. In: Proceedings of the Combustion Institute, 1941-1947, Elsevier Inc.

Reinhardt, B., Cordonnier, A. and P. Florent (1999). Use of an isokinetic sampling propane. Results in a cyclone. *Powder Technol.* 101, 81-90.

Rhodes, M.J., Laussmann, P., Villain, F. and D. Geldart (1988). Measurement of radial and axial solids flux variations in the riser of a circulating fluidized bed, In: Circulating Fluidized Bed Technology II (Basu, P. and J.F. Large (Eds)), 155-164, Pergamon Press, Oxford.

Rhodes, M.J. and P. Laussmann (1992). A simple non-isokinetic sampling probe for dense suspensions. *Powder Technol.* 70, 141-151

Van Breugel, J.W., Stein, J.J.M. and R.J. de Vries (1970). Isokinetic sampling in a dense gas-solids stream. *Proc. Instn. Mech. Engrs.* 184, 18-23.

Van der Vaart, D.R. (1988). Freeboard ignition of premixed hydrocarbon gas in a fluidised bed. *Fuel*, 67, 1003-1007.

Van der Meer, E.H., Thorpe, R.B. and J.F. Davidson (2000). Flow patterns in the square cross-section riser of a circulating fluidized bed and the effect of riser exit design. *Chem. Eng. Sci.* 55, 4079-4099.

Wen, C.Y. and L.H. Chen (1982). Fluidized bed freeboard phenomena: entrainment and elutriation. *AIChE J.* 28, 1, 117-128.

Werther, J. (1999). Measurement techniques in fluidized beds. *Powder Technol.* 102, 15-36.

ANNEXE 5 – ARTICLE PRESENTÉ À LA CONFÉRENCE FLUIDIZATION XIII (CORÉE DU SUD, 2010)

FLUIDIZED BED COMBUSTION OF C_1-C_4 N-ALKANES

Jean-Philippe Laviolette, Gregory S. Patience and Jamal Chaouki*

Department of Chemical Engineering, École Polytechnique de Montréal, P.O. Box 6079, Station Centre-ville, Montréal, Canada H3C 3A7

*Corresponding author. Tel.: +1 514 340 4711 ext. 4469; fax: +1 514 340 4159.
E-mail address: jamal.chaouki@polymtl.ca (J. Chaouki)

Abstract: The non-premixed combustion of C_1 to C_4 n-alkanes was investigated inside a bubbling fluidized bed of inert sand particles at intermediate temperatures: 923 K (650°C) ≤ T_B ≤ 1123 K (850°C). Lower (T_1) and upper (T_2) critical transition bed temperatures were measured for ethane, propane and n-butane as 923 K (650°C) and 1073 K (800°C), respectively. The values for methane were significantly higher with T_1 = 1023 K (750°C) and T_2 > 1123 K (850°C). Alkane conversion was accurately modeled with first-order kinetics and C_2 to C_4 n-alkanes combustion rates were characterized by a uniform Arrhenius expression: $r = (2.59 \times 10^7)\, C_i\, e^{-127300/RT}$. The reaction rate of methane was significantly slower with: $r_{CH4} = (1.99 \times 10^{12})\, C_{CH4}\, e^{-251008/RT}$.

Keywords: combustion, fluidized bed, methane, propane, ethane and n-butane

1. Introduction

The combustion of methane, LPG and propane in fluidized beds of inert particles has been the subject of several studies in premixed [1-10] and non-premixed modes [11-16]. Fluidized bed temperature has been reported as a key parameter that determines in-bed fuel conversion: combustion is initiated deeper inside the fluidized bed with increasing temperature. In premixed combustion, increasing temperature has been shown to move the combustion front towards the distributor - the combustion front moves first from the freeboard to the bubbles bursting at the upper surface of the bed, then to bubbles igniting in the bed and finally to small bubbles where

ignition occurs practically at the level of the distributor and the process appears flameless [7, 9]. While some studies have suggested that combustion did not occur to any significant extent inside the emulsion phase [9], methane and propane combustion have been observed in fixed beds of sand particles at temperatures above 1023 K (750°C) and 973 K (700°C), respectively [1, 17].

Two critical transition temperatures have been defined for fluidized bed combustion in inert particles. Below the lower critical temperature (T_1), combustion only occurs above the bed surface. Between T_1 and the upper critical temperature (T_2), combustion begins to move inside the bubbles within the bed. Finally, above T_2, combustion takes place entirely within the bed and close to the distributor. For methane combustion in inert sand particles, the values of T_1 and T_2 reported in the literature range between 823-1018 K (550-745°C) and 1133-1250 K (860-977°C), respectively [18]. For propane, T_2 was measured in a shallow bed ($H_B \approx 0.1$ m) of sand particles as 1123 K (850°C) [2, 9]. Investigations on the fluidized bed combustion of other alkanes in inert particles are scarce.

In-bed conversion for specific operating condition can also be estimated by reaction models that combine gas/solids hydrodynamics and reaction kinetics. Several microkinetic and first-order global kinetics schemes are available in the literature for gas-phase systems [5, 6, 19]. Gas-phase microkinetic models have also been modified to account for the “quenching” effect of solids particles on the free radicals [17, 20]. However, microkinetic models are very complex, while global kinetic models are valid only for a specific range of operating conditions such that both types of models may yield significant uncertainties. Furthermore, using global kinetics schemes for different hydrocarbons from various sources and measured under different experimental conditions may result in further errors in the modeling results.

It may be possible to express the first-order kinetics and conversion of C_2 and higher alkanes in terms of a single expression or correlation. Studies have reported similarities between the combustion chemistry of n-alkanes: their combustion rate is controlled by the same main chain branching path, which can be summarized by the following elementary reactions at intermediate temperatures (~ 850 K (577°C) to 1200 K (927°C)) [21-24]:

$$H + O_2 + M \rightarrow HO_2 + M \quad (1)$$

$$RH + HO_2 \rightarrow R + H_2O_2 \quad (2)$$

$$H_2O_2 + M \rightarrow OH + OH + M \quad (3)$$

In the above equations, RH is an alkane, R is an alkyl radical and M is a third body. Saxena *et al*. [23] have demonstrated that the high temperature induction time of propane and higher alkanes can be accurately estimated by employing rate parameters of elementary steps (2) to (4).

$$HO_2 + HO_2 \rightarrow H_2O_2 + O_2 \quad (4)$$

Consequently, the induction time of C_2 and higher n-alkanes have been shown to exhibit similar dependence on temperature, pressure and mixture composition such that it may be calculated from a single correlation with an uniform activation energy [21-22]. Methane, on the other hand, has been observed to yield significantly higher induction times, which can be explained by the production of a methyl radical in equation (2), which recombines to form ethane, resulting in chain termination. If the combustion chemistry and induction time correlations among C_2 and higher n-alkanes show such similarities, it seems reasonable to think that a parallel may also be made between the global reaction kinetics and conversion.

In the present study, the non-premixed combustion of methane, ethane, propane and n-butane was studied in a fluidized bed of sand particles at temperatures ranging from 923 K (650°C) to 1123 K (850°C). The flow of each hydrocarbon was adjusted to obtain a constant heat release rate of 3.8 kW and critical bed temperatures were measured for each hydrocarbon. Furthermore, a reaction model with first-order reaction kinetics was developed and compared to the experimental results. The first-order kinetic parameters were measured for each n-alkane and compared.

2. Experimental

The experiments were performed in a fluidized bed reactor with an inner diameter of 0.2 m and a height of approximately 1.0 m. Inert sand particles (d_p = 290 μm and U_{mf} = 0.08 m/s) were used as the bed material. The bed was fluidized with air, which was injected through the distributor, and the hydrocarbon fuels (methane, ethane, propane and n-butane) were separately injected through a downward-facing sparger whose the tip was located at a distance of 0.1 m above the

distributor. Prior to each experiment, the fluidized bed reactor was heated to the desired temperature with a natural gas burner connected to the windbox.

The experiments were conducted at a superficial gas velocity of 0.4 m/s and at five bed temperatures: 923 K (650°C), 973 K (700°C), 1023 K (750°C), 1073 K (800°C) and 1123 K (850°C). The temperature was measured at 9 different axial positions with thermocouples. Gas was sampled at six axial and five positions. The sampled gas was analyzed by a CO/CO_2 analyzer and a micro-GC connected in series to measure the volume fraction of the following species: H_2, CH_4, C_2H_4, C_2H_6, C_3H_8, n-C_4H_{10}, O_2, N_2, CO and CO_2. At each axial position, a cross-sectional average of species volume fraction was calculated from the measurements. The mixed-cup volume fraction at the injector tip was adjusted for each hydrocarbon to obtain a constant heat release rate of 3.8 kW. For methane, ethane, propane and n-butane, the mixed-cup volume fraction was 5.1%, 2.5%, 1.9% and 1.3%, respectively.

3. Results and discussion

3.1 Critical transition fluidized bed temperatures

Lower (T_1) and upper (T_2) critical transition bed temperatures were measured for methane, ethane, propane and n-butane. Figure 1a shows the axial profile of conversion for ethane, propane and n-butane inside the fluidized bed reactor at a bed temperature of 923 K (650°C). The corresponding axial profile of CO_2 volume fraction is presented in Figure 1b. The bed height was 0.55 m and it is shown on both figures as a dashed line. At 923 K (650°C), ethane, propane and n-butane conversion was not significant inside the fluidized bed: conversion fluctuated between 0-4%, 0-18% and 10-27% for ethane, propane and n-butane, respectively. Furthermore, the CO_2 volume fractions in the fluidized bed remained low at approximately 0.7%. Combustion occurred mainly at the bed surface and inside the freeboard as conversion reached 92%, 93% and 96% at 0.2 m above the bed surface (Z = 0.75 m) for ethane, propane and n-butane, respectively. This was accompanied by a significant increased in the CO_2 volume fraction, which reached approximately 5.5% for all alkanes. Complete conversion was obtained at Z = 0.97 m. Since in-bed conversion was limited and most hydrocarbons burned inside the freeboard, the lower critical temperature (T_1) was defined as 923 K (650°C) for ethane, propane and n-butane.

As the bed temperature was increased to 973 K (700°C), the combustion front moved upstream inside the fluidized bed for ethane, propane and n-butane. Figures 1c and 1d show the axial profile of conversion and CO_2: combustion was initiated within 0.15 m (Z = 0.25 m) of the injector tip where a conversion of 24%, 57% and 61% was measured for ethane, propane and n-butane, respectively. Conversion increased steadily in the fluidized bed and partial in-bed conversions of 60%, 79% and 84% were measured at 0.1 m below the bed surface (Z = 0.46 m) for ethane, propane and n-butane. The unconverted hydrocarbons burned inside the feeboard region and complete conversion was observed at 0.2 m above the bed surface (Z = 0.75 m). The measured conversion in the fluidized bed and freeboard regions was accompanied by a corresponding increase in the CO_2 volume fraction, which reached approximately 3.8% at 0.1 m below the fluidized bed surface (Z = 0.46 m) and 6.0% in the freeboard region at Z = 0.97 m.

Figures 1(e) and 1(f) show the axial profile of CO_2 and conversion for the three n-alkanes as the bed temperature was increased further to 1023 K (750°C). Near complete fuel conversion occurred in the fluidized bed with ethane, propane and n-butane: conversion reached 95%, 95% and 98%, respectively, only 0.36 m (Z = 0.46 m) downstream of the injector. At that position, the CO_2 volume fraction reached about 6.0%, which corresponded approximately to the theoretical value at 100% combustion. Complete conversion was observed 0.2 m over the bed surface (Z = 0.75 m).

At a bed temperature of 1073 K (800°C), the conversion of ethane, propane and n-butane, conversion reached 99% within 0.25 m of the sparger tip (Z = 0.35 m): this temperature was defined as the upper critical temperature (T_2). This value is lower than the 1123 K (850°C) previously reported for propane [2, 9]. However, this discrepancy may be explained by the fact that conversion was not measured at a bed temperature of 1073 K (800°C) – experiments were performed at bed temperatures of 1023 K (750°C) and 1123 K (850°C) [2, 9].

Methane fluidized bed combustion required significantly higher bed temperatures compared to ethane, propane and n-butane. Figure 2 shows the axial profile of methane conversion at four bed temperatures: 973 K (700°C), 1023 (750°C), 1073 (800°C) and 1123 K (850°C). At a bed temperature of 973 K (700°C), no methane conversion was measured in the fluidized bed and

combustion occurred entirely in the freeboard region: methane conversion increased from 37% at 0.06 m above the bed surface (Z = 0.61 m) to 99% at Z = 0.97 m, respectively.

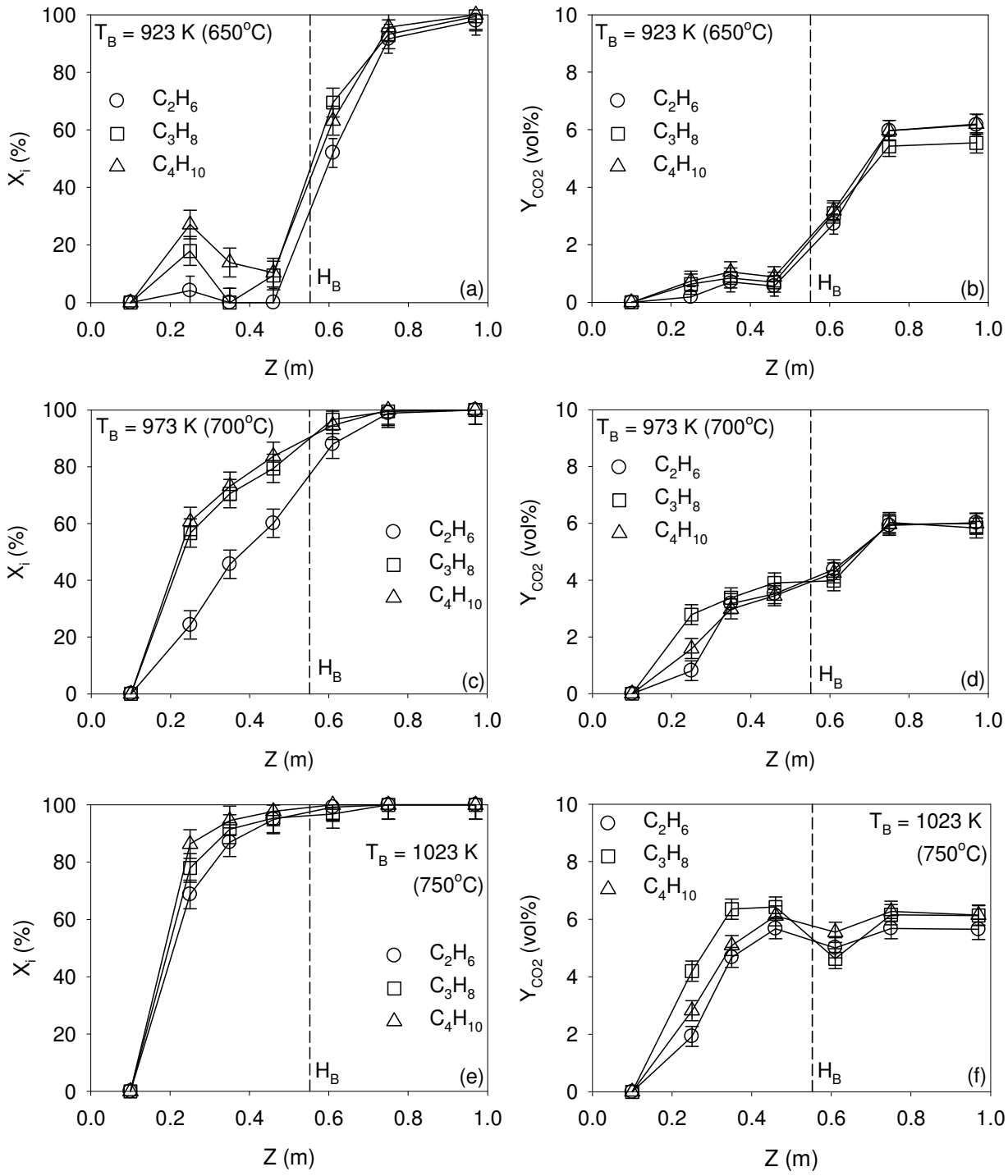

Figure 1: Conversion and Y_{CO2} axial profiles at 923 K and 973 K

As the temperature was increased to 1023 K (750°C), figure 2 shows that the methane in-bed conversion was small – the measured conversion fluctuated between 0% and 12% and the CO_2 volume fraction reached about 2.0%. Combustion mainly occurred at the bed surface – conversion increased to 64% at 0.06 m (Z = 0.61 m) above the bed surface. This was accompanied by a significant increase in the volume fraction of CO_2 in the freeboard. Complete methane conversion was observed at Z = 0.97 m. A bed temperature of 1023 K (750°C) was defined as the lower critical temperature (T_1), which is similar to the observations of previous studies [18].

At a higher bed temperature of 1073 K (800°C), significant in-bed conversion was observed: conversion reached 23% at a distance of 0.15 m downstream of the sparger (Z = 0.25 m) and increased to 40% at Z = 0.46 m. The unconverted methane burned in the freeboard and complete conversion was obtained at Z = 0.97 m.

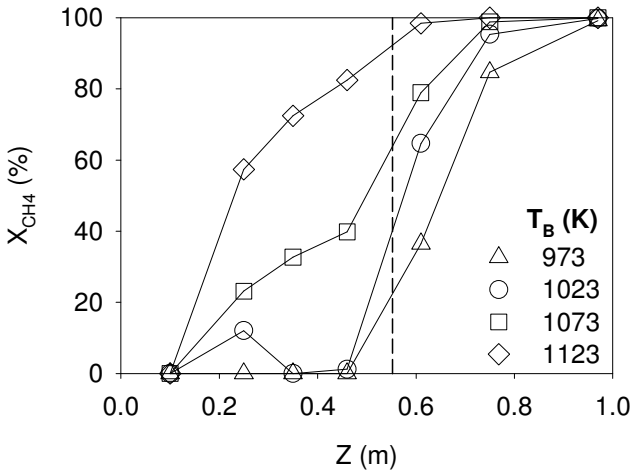

Figure 2: X_{CH4} axial profiles at various fluidized bed temperatures

The bed temperature was increased further to 1123 K (850°C) and metane conversion increased to 83% at 0.1 m below the bed surface (Z = 0.46 m). The unconverted methane burned inside the freeboard region and within 0.2 m of the bed surface. The upper critical temperature (T_2) for methane is higher than 1123 K (850°C) and this agrees with the reported values in the scientific literature [18].

3.2 C_1-C_4 n-alkanes global reaction rates

A reaction model was developed and compared to the experimental measurements. The fluidized bed gas-phase hydrodynamics and reaction kinetics were modeled as a plug flow reactor and a first-order reaction, respectively. The hydrocarbon conversion was calculated from equations (5) and (6):

$$X_i = 100\left(1 - e^{-k'(Z_{inj} - b_i)}\right) \quad (5)$$

$$k' = \frac{Ak_0}{v} e^{-E_A/RT} = k_0' e^{-E_A/RT} \quad (6)$$

In equation (5), the parameter b_i represents an induction delay: b_i increases with induction time. Furthermore, Z_{inj}, k, A, v, E_A and R corresponds to the height above the sparger tip (Z_{inj} = 0 m corresponds to Z = 0.1 m), the kinetic constant, the fluidized bed cross-sectional area, the volume flow rate in the fluidized bed, the activation energy and the universal gas constant. The use of this simple reaction model is consistent with the work of Lorences *et al.* [25], which have shown that the gas-phase hydrodynamics in fluidized beds are very close to plug flow when $U_g \leq 6 \times U_{mf}$. Also, several fluidized bed combustion studies have reported that fuel-lean combustion can be accurately represented as first order with respect to hydrocarbon concentration [17, 26-27].

Figure 3a shows the in-bed conversion of ethane, propane and n-butane as a function of Z_{inj} on a natural logarithmic scale for two bed temperatures: 973 K (700°C) and 1023 K (750°C). A linear relationship is observed between the ordinate [ln(1-X_i)] and Z_{inj}, which indicates that the model agrees well with the experimental results. The slope of the curve represents the first order reaction rate (k'): the same reaction rate was measured for ethane, propane and n-butane. For bed temperatures of 973 K (700°C) and 1023 K (750°C), k' was measured as 3.8 m^{-1} and 8.2 m^{-1}, respectively. Therefore, the temperature dependence of the reaction rate was uniform for C_2 to C_4 n-alkanes, which implies that the activation energy (E_A) was also the same. However, the parameter b_i in equation (6) was not uniform among C_2 to C_4 n-alkanes. Table 1 lists the different values of b_i measured at the different bed temperatures and used in the fluidized bed combustion model. Figure 3b compares the measured and predicted conversion of ethane, propane and n-butane as a function of (Z_i + b): the agreement between the model and the experimental results is very good.

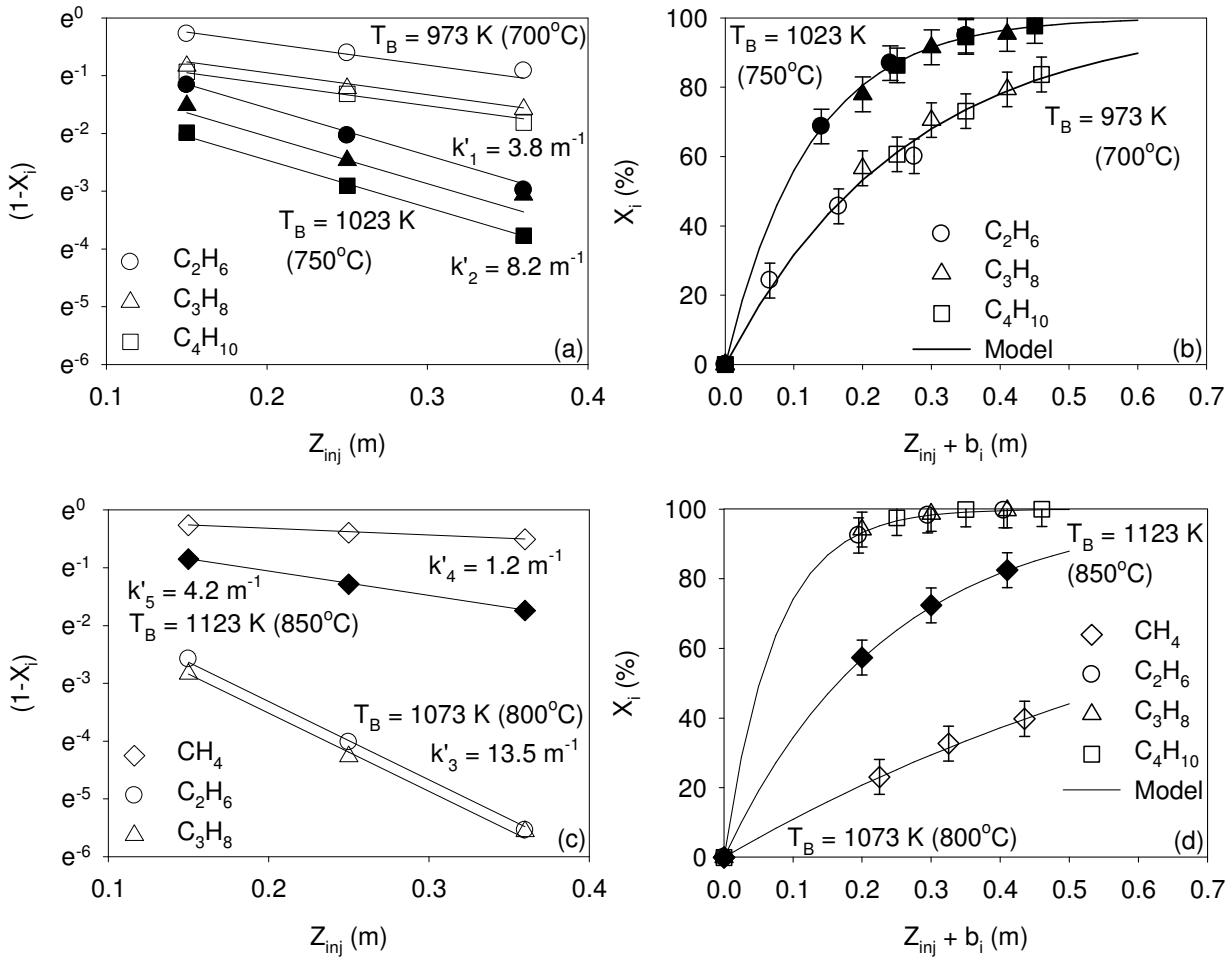

Figure 3: Comparison between the model and experiments at 973, 1023,1073 and 1123 K

Similar observations were made at higher bed temperatures. Figure 3c shows the in-bed conversion of methane, ethane and propane as a function of Z_{inj} on a natural logarithmic scale for two bed temperatures: 1073 K (800°C) and 1123 K (850°C). The first-order global reaction rate for ethane and propane was measured as 13.5 m^{-1} at 1073 K (800°C). N-butane conversion reached 100% and could therefore not included in Figure 3c. For methane, however, the reaction rate was significantly lower compared to C_2-C_4 n-alkanes: k' rose from 1.2 m^{-1} to 4.2 m^{-1} as the bed temperatures was increased from 1073 K (800°C) to 1123 K (850°C). Figure 3d compares the measured and predicted conversion of methane, ethane, propane and n-butane in the fluidized bed: at these higher bed temperatures, the agreement is also very good.

It is observed in Table 1 that the magnitude of b_i decreased with increasing alkane carbon number at a constant bed temperature. For methane and ethane, b_i decreased linearly with temperature, which is consistent with induction time studies: induction time decreased with increasing temperature. For ethane, b_i decreased from 0.085 m at 973 K (700°C) to -0.045 m at 1073 K (800°C). A negative b_i can be explained by a significant hydrocarbon conversion near the injector tip at high bed temperatures. Studies have shown that the jet originating from an injector enhances mixing, which can lead to significant conversion in that region when the mixture induction time is sufficiently low [18]. For methane, b_i decreased from 0.075 m at 1073 K (800°C) to -0.05 m at 1123 K (850°C). For propane and n-butane, b_i remained approximately constant at -0.05 m and -0.1 m, respectively.

Table 1: Parameter b_i at the different bed temperatures (T_B)

n-Alkane	**b_i (m)**	**Range (K)**
CH_4	-0.0025 T_B + 2.76	1073-1123
C_2H_6	-0.0013 T_B + 1.35	973-1073
C_3H_8	-0.05	973-1073
n-C_4H_{10}	-0.1	973-1073

The global reaction rates can be expressed in the Arrhenius form:

$$k'_{CH4} = (1.99 \times 10^{12})\, e^{-251008/RT} \quad (7)$$

$$k'_{C2H6} = k'_{C3H8} = k'_{C4H10} = (2.59 \times 10^{7})\, e^{-127300/RT} \quad (8)$$

The reaction rate constant and the activation energy for methane were calculated from the reactions rates measured at bed temperatures of 1073 K (800°C) and 1123 K (850°C). On the other hand, the parameters for ethane, propane and n-butane were calculated from the reactions rates at 973 K (700°C) and 1023 K (750°C). Equation (8) overpredicts the global reaction rate at 1073 K (800°C) and yields 16.4 m^{-1} compared to the measured value of 13.5 m^{-1}. This discrepancy can be explained by the fact that the in-bed conversions were very high at this

temperature (in the order of 93% to 100%). At these high conversions, a variation of 1.0% in the measured value greatly affected the measured slope in Figure 3c. The precision in the conversion measurements was estimated for the present study as ±5% absolute.

The fact that ethane, propane and n-butane have the same global kinetics is consistent with previous studies, which have shown that the induction times of C_2 and higher alkanes are of similar magnitude and are governed by the same temperature dependence or activation energy [21-22]. Methane is also known to be significantly less reactive than higher n-alkanes [22,24]. Table 1 shows that the parameter b_i increased with increasing number of carbons in the n-alkane molecule, which suggests that the mixture reactivity increased (and induction time decreased) with increasing fuel molecule size. This trend is consistent with previous studies [21-22] except for ethane, which was reported by Burcat *et al*. [22] to show the highest reactivity among C_1 to C_5 n-alkanes. This was also supported by Westbrook [24] with kinetic considerations. This discrepancy between the present results and the scientific literature can not be explained and the ± 5% (absolute) error in the measured conversion may be at cause.

4. Conclusions

The non-premixed combustion of methane, ethane, propane and n-butane was investigated in a fluidized bed of inert sand particles. The bed temperature was varied between 923 K (650°C) and 1123 K (850°C) while the superficial gas velocity was kept at 0.4 m/s. Critical transition bed temperatures (T_1 and T_2) were measured for each fuel. For ethane, propane and n-butane, combustion occurred mainly in the freeboard region at bed temperatures below: T_1 = 923 K (650°C). On the other hand, complete conversion occurred within 0.2 m of the injector at: T_2 = 1073 K (800°C). For methane, the measured values of T_1 and T_2 were significantly higher at 1023 K (750°C) and above 1123 K (850°C), respectively. A reaction model with first-order kinetics was developed and compared to the experimental measurements. The reaction rate of C_2 to C_4 n-alkanes could be characterized by a single kinetic expression and a uniform reaction rate constant and activation energy. On the other hand, the methane reaction rate was significantly slower with a higher activation energy.

References

[1] Hesketh RP, Davidson JF. Combust. Flame 1991;85:449-467.

[2] Van der Vaart DR. Combust. Flame 1988;71:35-39.

[3] Van der Vaart DR. Fuel 1988;67:1003-1007.

[4] Friedman J, Li H. Combust. Sci. Technol. **2005**; 177; 2211-2241.

[5] Dounit S, Hemati M, Andreux R. Chem. Eng. J. **2008**; 140; 457-465.

[6] Pre P, Hemati M, Marchand B. Chem. Eng. Sci **1998**; 53 (16); 2871-2883.

[7] Zukowski W. Combust. Flame **2003**; 134; 399-409.

[8] Baron J, Bulewicz EM, Zukowski W, Kandefer S, Pilawska M. Combust. Flame **2002**; 128; 410-421.

[9] Dennis JS, Hayhurst AN, Mackley IG. 19th Symp. (Intl.) on Combust. 1982; 1205-1212.

[10] Srinivasan RA, Sriramulu S, Kulasekaran S, Agarwal PK. Fuel **1998**; 77; 1033-1049.

[11] Mabrouk R, Chaouki J, Laviolette J-P, Patience GS. Proc. 9th Conference on Circulating Fluidized Beds, Hamburg, Germany, **2008**.

[12] Ross DP, Yan HM, Zhang DK. Combust. Flame 2001; 124; 156-164.

[13] Sotudeh-Gharebaagh R. PhD Thesis, Ecole Polytechnique, Montreal, Canada, **1998**.

[14] Singh B, Rigby GR, Callcott TG In: Inst. of Fuel Symp. Series, No.1, London (1975), C5.1–C5.9.

[15] Stubington JF, Davidson JF. AIChE J. 1981; 27 (1); 59-65.

[16] Sotudeh-Gharebaagh R, Chaouki J. Energy & Fuels 2007; 21; 2230-2237.

[17] Sotudeh-Gharebagh R, Chaouki J. Can. J. Chem. Eng. **2003**; 81; 1182-1191.

[18] Laviolette J-P, Sotudeh-Gharebagh R, Mabrouk R, Patience GS, Chaouki J. In A. Agarwal (ed.) Handbook of Combustion (vol.5), Wiley **2010**.

[19] Ross DP, Yan H-M, Zhang D-K. Fuel **2004**; 83; 1979-1990.

[20] Jeng R-S, Altwicker ER, Morgan III MM, Wilk RD. Combust. Sci. Technol. **2001**; 170; 119-149.

[21] Horning DC, Davidson DF, Hanson RK. Journal of Propulsion and Power **2002**; 18 (2); 363.

[22] Burcat A, Scheller K, Lifshitz A. Combust. Flame **1971**; 16; 29-33.

[23] Saxena P, Peters N, Williams FA. Combust. Flame **2007**; 149; 79-90.

[24] Westbrook, CK. Proc. Combust. Inst. 2000; 28; 1563-1577.

[25] Lorences M, Laviolette J-P. Powder Technol. 2006; 168 (1); 1-9.

[26] Foka M, Chaouki J, Guy C, Klvana D. Chem. Eng. Sci. **1994**; 49 (24A); 4269-4276.

[27] Chaouki J, Klvana D, Guy C. Korean J. Chem. Eng. **1999**; 16 (4); 494-500.

ANNEXE 6 – ARTICLE PRÉSENTÉ À LA CONFÉRENCE FLUIDIZATION XIII CONFERENCE (CORÉE DU SUD, 2010)

FIBRE-OPTIC PROBE FOR THE SIMULTANEOUS MEASUREMENT OF GASEOUS SPECIES COMPOSITION AND SOLIDS VOLUME FRACTION

Jean-Philippe Laviolette, Gregory S. Patience and Jamal Chaouki*

Department of Chemical Engineering, École Polytechnique de Montréal, P.O. Box 6079, Station Centre-ville, Montréal, Canada H3C 3A7

*Corresponding author. Tel.: +1 514 340 4711 ext. 4469; fax: +1 514 340 4159.
E-mail address: jamal.chaouki@polymtl.ca (J. Chaouki)

Abstract

A novel infrared fibre-optic probe was developed to measure quantitatively and simultaneously solids volume fraction (1-ε) and gaseous species composition (Y_i) in a gas/solid fluidized bed. The fibre-optic probe was used with a FT-IR spectrometer to perform real-time and in-situ measurements of absorbance in the fluidized bed. The effect of (1-ε) and Y_i on the absorbance spectra were additive and could be independently calibrated. To calibrate the probe, fuel mole fractions and (1-ε) were varied between 1.8 - 10.1 mol% and 0 - 0.45, respectively. A proof of concept for a novel application in fluidized beds was completed: the fibre-optic probe was used to measure the molar fraction of a tracer gas inside the emulsion and bubble phases during gas tracer experiments.

Keywords: solids volume fraction, FT-IR spectroscopy, fibre-optic probe, gaseous species composition, fluidization, bubble, emulsion

1. Introduction

Gas/solid fluidized bed processes are characterized through the measurement of gaseous species composition and solid volume fraction. These two parameters are dependent parameters that are coupled through the reaction kinetics and hydrodynamics. Solids volume fraction affects chemical reactions through catalytic and/or inhibitive effects as well as through

the thermal balance. For example, the chemical products from fast reactions, such as oxidation, are greatly affected by the gas/solid mixing at the tip of injectors. Furthermore, at the hydrodynamic level, fluidized beds are characterized by the emulsion and bubble phases: determining the species composition in these two regions is key to the process characterization.

Current measurement methods are incapable of measuring gas-phase chemical composition and solids volume fraction simultaneously and in-situ in a gas/solid fluidized beds. Gas-phase chemical composition is usually measured with sampling probes connected to analyzers. Furthermore, solids volume fraction is generally measured with capacitance probes and fibre-optic probes that record the forward- or back-scattering of visible light [1-4].

It may be possible to use a fibre-optic probe with infrared (IR) light to measure solids volume fraction and gas-phase chemical composition simultaneously and in-situ. IR fibre-optic probes used with IR spectroscopy have been previously used to measured chemical composition in multiphase systems [5-14]. However, current IR spectroscopic applications do not measure solids volume fraction and rely on the uniformity of the solid samples with time (between measurements) since the solid phase has been shown to affect the IR absorbance spectra. The solids volume fraction and particle size influence the interaction between the light and the solids, which affect the path length of the IR beam and the effective sample size [15-16]. However, since multiphase systems are generally characterized by solids volume fractions that are heterogeneous in space and time, in-situ and real-time measurement of species concentrations in the different regions of a multiphase system requires the simultaneous determination of solids volume fraction. The measurement volume can be made independent of the solid properties by inclining the emitting and receiving fibres to form a convergent scheme [17] and this principle can be applied to an IR fibre-optic probe to measure species concentrations.

In multiphase systems, the movement of powders can make spectroscopy measurements and interpretation more complex. Studies have shown that the movement of the particles produced artefacts on the measured spectrum at certain wavenumbers that depended on the timescale of the spectral scan compared to the rate of movement of the particles. The wavenumber at which the artefact appeared increased with increasing modulation frequencies such that the effects of

moving particles could be completely eliminated at the wavenumbers of interest with a sufficiently high modulation frequency [18-20].

In the present study, a IR fibre-optic probe was constructed to perform in-situ and real-time measurements in a gas/solid flow of methane/nitrogen and FCC particles (d_p = 83 μm). The fibre-optic probe was connected to a near- and mid-IR Fourier transform transmission spectrometer (6000-1000 cm^{-1}). Absorbance spectra were recorded at a frequency of 4.5 Hz for a period of 75 seconds and both Y_i and (1-ε) were evaluated from each spectrum. Methane molar fractions in nitrogen were measured over a range of 0-10.1 vol%. Furthermore, the solids volume fraction was varied between 0-0.45.

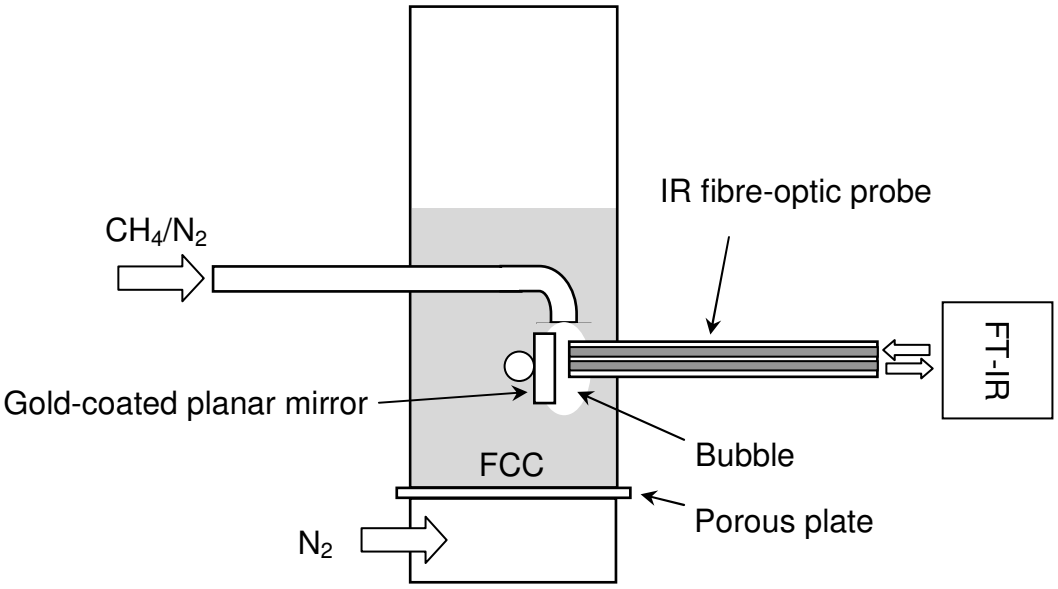

Figure 1: Fluidized bed apparatus

2. Experimental

Experiments were conducted with a mid-IR fibre-optic probe connected to FT-IR (Varian Excalibur series 3100). The probe was composed of two parallel fluoride glass fibre-optics (an emitting and a receiving fibre-optic) with a numerical aperture of 0.2 and a core diameter of 600 μm. The fibre-optic probe was connected to the FT-IR with a Harrick Fibremate™. A planar gold-coated mirror was positioned perpendicularly to the probe tip at a distance of 5 mm. The mirror reflected the emitted IR beam to the receiving fibre-optic, which resulted in a

measurement volume between the probe tip and the mirror. Experiments were conducted by first measuring a background spectrum - a CH_4/N_2 mixture was injected inside the measurement and a background spectrum was obtained from the co-addition of 20 spectra. Then, the measurement volume was flushed with air and the funnel was filled with sand particles to initiate a flow of solids. Absorbance spectra were measured at a frequency of 4.5 Hz (temporal resolution of 0.22 s) and the methane molar fraction was measured simultaneously to the solids volume fraction.

Gas tracer experiments were conducted in a small scale fluidized bed reactor (I.D. = 5 cm) illustrated in Figure 1 and the fibre-optic probe was used to measure the tracer molar fraction inside the bubble and emulsion phases. The reactor was filled with FCC particles (d_p = 83 μm and 14% fines ($d_p \leq 44$ μm)) and was fluidized with nitrogen at a superficial gas velocity of 2.6 mm/s (U_{mf} = 2.5 mm/s and U_{mb} = 2.7 mm/s). The expanded bed height was 12.5 cm and the fibre-optic probe was inserted in the bed at a height of 7 cm. A mirror was positioned perpendicularly at the probe tip and gas bubbles were produced in the fibre-optic probe measurement volume by injecting a mixture containing 10.1% CH_4 + 89.9% N_2 through a downward facing sparger. The CH_4/N_2 mixture was injected at a flow rate of 10 mL/s by manually opening a toggle valve for roughly 0.5 s at an interval of approximately 11 seconds.

3. Results and discussion

Both solid particles and gaseous species contribute to the absorbance spectrum during transmission spectroscopy in a gas/solid sample: the total absorbance at wavelength λ has a contribution from the solids volume fraction and from the gaseous species composition. Solid particles reduce the incident beam intensity by absorption, reflection and diffusion. Solids can also influence the path length and sample volume such that the absorbance due to the chemical species is a function of solids volume fraction:

$$A_{Total,\,\lambda} = A_{(1-\varepsilon),\,\lambda} + A_{Y_i,\,\lambda}\left[fn\left(1-\varepsilon\right)\right] \tag{1}$$

In the specific case of transmission spectroscopy where the effect of solids fraction on path length and sample volume can be neglected, equation (1) can be simplified to:

$$A_{Total,\lambda} = A_{(1-\varepsilon),\lambda} + A_{Y_i,\lambda} \quad (2)$$

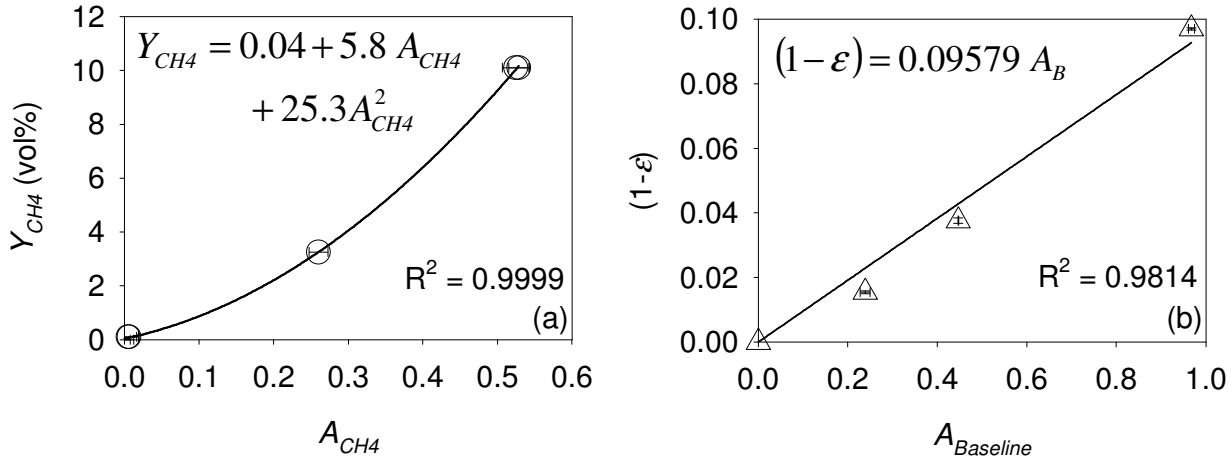

Figure 2: IR fibre-optic probe calibration

Equation (2) is valid when the reflected or diffused beam intensity measured is negligible compared to the transmitted light intensity. In equation (2), the effects of solids volume fraction and gaseous species composition on the absorbance spectrum are independent. Therefore, the effect of (1-ε) and Y_i can be calibrated independently. In the present experiments, the IR light intensity from diffused reflectance was negligible such that equation (2) was valid. This was verified experimentally be removing the mirror facing the probe tip.

A calibration was first performed with the fibre-optic probe to evaluate the effect of methane molar fraction and solids volume fraction on the absorbance spectrum. The effect of methane molar fraction (Y_{CH4}) was calibrated with four mixtures containing 0, 0.1, 3.25 and 10.1 vol% of methane in nitrogen. The average absorbance of the methane peak (A_{CH4}) was measured in the region of 3018.96-3016.86 cm^{-1} and it is shown as a function of methane molar fraction in Figure 2(a).

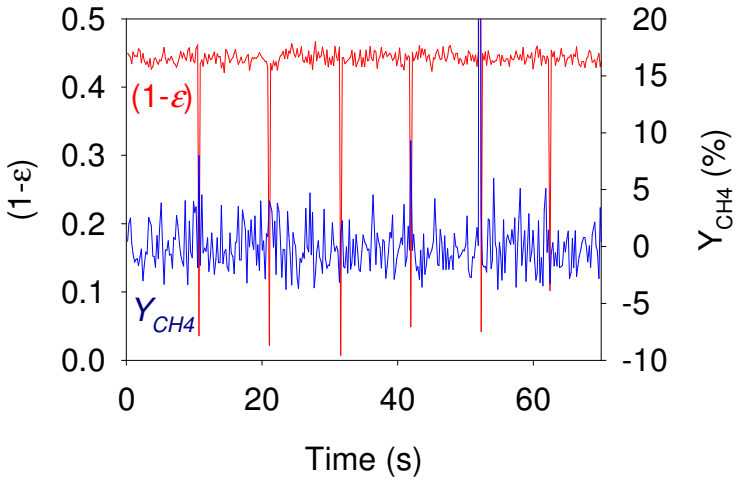

Figure 3: Time-history of (1-ε) and Y_{CH4} at the fibre-optic probe tip

The effect of solids volume fraction was calibrated by producing a flow of solids in the fibre-optic measurement volume with a funnel. The solids flow rate and solids volume fraction were varied by modifying the diameter of the funnel throat. Four solids volume fractions were used (0, 0.015, 0.038 and 0.097) and the average baseline absorbance ($A_{(1-\varepsilon)}$) was measured in the regions of 2997.73-2992.04, 3036.70-3030.72 and 3045.87-3040.39 cm^{-1} during 75 seconds at a frequency of 4.5 Hz. The average baseline absorbance is shown in Figure 2(b) as a function of solids volume fraction and the relationship is close to linear. Cutolo et al. [21] previously reported a linear relationship between absorbance and solids volume fractions. In the present case, solids volume fraction was measured by a conventional back-scattering fibre-optic probe with a different measurement volume than the IR fibre-optic probe. Since the flow of particles was heterogeneous, this may explain the observed deviation from the linear relationship.

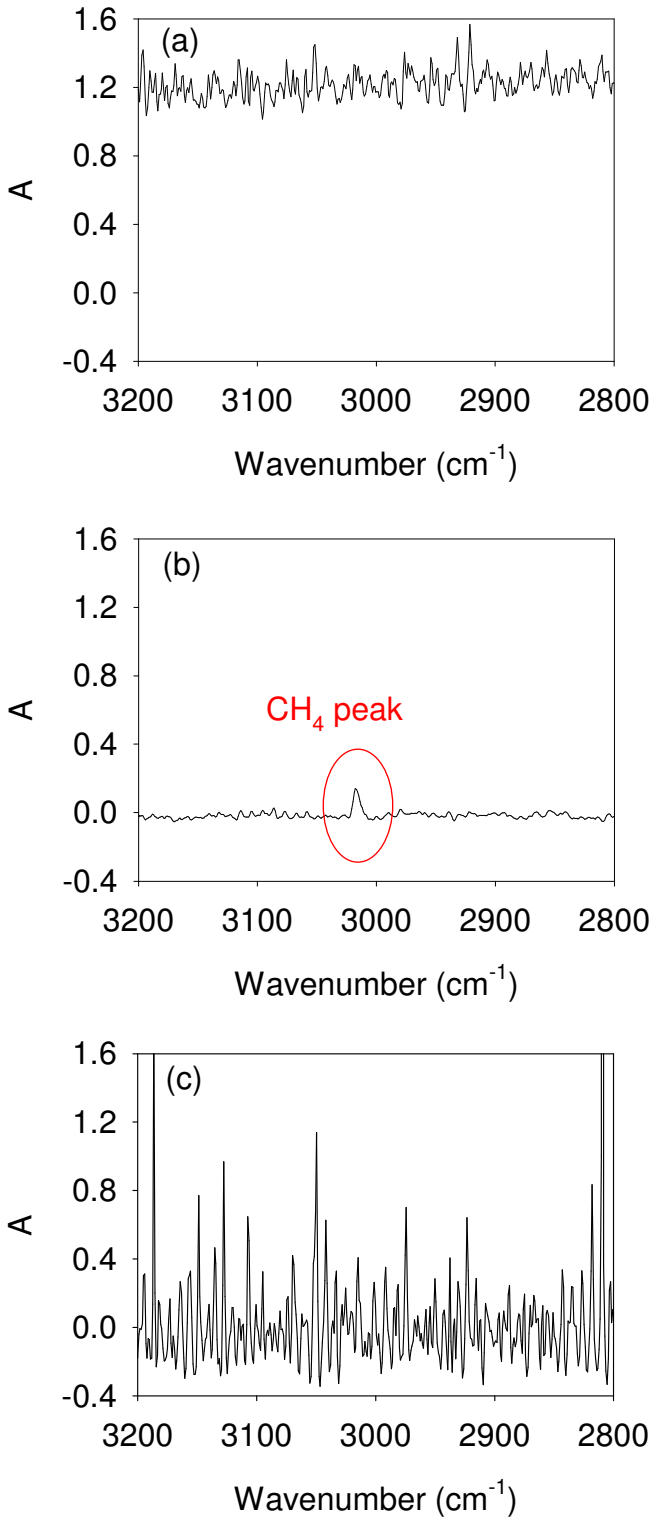

Figure 4: Measurement of Y_{CH4} in the fluidized bed

Gas tracer experiments were conducted in the fluidized bed of Figure 1 and the fibre-optic probe was used with the spectroscopic method to measure the molar fraction of a CH_4 tracer inside the bubble and emulsion phases. The bed of FCC particles was incipiently fluidized with nitrogen and bubbles were produced at the tip of the fibre-optic probe by the injection of a nitrogen/methane mixture (10.1% CH_4) through a sparger. Figure 3 shows the history of solids volume fraction and methane molar fraction measured by the fibre-optic probe during a typical experiment: the solids volume fraction was 0.45 in the emulsion phase and decreased significantly to 0.05-0 when gas bubbles of CH_4/N_2 were injected at intervals of approximately 11 seconds. The measured methane volume fraction in the emulsion phase fluctuated significantly (5% to -5%) due to the low intensity of the transmitted IR beam and the resulting low S/N. Figure 4(a) shows a typical absorbance spectrum measured in the emulsion phase: the low intensity of reflected signal resulted in a high absorbance throughout the spectrum. However, the time-average methane molar fraction was measured accurately as 0.0% (100% nitrogen).

Figure 4(b) shows an absorbance spectrum measured inside a bubble: a methane peak was observed at 3017.63 cm^{-1}. However, the injection of bubbles produced gas/solids movement, which caused noise in most recorded absorbance spectra: 5 spectra out of the 27 measured in the bubble phase were sufficiently clear to make a measurement of Y_{CH4}. Figure 4(c) shows a typical absorbance spectrum where noise was observed and the methane peak was indistinguishable. This noise could be eliminated in the wavelengths of interest by using a FT-IR with a higher modulation frequency.

The average peak height measured in the bubble phase corresponded to a methane molar fraction of 5% compared to the injected 10.1% CH_4 in nitrogen. This discrepancy may be due to mixing at the injector tip between the gas injected through the sparger and the fluidizing gas. Furthermore, the small number of clear spectra that were measured in the bubble phase could also explain the low value of Y_{CH4} measured since time-average measurements were more accurate than instantaneous measurements. During the present study, the measured absorbance spectra had to be exported and analyzed manually, which greatly reduced the number of spectra that could be considered to measure Y_{CH4} in the bubble phase. However, these results clearly show that the developed spectroscopic method with a fibre-optic probe can measure the gas composition in the bubble phase.

3.1 Limitation of the technique and future work

The fibre-optic probe used in this study is limited to ambient temperature applications: fluoride glass fibre-optics used can be exposed to temperatures below 150°C. However, fibre-optic probes have been developed with plastic fibre-optics for temperatures up to 1000°C [22]. Therefore, it is reasonable to assume that the measurement technique could be used to perform in-situ measurements in high temperature multiphase systems with an adequately designed fibre-optic probe.

This measurement technique is also limited by the modulation frequency of the spectrometer: the modulation frequency needs to be sufficiently high to avoid noise in the absorbance spectrum due to movement in the gas/solid system. The FT-IR used in the present study was purchased in 2001 and had a maximum modulation frequency of 80 kHz. New models are currently available with significantly higher modulation frequencies.

Another limitation of the technique is the IR beam intensity transmitted in the fibre-optic probe, which needs to be as high as possible in order to maximize the signal-to-noise ratio. The IR beam intensity can be increased by using a fibre-optic bundle, using a more sensitive detector, using a more powerful IR source, optimizing the signal transmission at the probe tip and at the FT-IR/fibre-optic probe interface (Harrick Fibremate™). More recent models of FT-IR also propose higher IR source intensity compared to the equipment used in the present study.

4. Conclusions

A novel IR fibre optic probe was used to measure quantitatively and simultaneously solids volume fraction ($1-\varepsilon$) and gaseous species composition (Y_i) in a gas/solid fluidized bed. The to a fibre-optic probe was connected to a FT-IR to perform real-time and in-situ measurements of absorbance. The effect of solids volume fraction and gaseous chemical composition on the absorbance spectra were additive and could be independently calibrated. Experiments were conducted with methane/nitrogen and propane/nitrogen mixtures and FCC particles. Fuel mole fraction and solids volume fraction were varied between 1.8 - 10.1 mol% and 0 - 0.45, respectively. The fibre-optic probe was used in a fluidized bed to measure the molar fraction of a

gas tracer inside the emulsion and bubble phases during gas tracer experiments. The measurement underestimated the methane volume fraction injected.

More measurements need to be performed in gas/solid systems at ambient and high temperatures to fully demonstrate the possibilities of this measurement method. High modulation frequencies from newer models of FT-IR should help resolve the problem of noise in the absorbance spectra caused by gas/solid movement. In theory, this method could also be used for liquid/solid, gas/liquid, liquid/liquid and gas/liquid/solid systems. However, work has to be performed in order to identify the limitations in these specific systems. It seems also that the accuracy of instantaneous fibre-optic probe measurements could be significantly improved by increasing the IR beam intensity. This could be achieved by using a fibre-optic bundle, using a more sensitive detector, using a more powerful IR source, optimizing the signal transmission at the probe tip and at the FT-IR/fibre-optic probe interface (Harrick Fibremate™). New FT-IR models also propose significantly higher IR signal intensity compared to the equipment used in the present study.

NOTATION

A	Absorbance
d_p	Average particle size (μm)
f	Modulation frequency (kHz)
t	Distance between probe tip and mirror (mm)
Y_i	Molar fraction of specie i (vol%)
$(1-\varepsilon)$	Solids volume fraction
λ	Wavelength (μm)

References

[1]Yates JG, Simons SRJ. Experimental methods in fluidization research. *International Journal of Multiphase Flow*. 1994; 20: 297-330.

[2]Ishida M, Tanaka H. Optical probe to detect both bubbles and suspended particles in a three-phase fluidized bed. *Journal of Chemical Engineering of Japan.* 1982; 15 (5): 389-391.

[3]Hu T, Yu B, Wang Y. Holdups and models of three phase fluidized beds. In: Ostergaard K, Sorensen A. *Fluidization V*. New York: Engineering Foundation, 1986: 353.

[4]Esmaeili B, Chaouki J, Dubois C. An evaluation of the solid hold-up distribution in a fluidized bed of nanoparticles using radioactive densitometry and fibre optics. *Canadian Journal of Chemical Engineering.* 2008; 86: 543-552.

[5]Cogdill RP, Anderson CA, Delgado M, Chisholm R, Bolton R, Herkert T, Afnan AM, Drennen III JK. Process analytical technology case study part I: feasibility studies for quantitative near-infrared method development. *AAPS PharmSciTech*. 2005; 6 (2): E273-E283.

[6]Andersson M, Josefson M, Langkilde FW, Wahlund K-G. Monitoring of a film coating process for tablets using near infrared reflectance spectrometry. *Journal of Pharmaceutical and Biomedical Analysis*. 1999; 20: 27-37.

[7]Kirsch JD, Drennen JK. Determination of film-coated tablet parameters by near-infrared spectroscopy. *Journal of Pharmaceutical and Biomedical Analysis*. 1995; 13: 1273-1281.

[8]Kirsch JD, Drennen JK. Near-infrared spectroscopic monitoring of the film coating process. *Pharmaceutical Research*. 1996; 13 (2): 234-237.

[9]Abrahamsson C, Johansson J, Andersson-Engels S, Svanberg S, Folestad S. Time-resolved NIR spectroscopy for quantitative analysis of intact pharmaceutical tablets. *Analytical Chemistry*. 2005; 77 (4): 1055-1059.

[10]Hailey PA, Doherty P, Tapsell P, Oliver T, Aldridge PK. Automated system for the on-line monitoring or powder blending processes using near-infrared spectroscopy part I. system development and control. *Journal of Pharmaceutical and Biomedical Analysis*. 1996; 14 (5): 551-559.

[11]Sonja Sekulic S, Wakeman J, Doherty P, Hailey PA. Automated system for the on-line monitoring of powder blending processes using near-infrared spectroscopy: Part II. Qualitative approaches to blend evaluation *Journal of Pharmaceutical and Biomedical Analysis*. 1998; 17: 1285-1309.

[12]Sonja Sekulic S, Ward HW, Brannegan DR, Stanley ED, Evans CL, Sciavolino ST, Hailey PA, Aldridge PK. On-line monitoring of powder blend homogeneity by near-infrared spectroscopy. *Analytical Chemistry*. 1996; 68: 509-513.

[13]Frake P, Greenhalgh D, Grierson SM, Hempenstall JM, Rudd DR. Process control and end-point determination of a fluid bed granulation by application of near infra-red spectroscopy. *International Journal of Pharmaceutics*. 1997; 151 (1): 75-80.

[14]Bellamy LJ, Nordon A, Littlejohn D. Real-time monitoring of powder mixing in a convective blender using non-invasive reflectance NIR spectrometry. *The Analyst*. 2008; 133: 58-64.

[15]Armaroli T, Bécue T, Gautier S. Diffuse reflection infrared spectroscopy (drifts) : application to the in situ analysis of catalysts. *Oil & Gas Science and Technology*. 2004 ; 59 (2): 215-237.

[16]Rantanen J, Räsänen E, Tenhunen J, Känsäkoski M, Mannermaa J-P, Yliruusi J. In-line moisture measurement during granulation with a four-wavelength near infrared sensor: an evaluation of particle size and binder effects. *European Journal of Pharmaceutics and Biopharmaceutics*. 2000a; 50 (2): 271-276.

[17]Cui H, Mostoufi N, Chaouki J. Comparison of measurement techniques of local particle concentration for gas-solid fluidization. In: Kwauk M, Li J, Yang W-C. *Fluidization X*. New York: Engineering Foundation, 2001: 779-786.

[18]De Paepe ATG, Dyke JM, Hendra PJ, Langkilde FW. Rotating samples in FT-RAMAN spectrometers. *Spectrochimica Acta Part A*. 1997; 53: 2261-2266.

[19]Berntsson O, Danielsson L-G, Folestad S. Characterization of diffuse reflectance fiber probe sampling on moving solids using a Fourier transform near-infrared spectrometer. *Analytical Chimica Acta.* 2001; 431: 125-131.

[20]Andersson M, Svensson O, Folestad S, Josefson M, Wahlund K-G. NIR spectroscopy on moving solids using a scanning grating spectrometer – impact on multivariate process analysis. *Chemometrics and Intelligent Laboratory Systems*. 2005; 75: 1-11.

[21]Cutolo A, Rendina I, Arena U, Marzocchella A, Massimilla L. Optoelectronic technique for the characterization of high concentration gas-solid suspension. Applied Optics 1990, 29 (9), pp. 1317-1322.

[22]Cui H, Sauriol P, Chaouki J. High temperature fluidized bed reactor: measurements, hydrodynamics and simulation. Chemical Engineering Science. 2003; 58: 1071-1077.

ANNEXE 7 – CHAPITRE 9 DU « WILEY HANDBOOK OF COMBUSTION » (VOLUME 5) (2010)

FLUIDIZED BED COMBUSTION OF NATURAL GAS AND OTHER HYDROCARBONS

Jean-Philippe Laviolette[1], Rahmat Sotudeh-Gharebagh[2], Rachid Mabrouk[3], Gregory S. Patience[1] and Jamal Chaouki[1*]

[1]Department of Chemical Engineering, Ecole Polytechnique, C.P. 6079, succ. Centre-Ville, Montréal, H3C 3A7, Canada

[2]School of Chemical Engineering, College of Engineering, University of Tehran, P.O. Box 11155-4563, Tehran, Iran

[3]Haldor Topsøe, Nymøllevej 55, 2800 Lyngby, Denmark

* Corresponding author (jamal.chaouki@polymtl.ca)

1 INTRODUCTION

This chapter reviews key features of methane combustion in the presence of solid catalytic or non-catalytic particles in fluidized bed reactors. Catalytic combustion has been defined as a flameless process that proceeds at lower temperature compared to homogeneous combustion. Catalytic combustion also results in lower pollutant (NO_X and CO) emissions and is not constrained by the flammability limits [1]. In the present work, the definition of catalytic combustion is broadened to include combustion with non-catalytic (inert) particles since it has been shown to satisfy many of the above criteria and since it is relevant to many applications.

Fluidized bed combustion is widely used in the chemical, petrochemical and energy industries and is central to many emerging technologies. Due to increasingly severe environmental regulations, increasing oil prices and the considerable natural gas world reserves, new technologies are currently under development such as:

- Co-firing of methane with different low calorific fuels (including solid) to increase combustion efficiency and heat value
- Methane combustion with solid catalytic and non-catalytic particles to minimize CO and NO_X in power and heat generation applications
- Syngas production from the catalytic partial oxidation of methane
- Chemical-looping combustion with a metal oxide oxygen carrier to eliminate NO_X and the cost of CO_2 separation [2]
- Biomass gasification and methane/biomass combustion to replace oil-based fuels

A thorough knowledge of fluidized bed combustion is essential for process control, optimization and minimization of pollutant emissions. In essence, fluidized bed combustion is governed by the reaction kinetics and the gas/solid hydrodynamics.

1.1 Heterogeneous and homogeneous kinetics

In the first section of this chapter, the intrinsic kinetics of combustion in gas/solid fixed beds are discussed. The intrinsic kinetics (without any limitations from the hydrodynamics) are characterized by simultaneous homogeneous and heterogeneous steps. Fixed bed reactors are generally used to study kinetics since the gas-phase hydrodynamics are considered to be ideal - plug flow - and mass transfer limitations are minimized when certain criteria regarding the ratio of particle diameter to tube diameter and to bed length are respected [3]. The kinetics are determined by the reaction conditions and the composition of the bed material. Three types of particles are considered in this chapter: combustion catalysts, inert particles (sand and alumina) and metal oxides. Several homogeneous and heterogeneous reaction networks have been published in the literature and range from simple single-step models to microkinetic models involving hundreds of elementary reactions. Several kinetic models are reviewed.

1.2 Mixing in gas/solid fluidized beds

Mixing is a critical phenomenon for fast and highly exothermic reactions, such as combustion, since it has a dominant influence on the prevailing mechanism and rate determining step. Although excellent gas-solid contact efficiency can be achieved in fixed bed reactors, the rise in bed temperature usually leads to the formation of hot spots, catalyst deactivation and even to conditions of homogeneous gas-phase combustion. Fluidized bed reactors are more attractive for highly exothermic reactions because of their superior heat management ability, proper mixing and excellent temperature control.

The schematic of a bubbling/turbulent fluidized bed reactor is shown in Figure 1.1. During operation, air is injected inside the windbox and then passes through the distributor (porous or perforated plate) to fluidize the bed of solid particles. The fuel can be premixed with air (premixed mode) or it can be separately injected inside the fluidized bed through a sparger (non-premixed mode). The gas/solid hydrodynamics depends strongly on the superficial gas velocity (U_g).

The bed of particles is in a fixed state (fixed bed) when U_g is below the minimum fluidization velocity ($U_g < U_{mf}$) and the gas-phase hydrodynamics is close to plug flow. When U_g is increased and equals U_{mf}, ($U_g = U_{mf}$) the upward drag forces exerted by the gas on the particles becomes sufficiently strong to suspend the solids. At this state, the bed of particles is said to be fluidized since it exhibits fluidic behaviour. As U_g is increased further ($U_g > U_{mf}$), bubbles of gas form at the distributor and rise inside the fluidized bed at several times the gas superficial velocity – this is the bubbling regime. Bubbles and the motion of solids result in gas by-passing and backmixing that produce a divergence from plug flow that amplifies with increasing superficial gas velocity

as the number and size of bubbles grow [4, 5, 6]. Particles disengage from the gas above the bed surface in the freeboard and disengagement regions. The cyclone collects the remaining solid particles in the off-gas and returns them to the fluidized bed through the dipleg.

At higher gas flow rates ($U_g >> U_{mf}$), in the turbulent fluidization regime, solids entrainment becomes significant, the upper bed surface becomes diffuse and the fluidized bed is characterized by a turbulent motion of clusters of solids and voids of various shapes and sizes. With a further increase in gas flow rate ($U_g >>> U_{mf}$), the solids are entrained out of the bed with the gas – this is lean-phase fluidization. Gas backmixing is significantly reduced in the lean fluidization regime. However, the void fraction increases considerably. A mode detailed review of fluidized beds can be found in Kunii *et al*. [6].

The main advantages of gas-solids fluidized bed reactors over fixed bed reactors are:

- Lower pressure drop (the pressure drop across the fluidized bed is constant and equals the weight of the bed independently of the gas velocity)
- Increased throughput
- Ability to inject the reactants separately
- Ability to add or remove particles continuously or intermittently without shutting down the process
- Improved heat transfer between the bed and the wall and immersed objects
- Reduced axial and radial temperature gradients, minimizing the risk of hot spots
- Increased catalyst effectiveness factors because of smaller particle sizes

However, fluidized bed reactors have some important disadvantages compared to fixed beds:

- Scale-up uncertainties due to more complex gas-solid hydrodynamics
- Particle attrition
- Wear on interior surfaces due to particle impingement
- Particle entrainment requiring gas-solid separation equipment

Fluidized beds are generally operated in a non-premixed mode to avoid combustion in the regions upstream (windbox and piping) and to allow operation in the flammable region. Efficient gas/solid mixing is therefore critical to achieve high reactant conversion. In the second section of this chapter, the effects of the following parameters on gas/solid mixing are reviewed: superficial gas velocity, sparger flow pattern, sparger design, particle size, solid fraction and baffles.

1.3 Fluidized bed combustion

Premixed and non-premixed methane fluidized bed combustion with inert and catalytic particles has been the subject of many investigations [7, 8, 9, 10, 11, 12, 13, 14, 15]. High-combustion

efficiency can be achieved at a remarkably low temperature ($T_b \leq 1173$ K) compared to conventional devices ($T > 1473$ K). The fluidized-bed reactors can be operated isothermally [16] and are capable of meeting all environmental requirements through the judicious selection of operating conditions and bed material [17]. In the third section of this chapter, the factors that influence methane conversion and pollutant emissions (CO and NO_X) in fluidized bed combustion are reviewed.

1.4 Fluidized bed combustion modelling

The optimization and scale-up of fluidized bed combustion processes necessitates the development of reaction models that include the effects of both kinetics (kinetics submodel) and hydrodynamics (hydrodynamics submodel). Various models have been proposed to describe the performance of fluidized beds and these models differ greatly in complexity. It is important to adopt a model with the optimum degree of sophistication with sufficient complexity to capture the mechanistic elements affecting the main aspects of interest. However, models should not be so complex such that they contain features whose inclusion is unjustified. In the fourth section of the present chapter, several fluidized bed combustion models are reviewed.

2 HETEROGENEOUS AND HOMOGENEOUS KINETICS

In gas/solid systems, the reaction kinetics is characterized by simultaneous homogeneous and heterogeneous steps.

2.1 Homogeneous kinetics

Homogeneous kinetics can be described by a set of global kinetics or by elementary reactions (microkinetics).

2.1.1 Global homogeneous combustion kinetics

Single-step models [18], two-step models [18, 19, 20] and more complex models [18] are available from the scientific literature. The main advantage of global models is their simplicity. The addition of intermediate species such as CO and others along with further refinement of the reaction mechanism into several steps can make the predicted product composition more detailed at the expense of increased complexity and uncertainty due to more estimated parameters. The kinetics of Dryer *et al.* [19] is described by the following two-step reaction:

$$CH_4 + \frac{3}{2}O_2 \xrightarrow{r_{CH4}} CO + 2H_2O \qquad (2.1)$$

$$CO + \frac{1}{2}O_2 \xrightarrow{r_{CO}} CO_2 \qquad (2.2)$$

$$r_{CH_4} = k_{CH_4}\, C_{CH_4}^{0.7}\, C_{O_2}^{0.8} \qquad k_{CH_4} = 235 \exp\left[-\frac{198\,000}{R}\left(\frac{1}{T}-\frac{1}{973}\right)\right] \qquad (2.3)$$

$$r_{CO} = k_{CO}\, C_{CO}\, C_{O_2}^{0.25}\, C_{CO_2}^{0.5} \qquad k_{CO} = 371000 \exp\left[-\frac{171000}{R}\left(\frac{1}{T}-\frac{1}{973}\right)\right] \qquad (2.4)$$

2.1.2 Microkinetic Combustion Models

Microkinetic models are constructed from a series of tens and sometimes hundreds of elementary reactions [21] and include many chemical species and free radicals. For example, the detailed Gas Research Institute mechanism (GRI-Mech release 3.0) for homogeneous combustion of methane consists of 325 elementary reaction steps and 53 species. Due to their complexity, microkinetic models allow more insight into reaction phenomena as the formation of many chemical products and intermediates can be tracked. In general, global models are unable to predict the formation of CO, NO_X and other intermediates [22]. Furthermore, the microkinetic models have been shown to successfully reproduce several combustion phenomena such as temperature regions, cool flames, induction time, etc. On the downside, they require several years of development, can hardly be used to describe multiphase systems with complex hydrodynamics (for the case of fluidized beds, for example) and involve the estimation of hundreds of parameters, which results in significant uncertainties concerning the results.

Microkinetic models are available from several research group websites [23, 24]. The GRI mechanism has been developed specifically for methane combustion. It is a product of significant computational and experimental work. The validity of the GRI approach has been demonstrated for a wide range of conditions [25].

2.1.2 Reduced GRI Mechanism

Microkinetic models are unsuitable for detailed reaction engineering modeling because of their complexity. Simple models are more readily modified to account for the effect of solids – catalytic and non-catalytic – compared to the detailed GRI mechanism. However, microkinetic models may also be simplified by eliminating minor reactions while conserving the fast reactions such that the overall behaviour is conserved.

Not all the reactions contribute equally to the combustion process at a specific set of operating conditions. Some of them may contribute significantly, others marginally and the rest do not contribute at all. Some species reach almost stationary mole fractions via very rapid elementary steps, while for others, this change happens very slowly compared to the time scale of interest. Moreover, the components with a small net rate may cause severe problems when solving large systems of differential equations. These considerations have been previously used to lower the number of species and elementary reactions in the GRI model. Tomlin *et al.* [26],

Warnatz *et al.* [27], Frenklach [28], Warnatz [29] have reviewed the main mathematical tools for the construction, investigation and reduction of complex reaction mechanisms.

To develop a reduced reaction network, the forward and reverse reactions rates that are small compared to the overall reaction rate are eliminated. This can be achieved by collecting rate information during the simulations with the complete mechanism and by setting a threshold value δ [26]. The non-contributing reactions can be identified by evaluating the following criterion for all grid points in the simulation:

$$\frac{|r_i|}{|r_{\max}|} \leq \delta \qquad (2.5)$$

Chang *et al.* [30] and Sotudeh-Gharebagh *et al.* [31] used equation (2.5) to reduce the GRI mechanism release 1.2 and 2.11 with $\delta = 0.02$ and $\delta = 0.005$, respectively. The mechanism with $\delta = 0.02$ contained a set of 104 reactions and 22 species. Using a smaller δ value of 0.005 produced a mechanism of 37 reactions and 17 species. This shows that the reduction technique is sensitive to the threshold value. Applying a uniform threshold value for different combustion conditions may either result in an oversimplified reaction scheme or the presence of non-contributing reactions. Therefore, a suitable δ threshold value should be chosen based on the combustion conditions.

The reduced mechanism of Sotudeh-Gharebagh *et al.* [31] is presented in Table 2.1. It was validated with methane-air combustion experiments performed in a flow reactor at the following conditions: 823 K $\leq T \leq$ 1250 K and $0.5 \leq \phi \leq 1$. The C_2 path was removed from the combustion chemistry. It is generally recognized in the scientific literature that the C_2 path is a sequence of less well-understood steps and becomes important for sufficiently fuel-rich mixtures [32, 33].

2.2 Combined homogeneous and heterogeneous kinetics

Solid particles can influence the gas-phase kinetics through a heterogeneous catalytic and/or inhibitive effect. Catalysts can increase or decrease the rate of specific elementary reactions and promote the formation of specific products and intermediates (including free radicals). Catalytic effects can also occur through intermediate species interaction in the heterogeneous and/or homogeneous phases. On the other hand, inert particles affect the intrinsic kinetics by inhibiting reactions through radical recombination at their surface [10].

Solid particles also influence combustion phenomena by modifying the thermal balance of the system. Solid particles have a significantly higher heat capacity compared to gas. The thermal balance of the system plays an important role in combustion [32]. For example, a higher heat capacity can quench the thermal run-away preceding the autoignition of a fuel/oxygen mixture.

2.2.1 Inert Particles

Inert particles are extensively used for power generation since they are inexpensive, widely available and resistant to high temperatures. Combustion with inert particles is also relevant to other applications such as biomass combustion and gasification. Inert particles can considerably alter the combustion process due to heterogeneous reactions. Inert particles can inhibit combustion by quenching free radicals and the extent of inhibition varies with temperature [34].

Sotudeh-Gharebagh *et al*. [31] performed premixed combustion experiments in a fixed bed reactor of sand particles. Figure 2.1 shows methane conversion at the reactor outlet as a function of reactor temperature for the empty reactor and the reactor filled with sand particles of 523 μm. The mean gas residence time was 3 s for a feed gas containing 2 mol% of methane in air. Based on Figure 2.1, it can be concluded that:

(1) $T < 1020$ K: The methane conversion was higher in the presence of sand particles - sand accelerated slightly the reaction.

(2) $1020\ \text{K} < T < 1150\ \text{K}$: In this moderately high temperature range, the methane conversion was significantly lower in the presence of sand particles as they inhibited the homogeneous combustion reactions. The inhibition occurred most probably via free radical recombination at the solids surface. Vlachos *et al*. (1994) reported that the operating conditions and spatial heterogeneity (presence of solid surface) could largely affect product distributions. For example, removal of H atoms and CH_3 radicals by adsorption can increase the ignition temperature. The inhibition effect from sand particles was observed in many studies [10, 35].

(3) $T > 1150$ K: Above this high temperature, methane conversion increased rapidly with increasing temperature. Moreover, the rate of increase of methane conversion was similar to the rate observed in the homogeneous reactor. At high temperatures, the free radical generation dominated the free radical quenching process. Hesketh *et al.* [10] made a similar observation in an incipient fluidized bed of sand.

The temperature required to achieve complete methane conversion depends on the average gas residence time inside the fixed bed reactor. Figure 2.1 shows that for an average gas residence time (τ) of 3 s, a reactor temperature of 1170 K was necessary. Figure 2.2 reports the methane conversion as a function of reactor temperature for $\tau = 6$, 2 and 1.2 s. The required temperature to obtain complete conversion increased from 1130 K to 1190 K as the gas residence time dropped from 6 s to 1.2 s, respectively.

Fuel lean methane combustion in a fixed bed of sand particles can be modeled as a first-order single-step reaction. Sotudeh-Gharebagh *et al*. [31] showed that the methane conversion is

independent of the initial methane mole fraction in the range of 2-4 mol%. Therefore, the overall methane conversion is first order with respect to methane concentration.

2.2.1.1 Effect of particle size distribution and alumina particles

The effects of particle size distribution have been investigated by Sotudeh-Gharebagh *et al.* [31] in a fixed bed of sand particles of three mean sizes (d_p = 230, 330 and 523 μm). The contact time index (h) was kept constant for all cases and particle size had no effect on conversion.

Sotudeh-Gharebagh *et al.* [31] also studied methane combustion in a fixed bed of alumina particles (d_p = 363 μm) and they observed that alumina particles had the same effect as sand particles.

2.2.1.2 CO production

Methane combustion in a fixed bed of sand particles can lower CO compared to homogeneous combustion. Figure 2.3 shows the CO mole fraction in the off-gas of a fixed bed as a function of reactor temperature: a maximum in CO was observed near $T = 1150$ K. For hydrocarbon combustion, the formation rate of CO is greater than its consumption rate at low temperatures. As the temperature is increased, the CO consumption rate dominates and this explains the presence of a maximum in CO emissions.

In Figure 2.3, the CO measurements are compared to the predictions of the full and the reduced GRI mechanisms (Table 2.1) for homogeneous combustion. The measured CO mole fractions were low compared to the homogeneous model predictions for $T < 1150$ K. Sotudeh-Gharebagh et al. [31] attributed this effect to the low concentration of OH radicals, which were substantially reduced by the recombination reactions at the particle surface.

2.2.2 Kinetics for methane combustion in inert particles

Figures 2.1 to 2.3 compare the methane conversion in a fixed bed of sand particles measured by Sotudeh-Gharebagh *et al*. [31] with the predictions of the full and reduced GRI mechanisms (Table 2.1) for homogeneous combustion. The homogeneous models failed to predict the methane conversion and CO outlet mole fraction as a function of reactor temperature for an empty reactor (Figure 2.1) and for a fixed bed of sand (Figures 2.1 to 2.3) in the second temperature interval (1020 K < T < 1150 K). The discrepancy between the results in the empty reactor (homogeneous system) and the model may be due to the alumina wall, which is known to have an inhibitive effect comparable to sand, as previously discussed. To better predict combustion in the presence of solid particles, homogeneous models need to be modified in order to account for the heterogeneous steps. In the third temperature interval (T > 1150 K), where complete conversion was achieved, good agreement was observed between fixed bed experiments and model predictions. At these high temperatures, radical generation dominated the inhibition mechanism.

As previously discussed, methane conversion during fuel-lean catalytic combustion can be modeled using a single-step first-order model. However, a more complex model is required to characterize the production of intermediate species (CO, NO_X, etc). Sotudeh-Gharebagh *et al*. [31] chose a certain number of reactions in their reduced mechanism (Table 2.1) and modified their reaction rates to represent the heterogeneous effects. The following assumptions were made:

- Free radical quenching occurs at the wall and particle surface [32, 36]
- The recombination of OH, O, H and CH_3 radicals retards homogeneous ignition [32]
- In the presence of inert particles, the most important radicals are OH and H radicals. Simulations with the reduced GRI mechanism (Table 2.1) showed that OH radicals play a major role in the inhibition process for the experimental conditions of Sotudeh-Gharebagh *et al.* [31].

Hence, the reaction rates (frequency factor and activation energy) of elementary steps #1, 2, 6, 12, 14, 16, 26, 27, 29 and 34 were modified in the reduced mechanism. They were changed based on a global reaction factor (f), which was defined as the ratio of the heterogeneous reaction rate to the homogeneous reaction rate:

$$f = \frac{r_{het}}{r_{\text{hom}}} = A \exp\left[\frac{-\Delta E_a}{R\,T}\right] \qquad (f < 1) \qquad (2.6)$$

The optimal values for the constant A and the activation energy (E_a) were found to be $A = 4.3\times10^9$ and $E_a = 217.2$ kJ/mol, respectively. At temperatures above 1170 K, the model returns to the homogeneous case ($f = 1$). The activation energy is of the order of magnitude found in the combustion literature [37]. The activation energies for the modified mechanism are presented in Table 2.1.

In Figures 2.3 and 2.4, the calculated methane conversion and CO mole fractions as a function of reactor temperature are compared to the experimental measurements of Sotudeh-Gharebagh *et al*. [31] obtained in a fixed bed of sand. The modified kinetics fits the experimental data well in all temperature intervals contrary to the reduced homogeneous GRI model.

2.2.3 Combustion catalysts

Combustion catalysts are generally in the form of solid porous micro-spheres that promote heterogeneous reactions and reduce the lower flammability limit below 5 mol% (in air). Low temperatures (in the range of 773 K) and excess oxygen can result in zero emissions of NO_X and CO. However, catalysts increase the operating costs for power generation. The kinetics of fuel-lean methane catalytic combustion has been reported as a first-order single-step mechanism [17,

38], which agrees with the observations of Sotudeh-Gharebagh *et al*. [31] with inert particles. More complex models are unnecessary since breakthrough of CO and NO_X are zero.

2.2.4 Oxygen carriers

In chemical-looping combustion, a solid oxygen carrier is used to bring the oxygen to the fuel for reaction. Oxygen carriers are composed of an active metal oxide (ZnO, CuO and Fe_2O_3, for example) and an inert support/binder. To fully describe chemical-looping combustion, both reduction and oxidation steps are required. Reactions schemes have been reviewed by Hossain *et al*. [2] – the solids act as a catalyst in some reactions and as a reactant in others.

3 MIXING IN GAS-SOLID FLUIDIZED BEDS

The complex gas/solid hydrodynamics in fluidized beds may have a dominant influence on the prevailing mechanisms and rate determining steps during combustion since the reaction rates are fast compared to the mass transfer rates. Dispersion and contacting of the gas and solids depend on the particle properties, operating conditions, reactor scale and geometry.

3.1 Superficial gas velocity and bubble size

In the bubbling fluidization regime, the bubbles produce gas by-passing that limits the gas/solid mixing. The bubble-emulsion inter-phase mass transfer decreases with increasing superficial velocity and increasing bubble size [39]. In the turbulent fluidization regime, at high superficial gas velocity, gas/gas and gas/solid contacting is significantly improved [40].

3.2 Particle size

The addition of catalyst fines and the use of a wider particle size distribution are critical in maintaining a good quality of fluidization and are often sited as a prime factor to optimize reactor performance [41]. Furthermore, many experimental investigations show that the addition of catalyst fines in the bed leads to significantly higher global conversion [42, 43]. Fines affect the reactor by reducing the mass transfer limitations, since the intrinsic properties of the catalyst remain unchanged [44].

A reported effect of the addition of fines on fluid bed hydrodynamics is an increase in the bed voidage. This was shown by Rowe *et al.* [45], who used an X-ray absorption technique to measure the change in voidage of the emulsion phase following the addition of fines. This was also observed by Pell *et al.* [44]. In essence, this results in a higher level of permeability of the emulsion phase and a more homogeneous fluidization. Hence, more gas flows through the solid-rich emulsion phase to the detriment of the bubble phase, resulting in smaller bubbles and a higher inter-phase mass transfer. This was concluded by several models [43, 45]. Smaller fractions of gas into bubbles should result in a lower degree of by-passing and gas phase hydrodynamics closer to plug flow. Some experimental investigations have also reported that fines can stay suspended in bubbles [46, 47].

The mean particle size also affects gas/solid mixing in fluidized beds. In the turbulent regime, Sotudeh-Gharebaagh *et al*. [40] observed better gas mixing ($U_g = 0.8$ m/s) with FCC ($d_p = 70$ μm) compared to sand ($d_p = 543$ μm). On the other hand, Wu *et al*. [14] reported a higher bubble-emulsion mass transfer in a bubbling fluidized bed close to incipient fluidization conditions ($U_g \sim U_{mf}$). Larger particles increase the minimum bubbling velocity (U_{mb}) and the transition to turbulent fluidization (U_c), which may partially explain these results.

3.3 Effect of baffles

Another means of reducing the divergence from plug flow of a bubbling fluidized bed may reside in the utilization of reactor internals. Reactor internals are often necessary for heat transfer purposes and several studies have suggested that they could be an effective means for improving gas-solid contacting; the bubble size distribution can be homogenized and reduced, such that the the solid and gas axial circulation rate can be lowered [4, 48, 49]. The goal is to promote bubble splitting and gas redistribution into the emulsion phase [50]. However, there are limitations as Volk et al. [51] have shown that the axial solid mixing can be reduced to the level at which segregation is promoted and the fluidization of each individual compartment becomes difficult. Furthermore, the effectiveness of internals greatly depends upon its design [52].

3.4 Sparger flow pattern for non-premixed operation

The injection gas velocity at the sparger nozzle may lead to a number of patterns ranging from the periodic formation of bubbles to the formation of a permanent jet. At relatively low gas injection velocities, gas bubbles form, grow, detach and travel through the bed. As the injection velocity increases, bubbles grow bigger and the distance between successive bubbles decreases. At higher gas injection velocities, bubbles coalesce to form a plume or a jet at the sparger tip. The flow pattern and jet penetration length, L_j, defined as the distance between the plate and centre of the bubble at the instant it detaches from the jet, are important for process design since:

- The gas injected from spargers entrains solids in the vicinity of the nozzle, which causes erosion on impinged surfaces and attrition
- Knowledge of the jet flow could help maximize gas-solid contact and minimize attrition
- For combustion processes, the reaction products largely depend on how the feed enters the bed

A vast body of experimental data is available in the literature for vertically upward gas injection into fluidized bed reactors. Correlations for jet length are available for various fluidized bed operating conditions [47, 53, 54, 55, 56, 57]. Significantly less information is available for downward facing nozzles [40, 58]. Criteria to determine the flow pattern (bubbling or jetting) at the tip of an upward facing sparger have been proposed by Grace *et al*. [59] and Roach [46] as shown in Table 3.1.

The transition velocity (U_{mj}) between the bubbling and jetting patterns can be measured experimentally by measuring the mean pressure fluctuations close to the sparger tip. Sotudeh-Gharebaagh *et al.* [40] measured a value of $U_{mj} = 115$ m/s with a downward facing sparger ($d_{or} = 2$ mm) inside a high temperature ($T_b = 713$ K) bubbling fluidized bed of sand particles and FCC catalyst. The criteria of Table 3.1 failed to correctly predict the flow pattern at the sparger tip most likely since they fall short of considering all reactor operating conditions (temperature, jet angle, injection velocity) and characteristics (reactor diameter and geometry). The formation of a jet is more likely with [59, 60]:

- Coarser and lighter particles
- Increasing fluid density
- Increasing orifice velocity
- Low superficial velocity
- Decreasing temperature
- Jets away from the vertical (attrition by downward jets is significantly higher than that of the upward jet [61]

In commercial fluidized bed reactors, where gas can be injected through a sparger with thousands of nozzles, the sparger is designed to operate under bubbling conditions ($U_j = 30$ m/s) to keep attrition low [6]. However, a jetting flow pattern at the sparger nozzle produces enhanced mixing compared to the bubbling pattern. Figure 3.1 shows the radial profiles of a non-reacting propane tracer at various axial positions above a downward facing sparger located at the centre of a fluidized bed [11]. At low gas injection velocity ($U_j = 14.8$ m/s) the tracer radial dispersion was poor - the tracer mole fractions reached a maximum at the bed centreline and decreased closer to the wall as shown in Figure 3.1(a). On the other hand, at a high gas injection velocity ($U_j = 92.6$ m/s), gas dispersion was enhanced as the tracer mole fraction was more uniformly distributed along the bed radius (Figure 3.1(b)). At low injection velocities, the tracer is mostly injected in bubbles that result in low gas-gas and gas-solid contacting.

The presence of the sparger may also limit mixing in its surrounding [40]. Figure 3.2 shows the methane concentration standard deviation as a function of axial position. Methane was injected from a downward facing sparger in a high temperature turbulent fluidized bed ($T_b = 673$ K and $U_g = 0.8$ m/s) and the standard deviation was calculated from the radial concentration profile. The sparger tip was located 170 mm above the distributor, which corresponds to $Z = 0$ mm on Figure 3.2. The data from two spargers are presented: a non-baffled sparger and a baffled sparger. The high standard deviation close to the spargers can be attributed to the fact that bubbles formed at the sparger nozzles and then rose close to the sparger wall. The wall acted as a barrier to mixing as it reduced contact between the sparger bubbles and the gas and solids inside the fluidized bed. As soon as the bubbles went past the sparger level, the tracer gas was well dispersed to the emulsion phase, due to intense gas-solid and gas-gas mixing in the turbulent fluidization regime. The standard deviation dropped significantly within less than 100 mm above the sparger. Figure 3.2 also shows the existence of three distinct mixing regions: null, partial and complete mixing. In the null mixing zone located below the sparger ($Z < 0$ mm), tracer gas is absent. In the acceleration zone ($0 \leq Z \leq 25$ mm), the axial and radial gas mixing is limited by the

sparger-nozzle walls. In the fully developed mixing zone ($Z > 25$ mm), above the tracer injection level, a fairly uniform mixing pattern is developed.

Figure 3.2 also shows that baffled spargers can enhance mixing compared to non-baffled spargers. At 2 mm below the sparger tip, for baffled spargers, the gas diffusion was deeper as compared to the non-baffled sparger and the equilibrium methane concentration was reached faster with the baffled sparger ($Z = 200$ mm) compared to the non-baffled sparger ($Z = 300$ mm).

4. METHANE FLUIDIZED BED COMBUSTION

Fluidized bed combustion is characterized by both kinetics and gas/solid hydrodynamics. Combustion can occur in different regions inside the fluidized bed (at the distributor, at the sparger tip, in the bubble/emulsion phases and in the freeboard region), which has a significant effect on fuel conversion and pollutant emissions. Combustion of gaseous mixtures, mostly methane-air, has been successfully implemented in fluidized bed reactors.

4.1 Inert Particles

Most studies on fluidized bed combustion with inert particles have been performed in premixed mode [7, 8, 9, 10, 15]. Few were achieved with fuel injection through a separate sparger [11, 12, 13].

4.1.1 Fluidized bed temperature

The fluidized bed temperature is a key parameter to ensure complete combustion. With increasing temperature, the combustion is initiated deeper inside the fluidized bed. In premixed combustion, increasing temperature moves the combustion front towards the distributor - the combustion front moves first from the freeboard to the bubbles bursting at the upper surface of the sand, then to bubbles igniting in the bed and finally to small bubbles where ignition occurs practically at the level of the distributor and the process appears flameless [9, 35]. Two critical transition temperatures have been defined for fluidized bed combustion. Below the lower critical temperature (T_1), combustion only occurs above the bed surface. Between T_1 and the upper critical temperature (T_2), combustion begins to move inside the bubbles within the bed. Finally, above T_2, combustion takes place entirely within the bed and close to the distributor.

Table 4.1 summarizes methane fluidized bed combustion studies that measured T_1 and/or T_2. The values of T_1 and T_2 reported vary by 100 - 200 K. This difference may be due to the difference in operating conditions and the method by which the critical temperatures were determined – temperature or species measurements. Van der Vaart [62] reported that T_1 increased with decreasing bed height, increasing excess fluidizing gas velocity and increasing particle size.

Combustion will occur inside the emulsion (particulate) phase if the fluidized bed temperature is sufficiently high above T_1. Hesketh *et al*. [10] observed in-bed combustion inside an incipient

fluidized bed for $T_b \geq 1188$ K. Sotudeh-Gharebagh *et al*. [31] observed complete methane conversion in a fixed bed of silica sand at $T_b \geq 1150$ K. At sufficiently high temperature, free radicals production outweighs the radical recombination at the surface of particles and combustion is possible in the emulsion phase.

In non-premixed combustion, increasing the temperature will bring the combustion front closer to the sparger. The sparger operating conditions and design should be chosen to maximize gas/gas and gas/solid contacting.

4.1.2 Bubble size and air-fuel ratio

Friedman *et al*. [8] reported that increasing the air-fuel ratio promotes the consumption of methane in the bed at lower bed temperatures (below 1173 K). Wu *et al*. [14] injected bubbles of pure methane (non-premixed combustion) inside a bubbling fluidized bed of alumina and sand particles. It was found that small bubbles enhanced bubble-emulsion mass transfer, which promoted oxygen diffusion inside the bubbles and bubble-phase combustion. Wu *et al.* [14] also reported that increasing the oxygen concentration in the emulsion promoted bubble-phase combustion.

Pilawska *et al.* [64] observed that when $T_b < T_1$ (1123 K in their case) only bubbles above a certain critical size ignite on leaving the fluidized bed. Complete methane combustion was only observed when the superficial velocity was sufficiently higher ($U_g/U_{mf} > 4$ for a bed height of 20 mm).

4.1.3 Fluidization regime

The turbulent fluidized bed regime shows better gas-gas and gas-solid contacting compared to the bubbling regime. Also, due to its higher throughput, the turbulent regime offers a higher power generation for the same operating temperature. The power generated in the combustion process is calculated using the following expression:

$$P = F_{CH4}\ X\ \Delta H \qquad (4.1)$$

4.1.4 CO formation

The combustion of hydrocarbons can be viewed as a two-step global process: combustion to CO and its conversion to CO_2. At lower temperatures and also in the presence of inert particles, consumption of CO is very small compared to its formation and conversely at higher temperatures. The bed temperature must be sufficiently high to completely oxidize CO to CO_2 within the bed.

Sotudeh-Gharebaagh *et al.* [65] showed that the conversion of CO to CO_2 occurs faster in a turbulent fluidized bed. Pure methane was injected through a downward facing sparger at two

injection gas velocities ($U_j = 30,\ 120$ m/s) at a bed temperature of 1173 K. These sparger velocities represented two different sparger hydrodynamics: bubbling and jetting. Furthermore, two gas superficial velocities ($U_g = 0.7,\ 1.5$ m/s) were tested, which corresponded to the bubbling and turbulent regimes, respectively.

In Figure 4.1, CO measurements along the reactor height at the four conditions are reported (the sparger tip was located at $Z = 170$ mm). For all cases, the CO volume fraction increased close to the sparger tip where combustion occurred under fuel-rich conditions due to incomplete gas mixing in that region. The CO volume fraction then reached a maximum value downstream and then declined as the gases mixed and reacted further with O_2 in the fluidized bed. All CO was converted to CO_2 since the bed temperature was sufficiently high.

As shown in Figure 4.1, increasing gas injection velocities resulted in greater CO peaks due to enhanced mixing at the sparger tip, which led to faster combustion and increased dispersion of gas in the emulsion phase. The complete reaction length for CO oxidation in the turbulent fluidization was also small compared to bubbling conditions due to improved gas mixing. The overall trend reported in Figure 4.1 is in close agreement with the predictions as well as with the experimental and theoretical findings of turbulent non-premixed combustion of methane in air [66] and of coal combustion [67].

Figure 4.2(a) shows the normalized concentration of CO (ppm) measured at the reactor outlet for non-premixed methane combustion in a bubbling and turbulent fluidized bed. For bed temperatures less than about 1123 K, high concentrations of CO were generated since the temperature was insufficient to completely convert the CO within the bed. In the temperature range of 1123-1273 K, both systems performed quite well. Turbulent fluidized beds generated less CO most probably due to higher contacting efficiency, while bubbling fluidized beds need to operate above 1170 K for low CO emission levels. This agrees with the observations of Friedman *et al*. [8]. Furthermore, Friedman *et al*. [8] reported that increasing gas superficial velocity in the bubbling fluidization regime reduced in-bed CO conversion because of increasing bubble size, which resulted in higher bubble rise velocities and gas by-passing.

4.1.5 NO_X formation

A major environmental concern for fluidized bed systems is to control NO_X emissions. NO_X formation and destruction in combustion processes result from a combination of fuel nitrogen oxidation, thermal processes, and reactor hydrodynamics. The success of natural gas combustors depends strongly on their operating temperature, which is critical for thermal NO_X emissions. Thermal NO_X are generated in conventional devices where the flame temperature is usually above 1473 K. Below 1073 K, no thermal NO_X is produced.

Fluidized beds are characterized by solids mixing that prevent the formation of hot spots, which reduces the NO_X compared to homogeneous gas-phase combustion. Friedman *et al*. [8] reported that NO_X emissions were considerably reduced when the combustion front moved from the

freeboard to the fluidized bed. NO_X emissions have been observed to increase with bed temperature until a critical temperature where the trend reverses. This critical temperature was measured as ~1100 K and 1200 K by Friedman *et al*. [8] and Pilawska *et al*. [64], respectively.

Friedman *et al*. [8] reported that increasing the gas superficial velocity (constant air-fuel ratio) increased NO_X emissions. It was argued that a denser bed could more easily quench hot spots. Pilawska *et al*. [64] observed an increase in NO_X with increasing U_g/U_{mf}. In this case, it was hypothesized that bigger bubbles resulted in enhanced gas by-passing and less in-bed combustion.

Sotudeh-Gharebaagh *et al.* [65] compared the NO_X emissions from a bubbling and a turbulent fluidized bed of sand particles. In Figure 4.2(b), NO_X fractions are reported for turbulent and bubbling conditions. The NO_X emission levels for turbulent fluidized-bed operation were higher compared to the bubbling bed. This was attributed to the higher availability of oxygen in the turbulent fluidized bed, which was almost 8% above stoichiometry. In comparison, the bubbling bed was operated with excess oxygen of less than 1%, which consequently led to lower NO_X formation. The experimental NO_X measurements in Figure 4.2(b) were significantly lower than the predictions of the GRI model for homogeneous combustion. For industrial reactors operating in the turbulent fluidization regime with an integrated heat exchanger inside of the reactor and less oxygen, NO_X emissions can be significantly lowered. NO_X emissions as low as 5 ppm were measured by Friedman *et al*. [8] and Pilawska *et al*. [64] in the bubbling regime with inert particles.

4.1.6 Particle type and size

Sotudeh *et al.* [40] reported that the CO generated in a turbulent fluidized bed of sand particles (~ 10 mol%) was greater compared to FCC particles (~ 2 mol%). Gas/gas and gas/solid mixing is significantly improved with small FCC particles (d_p = 70 μm) compared to large sand particles (d_p = 543 μm). With sand particles, limited mixing resulted in fuel-rich conditions and reactions that were mostly homogeneous.

4.2 Combustion catalysts

Studies have been performed with various combustion catalysts, which have shown that low temperature combustion (T_b ~ 773 K) of a fuel lean methane-air mixture can be achieved with zero CO and NO_X emissions in a turbulent fluidized bed [17, 38].

4.3 Oxygen carriers / chemical-looping combustion

Chemical-looping combustion is typically done in a circulating fluidized bed. The concept is based on shuttling catalyst between two zones: the oxygen carrier is reduced in a transport bed/riser and then re-oxidized in a fluidized bed regenerator [2].

5 FLUIDIZED BED COMBUSTION MODELLING

Methane conversion in gas-solid fluidized bed has been observed to vary from plug flow to backmixed flow, depending on the reaction and fluidization conditions. Various models have been proposed to describe the performance of fluidized beds and these models differ greatly in complexity.

Empirical models are seldom of much value due to the hydrodynamic complexity of fluidized beds and the large number of variables involved. Historically, mechanistic models have been based on a pseudo-homogeneous or a two-phase approach. The pseudo-homogeneous approach describes the fluidized bed hydrodynamics with single-phase models (well-mixed, plug flow and dispersion models), which constitutes a poor characterization.

In the two-phase approach, the fluidized bed is separated into two one-dimensional paths: one of high voidage that represents the bubble phase and one of high solids fraction that represents the dense (emulsion or particulate) phase. The mole balance is written for both phases and includes terms for the chemical reactions and the inter-phase mass transfer. The performance of two-phase models is dependent upon the inter-phase mass transfer, the volume of each phase, the solids fraction the chemical kinetics and the flow rate attributed to each phase. Two-phase models, reviewed in several studies [6, 68, 69, 70], are widely used and have been quite successful for steady-state fluidized bed gas-phase solid-catalyzed reactions.

5.1 Single-phase models

Single-phase models are reviewed in several studies [6, 69]. Lorences *et al*. [4] showed that for $U_g \leq 6\ U_{mf}$, the gas hydrodynamics is very close to plug flow such that the conversion for a first order reaction is within 0.8% of the value for plug flow.

5.2 Two-phase models

Two-phase models describe the fluidized bed with a molar conservation equation for the bubble and emulsion phases. The conservation equations contain an inter-phase transfer term and the two phases are generally modeled as ideal reactors (plug flow or CSTR). Several fluidized bed models have been published in the literature and include the model of Davidson and Harrison [71], bubbling bed models [6] and bubble assemblage models [72].

5.2.1 The model of Davidson and Harrison

General two-phase models have the following assumption [71]:

- All gas flow in excess of U_{mf} passes through the bed as bubbles
- Bubbles are of uniform size throughout the bed

- Interphase mass transfer occurs through a combined effect of molecular diffusion and gas throughflow
- The bubble and emulsion phases are either perfectly mixed or in plug flow

5.2.2 Bubbling bed models

The bubbling bed model of Kunii and Levenspiel [6] is a modified version of the two-phase model where a cloud-wake phase is also considered. Hence, the interphase mass transfer occurs between the bubble and the cloud-wake phase and between the later and the emulsion phases.

5.2.3 Bubble assemblage models

Other hydrodynamic models have used various combinations of assumptions. Among them, the Kato and Wen [72] model considers the change of bubble size with height inside the bed. Modified versions of this model have also been proposed by Dounit *et al*. [7].

5.2.2 Multiple region models

The grid region near the distributor, the region surrounding the tip of spargers and the freeboard zone above the fluidized bed are characterized by hydrodynamics significantly different from the main body of the fluidized bed. These regions are characterized by relatively high voidage due to the injection of gas (grid and sparger tip) and the disengagement of solids (freeboard).

5.2.2.1 Models for the grid region

A significant amount of reaction may occur in the grid region, especially for fast reactions such as combustion [73]. The jet of gas originating from the distributor results in good contacting. Behie *et al*. [74] calculated an inter-phase mass transfer coefficient 40 to 60 times higher in the grid region compared to the main body of the fluidized bed. Single-phase models have been proposed to describe the grid region [73, 75, 76]. Behie *et al*. [74], Grace *et al*. [77] and Sit *et al*. [78] proposed two-phase models with enhanced inter-phase mass transfer terms.

5.2.2.2 Models for the freeboard region

In the freeboard region, solid particles are projected due to the bubbles bursting at the bed surface. Reaction can occur in the freeboard region due to the high voidage. Studies have shown that the solids fraction decreases exponentially with height from the bed surface and reaches a constant value above the transport disengagement height (TDH) [79, 80]. Yates *et al*. [81] developed a single-phase model based on the assumption that the freeboard contained perfectly mixed particles derived from bubble wakes. Chen *et al*. [82] modeled the freeboard with an axial dispersion model and an exponential decrease in solids hold-up.

5.3 Kinetic models

Fluidized beds are characterized by complex gas/solid hydrodynamics, such that simple kinetic models are convenient. Methane conversion during fluidized bed combustion with inert particles has been modeled with global homogeneous models. Pre *et al.* [83] modelled high temperature ($T_b \geq 973$ K) methane combustion in a fluidized bed of silica sand particles with the two-step model of Dryer *et al.* [19], Bradley *et al.* [20] and Westbrook *et al.* [18]. The kinetics of Dryer *et al.* [19] fitted more closely the experimental data. Dounit *et al.* [7, 84] also modeled methane combustion in a fluidized bed of silica sand with reasonable agreement with the experimental data. Wu *et al.* [14] compared the three models and found that the model of Bradley *et al.* [20] reproduced their experimental fluidized bed combustion data more closely. This emphasizes the fact that global models are more accurate for the conditions for which they were developed. Furthermore, more detailed models are required to describe the formation of intermediates (CO, NO_X), such as the corrected model in Table 2.1 [85].

Notation

A	Constant (Eq. 2.6)
C	Concentration (kmol/m^3)
d_j	Nozzle diameter (m)
d_p	Mean particle diameter (μm)
d_{or}	Orifice diameter (m)
E_a	Activation energy (kJ/mol)
f	Ratio of heterogeneous to homogeneous reaction rates
F	Molar flow rate (mol/s)
g	Gravitational acceleration (9.81 m^2/s)
h	Contact time index (g s/mol)
ΔH	Heat of reaction (kJ/mol)
k	Reaction rate constant
L_j	Characteristic jet length (mm)
n	Temperature exponent
P	Power (kW)
R	Universal gas constant (8.314 J/mol K)
r	Reaction rate (kmol/m^3 s)
U_g	Superficial gas velocity (m/s)
Uc	Gas velocity at the onset of turbulent fluidization (m/s)
U_{mb}	Minimum bubbling velocity (m/s)
U_{mf}	Minimum fluidization velocity (m/s)
U_{mj}	Minimum jetting velocity (m/s)

U_j	Gas discharge velocity at nozzle tip (m/s)
T	Temperature (K)
T_b	Bed temperature (K)
T_1	Lower critical temperature (K)
T_2	Upper critical temperature (K)
X	Conversion (%)
Y	Molar fraction (mol%)
Z	Axial position (mm)

Greek symbols

δ	Threshold value
ε	Void fraction
ϕ	Fuel-air ratio
ρ	Density (kg/m^3)
τ	Average gas residence time (s)

Subscript

a	Refers to alumina particles
corr	Corrected
f	Gas-phase
het	Heterogeneous
hom	Homogeneous
i	ith reaction
max	Maximum
s	Solids
0	Conditions at the inlet

References

[1] R.E. Hayes, S.T. Kolaczkowski, *Introduction to catalytic combustion*, Gordon and Breach Science Publishers, The Netherlands, **1997**.

[2] M.M. Hossain, H.I. de Lasa, *Chem. Eng. Sci.* **2008**, 63, 4433-4451.

[3] J.R. Grace, *Gas Fluidization Technology*, Chapter 11, Wiley, Chichester, U.K., **1986**.

[4] M.J. Lorences, J-P Laviolette, G.S. Patience, M. Alonso, F.V. Diez, *Powder Technol.* **2006**, 168, 1-9.

[5] B. Du, L.-S. Fan, F. Wei, W. Warsito, *AIChE J*. **2002**, 48, 1896-1909.

[6] D. Kunii, O. Lenvenspiel, *Fluidization Engineering*, 2nd ed., Butterworth-Heinemann, Stoneham, MA, USA, **1991**.

[7] S. Dounit, M. Hemati, R. Andreux, *Chem. Eng. J.* **2008**, 140, 457.

[8] J. Friedman, H. Li, *Combust. Sci. Technol.* **2005**, 177, 2211-2241.

[9] W. Żukowski, *Combust. Flame* **2003**, 134, 399-409.

[10] R.P. Hesketh, J.F. Davidson, *Combust. Flame* **1991**, 85, 449-467.

[11] R. Mabrouk, J. Chaouki, J-P Laviolette, G.S. Patience, *Proc. 9th Conference on Circulating Fluidized Beds*, Hamburg, Germany, **2008**.

[12] R. Sotudeh-Gharebaagh, *PhD Thesis*, Ecole Polytechnique, Montreal, Canada, **1998**.

[13] B. Singh, G.R. Rigby, T.G. Callcott, *Inst. Fuel Symp. Series 1: Fluidised Combustion*, C5-1, **1975**.

[14] W. Wu, P.A. Dellenback, P.K. Agarwal, H.W. Haynes Jr., *Combust. Flame* **2005**, 140, 204-221.

[15] R.A. Srinivasan, S. Sriramulu, S. Kulasekaran, P.K. Agarwal, *Fuel* **1998**, 77, 1033-1049.

[16] J.R. Grace, *Chem. Eng. Sci.* **1990**, 45, 1953.

[17] M. Foka, J. Chaouki, C. Guy, D. Klvana, *Chem. Eng. Sci.* **1994**, 49 (24A), 4269-4276.

[18] C.K. Westbrook, F.L. Dryer, *Combust. Sci. Tech.* **1981**, 27, 31.

[19] F.L. Dryer, I. Glassman, *Proc. 14th Symp. (Intl.) on Combust.* **1973**, 987.

[20] D. Bradley, S.B. Chin, M.S. Draper, G. Hankinson, *Proc. 16th Symp. (Intl.) on Combust.* **1977**, 1571.

[21] W.C. Gardiner, *Combustion Chemistry*, Springer-Verlag, New York, **1984**.

[22] D.R. Van der Vaart, *Ind. Eng. Chem. Res.* **1992**, 31, 999-1007.

[23] URL: http://www.chem.leeds.ac.uk/Combustion/Combustion.html

[24] URL:http://ame-www.usc.edu/research/combustion/combustionkinetics/research.html

[25] URL: http://www.me.berkeley.edu/gri-mech/

[26] A.S. Tomlin, T. Turányi, M.J. Pilling, *Low Temperature Combustion and Autoignition*, Elsevier, Amsterdam, **1997**.

[27] J. Warnatz, U. Mass, R.W. Dibble, *Combustion*, Springler-Verlag, New York, **1999**.

[28] M. Frenklach, *Numerical Approaches to Combustion Modeling*, Progress in Astronautics and Aeronautics, AIAA, Washington, 135, **1991**, 129-154.

[29] J. Warnatz, *Proc. 24th Symp. (Intl.) on Combust.* **1992**, 553.

[30] W.C. Chang, J.Y. Cheng, *Reduced Mechanisms Based on GRI-Mech 1.2*, http://www.me.berkeley.edu/drm/.

[31] R. Sotudeh-Gharebagh, J. Chaouki, *Can. J. Chem. Eng.* **2003**, 81, 1182-1191.

[32] D.G. Vlachos, L.D. Schmidt, R. Aris, *AIChE J.* **1994**, 40, 1018-1025.

[33] R.J. Kee, F.M. Rupley, J.A. Miller, *SAND89-8009 Sandia National Laboratories Report*, CA, USA, **1989**.

[34] D.J. Tringham, *PhD Thesis*, Leeds, U.K. **1982**.

[35] J.S. Dennis J.S., A.N. Hayhurst, I.G. Mackley, *19th Symp. (Intl.) on Combust.* **1982**, p. 1205.

[36] B. Lewis, G. Von Elbe, *Combustion, Flames and Explosions of Gases*, 3rd ed., Academic Press, London, **1987**.

[37] P. Markatou, L.D. Pfefferle, M.D. Smooke, *Combust. Flame* **1993**, 93, 185-201.

[38] J. Chaouki, D. Klvana, C. Guy, *Korean J. Chem. Eng.* **1999**, 16 (4), 494-500.

[39] W. Wu, P.K. Agarwal, *Can. J. Chem. Eng.* **2003**, 81, 940-948.

[40] R. Sotudeh-Gharebaagh, J. Chaouki, *Can. J. Chem. Eng.* **2000**, 78, 65-74.

[41] J.R. Grace, G. Sun, *Can. J. Chem. Eng.* **1991**, 69, 1126-1134.

[42] S.C. Arnold, M. Cecchini, G. Fenati, *Fluidization X*, Engineering Foundation, New York, 181-188, **2001**.

[43] J.G. Yates, D. Newton, *Chem. Eng. Sci.* **1986**, 41, 801-806.

[44] M. Pell, S.P. Jordan, *Fluidization Engineering: Fundamentals and Applications* **1988**, 84, 68-73.

[45] P.N, Rowe, L. Santoro, J.G. Yates, *Chem. Eng. Sci.* **1978**, 33, 133-140.

[46] P.E. Roach, *Int. J. Multiphase Flow* **1993**, 19, 1159-1165.

[47] W.C. Yang, B. Ettehadieh, T.C. Anestis, R.E. Gizzie, G.B. Haldipur, *Fluidization V*, Engineering Foundation, New York, 95-102, **1986**.

[48] H.V. Nguyen, O.E. Potter, A.B. Whitehead, *Chem. Eng. Sci.* **1979**, 34, 1163-1164.

[49] S. Ramamoorthy, N. Subramanian, *Chem. Eng. J.* **1981**, 22, 237-42.

[50] N. Dropka, K. Jaehnisch, E.V. Kondratenko, V. Kondratenko, R. Kraehnert, N. Steinfeldt, *Int. J. Chem. React. Eng.* **2005**, 3, 1-16.

[51] W. Volk, C.A. Johnson, H.H. Stotler, *Chem. Eng. Prog.* **1962**, 58, 47-44.

[52] S. Dutta, G.D. Suciu, *J. Chem. Eng. Jpn.* **1992**, 25, 345-348.

[53] J.G. Yates, V. Bejcek, D.J. Cheesman, *Fluidization V*, Engineering Foundation, New York, 79-86, **1986**.

[54] J.M.D. Merry, *AIChE J.* **1975**, 21, 507-510.

[55] C.Y. Wen, M. Horio, R. Kirshnan, R. Khosravi, P. Rengarajan, *Proc. 2nd Pacific Chem. Eng. Cong.*, Nagoya, Japan, 1182-1189, **1977**.

[56] T.R. Blake, H. Wevv, P.B. Sunderland, *Chem. Eng. Sci.* **1990**, 45, 365-371.

[57] W.C. Yang, D.L. Keairns, *Ind. Eng. Chem. Fund.* **1979**, 18, 317-320.

[58] Z. Shen, C.L. Briens, M. Kwauk, M.A. Bergougnou, *Can. J. Chem. Eng.* **1990**, 68, 534-540.

[59] J.R. Grace, C.J. Lim, *Can. J. Chem. Eng.* **1987** 65, 160.

[60] L. Massimilla, *Fluidization*, 2nd ed., Academic Press, New York, **1985**.

[61] J. Werther, W. Xi, *Powder Tech.* **1993**, 76, 39-46.

[62] D.R. Van der Vaart, *Fuel* **1988**, 67, 1003-1007.

[63] R. Sotudeh-Gharebaagh, J. Chaouki, *Energ. Fuel.* **2007**, 21, 2230-2237.

[64] M. Pilawska, C.J. Butler, A.N. Hayhurst, D.R. Chadeesingh, *Combust. Flame* **2001**, 127, 2181-2193.

[65] R. Sotudeh-Gharebaagh, J. Chaouki, R. Legros, *Chem. Eng. Sci.* **1999**, 54, 2029-2037.

[66] A.R. Masri, R.W. Bilger, R.W. Dibble, *Combust. Flame* **1988**, 73, 261.

[67] J. Lufei, H.A. Becker, R.K. Code, *Can. J. Chem. Eng.* **1993**, 71, 10.

[68] T.C. Ho, *Handbook of Fluidization and Fluid-Particle Systems*, Chapter 9, Taylor & Francis, USA, **2003**.

[69] J.G. Yates, *Fundamentals of Fluidized-Bed Chemical Processes*, Butterworths, London, **1983**.

[70] C.A. McKnight, L.P. Hackman, J.R. Grace, A. Macchi, D. Kiel, J. Tyler, *Can. J. Chem. Eng.* **2003**, 81, 338–350.

[71] J.F. Davidson, D. Harrison, *Fluidized Particles*, Cambridge University Press, London, **1963**.

[72] K. Kato, C.Y. Wen, *Chem. Eng. Sci.* **1969**, 24, 1351-1369.

[73] J.G. Yates, P.N. Rowe, D.J. Cheesman, *AIChE J.* **1984**, 30 (6), 890-894.

[74] L.A. Beheie, P. Kehoe, *AIChE J.* **1973**, 19 (5), 1070-1072.

[75] P.N. Rowe, *Chem. Eng. Sci.* **1993**, 48 (14), 2519-2524.

[76] Y. Xiao-tian, D.G. Horne, J.G. Yates, P.N. Rowe, *AIChE Symposium Series* **1984**, 80 (241), 41-44.

[77] J.R. Grace, H.I. de Lasa, *AIChE J.* **1978**, 24 (2), 364-365.

[78] S.P. Sit, J.R. Grace, *Fluidization V*, Engineering Foundation, USA, 39-46, **1986**.

[79] C.Y. Wen, L.H. Chen, *AIChE J.* **1982**, 28 (1), 117-128.

[80] D. Kunii, O. Levenspiel, *Powder Technol.* **1990**, 61, 193-206.

[81] J.G. Yates, P.N. Rowe, *Trans. Inst. Chem. Eng.* **1977**, 55, 137-142.

[82] L.H. Chen, C.Y. Wen, *AIChE J.* **1982**, 28 (6), 1019-1027.

[83] P. Pré, M. Hemati, B. Marchand, *Chem. Eng. Sci.* **1998**, 53 (16), 2871.

[84] S. Dounit, M. Hemati, D. Steinmetz, *Powder Tech.* **2001**, 120, 49.

[85] R. Sotudeh-Gharebagh, J. Chaouki, P. Sauriol, *Fuel Process. Technol.* **2007**, 88, 847-858.

ANNEXE 8 – ARTICLE PUBLIÉ DANS LE JOURNAL « APPLIED CATALYSIS A: GENERAL » (2010)

La contribution à cet article se résume à l'écriture de la première version qui a été soumis aux co-auteurs de DuPont pour révision. Ces derniers ont apportés plusieurs changements avant la soumission au journal « Applied Catalysis A: General ». Il faut noter que les travaux expérimentaux et l'analyse initiale des résultats ont été effectués chez DuPont. Cet article est présenté dans cette thèse puisqu'il est pertinent et puisque l'auteur y a consacré plusieurs mois.

Parametric Study of *n*-Butane Oxidation in a Circulating Fluidized Bed Reactor

Manuscipt No. APCATA-D-09-01052

Keith W. Hutchenson[a*], Concetta La Marca[b], Gregory S. Patience[c],
Jean-Philippe Laviolette[c], Richard E. Bockrath[a]

[a]*DuPont Company, Experimental Station, Wilmington DE 19880, U.S.A.*

[b]*DuPont Company, DuPont Engineering Research & Technology, DuPont Building, Wilmington DE 19898, U.S.A.*

[c]*Department of Chemical Engineering, École Polytechnique de Montréal, C.P. 6079, Succ. "CV", Montréal, QC, Canada, H3C 3A7*

Submitted to Applied Catalysis A: General
Special Issue on "International VPO Workshop"

Revision of

January 23, 2010

Keywords: Autoignition, *n*-Butane Oxidation**,** Circulating Fluidized Bed, Combustion, Induction Time, Maleic Anhydride, Oxidation, Vanadyl Pyrophosphate

---

[*]To whom correspondence should be addressed. E-mail: Keith.W.Hutchenson@usa.dupont.com. Tel.: +1-302-695-1389, Fax: +1-302-695-2504

Abstract

DuPont's *n*-butane oxidation process uses a proprietary attrition-resistant vanadyl pyrophosphate (VPP) catalyst and circulating fluidized bed (CFB) technology for the selective oxidation of *n*-butane to maleic anhydride. In the redox mode, *n*-butane feed plus recycle gas are fed to the riser side of the CFB, and air is fed to the regenerator. To optimize both activity and selectivity, oxygen may be fed to the riser side together with *n*-butane. These conditions fall within the *n*-butane flammability envelope, and localized combustion reactions were experienced during operation of a pilot plant utilizing this reactor technology. Complementary experimental and theoretical investigations were conducted using a laboratory fluidized bed reactor and an elementary step kinetic model to study the local reaction behavior near an oxygen sparger placed in a fluidized bed of solid VPP catalyst and to evaluate the effect of operating conditions on the onset of combustion in the homogeneous gas phase regions of the reactor. The laboratory fluidized bed reactor was operated at temperatures of 320-390°C, pressures of 3-4 bar, freeboard residence times of 4-8 s, and *n*-butane and oxygen compositions of 4-10% and 1-6%, respectively. For the low solids regions of the reactor, both experimental and modeling results demonstrated pronounced pressure and temperature effects on the onset of combustion in this range of operating conditions and that decreasing the residence time delays the onset of complete combustion to longer time or higher relative molecular oxygen compositions. Kinetic model predictions also showed a significant influence of reactant composition and reactor pressure on oxidation induction time.

INTRODUCTION

Many industrial catalytic processes involve simultaneous heterogeneous and homogeneous reaction pathways. Homogeneous reactions generally result in yield loss of the desired product. Moreover, they may also represent a significant safety hazard in the case of fast and highly exothermic reactions such as those involving oxygen and hydrocarbons. Hydrocarbon selective oxidation processes are widespread in the industry, and new processes are presently being developed in the context of alkane functionalization. In fact, the direct oxidative conversion of lower alkanes is undergoing intensive research due to their lower cost compared to olefins. Fluidized bed reactors are currently being developed for a variety of these processes. To

maximize productivity, they may operate within the flammability limits while feeding the oxidant and hydrocarbon separately into the bed—through spargers, for example. This is possible due to the ability of the solids phase to suppress non-selective homogeneous reactions (combustion) and at the same time to promote the selective heterogeneous reactions. Feed compositions to fixed beds, on the other hand, are generally constrained by the flammability region. Mixing hydrocarbons and oxygen upstream of the reactor is a major safety concern, and thus the optimal feed composition may be dictated by flammability limits and not kinetics.

Oxidation processes may operate under partial reactant conversion because selectivity generally declines at high conversion due to an increase in the rate of product decomposition [1-3]. The combination of partial hydrocarbon conversion and high oxygen concentration results in potentially flammable mixtures either within the catalyst bed or at the exit. In fluidized beds, when the solids volume fraction is sufficiently high, free radicals may be quenched, thus reducing the flammability risk. However, downstream of the catalyst bed in the freeboard, cyclones, and associated piping, the risk of combustion is much greater since the effluent gas phase composition is potentially flammable due to the high hydrocarbon and oxygen concentrations and elevated temperatures, and the solids volume fraction may be insufficient to quench free radicals and non-selective homogeneous reactions [4, 5]. Minimizing the risk of gas phase combustion and deflagration in these regions remains an important design issue.

Maleic anhydride is currently produced in fixed and fluidized bed reactors via the selective oxidation of *n*-butane with vanadyl pyrophosphate catalysts (VPP) [6]: feed compositions in the fixed bed process are typically in the range of 2% *n*-butane in air, whereas the mixed cup composition in the fluidized bed process exceeds 4% *n*-butane in air. Fixed beds are further constrained to low hydrocarbon concentrations due to the poor heat transfer rates that may cause hot spots, which may deactivate the catalyst [7].

Flammable mixtures may form either at the entrance of the catalyst bed (in the case of fixed beds), in the bed of catalyst solids (in the bubble phase of fluidized beds, for example), or downstream of the solids. The threshold conditions leading to autoignition (self-initiated homogeneous combustion) must be known to minimize the safety hazards, not only during standard operation, but also during start-up as well as for emergency shut-down conditions. Several criteria to characterize a system's sensitivity to autoignition include flammability limits,

minimum oxygen concentration (MOC), autoignition temperature (AIT), and induction time. However, the induction time, defined as the minimum gas residence time that results in the onset of homogeneous combustion, is the only criterion that yields the time-scale of the ignition process. This information is key to maximizing the reactants' concentration since it may allow safe operation inside the flammability limits and above the AIT by ensuring that the induction time is lower than the gas residence time.

Hydrocarbon/oxygen induction times are measured by rapidly heating and pressurizing a mixture to a specific initial state, and then measuring the time it takes for the mixture to react (ignite). Butane/oxygen induction times have been previously measured in several types of experimental apparatus: static vessels, flow reactors [8], shock tubes [9], and high compression machines [10, 11]. A number of correlations have been developed relating the induction time to initial operating variables including mixture composition, pressure, and temperature. However, *n*-butane/oxygen induction times are unavailable in the temperature and pressure ranges of interest for the *n*-butane selective oxidation process (T = 320–420°C and P = 2–4 bar). Low temperature (≤ 450°C) gas-phase oxidation studies of *n*-butane have been performed at sub-atmospheric pressure [12-14]. Furthermore, investigations at moderate pressure (1-6 bar) have only been conducted at very high temperature (≥ 1000°C) [8, 15, 16]. Not only are the fluidized bed operating conditions outside the range of these correlations, but the presence of catalyst solids also affects the homogeneous reaction kinetics. Together with the quenching behavior due to the catalyst volume, the nature of the catalyst surface may also affect the homogeneous kinetics in different ways. Heterogeneous and homogeneous reactions are strongly coupled through heat and mass transfer as well as through reactive intermediates that are common to both pathways. Heterogeneous surface reactions can heat the catalyst boundary layer sufficiently to initiate homogeneous reactions, can deplete the boundary layer of a limiting reactant, and can act as a free radical source or sink. Previous studies have shown that flammability limits become narrower on several noble metal catalysts, which is most likely a consequence of reactant depletion in the catalyst boundary layer [17, 18]. Furthermore, Hesketh et al. [4] have shown that inert sand particles strongly inhibit homogeneous reactions via radical recombination. The effects of VPP catalyst on induction time have yet to be quantified.

This paper describes DuPont's pilot and commercial plant experience regarding non-selective gas phase oxidation reactions at gas spargers that were used to inject oxygen into a circulating

fluidized bed reactor (CFB) as well as the exit region of the CFB downstream of the cyclones. This experience resulted from the process development and commercialization of a process to manufacture tetrahydrofuran from *n*-butane. Scheme 1 shows the global reaction steps of the overall process, including the selective oxidation of *n*-butane to maleic anhydride, which was the reaction step conducted in this CFB reactor. This scheme also shows the alternative reaction pathway of non-selective combustion of the *n*-butane. Together with detailed reaction engineering modeling, an extensive parametric experimental program was developed to examine the effects of temperature, pressure, gas phase composition, and catalyst concentration on the phenomena. Some of these results are reported herein. This and subsequent work supported design modifications that led to a doubling of the commercial plant capacity.

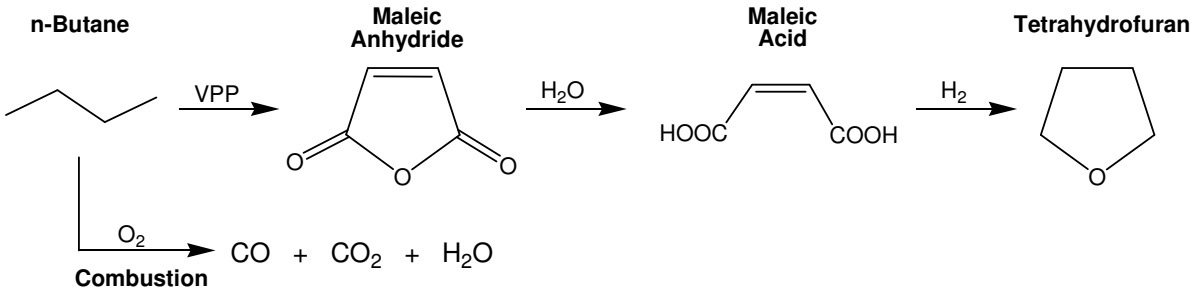

Scheme 1: DuPont's reaction sequence for tetrahydrofuran production via selective oxidation of *n*-butane to maleic anhydride.

EXPERIMENTAL

Commercial plant configuration

DuPont developed CFB technology to produce maleic anhydride from *n*-butane with a proprietary VPP catalyst [7, 19]. The concept was based on shuttling catalyst between two reactor zones: VPP was reduced by *n*-butane in a transport bed/riser and then re-oxidized in a fluidized bed regenerator. Transferring catalyst between the two zones was intended to maintain the catalyst in the most favorable oxidation state to achieve higher selectivity typical of fixed bed reactors while maintaining the superior heat transfer characteristics of fluidized bed reactors.

Lattice oxygen is more selective and active compared to molecular oxygen, thus not only are yields better, but also, the safety hazards are minimized.

Figure 1 shows the commercial CFB facility consisting of a transport bed operating in the dense phase fast or turbulent fluidization regime (fast bed), a riser, a stripper, and a regenerator. Catalyst entered the base of the fast bed through a tapered standpipe and was transported upwards to the riser. The fast bed contained two sets of cooling coils and three oxygen spargers with 926 nozzles per sparger. The riser operated at gas velocities of about 6 m/s and at catalyst suspension densities as high as 200 kg/m^3. The fast bed of the commercial reactor was 4.2 m in diameter and 11 m tall, while the riser was 1.8 m in diameter and 25 m tall. The gas-powder mixture exited the riser and entered the stripper tangentially, which provided a sufficiently high level of separation so that the cyclone was never overloaded. Based on iso-kinetic solids sampling in the horizontal duct between the stripper exit and cyclone entrance, the solids mass flow rate was 0.13 t/h, which represents a 96% stripping efficiency. The solids descended into a stripper bed equipped with horizontal coils. They descended along a standpipe and entered the air-fed regenerator from the top. The regenerator was equipped with horizontal cooling coils.

Pilot plant configuration

Figure 2 illustrates the sparger configuration in the fast bed of the pilot plant. During the final demonstration period, spargers were installed at three levels, with four nozzles in the bottom, two in the middle, and three in the top sparger. The shrouds were pointed inward at an angle of about 9° from the wall and at a 24° angle from vertical so that the oxygen would neither impinge onto the fast bed wall nor onto the cooling coils. The shroud was 51 mm in length with an inner diameter of 7 mm and an orifice diameter of 3.7 mm. The sparger design flow rate per shroud was about 7 kg/h, and nominal velocities through the shrouds were 9 to 20 m/s and as high as 40 m/s. This nozzle velocity and geometry are critical to the dispersion of oxygen into the catalyst bed. To illustrate, Figures 3a and 3b demonstrate the bubble formation of air sparged into a beaker of water at a rate of 14 and 40 m/s, respectively. At the lower gas velocity, bubbles form at the nozzle and detach at a constant frequency, whereas bubble formation and detachment are more random at the higher gas velocity. Figure 3c shows bubble formation at 40 m/s around a modified nozzle with a sintered metal filter substituted for the standard shroud. The bubbles are

much smaller with the sintered metal filter compared to the standard shroud, and the gas is distributed over a larger surface area, which presumably reduces the risk of homogeneous reactions.

Over the course of the pilot plant demonstration, the catalyst activity, as measured off-line in a standardized test, dropped over a short period of time, although extended testing in laboratory reactors indicated that activity was stable over several months. The drop in activity corresponded to a decrease in the catalyst surface area. In addition, a fraction of the catalyst turned from a gray color to black. Based on controlled thermal experiments, VPP powder became black when it was exposed to temperatures above 700°C. Such a high temperature was never recorded anywhere in the pilot plant even though it was well instrumented with dozens of thermocouples. Sudden changes were observed in the local temperature in the fast bed of as much as 20°C, but more often the temperature rise detected was on the order of 2°C. The sudden change in temperature was accompanied by a drop in the oxygen concentration and a corresponding increase in carbon dioxide. These local "exotherms" were at times self extinguishing but could continue for several hours (or more).

The exotherms were attributed to localized hot spots around the sparger nozzles in which pure oxygen was fed to the fast bed. Although the average gas-phase composition in the reactor was outside the flammability envelope, the local composition could cross the flammability envelope as the oxygen jet (or bubbles) was dispersed into the fast bed emulsion phase. Since the temperature was above the autoignition temperature, the onset of combustion was determined by the induction time of the local gas phase and solids concentration. Under mild conditions (low *n*-butane feed rates), the emulsion phase effectively quenched free radicals, and the induction time was longer than the time it takes for the oxygen to blend with the catalyst and recycle gas. However, at high *n*-butane and oxygen feed rates, the induction time was lower than the mixing time. Thus the emulsion phase was incapable of quenching free radicals, resulting in a sustained flame. The combination of an increase in temperature and CO_2 concentration and a decrease in oxygen concentration is referred to here as a "temperature excursion."

Laboratory Fluidized Bed Reactor Configuration

In the present study, a laboratory-scale bubbling fluidized bed reactor with VPP catalyst was used to investigate the effects of temperature, pressure, mixture composition, and solids fraction on the oxidation of *n*-butane/oxygen mixtures. The fluidized bed was operated in the bubbling regime with superficial gas velocities ranging from 0.3 to 0.6 m/s with mixtures of *n*-butane and oxygen in nitrogen to simulate the conditions in the fast bed, the cyclone/stripper, and the regenerator of a CFB reactor. The main objectives were to identify the operating conditions necessary to minimize *n*-butane combustion and to maximize maleic anhydride yield. In general, the fluidized bed was operated at temperatures between 320 and 390°C and pressures from 3 to 4 bar. Autoignition was detected by monitoring the temperature axially along the reactor while simultaneously sampling the gas phase. The sampled gas was analyzed with a gas chromatograph, a paramagnetic oxygen analyzer, and an FT-IR spectrometer to monitor the conversion of the oxygen and hydrocarbon species. A detailed description of the experimental apparatus follows.

Figure 4 shows a process flow diagram of the experimental apparatus. The process consists of a heated reactant delivery system, a 12.8 cm inner diameter (I.D.) fluidized bed reactor with a disengagement zone, reactor effluent and sampling lines, and various process and analytical instrumentation. Typical operating conditions for homogeneous gas phase combustion experiments include approximately 5 mol% *n*-butane, 2 mol% oxygen, 1 mol% maleic anhydride (MAN), (balance nitrogen), and a reactor temperature and pressure of 360°C and 4 bar, respectively.

The reactant delivery system incorporates nitrogen as the carrier gas which is metered using a mass flow controller (MFC, Brooks Model 5853E, 500 L/min). This stream is preheated to approximately 210°C using electric gas circulation heaters (Omega Engineering Model AHPF-122). *n*-Butane is metered as a liquid from a liquefied gas cylinder equipped with a dip tube and containing a nitrogen head pressure of about 7 bar. The *n*-butane cylinder mass is monitored and recorded using an electronic balance (Mettler model ID5 Multirange Weighing Terminal equipped with an Option 089 serial interface). A pressure regulator (PR) reduces the *n*-butane pressure prior to delivery to a diaphragm liquid metering pump (Pulsafeeder Model 7120-S-AE). A pulsation dampener and a back pressure regulator are used to maintain pressure on the pump effluent and to dampen pressure pulsations resulting from operation of the diaphragm pump. This liquid *n*-butane stream is then injected into the heated nitrogen stream and vaporized,

resulting in a gaseous *n*-butane/nitrogen stream of approximately 100°C and 4 bar. When desired, a syringe pump (Isco Model 500D) is used to meter additional molten or liquid materials into this reactor feed stream where they are similarly vaporized. For example, maleic anhydride (m.p. 55°C) can be melted *in situ* by heating the pump cylinder using a custom heating mantle (Glas-Col), and the molten material can then be metered into this feed mixing point. The combined gaseous feed stream then enters a gas circulation electric heater (Caloritech Model EX1609F467MRY, 9 kW) which raises the temperature to the desired reactor feed levels, and the stream is then delivered to the reactor inlet. The oxygen stream is fed from a cylinder through a two-stage gas regulator to a mass flow controller (Brooks Model 5851E, 100 L/min) before passing through a downward pointing Type 321SS oxygen sparger into the fluidized bed section of the reactor. The sparger is equipped with a 2.1 mm i.d. orifice and has overall dimensions of 10 mm o.d. by 5 mm i.d., with a 51 mm long shroud. This oxygen stream is heated by electrical heating tape on the external reactor feed tubing and by the sparger which is located in the hot reactor zone.

Figure 5 shows a cross-sectional view of the fluidized bed reactor. This approximately 46 L pressure vessel was custom designed by DuPont and fabricated by SL Piping Systems (Newport, Delaware). The reactor is equipped with a 0.32-cm thick, 10-micron sintered metal (316 SS) gas distribution plate that supports the solid catalyst at the bottom of the reactor. The heated feed mixture enters at the base of the reactor through a 1.6 cm I.D. pipe into a plenum and is then distributed by the sintered metal disk to fluidize and contact the catalyst. The fluidized bed portion of the reactor is constructed of 12.8 cm I.D. carbon steel pipe and has several threaded couplings which are used for pressure and temperature instrumentation, online gas sampling, and insertion of an oxygen sparger. This 12.8 cm section expands with a cone angle of approximately 22° to a flanged 31.9-cm I.D. section, which serves as a disengagement zone to separate the gases from the solids in the reactor. The overall height of the reactor is 157 cm. The reactor design specifies a maximum allowable working pressure of 6.2 bar, and the reactor was hydrostatically proof tested to 9.6 bar prior to installation. Pressure relief is provided by a 5-cm Inconel rupture disk (R/D, BS&B Model CSR reverse buckling type) rated at a burst pressure of 6.2 bar at 22°C. The reactor effluent gases exit through two sintered metal pipes (Mott Model 2232-A08-12-A00-0.5-AA, 5.1 cm O.D., 30.5 cm long, 0.5 micron porosity, 316SS) with a combined surface area of about 930 cm^2. The effluent from the two sintered metal pipes is then recombined and passes

through a back pressure regulator which is manipulated to maintain the desired reactor operating pressure. The reactor is charged with a commercial VPP catalyst (Geldart A, typically about 4-5 kg) which is fluidized by the inlet gas stream.

Gas samples from various sample ports in the reactor system were analyzed by an on-line gas chromatograph (GC). These analyses were performed using a Hewlett-Packard Model HP 5890 Series II GC equipped with both thermal conductivity (TCD) and flame ionization (FID) detectors and a multidimensional method using four columns located in the same GC oven. The relatively complex analysis method is a modification of that developed by Mills and Guise [20]. The TCD detector was used for analysis of oxygen, nitrogen, carbon dioxide, carbon monoxide, water, and unreacted *n*-butane in packed columns. The FID detector was used for the analysis of the hydrocarbons and oxygenates with capillary columns operated in the split mode (40:1) utilizing a split/splitless capillary injector. The on-line gas samples were injected from a 10-port Valco gas-sampling valve equipped with two 500-μL sample loops so that a given gas sample could be collected and injected to both sides of the multiple column and two-detector configuration. The FID side was equipped with a 30 m x 0.53 mm I.D. x 0.3 μm film Restek 1701 column and a 25 m x 0.53 mm I.D. Al_2O_3/KCl PLOT (Chrompack) column. These columns were connected to a six-port Valco switching valve so that the helium carrier gas flows through either the Restek 1701 column only, or through both columns in series. The TCD side uses two packed columns: a 61 cm x 0.32 cm O.D. column packed with 80/100 mesh Hayesep R and a 305 cm x 0.32 cm O.D. column packed with 60/80 mesh molecular sieve 5A. The analysis utilized a temperature program of 35°C for six minutes, and then the temperature was ramped at 10°C/min to 75°C, then another temperature ramp of 20°C/min to 165°C with a final hold period of 5.5 min. The GC was calibrated for the primary components using a certified gas mixture consisting of 5.00% carbon dioxide, 5.00% carbon monoxide, 5.00% oxygen, 1.50 % *n*-butane, balance nitrogen (MG Industries, Morrisville, PA).

Additional process equipment and instrumentation includes an on-line paramagnetic oxygen analyzer (Siemens model OXYMAT 5F), two on-line process infrared (IR) spectrometers for *n*-butane and carbon dioxide (Combustion Engineering model 501B Process IR Analyzers) and various pressure transducer indicators and Type K thermocouples. A data acquisition system (LabTech Notebook™, ver. 10.0, Laboratory Technologies Corporation, Wilmington, MA) records pertinent reactor temperatures and pressures, nitrogen and oxygen flow rates, the weight

of the *n*-butane feed cylinder, and the effluent oxygen, *n*-butane, and carbon dioxide concentrations from the on-line analyzers. The pressures at the top of the reactor and at the effluent back pressure regulator are used to measure the pressure drop across the exit filters.

The reactor is primarily heated by the hot feed gases entering the base of the reactor. A heating band is included on the upper 32-cm flange of the reactor since this was determined to be a primary source of reactor heat losses. Typical operations include running this and the main reactor feed heater overnight with site nitrogen flow to the reactor in order to maintain reactor temperatures in a "hot standby" condition and hence increase experimental productivity.

The apparatus is located in a process barricade designed to safely contain a burst reactor or auxiliary equipment. The system is equipped with an interlock system that closes the oxygen and *n*-butane feed streams and shuts off the *n*-butane pump if an "emergency stop" button is pressed, if a loss of barricade exhaust or nitrogen flow is sensed, or if a high pressure signal is sensed at the primary feed heater inlet or at the top of the reactor. If a loss of feed nitrogen is sensed, an automatic valve opens which allows a second nitrogen source to sweep the process free of any flammable gases. In addition, the heater controllers for the primary feed heater and the top reactor flange heater are equipped with high-temperature interlocks to prevent overheating during unattended "hot standby" operation.

MODEL DEVELOPMENT

In parallel with laboratory experiments, an elementary step level free-radical kinetics model was developed to describe the homogeneous, gas-phase chemistry using the Chemkin collection of programs and well-established reaction networks and associated parameters [21, 22], comprising 440 elementary reactions and 78 species.

n-Butane oxidation is known to exhibit cool flame behavior at moderate temperatures characterized by a negative temperature coefficient on reaction rate. This phenomenon has been well described by Dechaux and coworkers [12], where they show that the onset and end of this reaction regime is a function of *n*-butane concentration. For instance, at 10% *n*-butane, cool flame behavior was shown to be important between 335–390°C. Since the commercial *n*-butane oxidation reaction system operates within this general composition and temperature range, the description of these low temperature effects was essential to the development of a useful model.

The model developed by Pitz and coworkers [22] has been shown to accurately capture these phenomena and their impact on induction time.

Reaction simulations using the Chemkin model were run in several modes. The freeboard section of the laboratory fluidized bed was simulated as a perfectly mixed gas phase system using the experimental inlet composition to the reactor and gas residence time of the freeboard. These simulations were run in an adiabatic mode to approximate conditions in the freeboard of the laboratory reactor. Induction time predictions were performed using a constant pressure, batch simulation.

RESULTS AND DISCUSSION

Commercial experience

During the commissioning of the CFB reactor, the redox operating mode—where molecular oxygen is only fed to the regenerator, and *n*-butane and recycle gas are fed to the fast bed—was tested first. The production rate was 1,500 kg/h maleic acid (MAC). Oxygen addition to the fast bed middle sparger was the next step, and the production rate increased to 3,500 kg/h MAC. The third step was to begin oxygen addition to the upper sparger. While ramping up the oxygen feed rate, a high-high temperature interlock in the product gas stream downstream of the stripper shut the plant down. Inspection of the catalyst revealed that a small fraction turned black (less than 1%).

The high-high temperature interlock was caused by gas phase combustion in the freeboard region of the stripper/cyclone. A similar event was recorded in the pilot plant during a four hour period the day the plant was shut down. At that moment, the exit *n*-butane and oxygen concentrations were 10 and 3.7%, respectively, the pressure was 3 bar and the temperature was 399°C. Combustion in the exit pipe of the commercial plant occurred at 391°C and with *n*-butane and oxygen concentrations of only 6 and 1.6%, respectively. Maintaining oxygen concentrations at these elevated levels was essential to achieving high production rates.

The original configuration of the commercial plant included two spargers located at heights of 1.8 m and 5.5 m above the grid, as shown in Figure 1 immediately beneath each set of cooling coils. A third oxygen sparger was installed 0.5 m above the grid with the exact same design as the

original two spargers—926 nozzles distributed uniformly throughout the reactor cross-section and directed downward at an angle of 30°. To better distribute the oxygen, further modification was made to substitute the standard shrouds with sintered metal filters in the upper sparger. Several attempts to feed oxygen with the standard shrouds to the upper sparger at rates greater than 1000 kg/h were unsuccessful due to temperature excursions. Figure 3 illustrates the bubble formation around the sintered metal: the bubbles are much smaller with the sintered metal compared to the shrouds, and the gas is distributed over a larger surface area, which presumably reduces the risk of exotherms. Whereas oxygen feed rates of 1000 kg/h were unsustainable to the upper spargers with standard shrouds, feed rates of over 2600 kg/h were successfully demonstrated with the sintered metal filters. Note that the oxygen was diluted with nitrogen in all three spargers. As much as 1000 kg/h was continually fed to the lower and middle sparger, and between 200 to 500 kg/h was fed to the modified upper sparger.

Pilot plant experience

Three charges of catalyst were tested during the demonstration period that lasted about 18 months. During the first charge of catalyst, a single nozzle was installed at the center of the fast bed directly below the bottom coils about 1 m above the recycle gas sparger. Originally, the fast bed was 3 m tall. (An additional 3 m was added just before testing the second charge of catalyst.) The recycle gas together with fresh *n*-butane were introduced into the bed with a shower cap distributor. The distributor was found eroded following the first six months of operation leaving a single, large hole. The specific causes of this nozzle failure were not determined, but rather, the failed distributor was replaced with a conventional six-point candelabra sparger for testing with catalyst charges 2 and 3, and this distributor proved more durable. Despite the high oxygen flow rates through the single point nozzle—as much as 100 kg/h—and a compromised recycle gas sparger, only two temperature excursions were recorded with the first charge of catalyst. Two factors may account for the low frequency of excursions: (1) the solids from the standpipe below the fast bed may have risen into the bed as a plume, providing excellent gas-solids contacting at the nozzle, and (2) the *n*-butane feed during the first charge of catalyst contained as much as 30 ppm of sulfur, whereas the sulfur content in the *n*-butane was as little as 1 ppm for the following two catalyst charges. In the form of SO_2, sulfur is a known flame suppressant. As shown in

Figure 2, additional oxygen nozzles were added to distribute the oxygen more uniformly along the length of the fast bed. These nozzles were located near the wall and not in the center of the bed

During testing with the second catalyst charge, over 100 exotherms were recorded. Most were of short duration—a couple of minutes—with a temperature rise of about 1°C; the highest temperature rise recorded was 10°C, and the longest excursion lasted 8 hours. During the demonstration phase with the 3rd charge of catalyst, over 50 excursions were recorded, and Table 1 summarizes the conditions in the fast bed for those that were due to process conditions. (Some excursions occurred while ramping up and others were due to instability in the oxygen feed or solids circulation rate.) The table is organized sequentially with the time representing on stream operation while feeding *n*-butane. The average temperature, T, in the lower half of the fast bed is tabulated in the second column. At low maleic acid production rates (<20 kg/h), the average temperature rise in the fast bed varied between 0-6^{o}C. At high production rates (30-50 kg/h), the temperature rise reached about 8°C in the fast bed and as high as 8°C across the riser. The demonstration run was conducted at a riser exit temperature of 400^{o}C. The superficial gas velocity, U_g, assumes that all gas streams enter at the same point in the bottom of the fast bed (recycle gas + oxygen and nitrogen from all spargers + interstitial gas carried with the solids). High solids mass fluxes were tested early in the program, but superior *n*-butane utility was achieved with mass fluxes on the order of 76 kg/m^{2}s in the fast bed compared to 130 kg/m^{2}s. Excursions were recorded with as little as 7 and 5% mixed cup concentrations of *n*-butane and oxygen, respectively, and the recorded temperature rise varied from 2 to 6^{o}C. The catalyst surface area was initially 20 m^2/g, and after 1600 h of operation it dropped below 15 m^2/g. The successive drops in surface area seemed to correlate with the occurrence of exotherms.

The excursion at 5% oxygen was recorded at the lowest bed bulk density of 323 kg/m^3. The average bed density during the other excursions was close to 370 kg/m^3. Based on a multi-parameter regression analysis, feed oxygen concentration and bed suspension density were identified as critical parameters that initiated excursions.

Together with assessing catalyst performance, identifying operating parameters to extinguish temperature excursions became an objective of the third charge of catalyst. The combination of high *n*-butane and oxygen feed rates was a prime factor that correlated with frequency and

severity of excursions, and maximizing these parameters was critical for the overall process economics. Other risk factors that were identified included unstable catalyst circulation rate, high temperature, high gas velocity, and low overall pressure drop, which translated to low solids density. The most effective means of extinguishing an excursion was to reduce the oxygen feed rate to the sparger. Increasing the fraction of particles below 44 μm from 16% to 23% allowed an increase in the oxygen feed rate by 10%. Diluting the oxygen with nitrogen also was effective at extinguishing exotherms. During the last two weeks of the demonstration run, oxygen was fed at high rates with no temperature excursions, and at the same time, the design operating condition targets were achieved, including the space time yield. Initially, oxygen was fed through the bottom spargers with four shrouds. Temperature excursions were recorded with a combined total oxygen feed rate of about 10 kg/h per nozzle with a maximum *n*-butane concentration of 10%. To attempt to feed more oxygen to the reactor, the feed rate was reduced to the bottom sparger and increased to the upper sparger. A third sparger was installed in between the two at the end of the demonstration period. During the final stages of demonstration, total oxygen feed rates of 70 kg/h were achieved at 15% *n*-butane. The feed rates to the oxygen spargers were about 7.5 kg/h, and this rate was used for the commercial design.

Fluidized Bed Reactor and Modeling Evaluations

The laboratory fluidized bed reactor apparatus and theoretical modeling were utilized to address a number of design and operating issues related to the addition of molecular oxygen into the commercial CFB reactor. The objectives of this experimental and modeling program were to (1) study the local reaction behavior near an oxygen sparger placed in a fluidized bed of solid VPP catalyst, and (2) evaluate the effect of operating conditions on the onset of combustion in the homogeneous gas phase region of the *n*-butane oxidation reactor system. The fluidized bed reactor apparatus described above was used to simulate plant operating conditions (e.g., reactor temperature, pressure, concentrations, and solids density) and the effect of manipulating these experimental factors on suppression of gas phase combustion. Experimental factors investigated include these reactor conditions as well as the oxygen sparger design and operation. The primary goals of this work were to enhance production capacity by safely maximizing the free oxygen

concentration in the *n*-butane oxidation reactor and to optimize the operating conditions and oxygen sparger design to allow injection of the corresponding increased oxygen flow rates.

To illustrate the importance of the operating conditions on *n*-butane oxidation in the reactor, Figure 6 shows the impact of relatively modest pressure perturbations in the reactor freeboard on the oxidation chemistry occurring in the reactor. In general, the reactor pressure was held constant at about 3.3 bar, and the inlet *n*-butane composition was fixed at 4%. The initial inlet oxygen composition was about 4%, and then the oxygen flow rate was increased at about 17 min run time and again at 22 min run time to give inlet compositions of 5 and 6 %, respectively. Overall, the reactor temperature rose gradually during the course of this run until the second increase in oxygen composition, at which time the temperature rose exponentially, and the run was aborted.

The indicated pressure spikes of 0.3-0.6 bar were induced by back flushing the reactor filters with nitrogen for about a 3-second pulse to clear the filters of accumulated catalyst fines. These sudden spikes in the overall reactor pressure occurred because during the brief filter backflush, half of the normal effluent flow area (i.e., the flow through one of the two sintered metal filters) was temporarily removed from the effluent flow path, while at the same time, additional nitrogen was added to the reactor through the filter. The combination of reduced flow area and additional nitrogen flow into the reactor resulted in a sudden and rapid rise in pressure until the blowback valves were diverted back to their normal setting.

As shown in Figure 6, each pressure spike in the homogeneous gas phase region of the reactor resulted in an immediate corresponding spike in temperature from autoignition of the reaction mixture. The indicated temperature spikes at 7.0, 11.9, 20.2, and 25.1 min run time correspond exactly with the pressure spikes resulting from back flushing the filters. Replicate tests confirmed this temperature spiking at similar conditions and isolated the cause to that of the corresponding pressure spikes. These and similar experiments demonstrated that for these particular operating conditions, autoignition can be induced by pressure spikes of as little as 0.3-0.6 bar.

Effects of Operating Conditions within the Fluidized Bed

Initial experiments involved running parametric studies on the fluidized bed reactor to understand the influence of various operating parameters on the oxidation chemistry occurring within the fluidized catalyst section of the reactor. For these experiments, the gas-phase sampling system was configured to monitor the effluent from the fluidized bed section of the reactor. Figure 7 shows typical results from one of these parametric studies. In particular, this plot shows the effect of reactor temperature and inlet oxygen composition on the molecular oxygen conversion and both CO_2 and maleic anhydride (MAN) selectivity in the fluidized catalyst bed. These selectivities are calculated on the basis of the converted oxygen. The convention of tracking oxygen conversion, rather than n-butane conversion was selected because most conditions explored were in the fuel rich region. As expected, for a given initial oxygen composition, more of the inlet oxygen flow is converted with increasing temperature. However, since the selective partial oxidation to maleic anhydride is the dominant reaction at these conditions, the conversion of the inlet oxygen decreases with increasing excess oxygen composition. That is, the increasing amount of excess oxygen present in the fluidized catalyst bed with increasing inlet oxygen composition is not converted in the absence of significant homogeneous combustion. The selectivity to the partial oxidation product maleic anhydride increases marginally with increasing oxygen composition, but exhibits little influence of the operating temperature in this range. The selectivity to the combustion product carbon dioxide is essentially constant at about 15% over the range of temperatures and oxygen compositions evaluated.

During startup of the commercial reactor, approximately 25% of the bottom tier spargers and 50% of the top tier spargers developed pluggage from catalyst solids. As described above, porous metal nozzles were considered and ultimately installed on one of the reactor spargers to allow increased oxygen flow rates. In anticipation of this installation, a porous metal tipped sparger similar in design to that planned for the commercial reactor was tested in the laboratory fluidized bed reactor to determine if this modification could also produce undesired effects (e.g., the porous metal tending to stabilize a flame at the sparger tip). Initially, a standard sparger similar in design to the current plant spargers (0.082” i.d. orifice with a 0.405” o.d. x 0.197” i.d. x 2” long shroud) was run at base case conditions. An identical sparger was then modified by welding to the tip a standard 5-micron porous metal Inconel cup filter obtained from Mott Metallurgical Corp. (Mott P.N. 1200-.500-.375-1.00-5um, Mott CPN # 1204350-17-050). This sparger was then installed and run at similar conditions for comparison. Figure 8 shows typical

results comparing the two spargers. These results are plotted as molecular oxygen conversion versus the initial reactor oxygen composition at 362°C, 4.7% initial *n*-butane composition, and pressures of 3 and 4 bar. These results reflect analysis of gas samples taken from near the top of the fluidized bed section of the reactor prior to disengagement of the solids in the reactor freeboard. Figure 8 shows that varying the reactor pressure from 3 to 4 bar had a negligible effect on the molecular oxygen conversion at these conditions, and combined with analytical results for the effluent gas composition, demonstrates that complete combustion is not initiated at the sparger under these conditions in the fluidized catalyst bed. However, Figure 8 demonstrates a small but measureable difference in the molecular oxygen conversion obtained for the two spargers. The porous metal sparger resulted in lower oxygen conversion at both pressures. Similar results (not shown) indicating a small effect of sparger design were observed at the more stringent operating conditions of 385°C, 4 bar, and 7% *n*-butane feed composition, which approximated plant design conditions.

Figure 9 shows similar data using the porous metal sparger in the fluidized bed at 385°C, 4.1 bar, and both 7% and 10% *n*-butane feed compositions. Again, the former concentration approximates plant design conditions. These results and the effluent gas composition confirm that combustion is not initiated at the sparger under these conditions.

Effects of Operating Conditions within the Reactor Freeboard

The experimental and modeling efforts were next applied to dynamic testing of the impact of operating conditions in the reactor freeboard to simulate the low solids sections of the commercial reactor. The goal of these efforts was to better understand conditions contributing to homogeneous gas phase combustion in the low solids environment found in the riser stripper and cyclone with an intent of suppressing autoignition in these zones in commercial operations.

Figure 10a shows the influence of temperature on the molecular oxygen conversion in the reactor freeboard as a function of the initial oxygen composition. This figure plots the increase in temperature observed in the freeboard over the course of the experiment following introduction of oxygen at the indicated feed composition. Figure 10b shows the corresponding molecular oxygen conversion and the combined CO and CO_2 selectivity for these conditions. For the given operating conditions of 4% *n*-butane, 3.3 bar, and an approximate freeboard residence time of 6.3

sec, the exothermic temperature rise is only 6°C at the lowest initial reactor operating temperature shown of 320°C. The corresponding oxygen conversion and CO/CO_2 selectivity shown in Figure 10b are relatively constant with increasing molecular oxygen composition at approximately 13 and 26%, respectively. These data suggest that selective heterogeneous oxidation is the dominant mechanism at these conditions. Conversely, for these same operating conditions but at the higher initial temperatures shown of 335, 357, and 380°C, a significant exotherm is observed in the freeboard, which is combined with a dramatic increase in molecular oxygen conversion with high selectivity to CO and CO_2. These data are consistent with homogeneous gas phase combustion.

The laboratory fluidized bed reactor was also used to study residence time effects on the onset of autoignition in this low solids homogeneous gas phase section. The motivation for this work was to support a planned commercial reactor modification to decrease the diameter of the transfer line from the reactor stripper to the cyclone, which is a potential area for autoignition to occur. The intent was to decrease the residence time of the homogeneous gas phase mixture exiting the stripper, to let the material sweep through the system before the induction time for combustion.

Figure 11 shows the effect of residence time and initial molecular oxygen composition on the conversion of molecular oxygen at 362°C, 4.5% initial *n*-butane composition, and a pressure corresponding to the design pressure (4.1 bar) of the commercial reactor. Note that this conversion includes the oxygen consumption in both the fluidized bed and in the freeboard, but the freeboard residence time is estimated based on the low-solids reactor volume which excludes the fluidized bed section. The data show that at these conditions, decreasing the "low solids" gas-phase residence time in the freeboard delays the onset of complete combustion (as characterized by total oxygen conversion) to higher molecular oxygen compositions. This trend is expected for a free radical combustion chemistry mechanism with autoignition which characteristically includes an induction period for initiation.

The freeboard reaction was modeled using a perfectly mixed reactor model in an adiabatic mode. Initial conditions and process parameters for the model runs were selected to mimic the experimental conditions shown in Figure 11. The initial gas composition was assumed to contain 4.5% *n*-butane with varying amounts of O_2 ranging from 0.75–2.5% with the balance as N_2. Simulations were performed for three gas residence times, 4.5, 6.3 and 8.3 seconds, and at an

initial temperature of 362°C and pressure of 4.1 bar. The predicted oxygen conversion levels are lower than those observed experimentally; however, the shape of the response with respect to O_2 concentration, and the effect of increased residence time is qualitatively consistent with the experimental results. Lower predicted conversions can be explained by two factors. First, the model results do not reflect reactions that have occurred in the fast bed. These include both oxygen consuming reactions, as well as heterogeneous reactions that may contribute to a source of free radicals at the inlet to the freeboard. Based partially on these confirming experimental data and modeling results, the stripper transfer line in the commercial reactor was replaced with a smaller diameter pipe to decrease the residence time.

Figure 12 illustrates the pronounced effect of pressure on molecular oxygen conversion in the freeboard of the laboratory fluidized bed reactor at 360°C, 4.5% *n*-butane, 6.3 s freeboard residence time, and 3.1 and 4.1 bar—pressures corresponding to the operating pressure of the pilot plant and the commercial plant design pressure, respectively. These data suggest that at these conditions, increased oxygen conversion due to autoignition and combustion reactions will occur at a significantly lower molecular oxygen concentration at the higher design pressure than for the lower operating pressure. These results reinforce the results of Figure 6 presented previously.

The freeboard reactor model was run at 4.5% *n*-butane and oxygen compositions ranging from 1 to 2.5%, with an initial temperature of 360°C for two pressures, 3.1 and 4.1 bar. Clearly, oxygen conversion increases with increasing initial O_2 levels, and higher pressure promotes the homogeneous consumption of O_2 significantly. Again, predicted conversions are lower than what is observed experimentally for the same reasons cited above, however, qualitatively the trends predicted by the model are consistent with experiment.

This pressure effect is further explored in Figure 13 at the 1% initial O_2 level and 6.3 s residence time, where the molecular O_2 conversion is shown to increase from 42% at 2.75 bar, to nearly 88% at 4.1 bar for an initial reactor temperature of 360°C. Further increases in the reactor pressure at these conditions resulted in complete combustion in the freeboard as indicated by complete oxygen consumption with a simultaneous dramatic increase in the temperature and CO/CO_2 selectivity (not shown). The comparable model runs indicate very little conversion between 2.75 and 3 bar, however, reaction does appear to take off when the initial pressure is

raised to 3.12 bar, and then rises in a similar fashion to the experimental results. The lack of reaction at the lowest pressures indicates that the oxidation induction time at 1% O_2 and these pressures is longer than the time available for reaction. The fact that reaction is observed experimentally for these conditions suggests that free radicals created heterogeneously in the fastbed serve to seed the homogeneous reactions in the freeboard, thereby reducing induction time.

Modeling Oxidation Induction Time

Induction time is explored directly in model runs shown in Figures 14 and 15. In Figures 14(a) and (b), induction time in a constant pressure batch system is tested at two different initial *n*-butane concentrations, 7.4 and 4.4%, at an initial temperature of 385°C and 4.1 bar, parametric in initial O_2 concentration. For the higher 7.4% initial *n*-butane case, the induction time for all O_2 levels is on the order of about 6 s. At 4.4% *n*-butane, the induction time is about 14 s. The magnitude of the pressure rise, which is indicative of the reaction rate, is amplified at higher initial O_2 concentration, but the onset of reaction occurs at approximately the same time. Figure 15 shows the important impact of pressure on oxidation induction time. Here the 13 s induction time at 4 bar increases to 200 s at 1 bar. These results show that the onset of reaction, or oxidation induction time, is inversely proportional to the pressure squared. These induction time results do not map directly to the freeboard observations since the back-mixing of free radicals in the freeboard serve to accelerate reaction initiation, however all trends are consistent.

SUMMARY AND CONCLUSIONS

DuPont's *n*-butane oxidation process involves the use of a proprietary attrition-resistant VPP catalyst and CFB reactor technology for the selective oxidation of *n*-butane to maleic anhydride as an intermediate for the production of tetrahydrofuran. Reactor operating conditions fall within the flammability envelope of the reactant and products to maximize reactor productivity. Such operation is possible since the solids phase tends to suppress non-selective homogeneous reactions (combustion) while at the same time promoting the desired selective catalytic reactions. During operation of both a pilot plant and the commissioning of the commercial CFB reactor, "temperature excursions" resulting from localized combustion reactions were experienced both in

the vicinity of spargers supplying oxygen to the reactors and in the homogeneous gas phase or "free board" region in and downstream of the reactor cyclone.

A laboratory fluidized bed reactor and theoretical modeling were utilized to address design and operating issues related to the addition of molecular oxygen into the commercial CFB reactor with a goal of enhancing production capacity by safely maximizing the free oxygen concentration. The simulation consisted of an elementary step level free-radical kinetics model using the Chemkin collection of programs and well-established reaction networks and associated parameters comprising 440 elementary reactions and 78 species. The objectives of this experimental and modeling program were (1) to study the local reaction behavior near an oxygen sparger placed in a fluidized bed of solid VPP catalyst, and (2) to evaluate the effect of operating conditions on the onset of combustion in the homogeneous gas phase region of the *n*-butane oxidation reactor. Plant operating conditions (e.g., reactor temperature, pressure, residence time, and *n*-butane and oxygen compositions) were simulated in the fluidized bed reactor to determine the effect of manipulating these experimental factors on suppression of gas phase combustion.

In general, the laboratory fluidized bed reactor was operated at temperatures between 320 and 390°C, pressures from 3 to 4 bar, *n*-butane compositions of 4-10%, oxygen compositions of 1-6%, and freeboard residence times of 4-8 s. Parametric studies of the oxidation products are presented for both the fluidized bed and freeboard sections of the reactor. Both experimental and modeling results demonstrated a pronounced pressure effect on the onset of combustion in this range of operating conditions. In one example, multiple temperature excursions corresponding to autoignition were induced by small pressure spikes of as little as 0.3-0.6 bar. A significant impact of operating temperature on the onset of combustion was also noted between 320 and 335°C in the reactor freeboard, with combustion being the dominant oxidation mechanism at 335°C and higher temperatures. Both experimental and modeling results demonstrated that decreasing the residence time in the low solids regions of the reactor delays the onset of complete combustion to longer time or higher relative molecular oxygen compositions. Kinetic model predictions are presented that show a significant influence of reactant composition and reactor pressure on oxidation induction time. Finally, the effect of using porous metal oxygen spargers as alternatives to standard nozzles was also demonstrated. Little impact of this sparger design on inducing combustion in the fluidized bed was observed over a range of operating conditions.

Subsequent papers will include reports of additional work on mitigating combustion by quenching effluent gases from the high solids sections of the reactor, the effect of suspended catalyst fines on suppressing autoignition, the effect of the product MAN composition, and the impact of adding free radical scavengers to suppress combustion.

REFERENCES

[1] P. Botella, J.M. López Nieto, B. Solsona, J. Mol. Catal. A: Chem. 184 (2002) 335-347.

[2] M.J. Lorences, G.S. Patience, R. Cenni, F. Diez, J. Coca, Catal. Today 112 (2006) 45-48.

[3] T.V. Malleswara Rao, G. Deo, Ind. Eng. Chem. Res. 46 (2007) 70-79.

[4] R.P. Hesketh, J.F. Davidson, Combust. Flame 85 (1991) 449-467.

[5] D.R. van der Vaart, Fuel 67 (1988) 1003-1007.

[6] N. Ballarini, F. Cavani, C. Cortelli, S. Ligi, F. Pierelli, F. Trifiro, C. Fumagalli, G. Mazzoni, T. Monti, Topics Catal. 38 (2006) 147-156.

[7] R.M. Contractor, Chem. Eng. Sci. 54 (1999) 5627-5632.

[8] M. Cathonnet, J.C. Boettner, H. James, Eighteenth Symposium (International) on Combustion, The Combustion Institute, 1981, pp. 903-913.

[9] A. Burcat, K. Scheller, A. Lifshitz, Combust. Flame 16 (1971) 29-33.

[10] S. Kojima, T. Suzuoki, Combust. Flame 92 (1993) 254-265.

[11] R. Minetti, M. Ribaucour, M. Carlier, C. Fittschen, L.R. Sochet, Combust. Flame 96 (1994) 201-211.

[12] J.C. Déchaux, J.L. Flament, M. Lucquin, Combust. Flame 17 (1971) 205-214.

[13] G.A. Luckett, R.T. Pollard, Combust. Flame 21 (1973) 265-274.

[14] M.B. Neumann, P.M. Tutakin, Compt. Rend. Acad. Sci. URSS 4 (1936) 127-130.

[15] D.C. Horning, D.F. Davidson, R.K. Hanson, J. Propul. Power 18 (2002) 363-371.

[16] M.A. Oehlschlaeger, D.F. Davidson, J.T. Herbon, R.K. Hanson, Int. J. Chem. Kinet. 36 (2004) 67-78.

[17] R.J. Olsen, W.R. Williams, X. Song, L.D. Schmidt, R. Aris, Chem. Eng. Sci. 47 (1992) 2505-2510.

[18] M. Ziauddin, G. Veser, L.D. Schmidt, Catal. Lett. 46 (1997) 159-167.

[19] G.S. Patience, R.E. Bockrath, Appl. Catal., A, in press, this issue.

[20] P.L. Mills, W.E. Guise, Jr., J. Chromatogr. Sci. 34 (1996) 431-459.

[21] W.J. Pitz, C.K. Westbrook, Combust. Flame 63 (1986) 113-133.

[22] W.J. Pitz, R.D. Wilk, C.K. Westbrook, N.P. Cernansky, Western States Section/The Combustion Institute, Salt Lake City, UT, Paper No. WSSCI 88-51 (1988).

List of Tables

Table 1. Pilot Plant Temperature Excursions

Time (h)	T (^oC)	Gas Velocity (m/s)	Solids Mass Flux (kg/m^2s)	Pressure Drop (mbar)	Suspension Density (kg/m^3)	[n-C_4H_{10}] (mol%)	[O_2] (mol%)	Bottom Sparger (kg/h)	Top Sparger (kg/h)	Middle Sparger (kg/h)	BET S.A. (m^2/g)	ΔT (^oC)
83	372	1.1	98	618	379	7.6	11.1	45	0	0	20.2	2
85	371	1.3	115	640	366	7.3	9.5	41	0	0	20.1	2
97	375	1.3	117	616	347	8.7	8.5	41	0	0	19.9	2
98	378	1.3	117	612	345	10.0	7.8	41	0	0	19.9	2
99	377	1.3	117	612	345	10.0	8.0	41	0	0	19.9	2
100	377	1.3	116	614	345	8.0	8.6	41	0	0	19.9	2
102	376	1.3	117	616	345	9.2	8.4	41	0	0	19.9	4
105	374	1.3	113	629	363	10.0	8.2	40	0	0	19.8	4
107	370	1.3	116	644	372	10.9	7.9	39	0	0	19.8	4
109	372	1.3	126	652	364	10.3	8.3	40	0	0	19.8	2
137	375	1.2	116	646	370	10.6	9.0	35	8	0	19.3	3
141	374	1.2	114	642	369	10.6	9.8	38	8	0	19.3	2
144	369	1.2	114	654	376	11.1	9.7	36	7	0	19.2	2
146	371	1.2	115	640	376	10.7	9.6	36	7	0	19.2	2
207	371	1.3	121	638	365	11.1	7.3	36	0	0	18.3	2
213	370	1.2	123	675	387	10.9	10.3	36	9	0	18.2	2

214	371	1.2	124	673	387	10.9	10.1	36	9	0	18.2	2
216	374	1.2	123	669	382	10.6	9.9	36	9	0	18.2	2
217	372	1.2	124	672	387	10.8	9.7	35	9	0	18.1	2
222	370	1.2	127	682	392	10.1	10.0	35	8	0	18.1	2
574	374	1.5	116	559	324	15.1	4.4	0	0	0	17.4	4
579	373	1.5	121	566	323	14.1	5.7	31	0	0	17.4	2
607	381	1.3	129	694	416	13.8	9.0	31	0	0	17.4	2
1000	383	1.3	112	639	361	11.7	12.7	25	0	16	16.6	3
1004	382	1.3	111	637	360	11.6	13.9	27	0	30	16.6	4
1248	381	0.9	76	680	449	17.4	17.4	30	14	30	16.1	4
1525	383	0.9	61	621	338	15.5	15.3	30	14	30	15.1	3
1526	382	0.9	61	624	347	15.7	15.0	27	14	29	15.1	6
1552	384	0.9	61	602	340	15.1	15.6	25	10	24	14.8	4

List of Figures

Figures

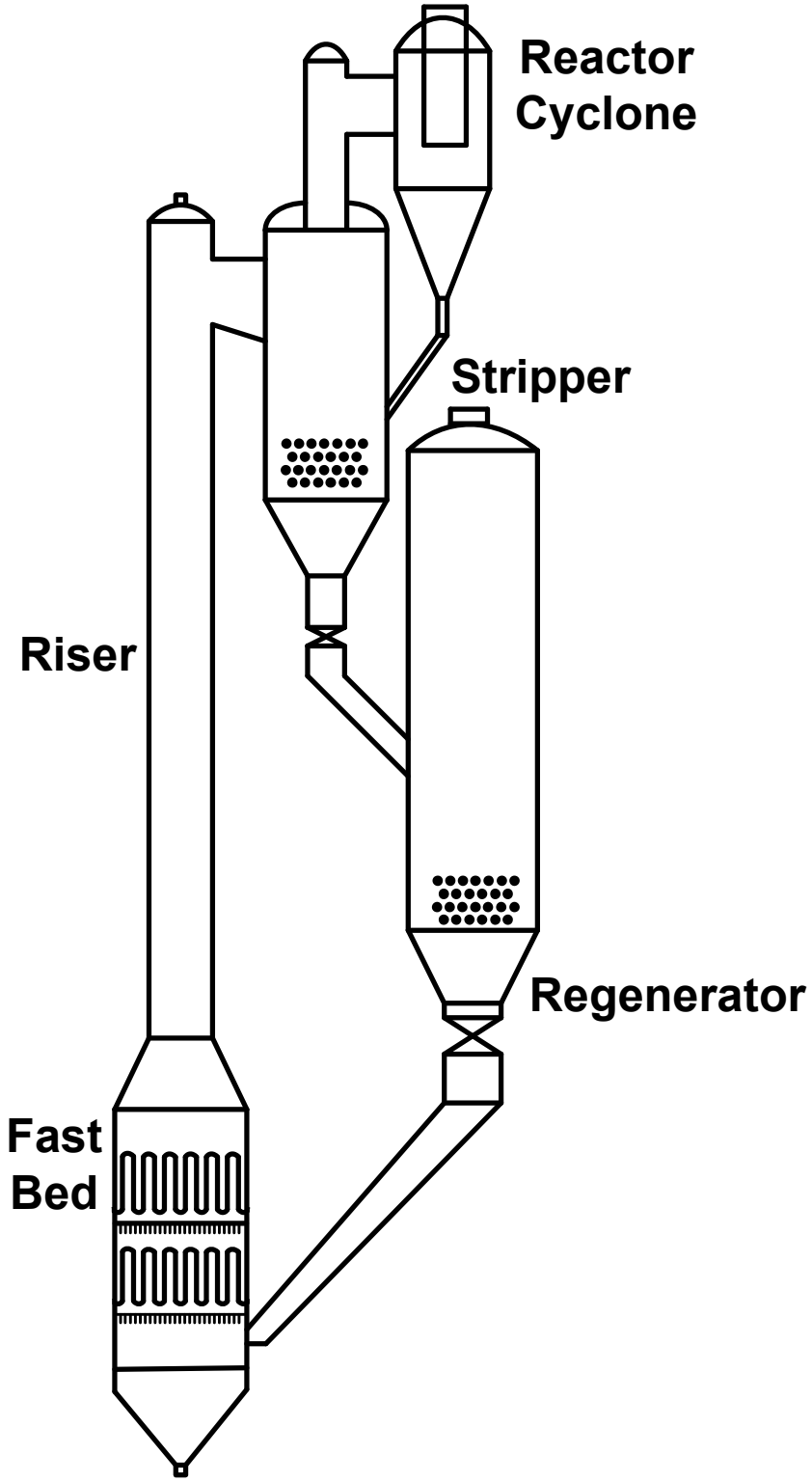

Figure 1. Circulating Fluidized Bed (CFB) configuration for the commercial facility.

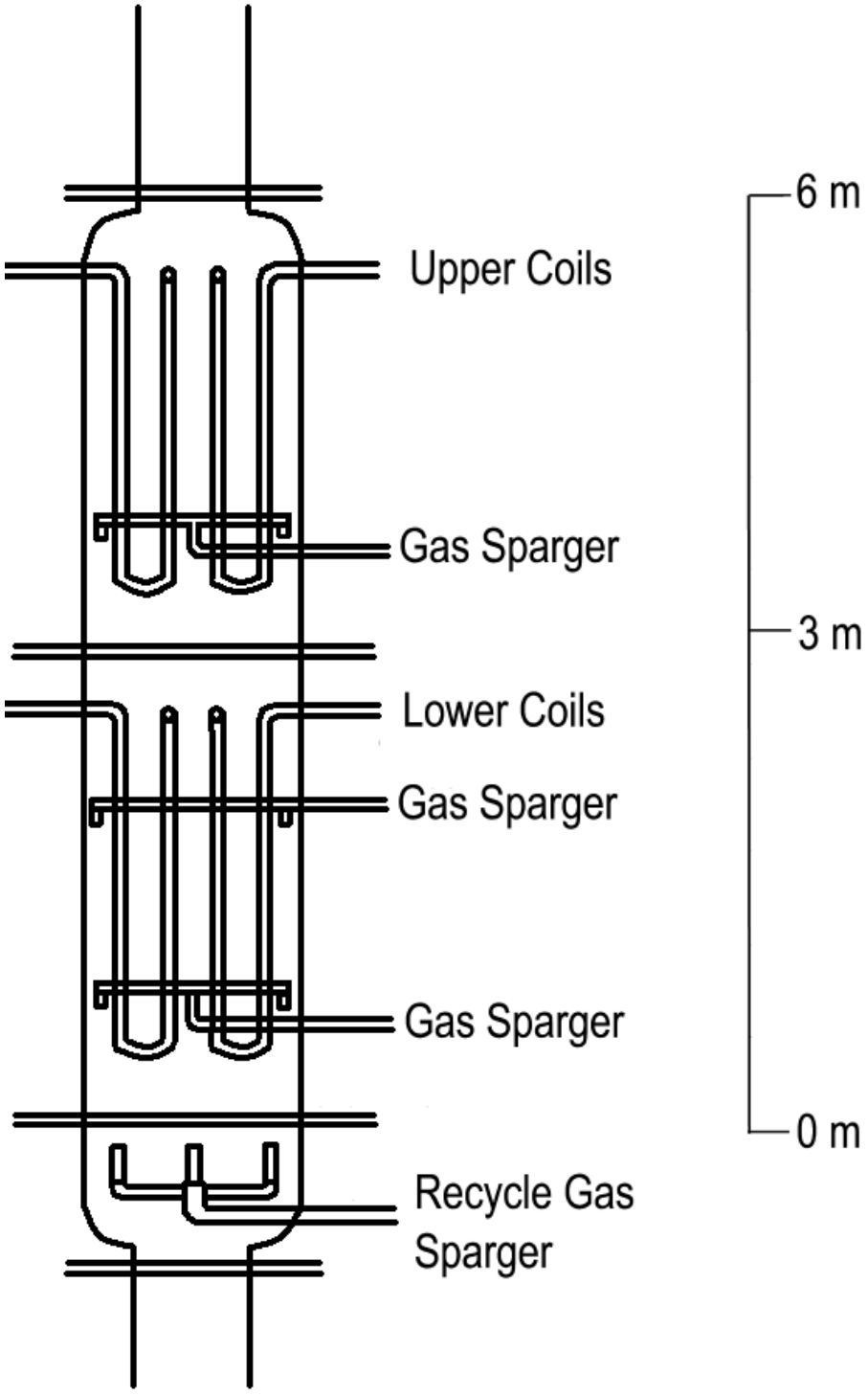

Figure 2. Pilot plant reactor fast bed configuration.

(a)

(b)

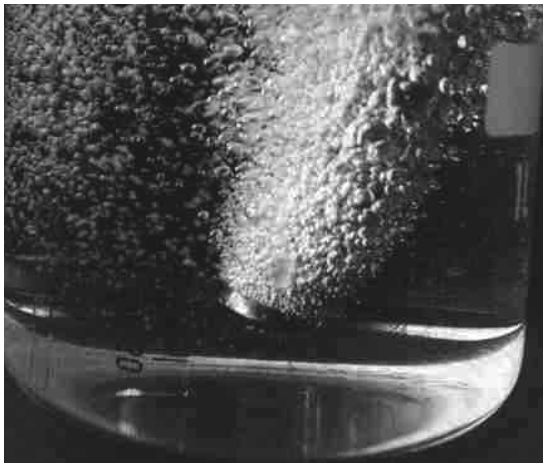

(c)

Figure 3. Sparger tests with air sparged through two nozzle geometries: Standard nozzle in water at (a) 14 m/s, (b) 40 m/s; (c) Sintered metal nozzle in ethanol at 40 m/s.

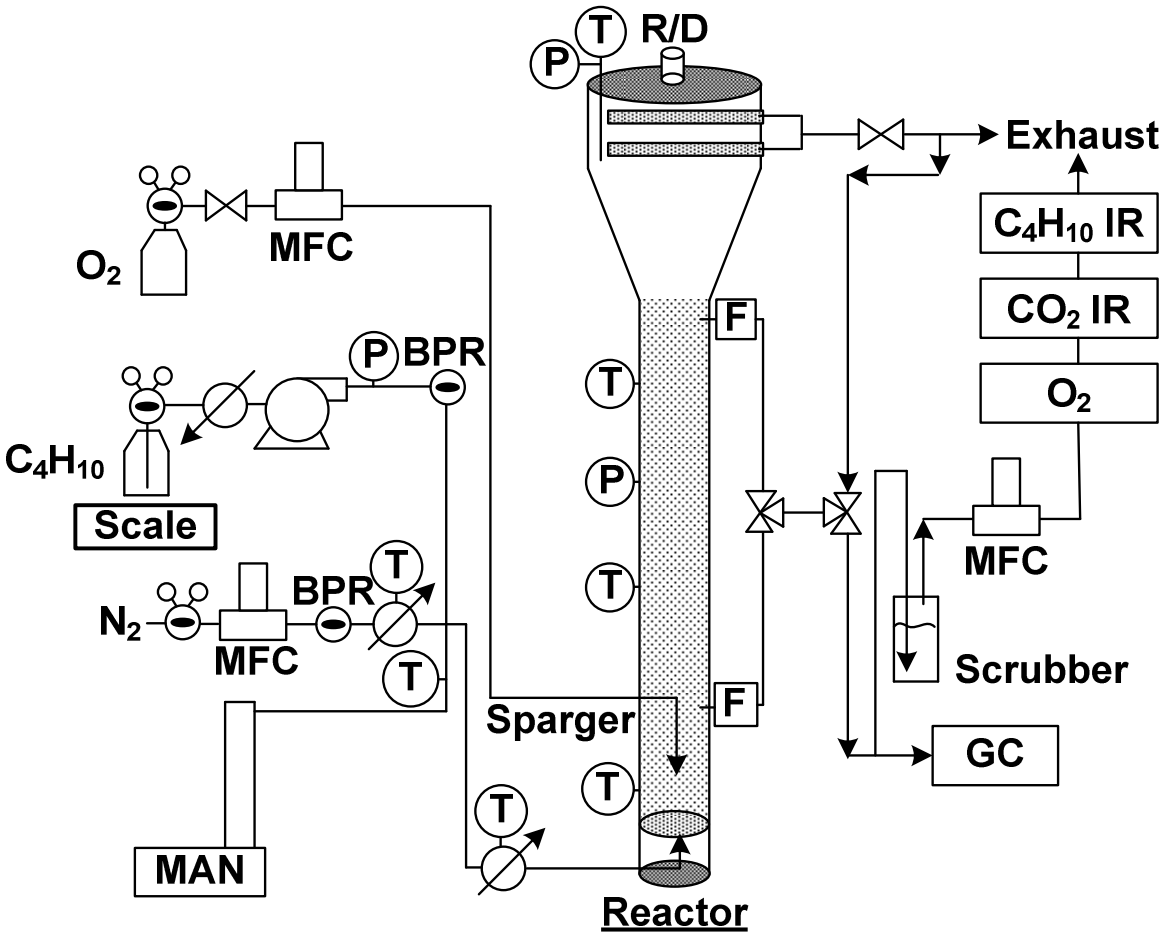

Figure 4. Experimental fluidized bed reactor apparatus.

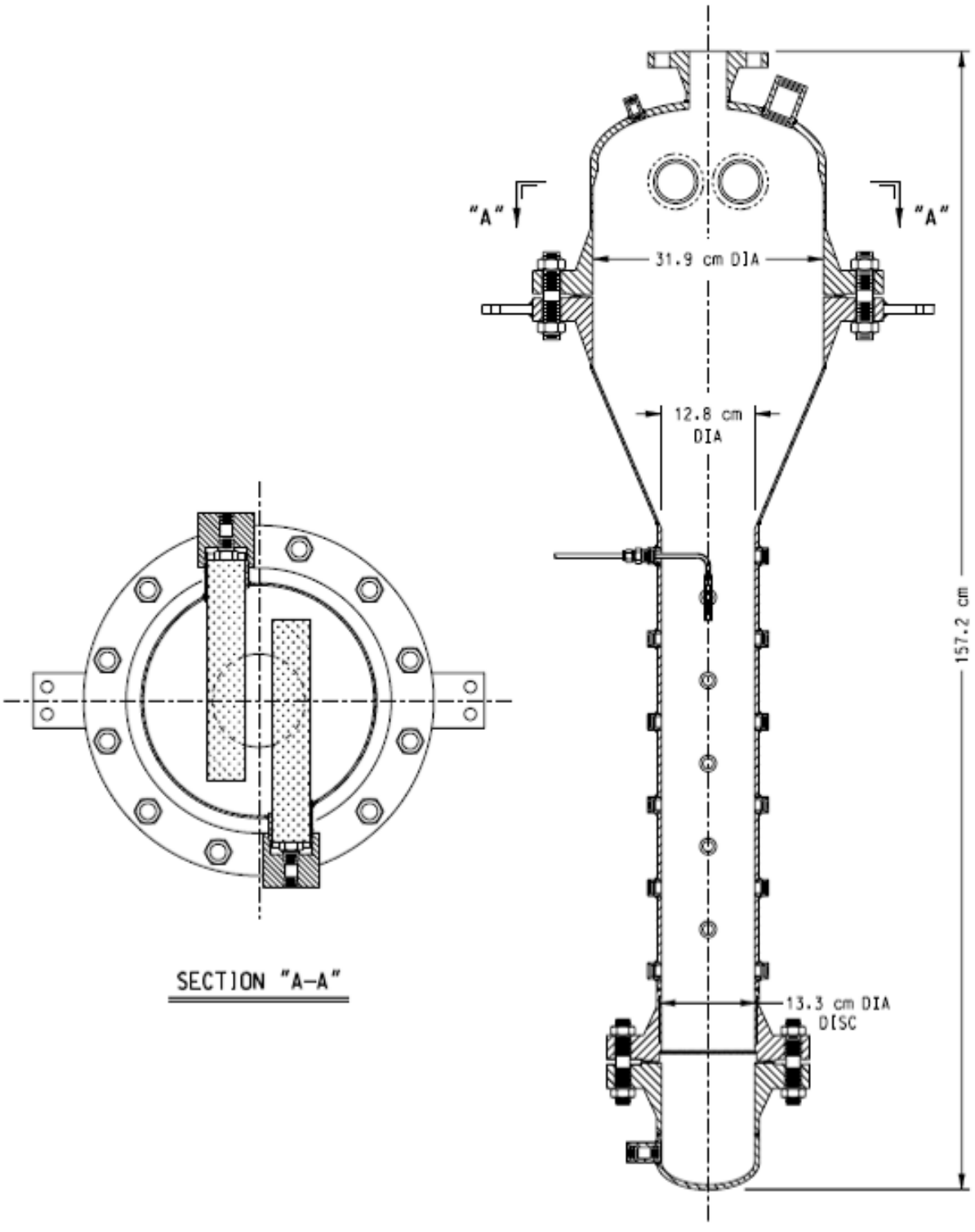

Figure 5. Cross-sectional view of the fluidized bed reactor.

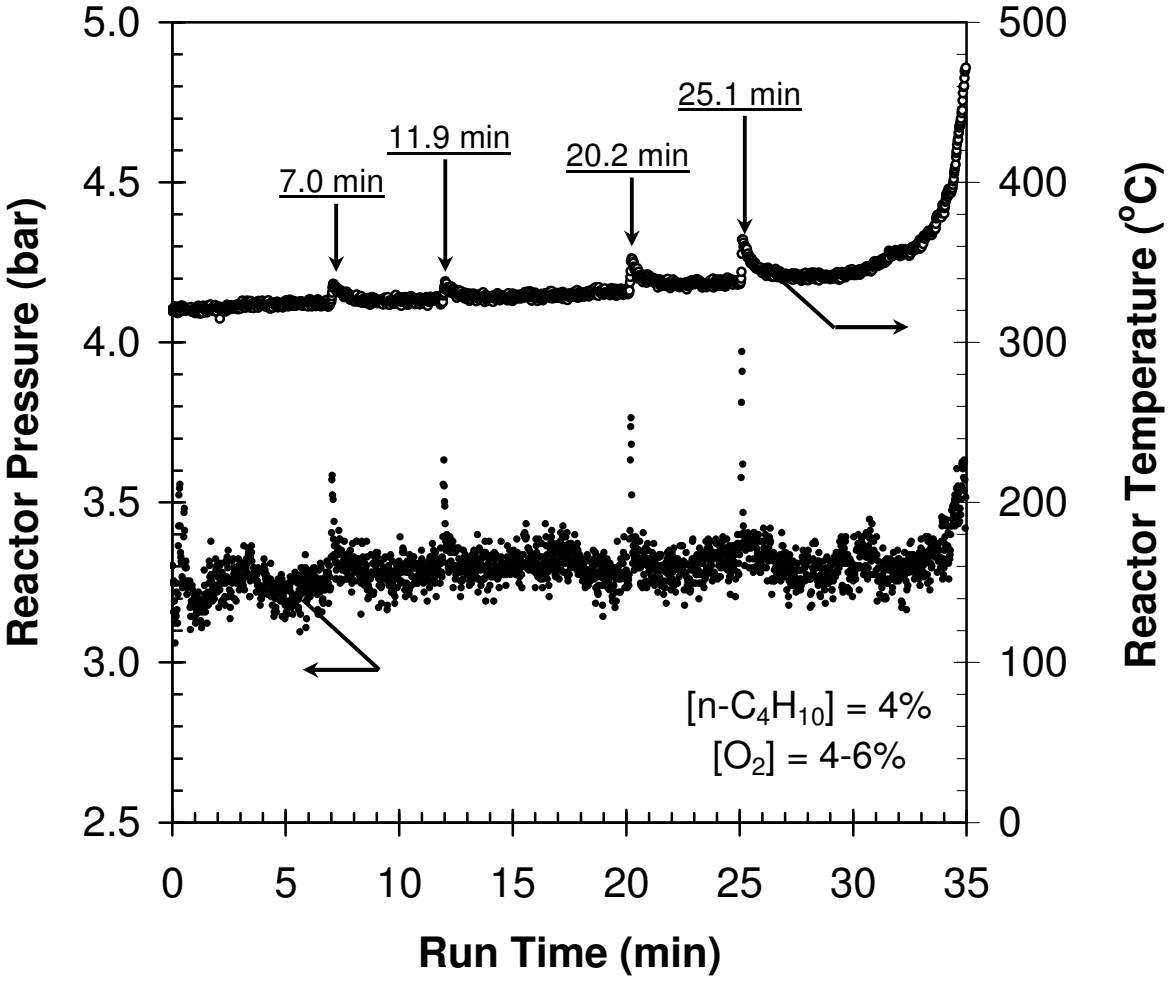

Figure 6. Pressure effect showing reactor freeboard temperature excursions induced by temporary reactor pressure spikes.

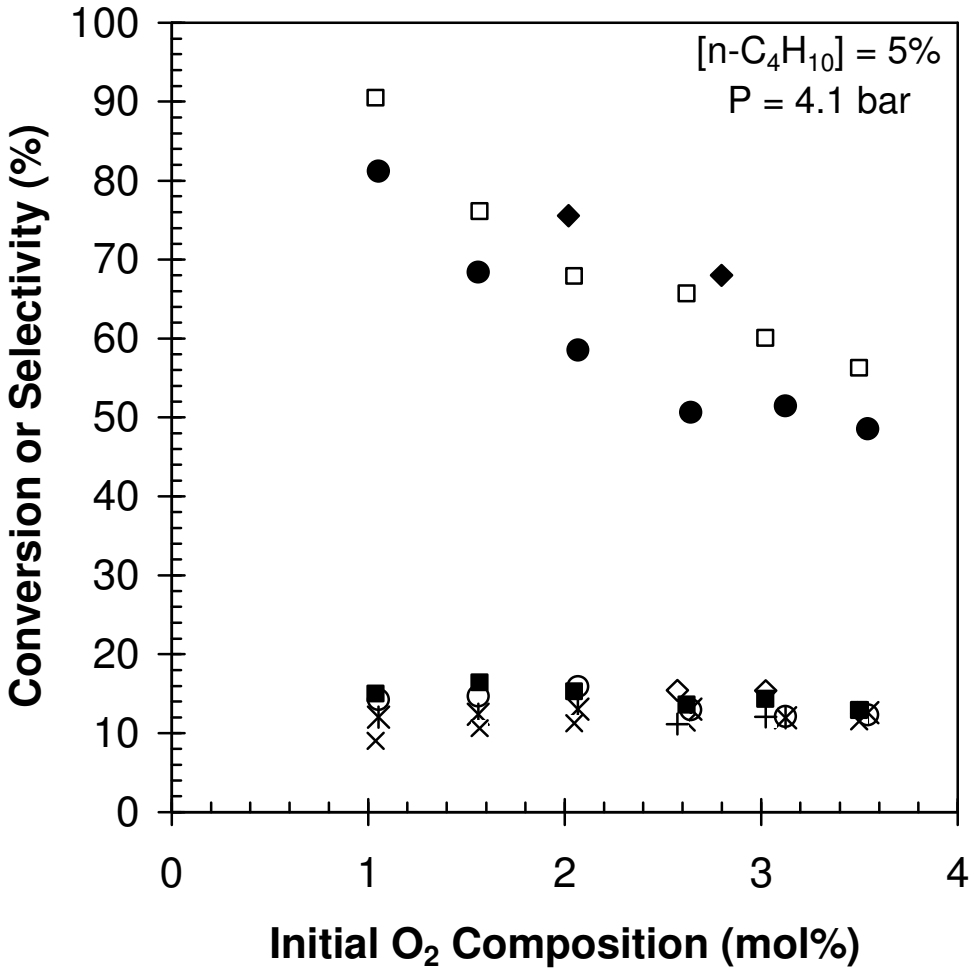

Figure 7. Effect of reactor temperature and initial oxygen composition on molecular oxygen conversion and CO_2 and maleic anhydride (MAN) selectivity in the fluidized catalyst bed: O_2 conversion at • 362°C, □ 375°C, ◆ 387°C; CO_2 selectivity at ○ 362°C, ■ 375°C, ◇ 387°C; MAN selectivity at ✳ 362°C, × 375°C, + 387°C.

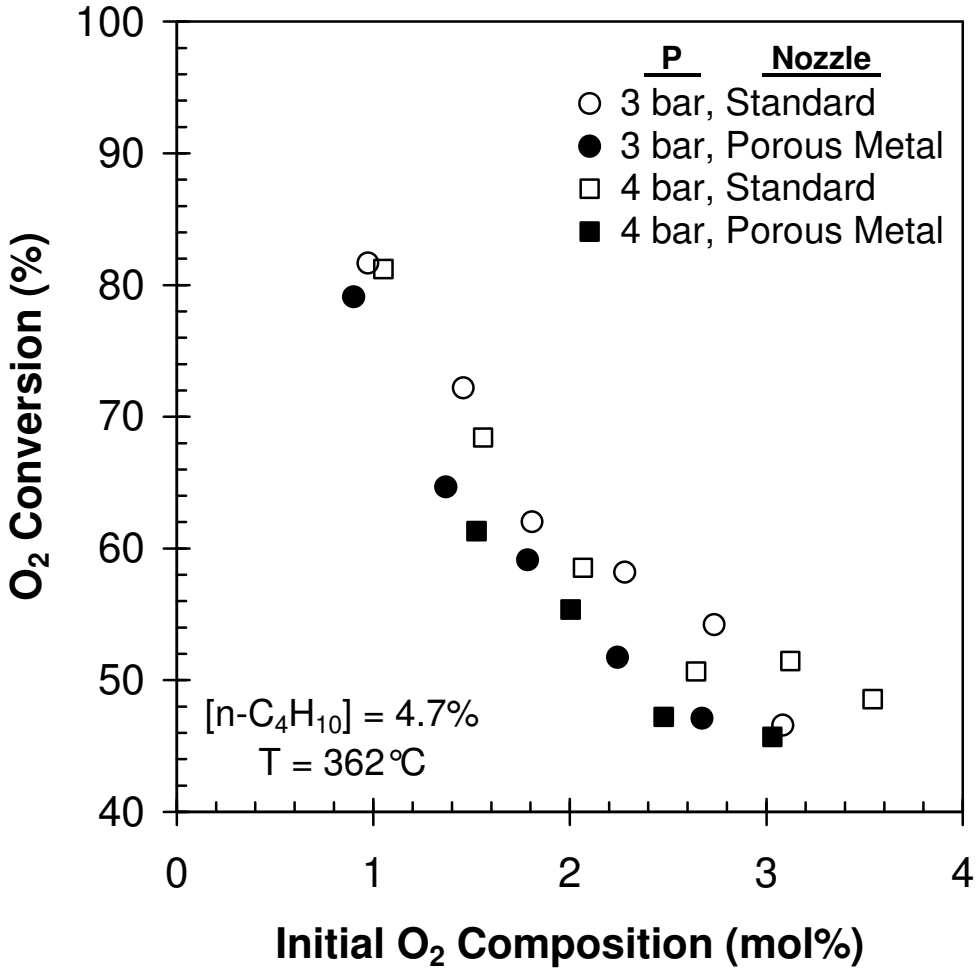

Figure 8. Influence of nozzle type and reactor pressure on molecular oxygen conversion in the fluidized catalyst bed.

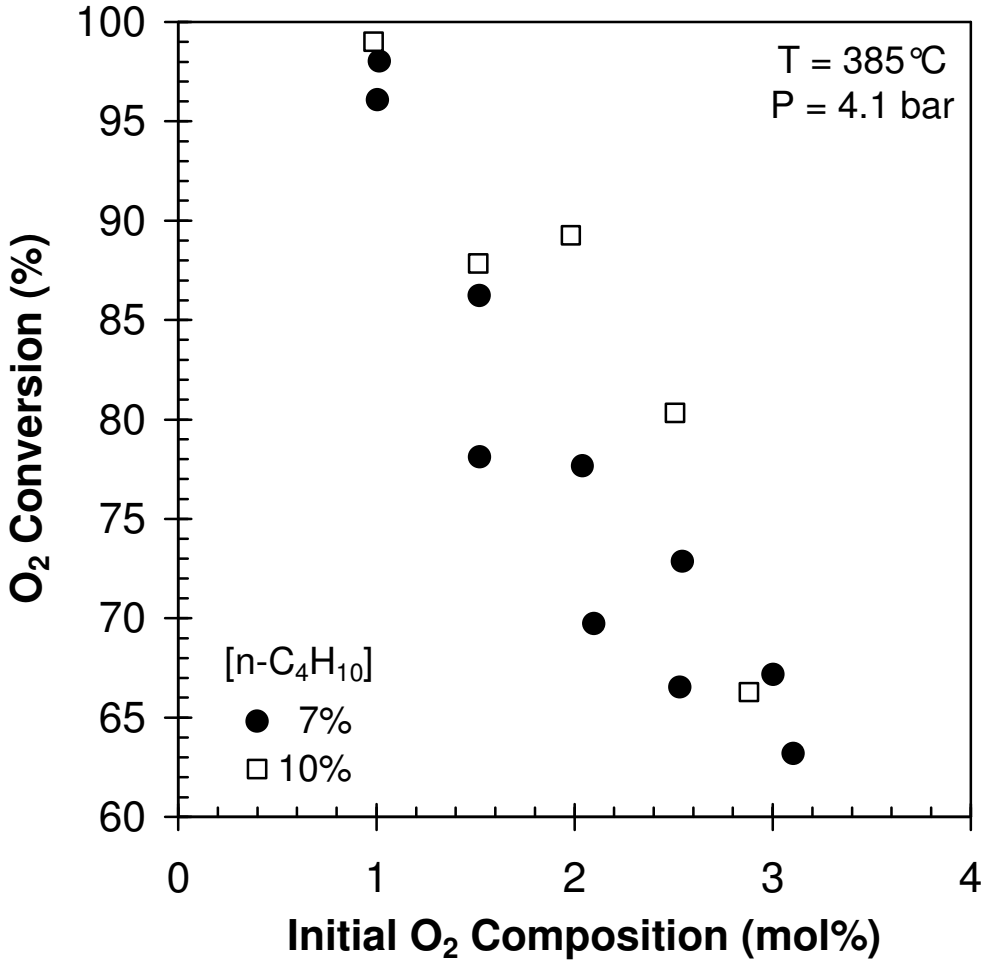

Figure 9. *n*-Butane concentration effect in fluidized bed with porous metal sparger.

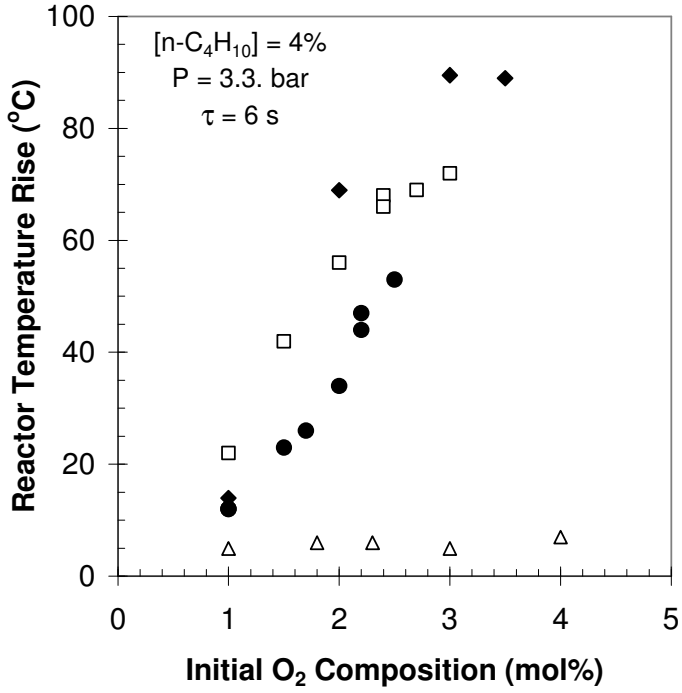

(a)

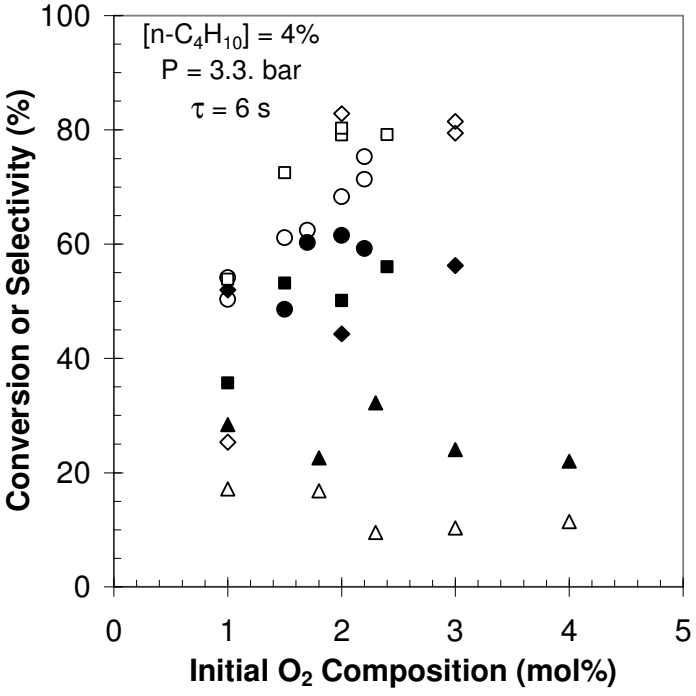

(b)

Figure 10. Influence of reactor temperature and initial oxygen composition on molecular oxygen conversion and CO/CO_2 selectivity in the reactor freeboard: (a) reactor temperature rise at • 380°C, □ 357°C, ◆ 335°C, Δ 320°C; (b) O_2 conversion at ○ 380°C, □ 357°C, ◇ 335°C, Δ 320°C; CO/CO_2 selectivity at • 380°C, ■ 357°C, ◆ 335°C, ▲ 320°C.

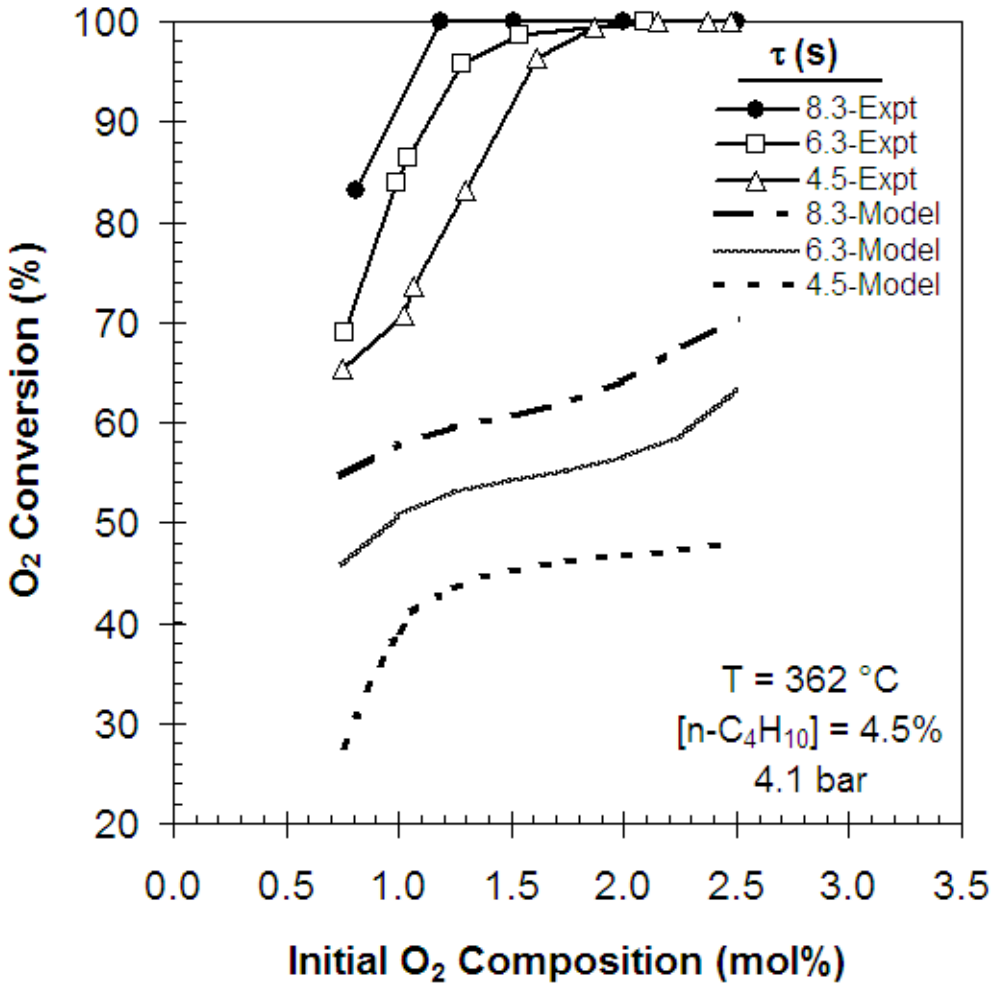

Figure 11. Effect of freeboard residence time and inlet oxygen composition on molecular oxygen conversion (lines in experimental data are to guide the eye).

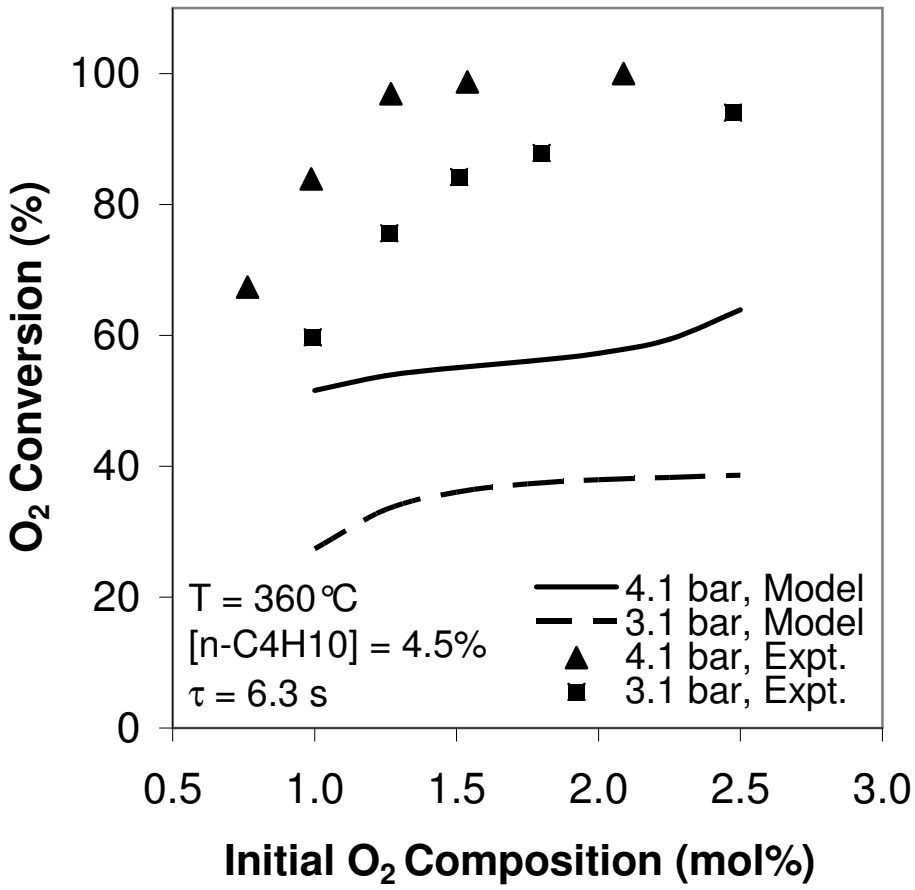

Figure 12. Effect of reactor pressure and inlet oxygen composition on molecular oxygen conversion in the reactor freeboard.

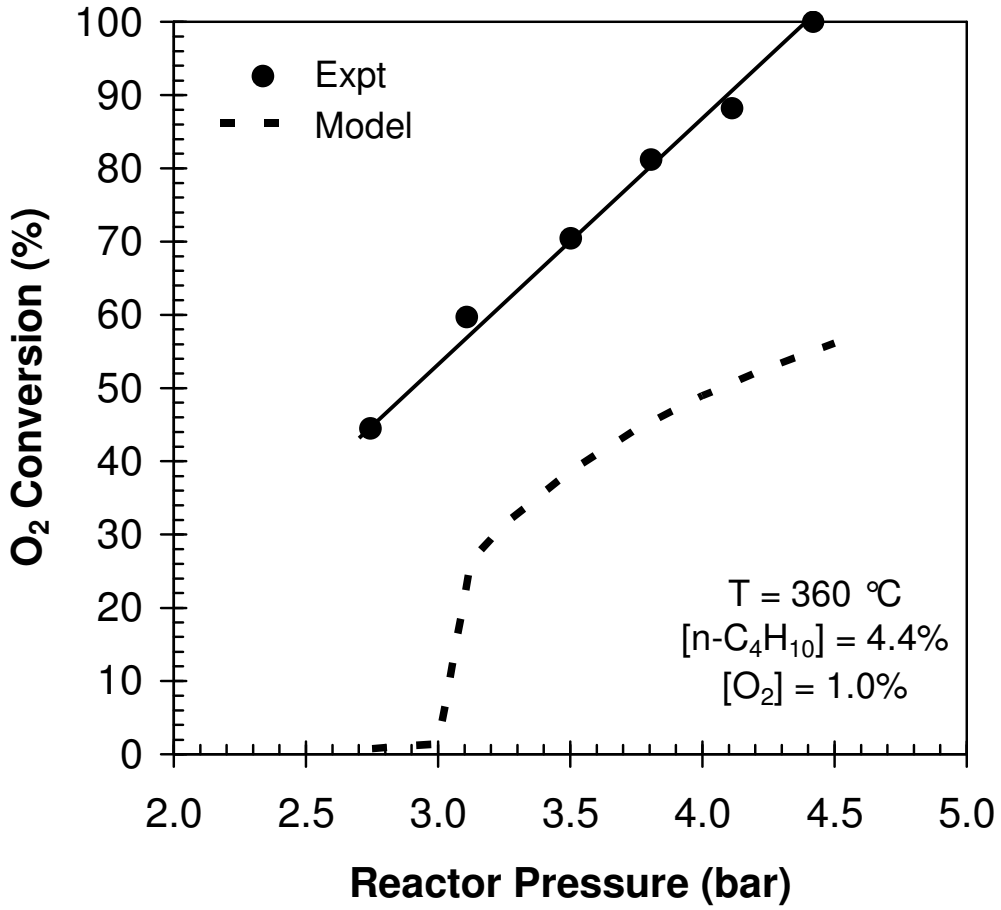

Figure 13. Effect of reactor pressure on molecular oxygen conversion in the reactor freeboard.

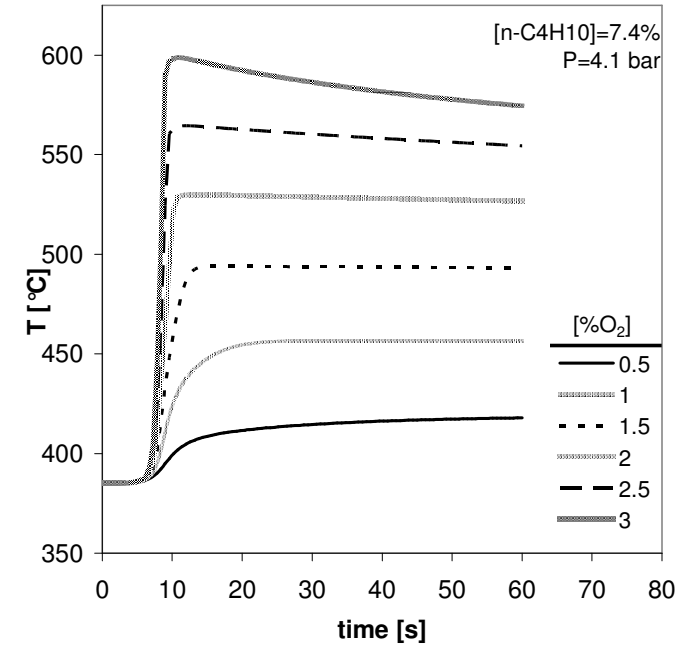

(a)

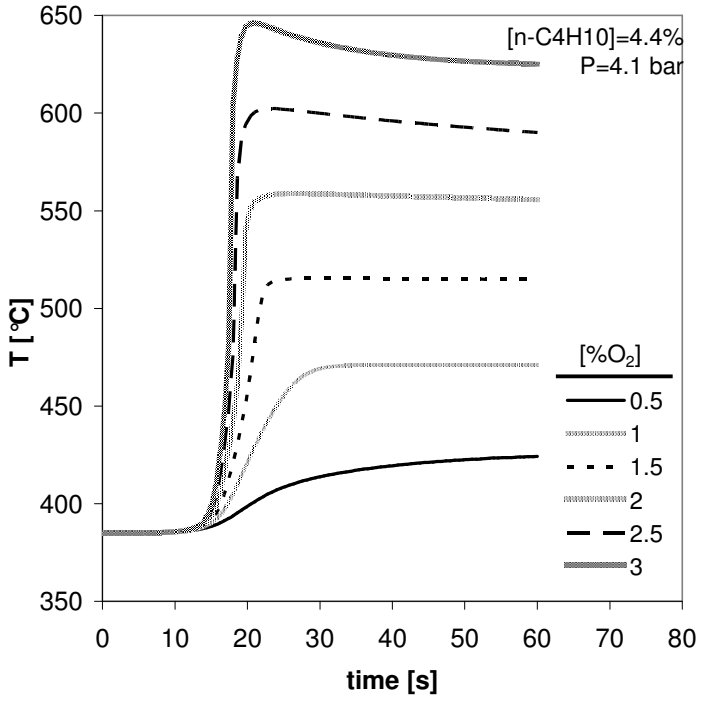

(b)

Figure 14. Effect of initial oxygen composition on induction time – constant pressure batch simulation: (a) 7.4% initial *n*-butane concentration (b) 4.4% initial *n*-butane concentration.

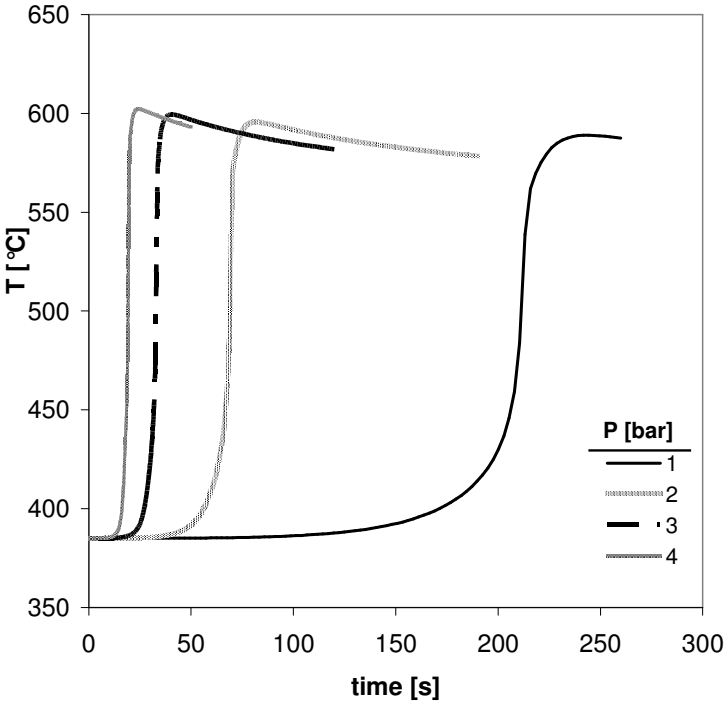

(a)

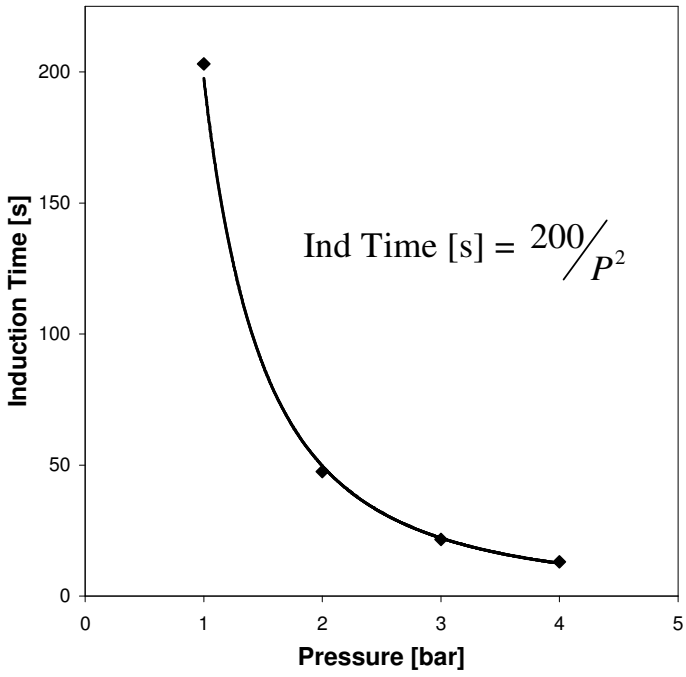

(b)

Figure 15. Model predictions of the effect of pressure on oxidation induction time: (a) Temperature rise vs time, parametric in pressure (b) Induction time vs P.

ANNEXE 9 – BREVET POUR LA MÉTHODE DE MESURE SIMULTANÉE DE LA FRACTION DE SOLIDES ET DE LA COMPOSITION CHIMIQUE DE LA PHASE GAZEUSE

UNITED STATES PATENT AND TRADEMARK OFFICE

UNITED STATES DEPARTMENT OF COMMERCE
United States Patent and Trademark Office
Address: COMMISSIONER FOR PATENTS
P.O. Box 1450
Alexandria, Virginia 22313-1450
www.uspto.gov

APPLICATION NUMBER	FILING or 371(c) DATE	GRP ART UNIT	FIL FEE REC'D	ATTY.DOCKET.NO	TOT CLAIMS	IND CLAIMS
61/272,481	09/29/2009		110	08400-150		

CONFIRMATION NO. 5814

61114
BCF LLP
1100 RENE'-LE'VESQUE BLVD. WEST
25TH FLOOR
MONTREAL, QC H3B-5C9
CANADA

FILING RECEIPT

OC000000038506691

Date Mailed: 11/02/2009

Receipt is acknowledged of this provisional patent application. It will not be examined for patentability and will become abandoned not later than twelve months after its filing date. Any correspondence concerning the application must include the following identification information: the U.S. APPLICATION NUMBER, FILING DATE, NAME OF APPLICANT, and TITLE OF INVENTION. Fees transmitted by check or draft are subject to collection. Please verify the accuracy of the data presented on this receipt. **If an error is noted on this Filing Receipt, please submit a written request for a Filing Receipt Correction. Please provide a copy of this Filing Receipt with the changes noted thereon. If you received a "Notice to File Missing Parts" for this application, please submit any corrections to this Filing Receipt with your reply to the Notice. When the USPTO processes the reply to the Notice, the USPTO will generate another Filing Receipt incorporating the requested corrections**

Applicant(s)

Jamal B. Chaouki, Dorval, CANADA;
Jean-Philippe Laviolette, Montreal, CANADA;
Gregory Patience, Ville Mont-Royal, CANADA;

Power of Attorney:
Ronald Kosie--28814

If Required, Foreign Filing License Granted: 10/28/2009
The country code and number of your priority application, to be used for filing abroad under the Paris Convention, is **US 61/272,481**
Projected Publication Date: None, application is not eligible for pre-grant publication
Non-Publication Request: No
Early Publication Request: No
**** SMALL ENTITY ****
Title

Simultaneous quantitative measurement of gaseous species composition and solids volum fraction in a gas/solid flow

PROTECTING YOUR INVENTION OUTSIDE THE UNITED STATES

Since the rights granted by a U.S. patent extend only throughout the territory of the United States and have no effect in a foreign country, an inventor who wishes patent protection in another country must apply for a patent in a specific country or in regional patent offices. Applicants may wish to consider the filing of an international application under the Patent Cooperation Treaty (PCT). An international (PCT) application generally has the same

effect as a regular national patent application in each PCT-member country. The PCT process **simplifies** the filing of patent applications on the same invention in member countries, but **does not result** in a grant of "an international patent" and does not eliminate the need of applicants to file additional documents and fees in countries where patent protection is desired.

Almost every country has its own patent law, and a person desiring a patent in a particular country must make an application for patent in that country in accordance with its particular laws. Since the laws of many countries differ in various respects from the patent law of the United States, applicants are advised to seek guidance from specific foreign countries to ensure that patent rights are not lost prematurely.

Applicants also are advised that in the case of inventions made in the United States, the Director of the USPTO must issue a license before applicants can apply for a patent in a foreign country. The filing of a U.S. patent application serves as a request for a foreign filing license. The application's filing receipt contains further information and guidance as to the status of applicant's license for foreign filing.

Applicants may wish to consult the USPTO booklet, "General Information Concerning Patents" (specifically, the section entitled "Treaties and Foreign Patents") for more information on timeframes and deadlines for filing foreign patent applications. The guide is available either by contacting the USPTO Contact Center at 800-786-9199, or it can be viewed on the USPTO website at http://www.uspto.gov/web/offices/pac/doc/general/index.html.

For information on preventing theft of your intellectual property (patents, trademarks and copyrights), you may wish to consult the U.S. Government website, http://www.stopfakes.gov. Part of a Department of Commerce initiative, this website includes self-help "toolkits" giving innovators guidance on how to protect intellectual property in specific countries such as China, Korea and Mexico. For questions regarding patent enforcement issues, applicants may call the U.S. Government hotline at 1-866-999-HALT (1-866-999-4158).

LICENSE FOR FOREIGN FILING UNDER

Title 35, United States Code, Section 184

Title 37, Code of Federal Regulations, 5.11 & 5.15

GRANTED

The applicant has been granted a license under 35 U.S.C. 184, if the phrase "IF REQUIRED, FOREIGN FILING LICENSE GRANTED" followed by a date appears on this form. Such licenses are issued in all applications where the conditions for issuance of a license have been met, regardless of whether or not a license may be required as set forth in 37 CFR 5.15. The scope and limitations of this license are set forth in 37 CFR 5.15(a) unless an earlier license has been issued under 37 CFR 5.15(b). The license is subject to revocation upon written notification. The date indicated is the effective date of the license, unless an earlier license of similar scope has been granted under 37 CFR 5.13 or 5.14.

This license is to be retained by the licensee and may be used at any time on or after the effective date thereof unless it is revoked. This license is automatically transferred to any related applications(s) filed under 37 CFR 1.53(d). This license is not retroactive.

The grant of a license does not in any way lessen the responsibility of a licensee for the security of the subject matter as imposed by any Government contract or the provisions of existing laws relating to espionage and the national security or the export of technical data. Licensees should apprise themselves of current regulations especially with

respect to certain countries, of other agencies, particularly the Office of Defense Trade Controls, Department of State (with respect to Arms, Munitions and Implements of War (22 CFR 121-128)); the Bureau of Industry and Security, Department of Commerce (15 CFR parts 730-774); the Office of Foreign AssetsControl, Department of Treasury (31 CFR Parts 500+) and the Department of Energy.

NOT GRANTED

No license under 35 U.S.C. 184 has been granted at this time, if the phrase "IF REQUIRED, FOREIGN FILING LICENSE GRANTED" DOES NOT appear on this form. Applicant may still petition for a license under 37 CFR 5.12, if a license is desired before the expiration of 6 months from the filing date of the application. If 6 months has lapsed from the filing date of this application and the licensee has not received any indication of a secrecy order under 35 U.S.C. 181, the licensee may foreign file the application pursuant to 37 CFR 5.15(b).